

Survey of Period Variations of Superhumps in SU UMa-Type Dwarf Novae. VIII: The Eighth Year (2015–2016)

Taichi KATO,^{1*} Franz-Josef HAMBSCH,^{2,3,4} Berto MONARD,^{5,6}
Tonny VANMUNSTER,⁷ Yutaka MAEDA,⁸ Ian MILLER,⁹ Hiroshi ITOH,¹⁰
Seiichiro KIYOTA,¹¹ Keisuke ISOGAI,¹ Mariko KIMURA,¹ Akira IMADA,¹²
Tamás TORDAI,¹³ Hidehiko AKAZAWA,¹⁴ Kenji TANABE,¹⁴ Noritoshi OTANI,¹⁴
Minako OGI,¹⁴ Kazuko ANDO,¹⁴ Naoki TAKIGAWA,¹⁴ Pavol A. DUBOVSKY,¹⁵
Igor KUDZEJ,¹⁵ Sergey Yu. SHUGAROV,^{16,18} Natalia KATYSHEVA,¹⁶
Polina GOLYSHEVA,¹⁶ Natalia GLADILINA,¹⁷ Drahomir CHOCHOL,¹⁸
Peter STARR,¹⁹ Kiyoshi KASAI,²⁰ Roger D. PICKARD,^{21,22}
Enrique de MIGUEL,^{23,24} Naoto KOJIGUCHI,²⁵ Yuki SUGIURA,²⁵
Daiki FUKUSHIMA,²⁵ Eiji YAMADA,²⁵ Yusuke UTO,²⁵ Taku KAMIBETSUNAWA,²⁵
Taiki TATSUMI,²⁵ Nao TAKEDA,²⁵ Katsura MATSUMOTO,²⁵ Lewis M. COOK,²⁶
Elena P. PAVLENKO,²⁷ Julia V. BABINA,²⁷ Nikolaj V. PIT,²⁷
Oksana I. ANTONYUK,²⁷ Kirill A. ANTONYUK,²⁷ Aleksei A. SOSNOVSKIJ,²⁷
Aleksei V. BAKLANOV,²⁷ Stella KAFKA,²⁸ William STEIN,²⁹
Irina B. VOLOSHINA,¹⁶ Javier RUIZ,^{30,31,32} Richard SABO,³³
Shawn DVORAK,³⁴ Geoff STONE,²⁸ Maksim V. ANDREEV,^{35,36}
Sergey V. ANTIPIN,^{16,17} Alexandra M. ZUBAREVA,^{17,16}
Anna M. ZAOSTROJNYKH,³⁷ Michael RICHMOND,³⁸ Jeremy SHEARS,^{39, 21}
Franky DUBOIS,⁴⁰ Ludwig LOGIE,⁴⁰ Steve RAU,⁴⁰ Siegfried VANAVERBEKE,⁴⁰
Andrei SIMON,⁴¹ Arto OKSANEN,⁴² William N. GOFF,⁴³ Greg BOLT,⁴⁴
Bartłomiej DĘBSKI,⁴⁵ Christopher S. KOCHANEK,⁴⁶ Benjamin SHAPPEE,⁴⁶
Krzysztof Z. STANEK,⁴⁶ José L. PRIETO,^{47, 48} Rod STUBBINGS,⁴⁹
Eddy MUYLLAERT,⁵⁰ Mitsutaka HIRAGA,⁵¹ Tsuneo HORIE,⁵²
Patrick SCHMEER,⁵³ Kenji HIROSAWA,⁵⁴

¹ Department of Astronomy, Kyoto University, Kyoto 606-8502, Japan

² Groupe Européen d'Observations Stellaires (GEOS), 23 Parc de Levesville, 28300 Bailleau l'Evêque, France

³ Bundesdeutsche Arbeitsgemeinschaft für Veränderliche Sterne (BAV), Munsterdamm 90, 12169 Berlin, Germany

⁴ Vereniging voor Sterrenkunde (VVS), Oude Bleken 12, 2400 Mol, Belgium

⁵ Bronberg Observatory, Center for Backyard Astrophysics Pretoria, PO Box 11426, Tiegterpoort 0056, South Africa

⁶ Kleinkaroo Observatory, Center for Backyard Astrophysics Kleinkaroo, Sint Helena 1B, PO Box 281, Calitzdorp 6660, South Africa

⁷ Center for Backyard Astrophysics Belgium, Walhostraat 1A, B-3401 Landen, Belgium

⁸ Kaminishiyamamachi 12-14, Nagasaki, Nagasaki 850-0006, Japan

- ⁹ Furzehill House, Ilston, Swansea, SA2 7LE, UK
- ¹⁰ Variable Star Observers League in Japan (VSOLJ), 1001-105 Nishiterakata, Hachioji, Tokyo 192-0153, Japan
- ¹¹ VSOLJ, 7-1 Kitahatsutomi, Kamagaya, Chiba 273-0126, Japan
- ¹² Kwasan and Hida Observatories, Kyoto University, Yamashina, Kyoto 607-8471, Japan
- ¹³ Polaris Observatory, Hungarian Astronomical Association, Laborc utca 2/c, 1037 Budapest, Hungary
- ¹⁴ Department of Biosphere-Geosphere System Science, Faculty of Informatics, Okayama University of Science, 1-1 Ridai-cho, Okayama, Okayama 700-0005, Japan
- ¹⁵ Vihorlat Observatory, Mierova 4, 06601 Humenne, Slovakia
- ¹⁶ Sternberg Astronomical Institute, Lomonosov Moscow State University, Universitetsky Ave., 13, Moscow 119992, Russia
- ¹⁷ Institute of Astronomy, Russian Academy of Sciences, Moscow 119017, Russia
- ¹⁸ Astronomical Institute of the Slovak Academy of Sciences, 05960 Tatranska Lomnica, Slovakia
- ¹⁹ Warrumbungle Observatory, Tenby, 841 Timor Rd, Coonabarabran NSW 2357, Australia
- ²⁰ Baselstrasse 133D, CH-4132 Muttenz, Switzerland
- ²¹ The British Astronomical Association, Variable Star Section (BAA VSS), Burlington House, Piccadilly, London, W1J 0DU, UK
- ²² 3 The Birches, Shobdon, Leominster, Herefordshire, HR6 9NG, UK
- ²³ Departamento de Física Aplicada, Facultad de Ciencias Experimentales, Universidad de Huelva, 21071 Huelva, Spain
- ²⁴ Center for Backyard Astrophysics, Observatorio del CIECEM, Parque Dunar, Matalascañas, 21760 Almonte, Huelva, Spain
- ²⁵ Osaka Kyoiku University, 4-698-1 Asahigaoka, Osaka 582-8582, Japan
- ²⁶ Center for Backyard Astrophysics Concord, 1730 Helix Ct. Concord, California 94518, USA
- ²⁷ Federal State Budget Scientific Institution "Crimean Astrophysical Observatory of RAS", Nauchny, 298409, Republic of Crimea
- ²⁸ American Association of Variable Star Observers, 49 Bay State Rd., Cambridge, MA 02138, USA
- ²⁹ 6025 Calle Paraiso, Las Cruces, New Mexico 88012, USA
- ³⁰ Observatorio de Cantabria, Ctra. de Rocamundo s/n, Valderredible, 39220 Cantabria, Spain
- ³¹ Instituto de Física de Cantabria (CSIC-UC), Avenida Los Castros s/n, E-39005 Santander, Cantabria, Spain
- ³² Agrupación Astronómica Cantabria, Apartado 573, 39080, Santander, Spain
- ³³ 2336 Trailcrest Dr., Bozeman, Montana 59718, USA
- ³⁴ Rolling Hills Observatory, 1643 Nightfall Drive, Clermont, Florida 34711, USA
- ³⁵ Terskol Branch of Institute of Astronomy, Russian Academy of Sciences, 361605, Peak Terskol, Kabardino-Balkaria Republic, Russia
- ³⁶ International Center for Astronomical, Medical and Ecological Research of NASU, Ukraine 27 Akademika Zabolotnoho Str. 03680 Kyiv, Ukraine
- ³⁷ Institute of Physics, Kazan Federal University, Ulitsa Kremlevskaya 16a, Kazan 420008, Russia
- ³⁸ Physics Department, Rochester Institute of Technology, Rochester, New York 14623, USA
- ³⁹ "Pemberton", School Lane, Bunbury, Tarporley, Cheshire, CW6 9NR, UK
- ⁴⁰ Public observatory Astrolab Iris, Verbrandemolenstraat 5, B 8901 Zillebeke, Belgium
- ⁴¹ Taras Shevchenko National University of Kyiv, the Faculty of Physics, Astronomy and Space Physics Department, 64/13, Volodymyrska Street, Kyiv 01601, Ukraine
- ⁴² Hankasalmi observatory, Jyvaskylan Sirius ry, Verkkoniementie 30, FI-40950 Muurame, Finland

- ⁴³ 13508 Monitor Ln., Sutter Creek, California 95685, USA
⁴⁴ Camberwarra Drive, Craigie, Western Australia 6025, Australia
⁴⁵ Astronomical Observatory, Jagiellonian University, ul. Orla 171 30-244 Kraków, Poland
⁴⁶ Department of Astronomy, the Ohio State University, Columbia, OH 43210, USA
⁴⁷ Núcleo de Astronomía de la Facultad de Ingeniería, Universidad Diego Portales, Av. Ejército 441, Santiago, Chile
⁴⁸ Department of Astrophysical Sciences, Princeton University, NJ 08544, USA
⁴⁹ Tetoora Observatory, 2643 Warragul-Korumburra Road, Tetoora Road, Victoria 3821, Australia
⁵⁰ Vereniging Voor Sterrenkunde (VVS), Moffelstraat 13 3370 Boutersem, Belgium
⁵¹ 19-27 Higashikannon-cho, Shimonoseki, Yamaguchi 752-0906, Japan
⁵² 759-10 Tokawa, Hadano-shi, Kanagawa 259-1306, Japan
⁵³ Bischmisheim, Am Probstbaum 10, 66132 Saarbrücken, Germany
⁵⁴ 216-4 Maeda, Inazawa-cho, Inazawa-shi, Aichi 492-8217, Japan

*E-mail: *tkato@kusastro.kyoto-u.ac.jp

Received 201 0; Accepted 201 0

Abstract

Continuing the project described by Kato et al. (2009), we collected times of superhump maxima for 128 SU UMa-type dwarf novae observed mainly during the 2015–2016 season and characterized these objects. The data have improved the distribution of orbital periods, the relation between the orbital period and the variation of superhumps, the relation between period variations and the rebrightening type in WZ Sge-type objects. Coupled with new measurements of mass ratios using growing stages of superhumps, we now have a clearer and statistically greatly improved evolutionary path near the terminal stage of evolution of cataclysmic variables. Three objects (V452 Cas, KK Tel, ASASSN-15cl) appear to have slowly growing superhumps, which is proposed to reflect the slow growth of the 3:1 resonance near the stability border. ASASSN-15sl, ASASSN-15ux, SDSS J074859.55+312512.6 and CRTS J200331.3–284941 are newly identified eclipsing SU UMa-type (or WZ Sge-type) dwarf novae. ASASSN-15cy has a short (~ 0.050 d) superhump period and appears to belong to EI Psc-type objects with compact secondaries having an evolved core. ASASSN-15gn, ASASSN-15hn, ASASSN-15kh and ASASSN-16bu are candidate period bouncers with superhump periods longer than 0.06 d. We have newly obtained superhump periods for 79 objects and 13 orbital periods, including periods from early superhumps. In order that the future observations will be more astrophysically beneficial and rewarding to observers, we propose guidelines how to organize observations of various superoutbursts.

Key words: accretion, accretion disks — stars: novae, cataclysmic variables — stars: dwarf novae

1 Introduction

This paper is one of series of papers Kato et al. (2009), Kato et al. (2010), Kato et al. (2012), Kato et al. (2013a), Kato et al. (2014b), Kato et al. (2014a) and Kato et al. (2015a) dealing with superhumps in SU UMa-type dwarf novae (DNe). SU UMa-type dwarf novae are a class of cataclysmic variables (CVs) which are close binary systems transferring matter from a low-mass dwarf secondary to a white dwarf, forming an accretion disk. In SU UMa-type dwarf novae, two types of outbursts are seen: normal outbursts and superoutbursts. During super-

outbursts, small-amplitude variations with period a few percent longer than the orbital period (P_{orb}) called superhumps are observed. These superhumps are considered to be a result of the precession of the eccentric (or flexing) disk deformed by the tidal instability at the 3:1 resonance [see e.g. Whitehurst (1988); Hirose, Osaki (1990); Lubow (1991); Wood et al. (2011); for general information of CVs, DNe, SU UMa-type dwarf novae and superhumps, see e.g. Warner (1995a)].

In recent years, it has been demonstrated that the periods of superhumps systematically vary during superoutburst and Kato

et al. (2009) introduced superhump stages (stages A, B and C): initial growing stage with a long period (stage A) and fully developed stage with a systematically varying period (stage B) and later stage C with a shorter, almost constant period (see figure 1). Although the origin of these stages was unknown at the time of Kato et al. (2009), the phenomenon has been repeatedly confirmed by observations reported in Kato et al. (2010)–Kato et al. (2015a). Quite recently, partly with the help of Kepler (Koch et al. 2010) observations, Osaki, Kato (2013b) proposed that stage A superhumps reflect the dynamical precession rate at the 3:1 resonance radius and that the rapid decrease of the period (stage B) reflects the pressure effect which has an effect of retrograde precession (Lubow 1992; Hirose, Osaki 1993; Murray 1998; Montgomery 2001; Pearson 2006). Kato, Osaki (2013b) further extended this interpretation and confirmed that stage A superhumps indeed reflect the dynamical precession rate at the 3:1 resonance radius by using objects with mass ratios (q) established by eclipse observations. After this physical identification of the superhump stages, observations of superhumps during superoutbursts became an important tool not only for diagnosing the accretion disk but also for obtaining q values, which are most essential in understanding the nature of binaries and their evolutions. Applications of the stage A superhump method have been numerous: e.g. Kato et al. (2013b); Nakata et al. (2013); Ohshima et al. (2014); Kato et al. (2014c); Nakata et al. (2014).

Outbursts and superoutbursts in SU UMa-type dwarf novae are considered to be a result of the combination of thermal and tidal instabilities [thermal-tidal instability (TTI) model by Osaki (1989); Osaki (1996)]. Although there have been claims of other mechanisms [the enhanced mass-transfer model (Smak 1991) and pure thermal instability model (Cannizzo et al. 2010)], it has been demonstrated using Kepler observations of V1504 Cyg and V344 Lyr that the TTI model is the best one to explain the observations (Osaki, Kato 2013a) (see also Osaki, Kato 2014).

In this paper, we report observations of superhumps and associated phenomena in SU UMa-type dwarf novae whose superoutbursts were observed mainly in 2015–2016. We present basic observational materials and discussions in relation to individual objects. Starting from Kato et al. (2014a), we have been intending these series of papers to be also a source of compiled information, including historical, of individual dwarf novae.

The material and methods of analysis are given in section 2, observations and analysis of individual objects are given in section 3, including discussions particular to the objects, the general discussion is given in section 4 and the summary is given in section 5. Some tables and figures are available online only.

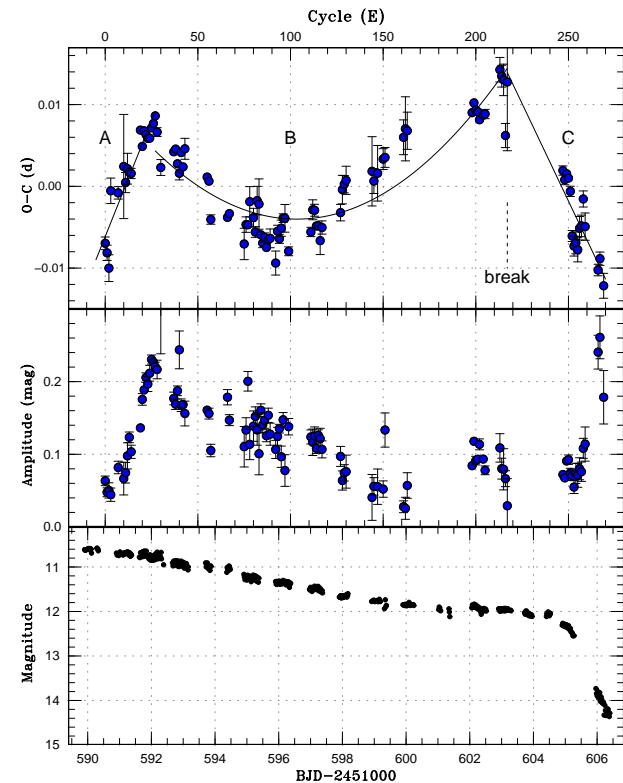


Fig. 1. Representative $O-C$ diagram showing three stages (A–C) of $O-C$ variation. The data were taken from the 2000 superoutburst of SW UMa. (Upper:) $O-C$ diagram. Three distinct stages (A – evolutionary stage with a longer superhump period, B – middle stage, and C – stage after transition to a shorter period) and the location of the period break between stages B and C are shown. (Middle:) Amplitude of superhumps. During stage A, the amplitude of the superhumps grew. (Lower:) Light curve. (Reproduction of figure 1 in Kato, Osaki 2013b)

2 Observation and Analysis

The data were obtained under campaigns led by the VSNET Collaboration (Kato et al. 2004b). We also used the public data for some objects from the AAVSO International Database¹. Outburst detections heavily relied on the ASAS-SN CV patrol (Davis et al. 2015)², Catalina Real-time Transient Survey (CRTS; Drake et al. 2009)³ in addition to outburst detections reported to VSNET, AAVSO⁴, BAAVSS alert⁵ and cvnet-outburst.⁶ There were some detections by the MASTER network (Gorbovskoy et al. 2013).

The majority of the data were acquired by time-resolved CCD photometry by using 30cm-class telescopes located world-wide. The details of these observations will be presented

¹ <<http://www.aavso.org/data-download>>.

² <<http://cv.asasn.astronomy.ohio-state.edu/>>.

³ <<http://nesssi.cacr.caltech.edu/catalina/>>.

For the information of the individual Catalina CVs, see <<http://nesssi.cacr.caltech.edu/catalina/AllCV.html>>.

⁴ <<https://www.aavso.org/>>.

⁵ <<https://groups.yahoo.com/group/baavss-alert/>>.

⁶ <<https://groups.yahoo.com/neo/groups/cvnet-outburst/>>.

in future papers dealing with analysis and discussion on individual objects of interest. The list of outbursts and observers is summarized in table 1. The data analysis was performed just in the same way described in Kato et al. (2009) and Kato et al. (2014a) and we mainly used R software⁷ for data analysis. In de-trending the data, we used both lower (1–3rd order) polynomial fitting and locally-weighted polynomial regression (LOWESS: Cleveland 1979). The times of superhumps maxima were determined by the template fitting method as described in Kato et al. (2009). The times of all observations are expressed in barycentric Julian days (BJD).

The abbreviations used in this paper are the same as in Kato et al. (2014a): P_{orb} means the orbital period and $\epsilon \equiv P_{\text{SH}}/P_{\text{orb}} - 1$ for the fractional superhump excess. Following Osaki, Kato (2013a), the alternative fractional superhump excess in the frequency unit $\epsilon^* \equiv 1 - P_{\text{orb}}/P_{\text{SH}} - 1 = \epsilon/(1 + \epsilon)$ has been introduced because this fractional superhump excess is a direct measure of the precession rate. We therefore used ϵ^* in discussing the precession rate.

We used phase dispersion minimization (PDM; Stellingwerf 1978) for period analysis and 1σ errors for the PDM analysis was estimated by the methods of Fernie (1989) and Kato et al. (2010). We introduced a variety of bootstrapping in estimating the robustness of the result of the PDM analysis since Kato et al. (2012). We typically analyzed 100 samples which randomly contain 50% of observations, and performed PDM analysis for these samples. The bootstrap result is shown as a form of 90% confidence intervals in the resultant PDM θ statistics.

If this paper provides the first solid presentation of a new SU UMa-type classification, we provide the result of PDM period analysis and averaged superhump profile.

The resultant P_{SH} , P_{dot} and other parameters are listed in table 3 in same format as in Kato et al. (2009). The definitions of parameters P_1 , P_2 , E_1 , E_2 and P_{dot} are the same as in Kato et al. (2009): P_1 and P_2 represent periods in stage B and C, respectively, and E_1 and E_2 represent intervals (in cycle numbers) to determine P_1 and P_2 , respectively.⁸ Comparisons of $O - C$ diagrams between different superoutbursts are also presented whenever available, since this comparison was one of the main motivations in of these series papers. In drawing combined $O - C$ diagrams, we usually used $E = 0$ for the start of the superoutburst, which usually refers to the first positive detection of the outburst. This epoch usually has an accuracy of ~ 1 d for well-observed objects, and if the outburst was not sufficiently observed, we mentioned in the figure caption how to estimate E in such an outburst. In some cases, this $E = 0$ is defined as the appearance of superhumps. This treatment is necessary

since some objects have a long waiting time before appearance of superhumps. Combined $O - C$ diagrams also help identifying superhump stages particularly when observations are insufficient. We also note that there is sometimes an ambiguity in selecting the true period among aliases. In some cases, this can be resolved by the help of the $O - C$ analysis. The procedure and example are shown in subsection 2.2 in Kato et al. (2015a).

We also present $O - C$ diagrams and light curves especially for WZ Sge-type dwarf novae. WZ Sge-type dwarf novae are a subclass of SU UMa-type dwarf novae characterized by the presence of early superhumps. They are seen during the early stages of superoutburst, and have period close to the orbital periods (Kato et al. 1996a; Kato 2002; Osaki, Meyer 2002; Kato 2015). These early superhumps are considered to be a result of the 2:1 resonance (Osaki, Meyer 2002). These objects usually show very rare outbursts (once in several years to decades) and often have complex light curves (Kato 2015) and are of special astrophysical interest since the origin of the complex light curves, including repetitive rebrightenings, is not well understood. They receive special attention since they are considered to represent the terminal stage of CV evolution and they may have brown-dwarf secondaries. We used the period of early superhumps as the approximate orbital period (Kato et al. 2014a; Kato 2015).

In figures, the points are accompanied by 1σ error bars whenever available, which are omitted when the error is smaller than the plot mark.

We used the same terminology of superhumps summarized in Kato et al. (2012). We especially call attention to the term “late superhumps”. Although this term has been used to express various phenomena, we only used the concept of “traditional” late superhumps when there is an ~ 0.5 phase shift [Vogt (1983); see also table 1 in Kato et al. (2012) for various types of superhumps], since we suspect that many of the past claims of detections of “late superhumps” were likely stage C superhumps before it became apparent that there are complex structures in the $O - C$ diagrams of superhumps (see discussion in Kato et al. 2009).

For objects detected in CRTS, we preferably used the names provided in Drake et al. (2014). If these names are not yet available, we used the International Astronomical Union (IAU)-format names provided by the CRTS team in the public data release⁹ As in Kato et al. (2009), we have used coordinate-based optical transient (OT) designations for some objects, such as apparent dwarf nova candidates reported in the Transient Objects Confirmation Page of the Central Bureau for Astronomical Telegrams¹⁰ and CRTS objects without registered designations in Drake et al. (2014) or in the CRTS public data release and listed the original identifiers in table 1.

⁷ The R Foundation for Statistical Computing: <http://cran.r-project.org/>.

⁸ The intervals (E_1 and E_2) for the stages B and C given in the table sometimes overlap because there is sometimes observational ambiguity (usually due to the lack of observations) in determining the stages.

⁹ <http://nessi.cacr.caltech.edu/DataRelease/>.

¹⁰ <http://www.cbat.eps.harvard.edu/unconf/tocp.html>.

We provided coordinates from astrometric catalogs for ASAS-SN (Shappee et al. 2014) CVs and two objects without coordinate-based names other than listed in the General Catalog of Variable Stars (Kholopov et al. 1985) in table 2. We used Sloan Digital Sky Survey (SDSS, Ahn et al. 2012), the Initial Gaia Source List (IGSL, Smart 2013) and Guide Star Catalog 2.3.2 (GSC 2.3.2, Lasker et al. 2007) and some other catalogs. The coordinates used in this paper are J2000.0. We also supplied SDSS g magnitudes and GALEX NUV magnitudes when counterparts are present.

3 Individual Objects

3.1 KV Andromedae

KV And was discovered as dwarf nova by Kurochkin (1977). Since Kurochkin (1977) reported very faint (22.5 mag) quiescent magnitude, this object was suspected to be a dwarf nova with a very large outburst amplitude. Later it turned out that Kurochkin (1977) underestimated the quiescent brightness since they used the paper print of the Palomar Observatory Sky Survey, and the true quiescent magnitude is now considered to be around 20. Kato et al. (1994) and Kato (1995) reported superhump observations in 1993 and 1994, respectively. Although this object was recognized as an SU UMa-type dwarf nova relatively early, none of observations sufficiently recorded the development of superhumps. Yet another superoutburst in 2002 (Kato et al. 2009) suffered from rather low signal-to-noise quality.

The 2015 superoutburst was visually detected by P. Dubovsky on August 25 (vsnet-alert 19005). Subsequent observations detected superhumps (vsnet-alert 19011, 19020, 19022). The times of superhump maxima are listed in table 4. The $O - C$ data suggest that the maxima for $E \leq 2$ probably recorded the final part of stage A. Although we give a comparison of the $O - C$ diagrams in figure 2, the starts of these superoutbursts were not well determined because this object has not been regularly monitored by visual observers. Since most of observations recorded large-amplitude superhumps, these observations, however, probably recorded the early phases of the superoutbursts and we treated these $O - C$ data as if the initial outburst detection refers to the start of the outburst. It is likely that the 1994 observation partly recorded stage A, which is compatible with low superhump amplitudes on the first two nights (the data quality was very poor, though).

3.2 EG Aquarii

EG Aqr was discovered as a blue eruptive object (BV number 3 in Luyten, Haro 1959) who reported a photographic magnitude of 14.8 on 1951 August 6. Haro, Chavira (1960) reported full photographic data, who gave a maximum of 14.0 mag (photo-

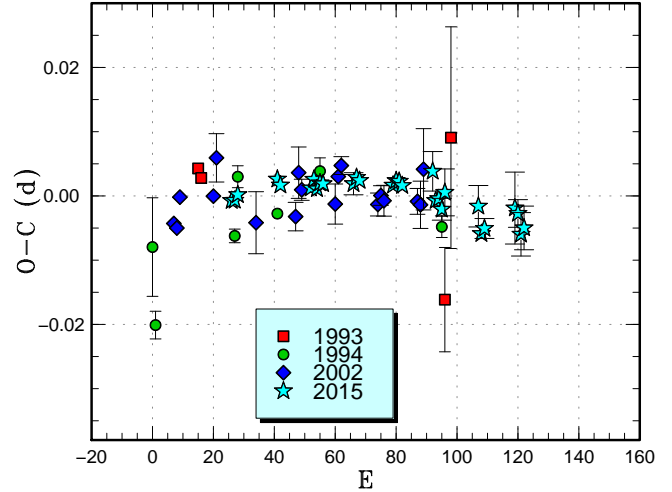


Fig. 2. Comparison of $O - C$ diagrams of KV And between different superoutbursts. A period of 0.07428 d was used to draw this figure. Approximate cycle counts (E) after the outburst detections were used. The actual starts of the outbursts were unknown. Since most of observations recorded large-amplitude superhumps, these observations probably recorded the early phases of the superoutbursts.

graphic) on 1958 November 5. The date in Luyten, Haro (1959) appears to have been a result of confusion. Vogt, Bateson (1982) did not detect any further outburst. Szkody, Howell (1992) obtained a K-type spectrum without emission lines, which was probably due to mis-identification.

The first well-confirmed outburst since the discovery was detected by R. Stubbings on 2006 November 8 at a visual magnitude of 12.4 (vsnet-alert 9103). In vsnet-alert 9105, P. Schmeer reported a CCD detection of the outburst earlier than R. Stubbings. This 2006 superoutburst was well studied by Imada et al. (2008). The 2008 and 2011 superoutbursts were also observed and analyzed in (Kato et al. 2009) and Kato et al. (2013a), respectively. There was also a normal outburst on 2013 October 1 at $V=15.0$ (ASAS-SN and R. Stubbings; vsnet-obs 76596, vsnet-outburst 16054). Although there was a bright outburst reaching a visual magnitude of 13.0 (R. Stubbings) on 2014 July 21, the nature of this outburst was unclear.

The 2015 superoutburst was visually detected by R. Stubbings at a magnitude of 12.1 on August 21 (vsnet-alert 18998). This outburst detection was sufficiently early and growing phase of superhumps was recorded (vsnet-alert 19003). There was, however, a long gap after the initial CCD observations and the outburst was not well covered by observations. The times of superhump maxima are listed in table 5. The maxima for $E \leq 2$ correspond to stage A superhumps (figure 3). The object showed a rebrightening on September 8 at $V=16.37$ (ASAS-SN detection, vsnet-alert 19038).

Table 1. List of Superoutbursts.

Subsection	Object	Year	Observers or references*	ID [†]
3.1	KV And	2015	DPV, RPc, Rui	
3.2	EG Aqr	2015	Aka, Kis	
3.3	NN Cam	2015	DPV, NKa, Aka, Trt	
3.5	V452 Cas	2016	RPc, IMi, Trt	
3.6	V1040 Cen	2015	HaC	
3.4	PU CMa	2016	GBo, Aka, Kis, SPE	
3.7	AL Com	2015	Kimura et al. (2016a)	
3.8	VW CrB	2015	Kis, Dub	
3.9	V550 Cyg	2015	Mdy	
–	V1006 Cyg	2015	Kato et al. (2016b)	
3.10	V1028 Cyg	2016	Aka, RPc, Trt	
3.11	V1113 Cyg	2015	Trt, Ter, Kai, Shu, COO, DPV, IMi, Kis, Rui	
3.12	HO Del	2015	Trt	
3.13	AQ Eri	2016	Aka, Kis, Mdy, AAVSO	
3.14	AX For	2015	HaC, Aka	
3.15	V844 Her	2015	OKU, DPV, IMi	
3.17	RZ Leo	2016	Kis, deM, HaC, Aka, AAVSO, CRI, Mdy, IMi, SWI, DKS, SRI, SGE, Trt, RPc	
3.16	MM Hya	2015	COO	
3.18	V585 Lyr	2015	RPc, DPV, OKU	
3.19	V2051 Oph	2015	HaC, Kis, Aka	

*Key to observers: Aka (H. Akazawa, OUS), Ant (S. Antipin and A. Zubareva team), COO (L. Cook), CRI (Crimean Astrophys. Obs.), Deb (B. Debski), deM (E. de Miguel), DKS[‡](S. Dvorak), DPV (P. Dubovsky), Dub (F. Dubois team), GBo (G. Bolt), GFB[‡](W. Goff), HMB (F.-J. Hamsch), HaC (F.-J. Hamsch, remote obs. in Chile), Han (Hankasalmi Obs., by A. Oksanen), IMi[‡](I. Miller), Ioh (H. Itoh), JSh[‡](J. Shears), KU (Kyoto U., campus obs.), Kai (K. Kasai), Kis (S. Kiyota), Les (Lesniki Obs.), MLF (B. Monard), Mdy (Y. Maeda), NKa (N. Katysheva and S. Shugarov), OKU (Osaya Kyoiku U.), OUS (Okayama U. of Science), RIT (M. Richmond), RPc[‡](R. Pickard), Rui (J. Ruiz), SGE[‡](G. Stone), SPE[‡](P. Starr), SRI[‡](R. Sabo), SWI[‡](W. Stein), Shu (S. Shugarov team), Ter (Terskol Obs.), Trt (T. Tordai), Van (T. Vanmunster), Vol (I. Voloshina), AAVSO (AAVSO database)

[†]Original identifications, discoverers or data source.

[‡]Inclusive of observations from the AAVSO database.

3.3 NN Camelopardalis

NN Cam = NSV 1485 was recognized as a dwarf nova by Khruslov (2005). For more history, see Kato et al. (2015a). The 2015 superoutburst was detected visually on August 11 by P. Dubovsky (vsnet-alert 18965). Although there were possible low-amplitude superhump-like modulations already on the next night (vsnet-alert 18972), we could not determine the period. On August 13, the superhumps were already stage B (vsnet-alert 18977, 18984). The times of superhump maxima are listed in table 6. The maxima for $E \geq 133$ refer to rapidly fading part of the superoutburst. The $O - C$ behavior was similar to that of past superoutbursts (figure 4). There was no indication of a phase jump as expected for traditional late superhumps.

3.4 PU Canis Majoris

This object was originally selected as an ROSAT source (RX J0640–24 = 1RXS J064047.8–242305: Voges et al. 1999). The object was classified as a dwarf nova based on the detection at mag 11 on one ESO B plate (cf. Downes et al. 1997). The dwarf nova-type nature was established by monitoring by P. Schmeer with a CCD attached to the 50-cm reflector at the Iowa Robotic Observatory. The object underwent an outburst in 2000 January and February. The rapid fading recorded in the 2000 January outburst suggested a normal outburst in an SU UMa-type dwarf nova (Kato et al. 2003b). Thorstensen, Fenton (2003) obtained an orbital period of 0.05669(4) d by a radial-velocity study. Using the data during superoutbursts in 2003, 2005 and 2008, Kato et al. (2009) established the superhump

Table 1. List of Superoutbursts (continued).

Subsection	Object	Year	Observers or references*	ID [†]
3.20	V368 Peg	2015	Trt	
3.21	V650 Peg	2015	HaC, Shu, Mdy, Aka, Kai, Trt, Ioh	
3.24	TY Psc	2015	Trt, Deb, Kis	
3.22	PU Per	2015	KU, Mdy, Vol, IMi, Kis	
3.22	QY Per	2015	Trt, Shu	
3.25	V493 Ser	2015	DPV, HaC, IMi	
3.26	V1212 Tau	2016	Mdy	
3.27	KK Tel	2015	HaC, SPE	
3.28	CI UMa	2016	SGE, Trt	
3.29	KS UMa	2015	Kis, Ioh, AAVSO, Aka, Kai	
3.30	MR UMa	2015	DPV	
3.31	NSV 2026	2015	AAVSO, IMi	
		2016	JSh, RPc, IMi, KU, Dub, AAVSO	
3.32	ASASSN-13ah	2016	Van, IMi	
3.33	ASASSN-13ak	2015	deM, KU, RPc, IMi	
3.34	ASASSN-13az	2016	Van	
3.35	ASASSN-14ca	2015	IMi	
–	ASASSN-14cc	2014	Kato et al. (2015b)	
3.36	ASASSN-14dh	2015	HaC, Mdy, Ioh	
3.37	ASASSN-14fz	2015	HaC	
3.38	ASASSN-14le	2014	KU	
3.39	ASASSN-15cl	2016	Kis, HaC, Ioh	
3.40	ASASSN-15cy	2015	MLF, HaC, deM, Kis	
3.41	ASASSN-15dh	2015	Van, SWI	
3.42	ASASSN-15dp	2015	DPV, Van, Trt, IMi, SWI	
3.43	ASASSN-15dr	2015	HaC, MLF	
3.44	ASASSN-15ea	2015	deM, Van	
3.45	ASASSN-15ee	2015	MLF, HaC, SPE	
3.46	ASASSN-15eh	2015	MLF	
3.47	ASASSN-15ev	2015	MLF, HaC	
3.48	ASASSN-15fo	2015	MLF, HaC	
3.49	ASASSN-15fu	2015	MLF, HaC	
3.50	ASASSN-15gf	2015	Van, Kai	

Table 1. List of Superoutbursts (continued).

Subsection	Object	Year	Observers or references*	ID [†]
3.51	ASASSN-15gh	2015	HaC, MLF	
3.52	ASASSN-15gi	2015	MLF, HaC	
3.53	ASASSN-15gn	2015	MLF, HaC, COO	
3.54	ASASSN-15gq	2015	Van, IMi, COO	
3.55	ASASSN-15gs	2015	MLF	
3.56	ASASSN-15hd	2015	Van, OKU, RIT, DPV, IMi, Kai, Ioh, deM, CRI, Trt, GFB, HMB, SRI, COO, DKS, HaC	
3.57	ASASSN-15hl	2015	MLF	
3.58	ASASSN-15hm	2015	HaC, Kis, COO	
3.59	ASASSN-15hn	2015	MLF, HaC, Ioh, COO, Kis, KU, deM	
3.60	ASASSN-15ia	2015	HaC	
3.61	ASASSN-15ie	2015	HaC	
3.62	ASASSN-15iv	2015	HaC	
3.63	ASASSN-15iz	2015	HaC	
–	ASASSN-15jd	2015	Kimura et al. (2016b)	
3.64	ASASSN-15jj	2015	HaC, MLF	
3.65	ASASSN-15kf	2015	MLF, HaC	
3.66	ASASSN-15kh	2015	MLF, HaC, SPE	
3.67	ASASSN-15le	2015	Van, HaC	
3.68	ASASSN-15lt	2015	HaC, SPE	
3.69	ASASSN-15mb	2015	HaC	
3.70	ASASSN-15mt	2015	Kis, Shu, Ant, Ioh, COO, IMi	
3.71	ASASSN-15na	2015	MLF, HaC	
3.72	ASASSN-15ni	2015	OKU, DPV, IMi, Van, Kis, Shu, SPE, Ioh, Trt, AAVSO	
3.73	ASASSN-15nl	2015	Shu, Van, Trt	
3.74	ASASSN-15ob	2015	CRI, HaC	
3.75	ASASSN-15oj	2015	MLF	
3.76	ASASSN-15ok	2015	MLF, HaC	

period. The 2008 superoutburst was preceded by a precursor outburst during which a long superhump period (now known as stage A) was recorded (Kato et al. 2009). The 2009 superoutburst was reported in Kato et al. (2010). Kato, Osaki (2013b) estimated the mass ratio $q=0.110(11)$ by using stage A superhumps.

The 2016 superoutburst was visually detected by T. Horie and R. Stubbings on February 29 (vsnet-alert 19543). The object showed a precursor on March 1, as in the 2008 superoutburst. Due to the 1 d gap between observations on March 1 and 2, we could not determine the period of stage A superhumps. The times of superhump maxima are listed in table 7. The evolution of the $O - C$ variation was similar to the past superoutbursts (figure 5).

3.5 V452 Cassiopeiae

V452 Cas was discovered as a dwarf nova (=S 10453) with a photographic range of 14–17.5 by Richter (1969). The SU UMa-type nature was confirmed by T. Vanmunster in 2000 (vsnet-alert 3698, 3707). Shears et al. (2009) studied this object between 2005 and 2008, and obtained supercycle lengths of 146 ± 16 d. For more history, see Kato et al. (2014a).

The 2016 superoutburst was detected on February 9 by M. Hiraga at an unfiltered CCD magnitude of 15.5 (cf. vsnet-alert 19486). This outburst was also detected by I. Miller on February 10 and subsequent observations detected superhumps (vsnet-alert 19486). The times of superhump maxima are listed in table 8. The initial part ($E < 11$) probably refers to stage A. A comparison of $O - C$ diagrams (figure 6) suggests that

Table 1. List of Superoutbursts (continued).

Subsection	Object	Year	Observers or references*	ID [†]
3.77	ASASSN-15pi	2015	Van	
–	ASASSN-15po	2015	K. Namekata et al. in preparation	
3.78	ASASSN-15pu	2015	MLF, SPE, HaC	
3.79	ASASSN-15qe	2015	KU, Mdy, Van, Ioh	
3.80	ASASSN-15ql	2015	HaC	
3.81	ASASSN-15qo	2015	IMi, Van, Ioh	
3.82	ASASSN-15qq	2015	MLF, HaC	
3.83	ASASSN-15rf	2015	HaC	
3.84	ASASSN-15rj	2015	Mdy, KU, CRI	
3.85	ASASSN-15ro	2015	Mdy	
3.86	ASASSN-15rr	2015	MLF	
3.87	ASASSN-15rs	2015	Mdy, Ioh, Trt, Kis	
3.88	ASASSN-15ry	2015	Kis, OUS, Ioh	
3.89	ASASSN-15sc	2015	Ioh, Rui, Mdy, SWI, DPV, Van, CRI, Kis, OUS, Les, Kai, IMi	
3.90	ASASSN-15sd	2015	HaC, MLF	
3.91	ASASSN-15se	2015	OKU, Van, Kis, Rui, IMi, HaC	
3.92	ASASSN-15sl	2015	Shu, Ioh, Trt, Van, IMi, CRI	
3.93	ASASSN-15sn	2015	Kai, Mdy	
3.94	ASASSN-15sp	2015	HaC	
3.95	ASASSN-15su	2015	Trt	
3.96	ASASSN-15sv	2015	Kai, Shu	
3.97	ASASSN-15ud	2015	Mdy	
3.98	ASASSN-15uj	2015	MLF, HaC, SPE	
3.99	ASASSN-15ux	2015	deM, Ioh, KU, Mdy, Van, Kis, Shu, IMi	
3.100	ASASSN-16af	2016	Mdy, Van, HaC, Ioh	
3.101	ASASSN-16ag	2016	Mdy, IMi, Van, Ioh	
3.102	ASASSN-16ao	2016	MLF	
3.103	ASASSN-16aq	2016	IMi	

V452 Cas has long-lasting stage A, which has been recently established in long- P_{orb} systems such as V1006 Cyg (Kato et al. 2016b; Kato et al. 2014a; subsection 4.4). Having a long superhumps period, V452 Cas is an excellent candidate for this class of objects. Since stage A superhumps appears to be easily observable, determination of the orbital period and the period of stage A superhumps by systematic observations will lead to an estimation of q by the stage A superhump method (Kato, Osaki 2013b).

3.6 V1040 Centauri

This object was originally selected as an X-ray source (RX J1155.4–5641: Motch et al. 1998). After monitoring since

1999, B. Monard detected an outburst on 2000 July 4 (vsnet-alert 5064). The variable star name V1040 Cen was given based on this observation (Kazarovets et al. 2003). The 2002 superoutburst was relatively well observed. Patterson et al. (2003) reported a superhump period of 0.06215(10) d and an orbital signal with a period of 0.06028(6) d. Using the available data (part of the data used in Patterson et al. 2003), Kato et al. (2009) studied the evolution of superhumps and identified a period of 0.060296(8) d during the post-superoutburst phase. This period has been listed as the orbital period in Ritter, Kolb (2003). This period, however, was not confirmed during the quiescent phase in 2008 (Kato et al. 2009). Woudt, Warner (2010) studied this object on three nights in 2008 when the object was returning to quiescence from a normal outburst. Although Woudt,

Table 1. List of Superoutbursts (continued).

Subsection	Object	Year	Observers or references*	ID [†]
3.104	ASASSN-16bh	2016	MLF, SPE, DKS, Kis, Mdy, HaC, Ioh	
3.105	ASASSN-16bi	2016	MLF, SPE, HaC	
3.106	ASASSN-16bu	2016	OKU, Ioh, Kis, IMi, Van, Mdy, deM	
3.107	ASASSN-16de	2016	Van, HaC	
3.108	CRTS J081936	2015	Kai	CRTS J081936.1+191540
3.109	CRTS J095926	2015	MLF, HaC	CRTS J095926.4–160147
3.110	CRTS J120052	2011 2016	Kato et al. (2012) OKU, HaC	CRTS J120052.9–152620
3.111	CRTS J163120	2015	RIT	CRTS J163120.9+103134
3.112	CRTS J200331	2015	HaC	CRTS J200331.3–284941
3.113	CRTS J212521	2015	Shu, Ter	CRTS J212521.8–102627
3.114	CRTS J214738	2015	Ioh	CRTS J214738.4+244554
3.115	CSS J221822	2015	Mdy, Van, Vol	CSS120812:221823+344509
3.116	DDE 26	2015	Kai, Ioh, Mdy	
3.117	IPHAS J230538	2015	CRI, IMi, Van	IPHAS J230538.39+652158.7
3.118	MASTER J003831	2016	HaC	MASTER OT J003831.10–640313.7
3.119	MASTER J073325	2016	Mdy, Van, DPV, RPc, NKa	MASTER OT J073325.52+373744.9
3.120	MASTER J120251	2015	MLF, HaC, SPE	MASTER OT J120251.56–454116.7
3.121	MASTER J131320	2016	Van, SGE	MASTER OT J131320.24+692649.1
3.122	MASTER J181523	2015	Van	MASTER OT J181523.78+692037.4
3.123	MASTER J212624	2015	Shu, Ioh	MASTER OT J212624.16+253827.2
3.124	N080829A	2015	KU, Mdy, OUS, SWI, Vol, Ioh	
3.125	OT J191443	2015	Mdy, OKU	OT J191443.6+605214
–	PM J03338+3320	2015	Kato et al. (2016a)	
3.126	SDSS J074859	2015	Mdy, RPc, Kis	SDSS J074859.55+312512.6
3.127	SDSS J145758	2015	Vol, JSh, AAVSO, Shu, IMi, SRI, Han, deM, Mdy, RPc, Ioh	SDSS J145758.21+514807.9
3.128	SDSS J164248	2016	HaC, Van	SDSS J164248.52+134751.4

Warner (2010) reported dwarf nova oscillations (DNOs) and quasi-periodic oscillations (QPOs), there was no information about the orbital variation. Longa-Peña et al. found a spectroscopic orbital period of $0.06049(10)$ d¹¹. Rutkowski et al. (2011) studied this object in 2009 in quiescence and two normal outbursts. Rutkowski et al. (2011) derived an orbital period of $0.060458(80)$ d using their photometric data.

The 2015 superoutburst was detected by R. Stubbings on April 4 at a visual magnitude of 12.0 (vsnet-outburst 18159). This observation later turned out to be a precursor outburst. The object once faded and the rising branch of the main superoutburst was recorded in April 7 at $V=13.49$ by P. Starr. The object took another 2 d to reach the maximum around $V=11.4$. Our time-resolved photometry started 1 d after this peak and imme-

diately detected superhumps (vsnet-alert 18532, 18560). The times of superhump maxima are listed in table 9. The maxima after $E=129$ are post-superoutburst superhumps. There was no phase jump around the termination of the superoutburst. A comparison of the $O-C$ diagrams (figure 7) suggests that the $O-C$ diagrams between the 2002 and 2015 do not agree if we assume that superhumps immediately started evolving around the precursor outburst. This comparison suggests that superhumps started to develop ~ 40 cycles (~ 2.5 d) following the peak of the precursor outburst. This epoch corresponds to 0.5 d before the rising phase to the main superoutburst. This observation gives a support to the suggestion that it can take a long time to fully develop stage B superhumps when the precursor occurred well before the main superoutburst and the system stayed in low state for a long time before the main superoutburst starts [see subsection 5.4 in Kato et al. (2016a); the case of CY UMa in Kato

¹¹<http://www.noao.edu/meetings/wildstars2/posters/monday/p-longa-poster.png>.

Table 2. Coordinates of objects without coordinate-based names.

Object	Right Ascension	Declination	Source*	SDSS g	GALEX NUV
ASASSN-13ah	18 ^h 32 ^m 11 ^s .37	+61°55′05″.6	IGSL	–	20.6(2)
ASASSN-13ak	17 ^h 48 ^m 27 ^s .88	+50°50′39″.7	SDSS	19.9	–
ASASSN-13az	18 ^h 42 ^m 58 ^s .18	+73°42′28″.4	ASAS-SN [†]	–	20.9(3)
ASASSN-14ca	23 ^h 53 ^m 13 ^s .22	+27°42′01″.8	SDSS [†]	20.6	–
ASASSN-14dh	21 ^h 23 ^m 25 ^s .65	–15°39′54″.3	IGSL	–	19.7(1)
ASASSN-14fz	19 ^h 00 ^m 05 ^s .25	–49°30′34″.4	IGSL	–	–
ASASSN-14le	21 ^h 43 ^m 21 ^s .84	+73°41′12″.9	SDSS	22.4	–
ASASSN-15cl	07 ^h 39 ^m 51 ^s .35	–15°41′00″.3	IGSL	–	–
ASASSN-15cy	08 ^h 11 ^m 50 ^s .53	–12°27′51″.5	Kis [†]	–	–
ASASSN-15dh	04 ^h 59 ^m 55 ^s .75	+77°11′17″.9	IGSL	–	17.44(3)
ASASSN-15dp	04 ^h 49 ^m 32 ^s .28	+36°05′14″.0	GSC2.3.2	–	–
ASASSN-15dr	11 ^h 05 ^m 49 ^s .38	–42°41′15″.9	IGSL	–	–
ASASSN-15ea	18 ^h 50 ^m 50 ^s .59	+40°44′06″.0	deM	–	–
ASASSN-15ee	06 ^h 36 ^m 17 ^s .49	–31°14′43″.6	IGSL	–	–
ASASSN-15eh	17 ^h 53 ^m 51 ^s .25	–64°17′40″.2	GSC2.3.2	–	–
ASASSN-15ev	07 ^h 38 ^m 19 ^s .36	–82°50′40″.2	IGSL	–	–
ASASSN-15fo	12 ^h 39 ^m 56 ^s .28	–47°16′23″.9	IGSL	–	–
ASASSN-15fu	11 ^h 10 ^m 46 ^s .21	–23°37′44″.2	IGSL	–	21.6(2)
ASASSN-15gf	06 ^h 10 ^m 04 ^s .01	+12°40′08″.5	IPHAS DR2	–	–
ASASSN-15gh	17 ^h 48 ^m 16 ^s .13	–57°33′16″.3	ASAS-SN	–	–
ASASSN-15gi	09 ^h 11 ^m 51 ^s .74	–77°56′33″.8	IGSL	–	–
ASASSN-15gn	15 ^h 19 ^m 29 ^s .60	–24°40′00″.7	GSC2.3.2	–	–
ASASSN-15gq	10 ^h 15 ^m 11 ^s .32	+81°24′17″.5	ASAS-SN [†]	21.6?	–
ASASSN-15gs	13 ^h 59 ^m 17 ^s .48	–37°52′42″.2	GSC2.3.2	–	–
ASASSN-15hd	17 ^h 31 ^m 25 ^s .45	+27°54′28″.5	SDSS	21.4–21.9	–
ASASSN-15hl	05 ^h 53 ^m 30 ^s .40	–48°06′23″.2	GSC2.3.2	–	–

*source of the coordinates: 2MASS (2MASS All-Sky Catalog of Point Sources; Cutri et al. 2003), ASAS-SN (ASAS-SN measurements), Gaia (Gaia measurements), GSC2.3.2 (The Guide Star Catalog, Version 2.3.2, Lasker et al. 2007), IGSL (The Initial Gaia Source List 3, Smart 2013), IPHAS DR2 (INT/WFC Photometric H α Survey, Witham et al. 2008), KIC (The Kepler Input Catalog, Kepler Mission Team 2009), SDSS (The SDSS Photometric Catalog, Release 9, Ahn et al. 2012), USNO-A2.0 (The USNO-A2.0 Catalogue, Monet et al. 1998), the others are observers' symbols (see table 1).

[†]See text for more details.

et al. (2015a) might have been similar].

The evolutionary phase of superhumps also well match between the 2002 and 2015 superoutburst by assuming that superhumps started to develop ~ 40 cycles following the peak of the precursor outburst (figure 8). Secondary maxima of superhumps are relatively prominent in this system and became stronger than the original maxima during the later course of the superoutburst. The same feature was recorded in the Kepler data of V344 Lyr, which was considered to arise from the accretion stream resulting a bright spot that sweeps around the rim of the non-axisymmetric disk (Wood et al. 2011). The maxima for $E \geq 97$ in table 9 correspond to these secondary maxima, and are excluded for obtaining the period in table 3. The interpretation in Wood et al. (2011) would suggest a high mass-transfer rate,

and indeed “traditional” late superhumps with an ~ 0.5 phase jump are seen only in systems with frequent outbursts (e.g. Kato et al. 2013a). V1040 Cen, however, lacks frequent normal outbursts which are expected for a high mass-transfer rate. The small outburst amplitude (~ 3.0 mag for superoutbursts) of this systems suggests a bright disk in quiescence, which may in turn suggest a high mass-transfer rate. Normal outbursts in this system may be somehow suppressed. The duration of superoutbursts are somewhat short for a short P_{orb} object (the duration of the plateau phase were ~ 8 d in 2015).

Table 2. Coordinates of objects without coordinate-based names (continued).

Object	Right Ascension	Declination	Source*	SDSS g	GALEX NUV
ASASSN-15hm	11 ^h 00 ^m 38 ^s .05	−11°56′46″.4	IGSL	–	21.7(3)
ASASSN-15hn	09 ^h 07 ^m 05 ^s .42	−10°42′45″.4	GSC2.3.2	–	–
ASASSN-15ia	18 ^h 10 ^m 33 ^s .83	−53°49′45″.9	IGSL	–	21.1(3)
ASASSN-15ie	20 ^h 36 ^m 44 ^s .20	−13°11′56″.5	IGSL	–	21.4(2)
ASASSN-15iv	14 ^h 36 ^m 15 ^s .50	−36°04′17″.0	IGSL	–	–
ASASSN-15iz	13 ^h 12 ^m 13 ^s .26	−42°18′00″.4	ASAS-SN	–	–
ASASSN-15jj	19 ^h 17 ^m 56 ^s .80	−56°57′58″.1	IGSL	–	–
ASASSN-15kf	15 ^h 38 ^m 38 ^s .23	−30°35′49″.4	IGSL	–	–
ASASSN-15kh	10 ^h 38 ^m 59 ^s .93	−36°54′41″.5	ASAS-SN	–	–
ASASSN-15le	18 ^h 21 ^m 13 ^s .93	+17°09′16″.2	IGSL	–	19.5(1)
ASASSN-15lt	20 ^h 03 ^m 59 ^s .59	−39°28′30″.7	IGSL	–	20.6(2)
ASASSN-15mb	02 ^h 52 ^m 48 ^s .21	−39°59′11″.3	IGSL	–	–
ASASSN-15mt	19 ^h 12 ^m 35 ^s .54	+50°34′31″.3	IGSL	–	–
ASASSN-15na	19 ^h 19 ^m 08 ^s .77	−49°45′41″.7	IGSL	–	21.0(2)
ASASSN-15ni	18 ^h 39 ^m 57 ^s .96	+22°21′18″.7	ASAS-SN	–	–
ASASSN-15nl	14 ^h 14 ^m 59 ^s .70	+38°35′47″.8	SDSS	19.3	20.1(1)
ASASSN-15ob	16 ^h 50 ^m 59 ^s .48	+01°20′06″.5	SDSS	21.1	–
ASASSN-15oj	13 ^h 45 ^m 18 ^s .90	−36°30′15″.0	IGSL	–	–
ASASSN-15ok	00 ^h 24 ^m 30 ^s .76	−66°35′52″.7	2MASS	–	20.7(2)
ASASSN-15pi	18 ^h 50 ^m 22 ^s .29	+74°56′03″.3	ASAS-SN	–	–
ASASSN-15pu	21 ^h 11 ^m 04 ^s .70	−39°56′33″.9	GSC2.3.2	–	–
ASASSN-15qe	22 ^h 53 ^m 44 ^s .43	+35°53′54″.4	GSC2.3.2	–	–
ASASSN-15ql	20 ^h 21 ^m 56 ^s .11	−85°59′09″.5	IGSL	–	–
ASASSN-15qo	18 ^h 11 ^m 22 ^s .86	+22°42′06″.7	SDSS	22.0	–
ASASSN-15qq	22 ^h 54 ^m 35 ^s .69	−36°12′27″.6	IGSL	–	21.0(2)
ASASSN-15rf	21 ^h 57 ^m 23 ^s .06	+10°49′59″.3	SDSS	20.7–20.8	21.6(2)
ASASSN-15rj	02 ^h 59 ^m 38 ^s .33	+44°57′04″.7	SDSS	21.3	–
ASASSN-15ro	01 ^h 33 ^m 07 ^s .56	+41°07′18″.6	SDSS	21.6	–
ASASSN-15rr	19 ^h 08 ^m 47 ^s .24	−58°31′06″.8	GSC2.3.2	–	–
ASASSN-15rs	04 ^h 46 ^m 33 ^s .68	+48°57′55″.6	2MASS	–	17.89(4)
ASASSN-15ry	05 ^h 28 ^m 55 ^s .66	+36°18′38″.9	IGSL	–	–

3.7 AL Comae Berenices

We provide the table of superhumps maxima during the 2015 superoutburst which was not presented in Kimura et al. (2016a) as a form of table 10. The maxima for $E \leq 20$ were not included in Kimura et al. (2016a) and some maxima with poor statistics have been removed. The resultant updated P_{dot} was $+1.6(0.8) \times 10^{-5}$. The main conclusions in Kimura et al. (2016a) are unchanged.

A comparison of $O - C$ diagrams between different superoutbursts is shown in figure 9. In order to match the other $O - C$ diagrams, the 2015 one had to be shifted by 60 cycles. This implies that stage A superhumps started to appear ~ 3 d before the initial superhump observation on BJD 2457087 (2015 March 6). Since the object was detected on the rise on March 4, superhumps should have already started to appear when the object

was on the rise to the superoutburst maximum. This is consistent with the lack of stage A superhumps in Kimura et al. (2016a), in which the earliest part of the superoutburst was not well observed.

3.8 VW Coronae Borealis

VW CrB was discovered as a dwarf nova (Antipin Var 21) by Antipin (1996a). The observations by Antipin (1996a) indicated the presence of two types of outbursts, which was already suggestive of an SU UMa-type dwarf nova. During the 1997 superoutburst, Novák (1997) observed this object on one night and detected superhumps. Liu et al. (1999) obtained a spectrum in outburst ($B=15.8$). This observation was made approximately one month after the superoutburst observed in Novák (1997), and was likely a normal outburst. Nogami et al. (2004) reported

Table 2. Coordinates of objects without coordinate-based names (continued).

Object	Right Ascension	Declination	Source*	SDSS g	GALEX NUV
ASASSN-15sc	02 ^h 21 ^m 11 ^s .94	+60°19′49″.2	ASAS-SN [†]	–	–
ASASSN-15sd	23 ^h 18 ^m 33 ^s .27	–35°37′22″.7	IGSL	–	18.75(5)
ASASSN-15se	09 ^h 33 ^m 09 ^s .37	+10°28′02″.1	SDSS	20.5–20.6	–
ASASSN-15sl	07 ^h 23 ^m 12 ^s .73	+50°50′07″.7	IGSL	–	21.6(4)
ASASSN-15sn	20 ^h 04 ^m 23 ^s .09	+44°20′30″.2	KIC	–	–
ASASSN-15sp	07 ^h 58 ^m 08 ^s .47	–57°22′41″.9	IGSL	–	–
ASASSN-15su	05 ^h 05 ^m 03 ^s .08	+22°25′30″.3	IGSL	–	–
ASASSN-15sv	00 ^h 39 ^m 00 ^s .55	+27°13′45″.6	SDSS	22.1–22.6	–
ASASSN-15ud	08 ^h 52 ^m 28 ^s .59	–08°44′11″.4	GSC2.3.2	–	–
ASASSN-15uj	04 ^h 36 ^m 21 ^s .63	–55°25′07″.4	IGSL	–	–
ASASSN-15ux	06 ^h 52 ^m 26 ^s .66	+47°10′56″.5	ASAS-SN	–	–
ASASSN-16af	09 ^h 06 ^m 06 ^s .44	+00°04′34″.7	SDSS	21.1–21.9	–
ASASSN-16ag	01 ^h 34 ^m 38 ^s .24	+52°06′16″.5	SDSS	19.7	21.0(3)
ASASSN-16ao	04 ^h 40 ^m 47 ^s .12	–58°07′28″.5	GSC2.3.2	–	21.8(3)
ASASSN-16aq	16 ^h 55 ^m 25 ^s .06	+37°21′36″.8	SDSS	22.2	22.1(4)
ASASSN-16bh	13 ^h 24 ^m 57 ^s .23	–27°56′10″.6	GSC2.3.2	–	21.5(4)
ASASSN-16bi	07 ^h 46 ^m 22 ^s .50	–77°47′16″.7	Gaia	–	–
ASASSN-16bu	07 ^h 27 ^m 31 ^s .65	+33°46′35″.1	SDSS	22.1	22.8(5)
ASASSN-16de	18 ^h 42 ^m 34 ^s .00	+17°41′22″.7	USNO-A2.0	–	–
DDE 26	22 ^h 03 ^m 28 ^s .22	+30°56′36″.4	SDSS	19.6	–
N080829A	21 ^h 42 ^m 54 ^s .30	+15°36′42″.3	SDSS	22.6	–

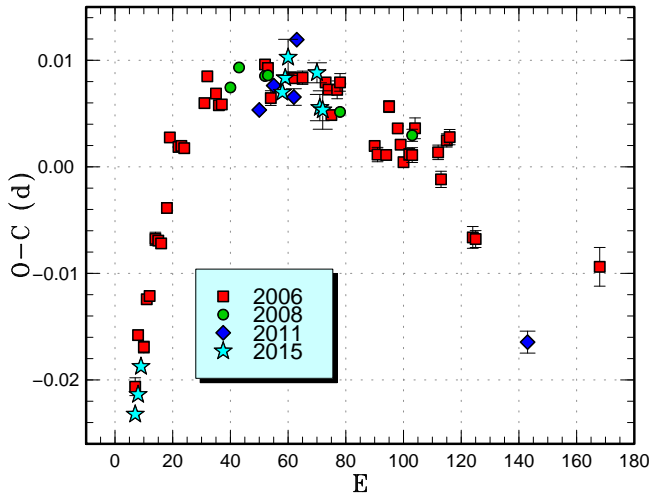
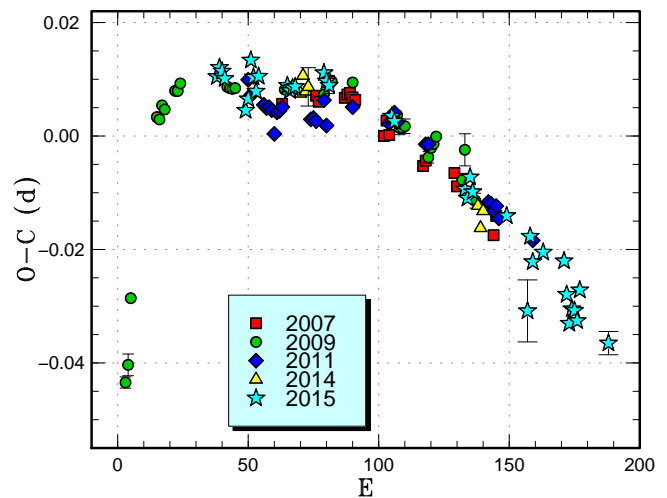
**Fig. 3.** Comparison of $O - C$ diagrams of EG Aqr between different superoutbursts. A period of 0.07885 d was used to draw this figure. Approximate cycle counts (E) after the start of the superoutburst were used. Since the starts of the 2008, 2011 and 2015 superoutbursts were not well constrained, we shifted the $O - C$ diagrams to best fit the best-recorded 2006 one.**Fig. 4.** Comparison of $O - C$ diagrams of NN Cam between different superoutbursts. A period of 0.07425 d was used to draw this figure. Approximate cycle counts (E) after the start of the superoutburst were used.

Table 3. Superhump Periods and Period Derivatives

Object	Year	P_1 (d)*	err	E_1 †	$P_{\dot{\text{dot}}}$ ‡	err‡	P_2 (d)*	err	E_2 †	P_{orb} (d)§	Q		
KV And	2015	0.074283	0.000011	15	56	0.0	2.6	0.074108	0.000054	66	96	–	B
EG Aqr	2015	0.078688	0.000122	51	65	–	–	–	–	–	–	–	C
NN Cam	2015	0.074226	0.000037	0	43	11.6	7.8	0.073768	0.000035	67	150	0.0717	B
V452 Cas	2016	0.088828	0.000088	11	57	–	–	–	–	–	–	–	C
V1040 Cen	2015	0.062244	0.000024	0	67	–	–	–	–	–	0.06049	–	CG2
PU CMa	2016	0.057968	0.000018	0	107	6.9	1.7	–	–	–	0.056694	–	B
AL Com	2015	0.057293	0.000010	0	128	1.6	0.8	–	–	–	0.056669	–	B
VW CrB	2015	0.072820	0.000038	0	112	3.6	3.1	–	–	–	–	–	C
V1006 Cyg	2015	0.105407	0.000044	36	94	20.8	2.0	0.104437	0.000050	102	200	0.09903	B
V1028 Cyg	2016	0.062009	0.000055	0	58	11.8	8.3	–	–	–	–	–	C
V1113 Cyg	2015	0.078937	0.000018	0	107	–4.3	1.3	–	–	–	–	–	BG
HO Del	2015	0.064326	0.000018	0	33	–	–	–	–	–	0.06266	–	C
AQ Eri	2016	0.062432	0.000030	0	83	10.8	2.5	–	–	–	0.06094	–	C
AX For	2015	–	–	–	–	–	–	0.081041	0.000073	0	26	–	C
V844 Her	2015	0.055902	0.000025	32	120	10.4	2.6	0.055819	0.000047	174	228	0.054643	C
RZ Leo	2016	0.078675	0.000035	0	48	15.6	5.9	0.078229	0.000022	53	138	0.076030	A
V585 Lyr	2015	0.060360	0.000018	11	84	9.9	2.4	–	–	–	–	–	C
V2051 Oph	2015	0.064708	0.000088	0	16	–	–	0.064144	0.000044	40	72	0.062428	Ce
V650 Peg	2015	0.069777	0.000020	0	125	6.7	0.9	0.069271	0.000029	135	210	–	C

* P_1 and P_2 are mean periods of stage B and C superhumps, respectively.

† Interval used for calculating the period (corresponding to E in the individual tables in section 3).

‡ $P_{\dot{\text{dot}}} = \dot{P}/P$ for stage B superhumps, unit 10^{-5} .

§ References: NN Cam (Denisenko, D. 2007, vsnet-alert 9557), V1040 Cen (Longa-Peña et al., see text), PU CMa (Thorstensen, Fenton 2003), AL Com (Kato et al. 2014a), V1006 Cyg (Sheets et al. 2007), HO Del (Patterson et al. 2003), AQ Eri (Thorstensen et al. 1996), V844 Her (Thorstensen et al. 2002), RZ Leo (Dai et al. 2016; improved by this work), V2051 Oph (this work), TY Psc (Thorstensen et al. 1996), V493 Ser (Kato et al. 2009), KS UMa (Patterson et al. 2003), PM J03338 (Skinner et al. 2014), SDSS J145758 (Uthas 2011), ASASSN-15gq, ASASSN-15hd, ASASSN-15na, ASASSN-15ni, ASASSN-15pu, ASASSN-15sc, ASASSN-15uj, ASASSN-15ux, ASASSN-16bh, ASASSN-16bi, ASASSN-16bu, CRTS J095926, CRTS J200331 (this work), ASASSN-15po (K. Namekata et al. in preparation)

|| Data quality and comments. A: excellent, B: partial coverage or slightly low quality, C: insufficient coverage or observations with large scatter, G: $P_{\dot{\text{dot}}}$ denotes global $P_{\dot{\text{dot}}}$, M: observational gap in middle stage, U: uncertainty in alias selection, 2: late-stage coverage, the listed period may refer to P_2 , E: P_{orb} refers to the period of early superhumps, e: eclipsing system.

observations of two superoutbursts in 2001 and 2003, and detected a positive $P_{\dot{\text{dot}}}$ despite the relatively long superhump period. These observations and the 2006 superoutburst were analyzed in Kato et al. (2009).

The 2015 superoutburst was detected by D. Denisenko using the MASTER network (vsnet-alert 18577). Subsequent observations detected superhumps (vsnet-alert 18583). The times of superhump maxima are listed in table 11. A comparison of $O - C$ diagrams between different superoutbursts is shown in figure 10. The 2015 observation most likely covered stage B.

3.9 V550 Cygni

V550 Cyg was discovered by Hoffmeister (1949) as a dwarf nova (=S 3847) with a photographic range of 15 to fainter than

18 mag. Ahnert-Rohlfs (1952) reported a photographic range of 14.8 to fainter than 16.3. Although the finding chart was provided by Hoffmeister (1957) (Nr. 291), the scale was insufficient to identify the object in quiescence. Pinto, Romano (1972) recorded an outburst at a photographic magnitude of 14.2 on 1961 September 20. Skiff (1999) was the first to identify the object in 1999 and two outbursts were detected in 2000 (vsnet-alert 3993, 5191). During the 2000 August outburst, superhumps were detected (Kato et al. 2009).

The 2015 outburst was detected by E. Muyliaert on October 11 at an unfiltered CCD magnitude of 15.12 (cf. vsnet-alert 19156). Only single-night observations (vsnet-alert 19173) yielded two superhumps maxima: BJD 2457313.0659(5) ($N=137$) and 2457313.1256(18) ($N=87$).

Table 3. Superhump Periods and Period Derivatives (continued)

Object	Year	P_1	err	E_1	P_{dot}	err	P_2	err	E_2	P_{orb}	Q		
PU Per	2015	–	–	–	–	–	0.067975	0.000020	0	51	–	C	
QY Per	2015	0.078593	0.000032	0	40	14.7	2.8	–	–	–	–	C	
TY Psc	2015	0.070093	0.000330	0	10	–	–	–	–	–	0.068348	C	
V493 Ser	2015	0.082793	0.000062	39	76	–	–	0.082576	0.000033	87	173	0.08001	B
KK Tel	2015	0.087606	0.000023	42	136	0.8	1.9	–	–	–	–	–	B
CI UMa	2016	0.063283	0.000354	0	5	–	–	–	–	–	–	–	C
KS UMa	2015	0.069948	0.000058	0	19	–	–	0.069763	0.000086	75	93	0.06796	C
NSV 2026	2015	0.069829	0.000015	0	102	0.4	1.5	–	–	–	–	–	CG
NSV 2026	2016	0.069795	0.000013	0	130	–0.4	1.1	–	–	–	–	–	CG
ASASSN-13ah	2016	0.066141	0.000013	0	33	–	–	–	–	–	–	–	C
ASASSN-13ak	2015	0.086655	0.000040	0	34	–	–	–	–	–	–	–	C
ASASSN-14cc	2014	0.015610	0.000010	–	–	–	–	–	–	–	–	–	C
ASASSN-14dh	2015	–	–	–	–	–	–	0.073629	0.000031	0	91	–	C
ASASSN-14fz	2015	0.078028	0.000030	13	103	–2.9	3.0	–	–	–	–	–	CG
ASASSN-15cl	2016	0.094633	0.000104	22	33	–	–	0.093907	0.000071	43	96	–	B
ASASSN-15cy	2015	0.049955	0.000009	0	122	3.4	1.2	–	–	–	–	–	C
ASASSN-15dh	2015	0.088014	0.000087	0	19	–103.2	14.1	–	–	–	–	–	CG
ASASSN-15dp	2015	0.060005	0.000015	49	200	0.4	1.1	–	–	–	–	–	B
ASASSN-15dr	2015	0.056387	0.000045	25	80	–	–	–	–	–	–	–	C
ASASSN-15ea	2015	0.095225	0.000034	–	–	–	–	–	–	–	–	–	CU
ASASSN-15ee	2015	0.057136	0.000018	15	120	8.1	1.2	–	–	–	–	–	B
ASASSN-15eh	2015	0.085665	0.000033	0	60	–10.3	2.4	–	–	–	–	–	CG
ASASSN-15ev	2015	0.058015	0.000041	0	20	–	–	–	–	–	–	–	C
ASASSN-15fo	2015	0.0630	0.0030	0	4	–	–	–	–	–	–	–	C
ASASSN-15fu	2015	0.074770	0.000062	0	44	–	–	0.074001	0.000228	43	71	–	C
ASASSN-15gf	2015	0.06690	0.00012	0	15	–	–	–	–	–	–	–	CU
ASASSN-15gh	2015	0.05905	0.00030	0	68	–	–	–	–	–	–	–	CU
ASASSN-15gi	2015	0.061270	0.000050	0	66	15.5	8.1	0.060928	0.000038	64	130	–	C
ASASSN-15gn	2015	0.063641	0.000033	18	112	–3.2	3.8	–	–	–	–	–	C
ASASSN-15gq	2015	0.066726	0.000034	15	120	11.9	0.8	–	–	–	–	0.06490	BE
ASASSN-15hd	2015	0.056105	0.000007	22	273	1.5	0.3	–	–	–	–	0.05541	BE
ASASSN-15hl	2015	0.067947	0.000035	0	89	–5.9	3.6	–	–	–	–	–	CG

3.10 V1028 Cygni

V1028 Cyg was discovered as a dwarf nova (=S 7854) by Hoffmeister (1963a). The object has been famous for the low frequency of outbursts (see e.g. Mayall 1968; Mayall 1970). Early observations (Tchäpe 1963) were already indicative of an SU UMa-type dwarf nova. Bruch, Schimpke (1992) reported a typical dwarf nova-type spectrum in quiescence. The 1995 superoutburst was the best recorded (cf. vsnet-alert 166, 168, 169, 172, 175, 177, 192, 193, 205). This superoutburst was one of the first examples showing positive P_{dot} , although the publication took some time (Baba et al. 2000). Other superoutburst (not well observed) in 1996, 1999, 2001, 2002, 2004 and 2008 were reported in Kato et al. (2009).

The 2016 outburst was detected on March 14 probably on

the rising phase ($V=14.8$) by the ASAS-SN team and M. Hiraga (vsnet-alert 19601). Since the initial detection magnitude was faint, the outburst did not receive attention. The initial time-resolved photometry started on March 18 when the superoutburst state was confirmed. Superhumps were soon recorded (vsnet-alert 19632). The times of superhump maxima are listed in table 12. The $O - C$ analysis (figure 11) clearly indicates that the present observation recorded the later part of stage B and stage C. The period of stage C superhumps was not determined due to the lack of data. In figure 11, we had to shift 90 cycles to match the $O - C$ curve to the 1995 one, although initial superhump observations started ~ 60 cycles after the outburst detection. It may have been that the 2016 superoutburst was shorter than other ones, or it had a separate precursor during which superhumps already started to develop.

Table 3. Superhump Periods and Period Derivatives (continued)

Object	Year	P_1	err	E_1	$P_{\dot{d}ot}$	err	P_2	err	E_2	P_{orb}	Q		
ASASSN-15hm	2015	0.056165	0.000031	34	159	5.4	2.0	–	–	–	–	C	
ASASSN-15hn	2015	0.061831	0.000018	32	178	–0.5	1.5	–	–	–	–	B	
ASASSN-15ia	2015	0.070281	0.000072	0	29	–	–	0.069882	0.000059	28	72	–	C
ASASSN-15ie	2015	0.058616	0.000022	35	224	4.0	0.9	–	–	–	–	–	C
ASASSN-15iv	2015	0.067435	0.000051	0	89	17.4	2.9	0.067099	0.000068	87	149	–	C
ASASSN-15iz	2015	0.081434	0.000049	0	61	–	–	–	–	–	–	–	CU
ASASSN-15jd	2015	0.064981	0.000008	24	90	9.9	4.2	–	–	–	–	–	C
ASASSN-15jj	2015	0.062388	0.000025	0	146	8.1	0.6	0.062124	0.000067	161	209	–	B
ASASSN-15kf	2015	0.019251	0.000097	0	3	–	–	–	–	–	–	–	C
ASASSN-15kh	2015	0.060480	0.000017	43	175	1.2	1.6	–	–	–	–	–	B
ASASSN-15le	2015	0.078000	0.000053	0	43	–	–	–	–	–	–	–	CU
ASASSN-15lt	2015	0.059815	0.000024	49	189	–	–	0.059633	0.000053	188	266	–	CM
ASASSN-15mb	2015	–	–	–	–	–	–	0.068838	0.000056	43	203	–	CU
ASASSN-15mt	2015	0.076342	0.000020	0	31	–	–	0.076032	0.000041	42	97	–	B
ASASSN-15na	2015	0.063720	0.000027	0	111	3.1	2.6	–	–	–	–	0.06297	CE
ASASSN-15ni	2015	0.055854	0.000009	32	205	3.4	0.6	–	–	–	–	0.05517	BE
ASASSN-15nl	2015	0.060095	0.000098	0	33	–	–	–	–	–	–	–	C
ASASSN-15ob	2015	0.060525	0.000060	0	83	15.1	2.8	–	–	–	–	–	C
ASASSN-15ok	2015	0.078931	0.000122	0	25	–	–	0.078476	0.000022	25	115	–	C
ASASSN-15pi	2015	0.078307	0.000300	0	4	–	–	–	–	–	–	–	C
ASASSN-15po	2015	0.050916	0.000002	49	329	1.1	0.1	–	–	–	–	0.050457	AE
ASASSN-15pu	2015	0.058254	0.000024	34	146	3.3	2.1	–	–	–	–	0.05757	BE
ASASSN-15qe	2015	0.061092	0.000017	0	62	–	–	–	–	–	–	–	C
ASASSN-15qq	2015	0.077131	0.000026	0	81	–1.0	2.6	–	–	–	–	–	CG2
ASASSN-15rj	2015	0.092463	0.000164	0	15	–	–	–	–	–	–	–	C
ASASSN-15ro	2015	0.072909	0.000088	0	29	–	–	–	–	–	–	–	C
ASASSN-15rr	2015	0.054938	0.000039	0	75	–	–	–	–	–	–	–	CU
ASASSN-15rs	2015	0.097854	0.000207	0	22	–	–	–	–	–	–	–	C
ASASSN-15ry	2015	0.060876	0.000270	0	3	–	–	–	–	–	–	–	C
ASASSN-15sc	2015	0.057735	0.000015	21	208	5.8	0.3	–	–	–	–	–	A
ASASSN-15sd	2015	–	–	–	–	–	–	0.068894	0.000028	0	93	–	C
ASASSN-15se	2015	0.063312	0.000042	10	58	–	–	–	–	–	–	–	C

3.11 V1113 Cygni

V1113 Cyg was discovered as a dwarf nova (=S 9382) by Hoffmeister (1966). Kato et al. (1996b) reported the detection of superhumps. Kato (2001b) reported a mean supercycle of 189.8 d and that the number of normal outbursts is too small for this short supercycle. Bakowska et al. (2010) studied the 2003 and 2005 superoutbursts, and also confirmed the low frequency of normal outbursts. Although Bakowska et al. (2010) reported large negative $P_{\dot{d}ot}$, they probably recorded stage B-C transition (Kato et al. 2010).

The 2015 superoutburst was detected by the ASAS-SN team on August 28 at $V=13.95$ (cf. vsnet-alert 19014). Subsequent observations detected superhumps (vsnet-alert 19018, 19019, 19023). The times of superhump maxima are listed in table 13.

The stages are not distinct (see also figure 12) and we adopted a globally averaged period except the rapidly fading part in table 3.

3.12 HO Delphini

HO Del (=S 10066) was discovered as a dwarf nova by Hoffmeister (1967). Hoffmeister (1967) recorded two outbursts in 1963 October and 1966 September. The coordinates of this object was wrongly given in Hoffmeister (1967) and it was only corrected in the third volume of the fourth edition of the GCVS (Kholopov et al. 1985) (the correct identification was found by T.K. in 1990 while preparing charts by comparison with the Palomar Sky Survey; the observations since 1990 by the VSOLJ members referred to the correct object). Munari, Zwitter (1998)

Table 3. Superhump Periods and Period Derivatives (continued)

Object	Year	P_1	err	E_1	P_{dot}	err	P_2	err	E_2	P_{orb}	Q
ASASSN-15sl	2015	0.091065	0.000066	0	97	9.1	2.6	–	–	0.087048	CGe
ASASSN-15sn	2015	0.064684	0.000090	0	48	–50.5	11.5	–	–	–	C
ASASSN-15sp	2015	0.058366	0.000018	33	138	7.7	0.9	0.058292	0.000040	–	B
ASASSN-15ud	2015	0.05649	0.00023	0	3	–	–	–	–	–	C
ASASSN-15uj	2015	0.055805	0.000012	35	129	–1.1	1.6	–	–	0.055266	BE
ASASSN-15ux	2015	0.056857	0.000012	73	131	–	–	–	–	0.056109	Ce
ASASSN-16af	2016	0.064204	0.000025	0	75	13.0	2.8	–	–	–	B
ASASSN-16ag	2016	0.058479	0.000071	0	96	–	–	–	–	–	C
ASASSN-16bh	2016	0.054027	0.000006	32	206	3.7	0.3	–	–	0.05346	AE
ASASSN-16bu	2016	0.060513	0.000071	42	82	–	–	–	–	0.05934	BE
CRTS J095926	2015	0.089428	0.000041	10	67	–4.4	5.0	–	–	–	C
CRTS J120052	2016	0.088950	0.000038	0	85	–5.5	3.2	–	–	–	CG2
CRTS J163120	2015	0.0645	0.0005	0	3	–	–	–	–	–	C
CRTS J200331	2015	0.059720	0.000088	49	84	–	–	–	–	0.058705	Ce
CRTS J212521	2015	0.079090	0.000119	0	26	–	–	–	–	–	C
CSS J221822	2015	0.069294	0.000035	0	50	–	–	–	–	–	C
DDE 26	2015	0.088617	0.000042	0	49	10.3	2.5	–	–	–	C
IPHAS J230538	2015	0.072772	0.000017	15	83	4.6	2.4	0.072493	0.000060	82 125	C
MASTER J003831	2016	0.061605	0.000038	0	114	11.5	0.9	0.061310	0.000038	114 179	B
MASTER J073325	2016	0.061218	0.000027	32	162	5.5	1.1	–	–	–	C
MASTER J120251	2015	0.063372	0.000018	0	131	–1.7	3.1	–	–	–	CGM
MASTER J131320	2016	0.069709	0.000044	0	34	–	–	–	–	–	CU
MASTER J181523	2015	0.058512	0.000056	0	20	–	–	–	–	–	C
MASTER J212624	2015	0.091193	0.000148	0	31	–	–	–	–	–	C
N 080829A	2015	0.064282	0.000027	0	100	11.4	2.4	–	–	–	B
PM J03338	2015	0.069013	0.000021	70	115	–12.7	4.7	0.068629	0.000020	115 246	A
SDSS J074859	2015	0.05958	0.00030	–	–	–	–	–	–	0.058311	Ce
SDSS J145758	2015	0.054912	0.000018	0	128	2.2	2.9	–	–	0.054087	C
SDSS J164248	2016	0.079327	0.000093	0	54	–	–	–	–	–	CG

confirmed the dwarf nova-type nature by recording relatively strong Balmer and HeI emission lines. Observations of superhumps during the 1994, 1996 and 2001 superoutbursts were analyzed in Kato et al. (2003a). Patterson et al. (2003) also reported the 1996 superoutburst and the spectroscopic orbital period. In Kato et al. (2003a), HO Del was chosen as a prototypical object showing the brightening trend near the end of the plateau phase. This phenomenon was later identified as emergence of stage C superhumps (Kato et al. 2009). The 2008 superoutburst was also reported in Kato et al. (2009).

The 2015 outburst was detected by R. Stubbings and ASASSN on July 18 (vsnet-alert 18865). Superhump were detected by observations which started 2 d later (vsnet-alert 18871). The times of superhump maxima are listed in table 14. The superhump period indicates that these observations were already in stage B. A comparison of $O - C$ diagrams between different superoutbursts is shown in figure 13. It is likely that stage A is short in this system since stage B superhumps already appeared

2 d after the outburst detection despite that the outburst was detected sufficiently early at least in 2001.

3.13 AQ Eridani

AQ Eri was discovered as a dwarf nova (=AN 431.1934) by Morgenroth (1934). Hoppe (1935) studied this object using 232 plates and found it unlikely a Mira variable since it was invisible most of the time. Hoppe (1935) derived a possible period of 78 d using three observed maxima (outbursts). Petit (1960) listed the object as a U Gem-type object with a cycle length of 78 d. Bond (1978) obtained a spectrum and recorded diffuse (broad) hydrogen emission lines superposed on a blue continuum. Vogt, Bateson (1982) also listed the object as a U Gem-type variable. Kholopov et al. (1985) (printed version) listed the object as a possible Z Cam-type dwarf nova based on Bateson (1982). Photometric observations in quiescence, however, suggested a short orbital period Szkody (1987).

Table 4. Superhump maxima of KV And (2015)

E	max*	error	$O - C^\dagger$	N^\ddagger
0	57261.4236	0.0006	-0.0036	40
1	57261.4979	0.0005	-0.0035	40
2	57261.5730	0.0006	-0.0026	31
15	57262.5411	0.0010	0.0006	41
16	57262.6144	0.0012	-0.0003	45
26	57263.3568	0.0005	-0.0002	60
27	57263.4324	0.0005	0.0012	53
28	57263.5051	0.0004	-0.0003	108
29	57263.5804	0.0004	0.0008	115
30	57263.6546	0.0003	0.0007	35
40	57264.3974	0.0017	0.0013	30
41	57264.4726	0.0009	0.0023	37
42	57264.5464	0.0004	0.0019	39
53	57265.3628	0.0009	0.0018	38
54	57265.4378	0.0008	0.0025	38
55	57265.5119	0.0005	0.0025	39
56	57265.5855	0.0006	0.0019	30
66	57266.3306	0.0031	0.0047	31
67	57266.4003	0.0009	0.0002	38
68	57266.4749	0.0010	0.0005	40
69	57266.5475	0.0017	-0.0011	37
70	57266.6244	0.0037	0.0016	9
81	57267.4393	0.0032	0.0001	20
82	57267.5093	0.0014	-0.0041	37
83	57267.5844	0.0015	-0.0033	39
93	57268.3304	0.0056	0.0005	18
94	57268.4039	0.0022	-0.0003	38
95	57268.4749	0.0034	-0.0035	25
96	57268.5502	0.0034	-0.0024	24

*BJD-2400000.

 † Against max = 2457261.4271 + 0.074224*E*. ‡ Number of points used to determine the maximum.**Table 5.** Superhump maxima of EG Aqr (2015)

E	max*	error	$O - C^\dagger$	N^\ddagger
0	57257.0963	0.0007	-0.0024	137
1	57257.1770	0.0006	-0.0011	107
2	57257.2585	0.0005	0.0011	131
51	57261.1478	0.0005	0.0032	72
52	57261.2281	0.0006	0.0041	81
53	57261.3088	0.0017	0.0055	35
63	57262.0959	0.0009	-0.0007	52
64	57262.1715	0.0012	-0.0045	53
65	57262.2501	0.0018	-0.0052	42

*BJD-2400000.

 † Against max = 2457257.0987 + 0.079332*E*. ‡ Number of points used to determine the maximum.**Table 6.** Superhump maxima of NN Cam (2015)

E	max*	error	$O - C^\dagger$	N^\ddagger
0	57248.3330	0.0002	-0.0055	67
1	57248.4089	0.0002	-0.0035	76
2	57248.4825	0.0002	-0.0039	76
3	57248.5554	0.0003	-0.0049	56
11	57249.1438	0.0017	-0.0080	40
12	57249.2201	0.0011	-0.0057	65
13	57249.3012	0.0015	0.0015	79
14	57249.3725	0.0004	-0.0012	75
15	57249.4442	0.0003	-0.0034	77
16	57249.5211	0.0004	-0.0005	77
27	57250.3362	0.0004	0.0013	76
28	57250.4096	0.0003	0.0007	76
29	57250.4843	0.0005	0.0016	75
30	57250.5588	0.0004	0.0021	69
41	57251.3780	0.0005	0.0079	76
42	57251.4508	0.0005	0.0068	76
43	57251.5242	0.0005	0.0063	64
67	57253.3008	0.0009	0.0083	48
68	57253.3742	0.0006	0.0077	42
95	57255.3670	0.0013	0.0042	41
96	57255.4396	0.0007	0.0029	103
97	57255.5176	0.0009	0.0069	258
98	57255.5892	0.0015	0.0046	63
111	57256.5503	0.0005	0.0044	180
119	57257.1275	0.0055	-0.0099	27
120	57257.2149	0.0009	0.0036	54
121	57257.2847	0.0009	-0.0006	55
125	57257.5833	0.0006	0.0023	76
133	57258.1758	0.0011	0.0033	52
134	57258.2442	0.0006	-0.0023	55
135	57258.3133	0.0010	-0.0071	109
136	57258.3901	0.0006	-0.0042	139
137	57258.4641	0.0004	-0.0042	104
138	57258.5365	0.0008	-0.0057	115
139	57258.6162	0.0013	0.0000	42
150	57259.4236	0.0021	-0.0059	54

*BJD-2400000.

 † Against max = 2457248.3385 + 0.073940*E*. ‡ Number of points used to determine the maximum.

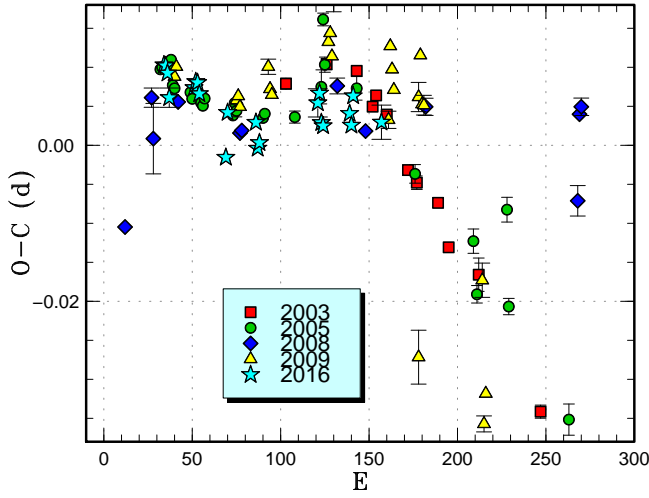


Fig. 5. Comparison of $O - C$ diagrams of PU CMa between different superoutbursts. A period of 0.05801 d was used to draw this figure. Approximate cycle counts (E) after the start of the superoutburst were used.

Table 7. Superhump maxima of PU CMa (2016)

E	max*	error	$O - C^\dagger$	N^\ddagger
0	57449.9334	0.0005	0.0032	43
1	57449.9913	0.0003	0.0031	48
2	57450.0483	0.0003	0.0022	146
3	57450.1032	0.0012	-0.0009	64
17	57450.9166	0.0008	0.0009	22
18	57450.9754	0.0001	0.0018	139
19	57451.0333	0.0002	0.0017	152
20	57451.0899	0.0005	0.0003	113
35	57451.9519	0.0010	-0.0073	10
36	57452.0156	0.0004	-0.0015	30
52	57452.9425	0.0007	-0.0021	42
53	57452.9972	0.0005	-0.0054	38
54	57453.0559	0.0010	-0.0046	41
87	57454.9754	0.0018	0.0018	43
88	57455.0346	0.0011	0.0031	102
89	57455.0889	0.0011	-0.0006	134
90	57455.1465	0.0005	-0.0010	117
105	57456.0182	0.0006	0.0012	117
106	57456.0747	0.0005	-0.0003	117
107	57456.1365	0.0008	0.0035	115
123	57457.0613	0.0022	0.0008	40

*BJD-2400000.

† Against max = 2457449.9302 + 0.057970 E .

‡ Number of points used to determine the maximum.

Table 8. Superhump maxima of V452 Cas (2016)

E	max*	error	$O - C^\dagger$	N^\ddagger
0	57429.2812	0.0013	-0.0040	60
1	57429.3731	0.0002	-0.0009	231
11	57430.2660	0.0012	0.0028	30
12	57430.3563	0.0016	0.0042	34
45	57433.2818	0.0047	-0.0044	46
46	57433.3757	0.0013	0.0006	71
56	57434.2695	0.0094	0.0053	18
57	57434.3494	0.0011	-0.0037	89

*BJD-2400000.

† Against max = 2457429.2851 + 0.088911 E .

‡ Number of points used to determine the maximum.

Table 9. Superhump maxima of V1040 Cen (2015)

E	max*	error	$O - C^\dagger$	N^\ddagger
0	57122.5102	0.0012	-0.0045	21
1	57122.5747	0.0009	-0.0022	25
2	57122.6365	0.0014	-0.0025	13
3	57122.6976	0.0011	-0.0036	16
4	57122.7589	0.0007	-0.0044	17
49	57125.5602	0.0019	0.0008	21
50	57125.6289	0.0013	0.0074	13
51	57125.6873	0.0020	0.0036	16
65	57126.5543	0.0015	0.0007	24
66	57126.6193	0.0014	0.0036	13
67	57126.6803	0.0028	0.0025	17
68	57126.7425	0.0023	0.0026	17
97	57128.5492	0.0022	0.0072	24
98	57128.6025	0.0018	-0.0016	16
99	57128.6760	0.0026	0.0098	17
100	57128.7181	0.0030	-0.0103	16
113	57129.5287	0.0025	-0.0074	25
129	57130.5355	0.0024	0.0052	24
146	57131.5855	0.0015	-0.0011	18
147	57131.6482	0.0019	-0.0006	17
148	57131.7175	0.0046	0.0066	16
149	57131.7757	0.0018	0.0027	10
177	57133.5124	0.0012	-0.0004	30
178	57133.5760	0.0012	0.0010	28
179	57133.6301	0.0015	-0.0070	15
180	57133.6927	0.0014	-0.0065	16
181	57133.7597	0.0018	-0.0017	13

*BJD-2400000.

† Against max = 2457122.5147 + 0.062136 E .

‡ Number of points used to determine the maximum.

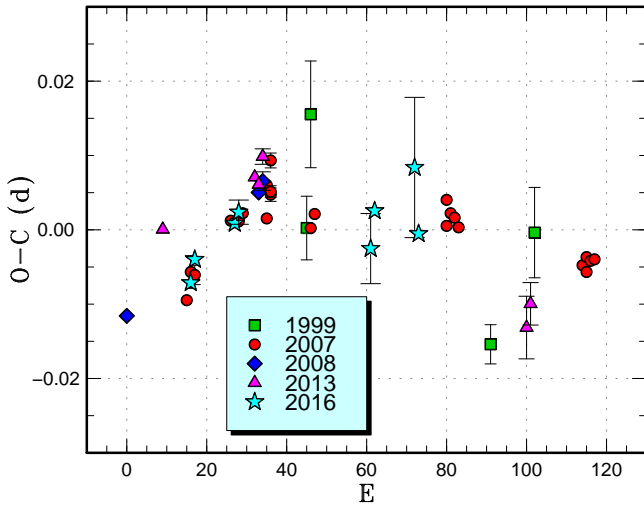


Fig. 6. Comparison of $O - C$ diagrams of V452 Cas between different superoutbursts. A period of 0.08880 d was used to draw this figure. Approximate cycle counts (E) after the start of the superoutburst were used. Since the start of the 2016 superoutburst was well observed, the 2007 $O - C$ diagram has been shifted by 15 cycles to match the 2016 one.

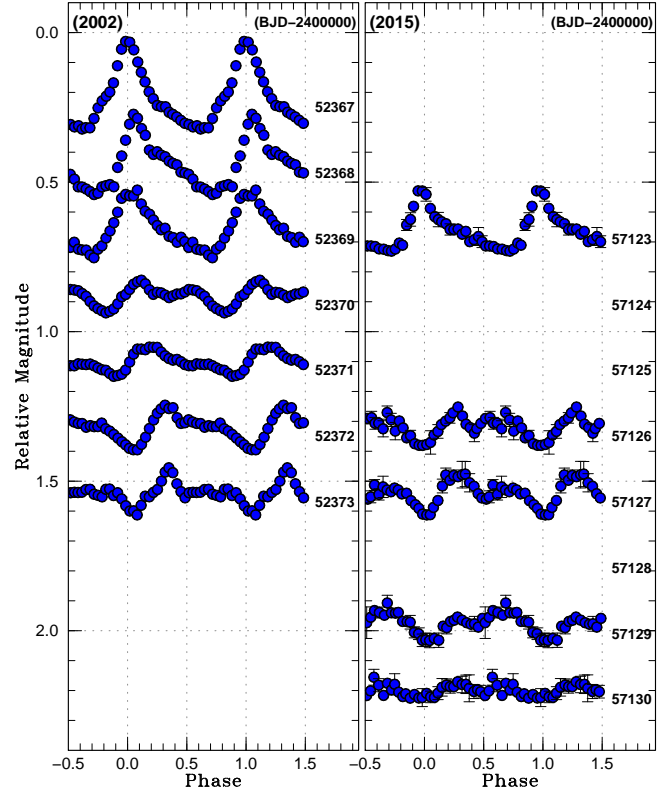


Fig. 8. Evolution of superhumps in V1040 Cen during the 2002 and 2015 superoutbursts. A period of 0.06190 d was used to draw this figure. The 2015 data were shifted by 2 d to reflect the shift in the cycle count in figure 7.

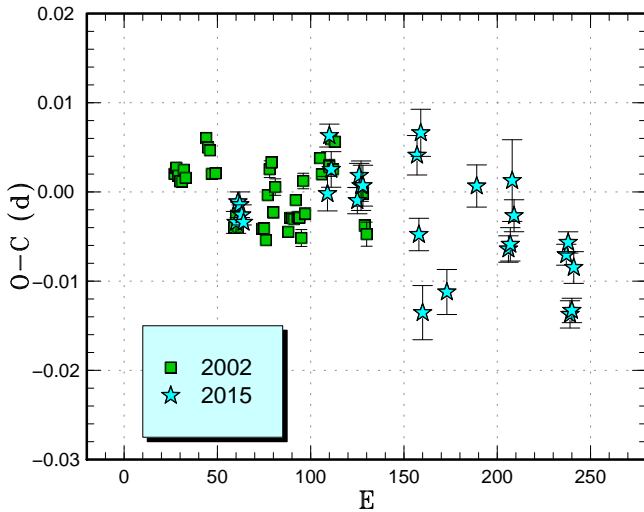


Fig. 7. Comparison of $O - C$ diagrams of V1040 Cen between different superoutbursts. A period of 0.06218 d was used to draw this figure. Approximate cycle counts (E) after the start of the superoutburst were used. Since there was a separate precursor outburst in 2015, we shifted the $O - C$ diagram so that it best matches the 2002 one. The maxima for $E > 150$ for the 2015 superoutburst probably refer to the secondary maxima (see text for details).

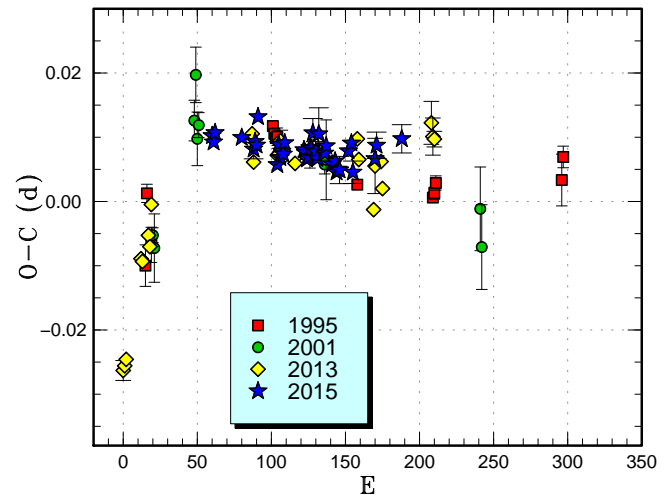
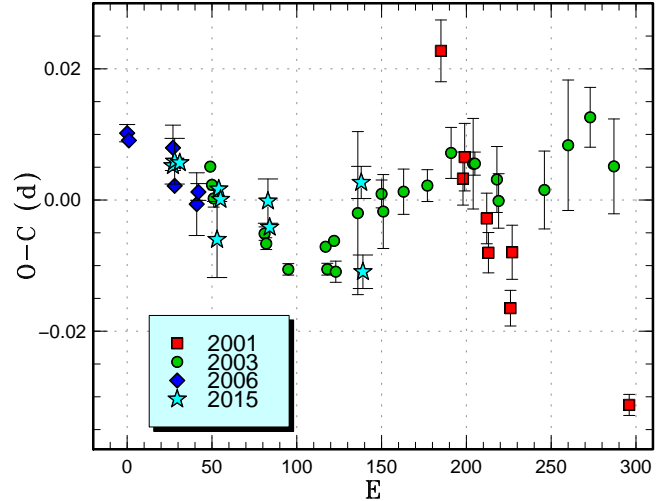


Fig. 9. Comparison of $O - C$ diagrams of AL Com between different superoutbursts. A period of 0.05732 d was used to draw this figure. Approximate cycle counts (E) after the emergence of superhump were used. Assuming that the stage A was best observed in 2013, the 1995 and 2001 $O - C$ diagrams were shifted within 20 cycles to best match the stage A-B transition in 2013. The 2015 $O - C$ diagram was shifted by 60 cycles to best match the others.

Table 10. Superhump maxima of AL Com (2015)

E	max*	error	$O - C^\dagger$	N^\ddagger
0	57087.8281	0.0006	0.0006	22
1	57087.8845	0.0006	-0.0004	26
2	57087.9432	0.0005	0.0011	26
20	57088.9743	0.0008	0.0008	18
28	57089.4310	0.0015	-0.0008	30
29	57089.4895	0.0004	0.0004	59
30	57089.5463	0.0003	-0.0001	56
31	57089.6080	0.0010	0.0043	28
44	57090.3457	0.0012	-0.0028	43
45	57090.4062	0.0005	0.0004	65
46	57090.4615	0.0007	-0.0016	78
47	57090.5198	0.0008	-0.0006	128
48	57090.5766	0.0008	-0.0010	90
49	57090.6357	0.0007	0.0008	53
62	57091.3798	0.0004	0.0000	41
63	57091.4367	0.0003	-0.0004	57
64	57091.4930	0.0003	-0.0013	57
65	57091.5506	0.0005	-0.0010	110
66	57091.6094	0.0006	0.0005	85
67	57091.6666	0.0007	0.0004	63
68	57091.7263	0.0022	0.0028	21
70	57091.8381	0.0016	-0.0000	53
71	57091.8943	0.0006	-0.0011	81
72	57091.9555	0.0041	0.0028	20
76	57092.1817	0.0012	-0.0001	112
77	57092.2402	0.0015	0.0011	119
81	57092.4666	0.0014	-0.0017	30
83	57092.5818	0.0013	-0.0011	46
84	57092.6374	0.0011	-0.0028	55
85	57092.6951	0.0007	-0.0024	63
86	57092.7523	0.0021	-0.0024	26
92	57093.0992	0.0010	0.0007	121
94	57093.2151	0.0007	0.0019	121
95	57093.2679	0.0017	-0.0026	55
110	57094.1298	0.0012	-0.0001	119
111	57094.1892	0.0021	0.0021	120
128	57095.1646	0.0022	0.0035	104

*BJD-2400000.

 \dagger Against max = 2457087.8276 + 0.057293*E*. \ddagger Number of points used to determine the maximum.**Fig. 10.** Comparison of $O - C$ diagrams of VW CrB between different superoutbursts. A period of 0.07290 d was used to draw this figure. Approximate cycle counts (E) after the start of the superoutburst were used.**Table 11.** Superhump maxima of VW CrB (2015)

E	max*	error	$O - C^\dagger$	N^\ddagger
0	57140.1102	0.0006	0.0018	155
1	57140.1838	0.0035	0.0026	76
4	57140.4022	0.0004	0.0026	41
26	57141.9943	0.0058	-0.0073	75
27	57142.0749	0.0006	0.0005	157
28	57142.1462	0.0006	-0.0010	155
56	57144.1872	0.0034	0.0009	51
57	57144.2561	0.0011	-0.0030	133
111	57148.1995	0.0025	0.0082	126
112	57148.2588	0.0026	-0.0053	105

*BJD-2400000.

 \dagger Against max = 2457140.1083 + 0.072820*E*. \ddagger Number of points used to determine the maximum.

Based on historical instances in which superoutbursts were confused with Z Cam-type standstills, Kato et al. (1989) studied this object during a long, bright outburst in 1987 November both in photographic and visual observations. The detection of superhumps confirmed the SU UMa-type nature.

Kato (1991) and Kato (2001a) reported observations of superhumps using a CCD in 1991 and 1992, respectively. Kato, Matsumoto (1999b) also reported observations of a normal outburst in 1998 December. The spectroscopic orbital period was determined by Mennicken, Vogt (1993) and by Thorstensen et al. (1996). Tappert et al. (2003) reported a line-profile analysis. Further superoutbursts were observed and reported in Kato et al. (2009) (the 2006, 2008 superoutbursts), Kato et al. (2010) (the 2010 superoutburst), Kato et al. (2013a) (the 2011 super-

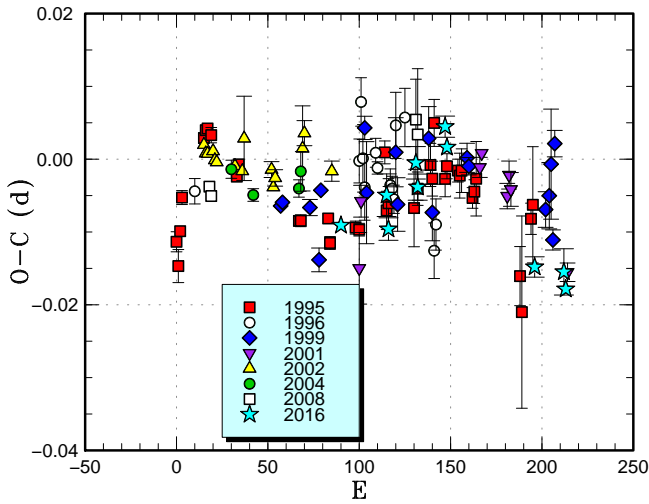


Fig. 11. Comparison of $O - C$ diagrams of V1028 Cyg between different superoutbursts. A period of 0.06178 d was used to draw this figure. Approximate cycle counts (E) after the start of the superoutburst (the start of the main superoutburst when preceded by a precursor) were used. The E for the 2008 superoutburst was somewhat uncertain due to the lack of observations at the early stage. The 2016 superoutburst was shifted by 90 cycles to match the best observed 1995 one.

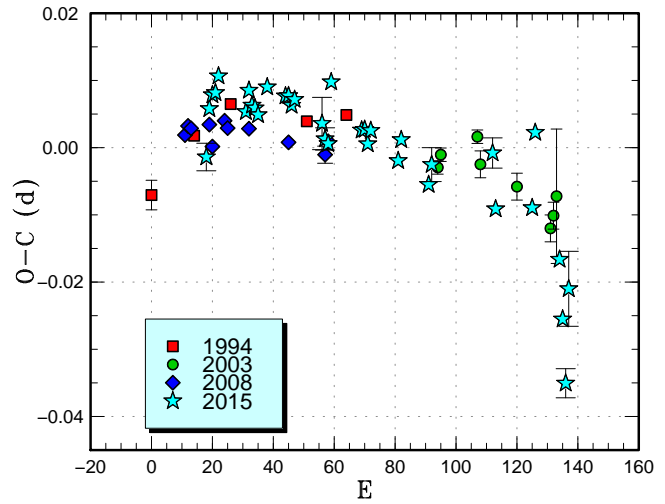


Fig. 12. Comparison of $O - C$ diagrams of V1113 Cyg between different superoutbursts. A period of 0.07911 d was used to draw this figure. Approximate cycle counts (E) after the start of the superoutburst were used.

Table 12. Superhump maxima of V1028 Cyg (2016)

E	max*	error	$O - C^\dagger$	N^\ddagger
0	57465.7060	0.0007	-0.0081	51
25	57467.2547	0.0029	-0.0014	34
26	57467.3118	0.0015	-0.0060	46
41	57468.2476	0.0022	0.0046	33
42	57468.3061	0.0018	0.0014	47
57	57469.2411	0.0015	0.0112	44
58	57469.3000	0.0008	0.0084	47
106	57472.2490	0.0014	-0.0032	27
122	57473.2368	0.0032	-0.0023	34
123	57473.2962	0.0010	-0.0046	35

*BJD-2400000.

† Against max = 2457465.7141 + 0.061680 E .

‡ Number of points used to determine the maximum.

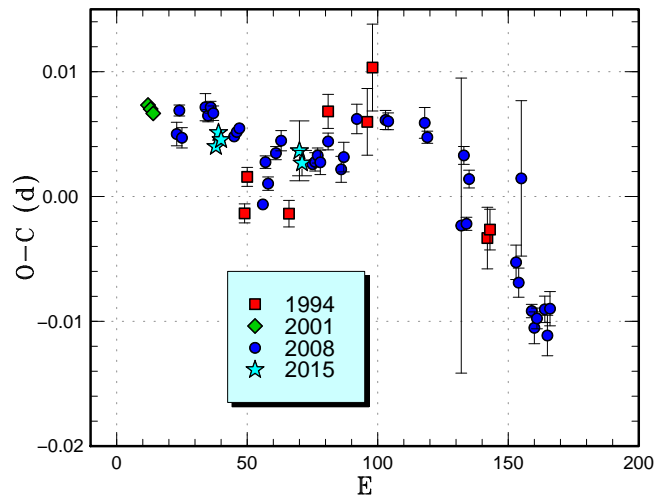


Fig. 13. Comparison of $O - C$ diagrams of HO Del between different superoutbursts. A period of 0.06437 d was used to draw this figure. Approximate cycle counts (E) after the start of the superoutburst were used. The 1994 superoutburst were artificially shifted to match the others.

Table 13. Superhump maxima of V1113 Cyg (2015)

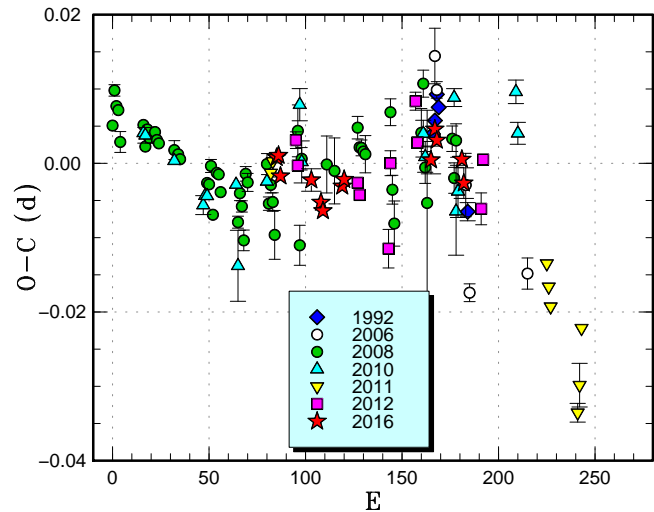
E	max*	error	$O - C^\dagger$	N^\ddagger
0	57264.2780	0.0021	-0.0126	74
1	57264.3643	0.0003	-0.0052	308
2	57264.4455	0.0003	-0.0029	306
3	57264.5249	0.0004	-0.0023	223
4	57264.6065	0.0009	0.0004	32
13	57265.3132	0.0005	-0.0028	106
14	57265.3955	0.0003	0.0006	166
15	57265.4724	0.0004	-0.0014	166
16	57265.5511	0.0004	-0.0016	165
17	57265.6292	0.0006	-0.0024	161
20	57265.8706	0.0011	0.0025	64
26	57266.3440	0.0005	0.0026	103
27	57266.4231	0.0004	0.0028	232
28	57266.5008	0.0004	0.0016	282
29	57266.5808	0.0007	0.0028	210
38	57267.2891	0.0034	0.0012	23
39	57267.3660	0.0017	-0.0008	61
40	57267.4444	0.0011	-0.0013	42
41	57267.5327	0.0009	0.0082	61
51	57268.3166	0.0005	0.0033	40
52	57268.3958	0.0002	0.0037	278
53	57268.4728	0.0003	0.0018	187
54	57268.5539	0.0003	0.0040	176
63	57269.2614	0.0005	0.0017	146
64	57269.3436	0.0002	0.0050	238
73	57270.0489	0.0014	0.0004	138
74	57270.1310	0.0025	0.0037	125
94	57271.7150	0.0022	0.0101	113
95	57271.7857	0.0006	0.0020	183
103	57272.4141	0.0010	-0.0006	82
104	57272.4948	0.0006	0.0012	80
105	57272.5739	0.0009	0.0015	82
107	57272.7352	0.0012	0.0050	115
116	57273.4396	0.0014	-0.0005	73
117	57273.5098	0.0012	-0.0091	76
118	57273.5795	0.0022	-0.0183	79
119	57273.6725	0.0056	-0.0042	23

*BJD-2400000.

 † Against max = 2457264.2907 + 0.078874E. ‡ Number of points used to determine the maximum.**Table 14.** Superhump maxima of HO Del (2015)

E	max*	error	$O - C^\dagger$	N^\ddagger
0	57224.3507	0.0004	-0.0006	59
1	57224.4162	0.0005	0.0006	72
2	57224.4800	0.0005	0.0000	59
32	57226.4102	0.0024	0.0005	51
33	57226.4736	0.0010	-0.0005	66

*BJD-2400000.

 † Against max = 2457224.3513 + 0.064326E. ‡ Number of points used to determine the maximum.**Fig. 14.** Comparison of $O - C$ diagrams of AQ Eri between different superoutbursts. A period of 0.06238 d was used to draw this figure. Approximate cycle counts (E) after the start of the superoutburst were used. Since the starts of the 2012 and 2016 superoutbursts were not well constrained, we shifted the $O - C$ diagram to best fit the best-recorded 2008 one.

outburst) and Kato et al. (2014b) (the 2012 superoutburst).

The 2016 superoutburst was visually detected by R. Stubbings on January 24 (vsnet-alert 19438). Subsequent observations detected superhumps (vsnet-alert 19444). The times of superhump maxima are listed in table 15. We observed stage B and initial part of stage C as inferred from figure 14.

3.14 AX Fornacis

This object was cataloged as 2QZ J021927.9-304545 in the 2dF QSO Redshift Survey (Boyle et al. 2000). B. Monard monitored this object since 2005 January and detected a bright (unfiltered CCD magnitude 11.9) on 2005 July 2 (vsnet-alert 8521). There were several past outbursts in the ASAS-3 (Pojmański 2002) data (vsnet-alert 8523). The object was then established to be an SU UMa-type dwarf nova by the detection of superhumps (Imada et al. 2006). These two superoutbursts were studied further in Kato et al. (2009). The object was given a

Table 15. Superhump maxima of AQ Eri (2016)

E	max*	error	$O - C^\dagger$	N^\ddagger
0	57412.9419	0.0006	0.0032	69
1	57413.0046	0.0006	0.0034	69
2	57413.0642	0.0007	0.0006	69
18	57414.0617	0.0015	-0.0004	21
23	57414.3706	0.0007	-0.0036	50
24	57414.4319	0.0009	-0.0047	44
34	57415.0590	0.0006	-0.0018	162
35	57415.1222	0.0005	-0.0009	142
80	57417.9320	0.0019	0.0003	97
82	57418.0609	0.0008	0.0044	154
83	57418.1218	0.0010	0.0029	18
96	57418.9301	0.0012	-0.0001	104
97	57418.9893	0.0021	-0.0033	34

*BJD-2400000.

† Against max = 2457412.9392 + 0.062463E.

‡ Number of points used to determine the maximum.

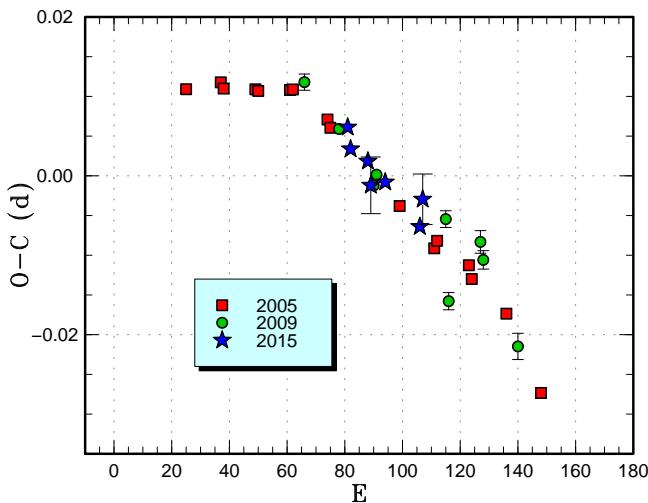


Fig. 15. Comparison of $O - C$ diagrams of AX For between different superoutbursts. A period of 0.08140 d was used to draw this figure. Approximate cycle counts (E) after the start of the superoutburst were used.

permanent name of AX For in Kazarovets et al. (2011).

The 2015 superoutburst was visually detected by R. Stubbings at a magnitude of 12.0 on November 10 (cf. vsnet-alert 19255). The times of superhump maxima are listed in table 16. A comparison of $O - C$ diagrams between different superoutbursts (figure 15) indicates that we only observed stage C superhumps in 2015. Although individual superhumps were not measured, a PDM analysis of the post-superoutburst data (BJD 2457346-2457350) yielded a strong signal of 0.08109(6) d, indicating that stage C superhumps persisted after the rapid fading from the outburst plateau.

Table 16. Superhump maxima of AX For (2015)

E	max*	error	$O - C^\dagger$	N^\ddagger
0	57341.5599	0.0008	0.0020	44
1	57341.6386	0.0006	-0.0004	36
7	57342.1254	0.0007	0.0002	111
8	57342.2038	0.0036	-0.0024	76
13	57342.6112	0.0010	-0.0002	45
25	57343.5824	0.0006	-0.0015	44
26	57343.6673	0.0032	0.0023	14

*BJD-2400000.

† Against max = 2457341.5579 + 0.081041E.

‡ Number of points used to determine the maximum.

3.15 V844 Herculis

This object was discovered as a dwarf nova (Antipin Var 43) by Antipin (1996b). The long outbursts were already suggestive of an SU UMa-type dwarf nova. The first superhump detection was made by T. Vanmunster during an outburst in 1996 October (vsnet-obs 4061, 4075). The superhump period was first determined during the 1997 superoutburst by T. Vanmunster and L. Jensen (Cataclysmic Variables Circular, No. 141, also in vsnet-alert 935; vsnet-obs 5854). Patterson (1998) cited a superhump period of 0.05597(2) d determined from their observations. Kato, Uemura (2000) was the first solid publication of superhumps in this system and reported a period of 0.05592(2) d. Thorstensen et al. (2002) obtained a spectroscopic orbital period of 0.054643(7) d. Oizumi et al. (2007) reported observations of the 2002, 2003 and 2006 superoutbursts. Positive P_{dot} was detected for the 2002 and 2006 superoutbursts. Oizumi et al. (2007) also summarized the known outbursts of this object. Most of the outbursts of this object were superoutbursts and only two out of 13 known outbursts were normal outbursts at the time of Oizumi et al. (2007). The 2008 superoutburst was reported in Kato et al. (2009). The 2009 and 2010 superoutbursts were reported in Kato et al. (2010). The second superoutburst in 2010 (hereafter 2010b) was reported in Kato et al. (2012). Another superoutburst in 2012 was reported in Kato et al. (2013a).

The 2015 superoutburst was detected by the ASAS-SN team (cf. vsnet-alert 18617). This detection was early enough and stage A superhumps were partly observed (vsnet-alert 18625, 18645). The times of superhump maxima are listed in table 17. The maxima for $E \leq 4$ correspond to the growing stage of superhumps and are stage A superhumps. Stage B-C transition probably fell in the observational gap between $E=119$ and $E=173$ and the late phase of stage B (with a long superhump period) was not properly observed.

A comparison of $O - C$ diagrams between different superoutbursts is shown in figure 16. Note that a different base pe-

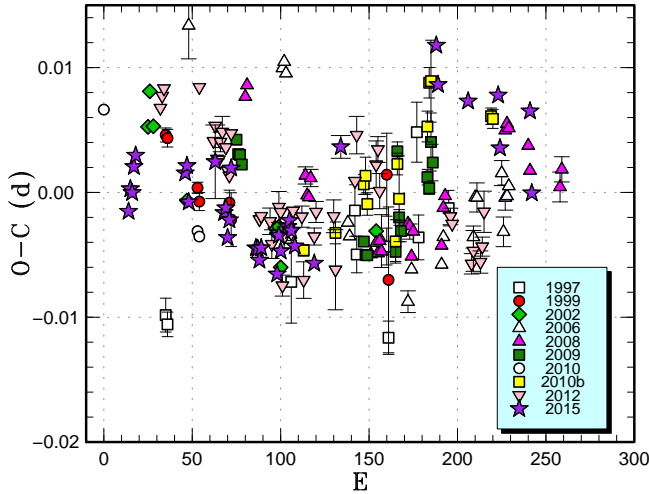


Fig. 16. Comparison of $O - C$ diagrams of V844 Her between different superoutbursts. A period of 0.05595 d was used to draw this figure. Approximate cycle counts (E) after the start of the superoutburst were used. The 2010b superoutburst were artificially shifted by 40 cycles to match the others.

riod was used to draw the figure compared to the earlier ones. The 2010b superoutburst were artificially shifted by 40 cycles to match the others. This superoutburst was either unusual (there was a normal outburst ~ 60 d preceding the superoutburst, and superhumps may have started to develop before the superoutburst) or the initial part of the superoutburst was missed (there were only one negative observation with a meaningful upper limit immediately before this superoutbursts).

3.16 MM Hydrae

MM Hya was originally selected as a CV by the Palomer-Green survey (Green et al. 1982). The SU UMa-type nature was confirmed by Patterson et al. (2003). See Kato et al. (2015a) for more history. The 2015 superoutburst was detected by R. Stubbings on March 9 (vsnet-alert 18395). Two superhumps were recorded on March 19, when the object apparently entered the rapid fading phase: BJD 2457096.9366(12) ($N=36$) and 2457096.9936(17) ($N=43$).

3.17 RZ Leonis

RZ Leo (=AN 30.1919) was discovered as a variable star or a nova by Wolf (1919). The object was detected at a photographic magnitude of 10–11 on 1918 March 13. This magnitude scale was probably 1–2 mag too bright compared to the modern scale (this tendency is common to other Astron. Nach. papers in the 1910s, see e.g. GR Ori in Kato et al. 2014b). Bertaud (1951) listed the object as a probable nova. Herbig (1958) provided an identification chart. The identification by Khatisov (1971)

Table 17. Superhump maxima of V844 Her (2015)

E	max*	error	$O - C^\dagger$	N^\ddagger
0	57157.3198	0.0003	0.0013	86
1	57157.3776	0.0004	0.0031	104
2	57157.4332	0.0002	0.0027	101
3	57157.4912	0.0003	0.0048	100
4	57157.5481	0.0002	0.0056	91
32	57159.1133	0.0002	0.0033	51
33	57159.1698	0.0002	0.0039	62
34	57159.2229	0.0006	0.0009	23
49	57160.0653	0.0029	0.0037	65
54	57160.3410	0.0002	-0.0005	103
55	57160.3973	0.0002	-0.0002	104
56	57160.4509	0.0002	-0.0026	104
57	57160.5083	0.0001	-0.0012	99
58	57160.5684	0.0005	0.0029	33
72	57161.3453	0.0003	-0.0039	57
73	57161.4012	0.0002	-0.0040	57
74	57161.4562	0.0003	-0.0050	58
75	57161.5131	0.0002	-0.0040	57
84	57162.0146	0.0004	-0.0064	71
85	57162.0736	0.0003	-0.0034	119
86	57162.1283	0.0004	-0.0046	96
90	57162.3541	0.0005	-0.0028	57
91	57162.4105	0.0003	-0.0023	58
92	57162.4657	0.0005	-0.0032	53
94	57162.5763	0.0005	-0.0045	87
105	57163.1904	0.0005	-0.0062	64
120	57164.0390	0.0009	0.0026	72
174	57167.0684	0.0007	0.0091	98
175	57167.1212	0.0004	0.0059	84
192	57168.0710	0.0006	0.0040	57
209	57169.0227	0.0005	0.0039	115
210	57169.0744	0.0003	-0.0003	120
227	57170.0285	0.0004	0.0021	76
228	57170.0779	0.0005	-0.0045	119

*BJD-2400000.

† Against max = 2457157.3185 + 0.055982 E .

‡ Number of points used to determine the maximum.

was incorrect. Brun, Petit (1957) and Petit (1960) listed this object as a dwarf nova. Vogt, Bateson (1982) listed this object as a possible WZ Sge-type object (probably based on the large outburst amplitude).

Since the object had been suspected to be a dwarf nova with rare outbursts, it had been sporadically monitored by amateur observers since the 1970s. Since 1982, it had been monitored more systematically and the second historical outburst was detected by R. Ducoty on 1984 December 29 at a visual magnitude of 12.9 (Mattei et al. 1985; Cristiani et al. 1985; McNaught 1985). Richter (1985) studied past photographic plates and detected several (some of them were questionable) outbursts only reaching 13 mag. Richter (1985) suggested that the cycle length might be as short as 6 yr. Although spectroscopic observation in outburst confirmed the dwarf nova-type nature (Cristiani et al. 1985), the object was listed as a recurrent nova in Kholopov et al. (1985). Szkody (1987) reported *JHK* photometry on 1985 January 21, 23 d after the outburst detection. Szkody (1987) ascribed the magnitude $J=14.0$ to the intermediate (“Mid”) state. In modern knowledge, this observation probably reflected the “red phase” following a superoutburst (e.g. see subsection 4.6 in Kato 2015).

On 1987 November 28, there was another outburst reaching a visual magnitude of 12.3–12.5 detected by S. Lubbock (Hurst et al. 1987; Mattei et al. 1987). This outburst lasted at least for 12 d. In the meantime, Howell, Szkody (1988) performed time-resolved CCD photometry in quiescence and detected 0.4 mag modulations with a period of 104 min and suggested the SU UMa-type classification. Since the object had been suspected to be a WZ Sge-type dwarf nova (Vogt, Bateson 1982), it has been discussed assuming this classification (Downes 1990; O’Donoghue et al. 1991. In O’Donoghue et al. (1991), the presence of a short (normal) outburst in 1989 (Narumi et al. 1989) was in particular discussed since various authors had claimed the absence of short outbursts in WZ Sge.

Despite these outburst detections, no secure outburst had been detected before 2000 (there was a possible outburst in 1990 October–November in the AAVSO data, only detected by a single observer). The 2000 outburst was detected by R. Stubbings on December 20 at a visual magnitude of 12.1 (vsnet-alert 5437; Mattei et al. 2000). The detection of superhumps finally led to the identification of an SU UMa-type dwarf nova (vsnet-alert 5446, 5448, Ishioka et al. 2000; Ishioka et al. 2001). Since the orbital period had already been measured to be 0.07651(26) d (Mennickent, Tappert 2001; Mennickent et al. 1999), Ishioka et al. (2001) identified the modulations with a period of 0.07616(21) d detected during the early stage of the outburst to be early superhumps. The orbital period has been updated to be 0.0760383(4) d by photometric observations in quiescence (Patterson et al. 2003). Dai et al. (2016) further determined the orbital period to be 0.07602997(4) d using the

Kepler K2 mission data. More analyses of superhumps during the 2000 superoutburst were reported in Patterson et al. (2003) and Kato et al. (2009).

There was another superoutburst in 2006 detected by S. Kerr on May 27 at a visual magnitude of 12.5 (vsnet-outburst 6885). This outburst was not very well observed due to the limited visibility in the evening sky. An analysis of superhumps was reported in Kato et al. (2009). There have been no confirmed normal outburst other than the 1989 one.

Howell et al. (2010) and Hamilton et al. (2011) reported the spectral type of the secondary to be M3–M4V and $M4\pm 1$, respectively, by infrared observations. These results were consistent with the analysis of spectral energy distribution by Mennickent, Diaz (2002), who suggested the spectral type M5 for the secondary.

The 2016 outburst was detected by R. Stubbings at a visual magnitude of 13.0 on January 31 (vsnet-alert 19448). Subsequent observations already recorded fully developed superhumps (vsnet-alert 19452, 19458, 19466). The object rapidly faded on February 11–12 (vsnet-alert 19499). There was also a post-superoutburst rebrightening at a visual magnitude of 14.1 on February 15 (vsobs-share 12235). The times of superhump maxima are listed in table 18. There were clear stages B and C (figure 17). In this figure, the amplitudes of superhumps cyclically varied with a period of ~ 30 cycles, particularly in the early stage of the superoutburst. This variation most likely reflects the beat phenomenon between the superhump period and orbital period (the estimated beat period is 2.3 d or 29 superhump cycles).

A comparison of the $O - C$ diagrams (figure 18) suggests that superhumps started ~ 3 d before the initial time-resolved observation in 2016. It means that superhumps already started to develop at the time of Stubbings’ initial outburst detection. The true start of the outburst was unknown due to a 6 d gap in the observation. The $O - C$ diagrams have stages B and C and a large positive P_{dot} typical for short- P_{orb} systems. It would be worth noting that stage C superhumps persisted long after the main superoutburst and there was no phase shift at the time of the rapid fading.

Although the existence of early superhumps was reported (Ishioka et al. 2001), these reported early superhumps may have been different from those of typical WZ Sge-type objects since the phase of early superhumps was apparently short. The period of these modulations was not sufficiently determined to make a secure comparison with the orbital period. Although Kato et al. (2009) concluded that these modulations could not be considered as an extension of stage A superhumps, the exact identification of modulations in the earliest stage in RZ Leo still awaits confirmation. It was a pity that both the 2006 and 2016 superoutbursts were not detected sufficiently early to confirm these modulations. Future intensive observations on the next occa-

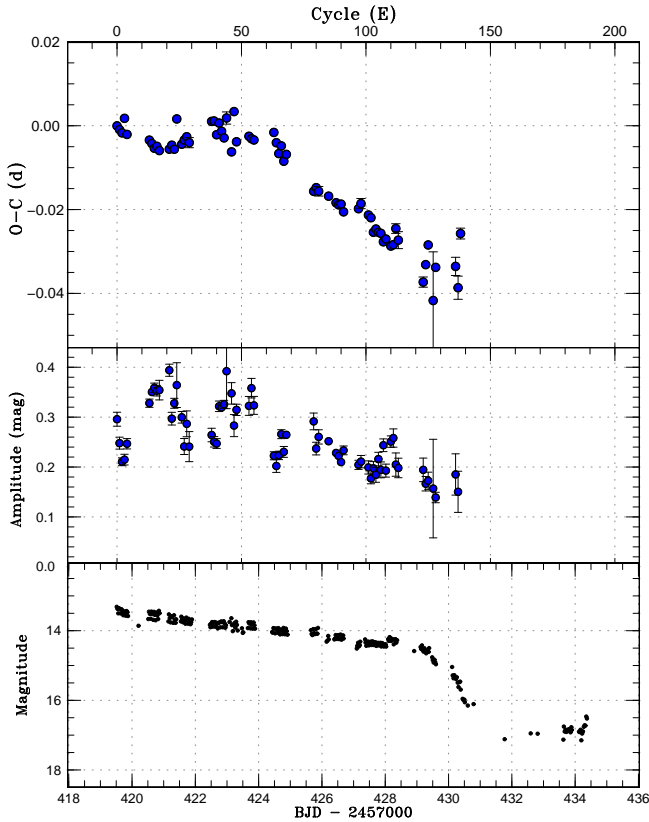


Fig. 17. $O - C$ diagram of superhumps in RZ Leo (2016). (Upper:) $O - C$ diagram. We used a period of 0.07865 d for calculating the $O - C$ residuals. (Middle:) Amplitudes of superhumps. The modulations of the amplitudes with a period of ~ 30 cycles in the initial part are the beat phenomenon between superhump period and the orbital period. (Lower:) Light curve. The data were binned to 0.026 d.

sion are still strongly desired since RZ Leo is supposed to be an atypical (long- P_{orb}) WZ Sge-type system (cf. Kato 2015) and confirmation of early superhumps is very important to verify this classification.

Since RZ Leo apparently has a high orbital inclination (doubly peaked emission lines, ellipsoidal variations in quiescence and beat phenomenon during superoutburst), we attempted to detect the orbital variations during the three superoutbursts (2000, 2006 and 2016). All the combinations of these superoutbursts yielded a consistent period (the alias was selected within the range considering the error in Dai et al. 2016) within respective errors and we identified 0.07603005(2) d to be the updated orbital period (figure 19).

3.18 V585 Lyrae

V585 Lyr was discovered as a dwarf nova (TK 4) by Kryachko (2001). Kryachko (2001) already suggested the SU UMA-type classification based on the presence of long and short outbursts. The 2003 superoutburst was well observed and analyzed in de-

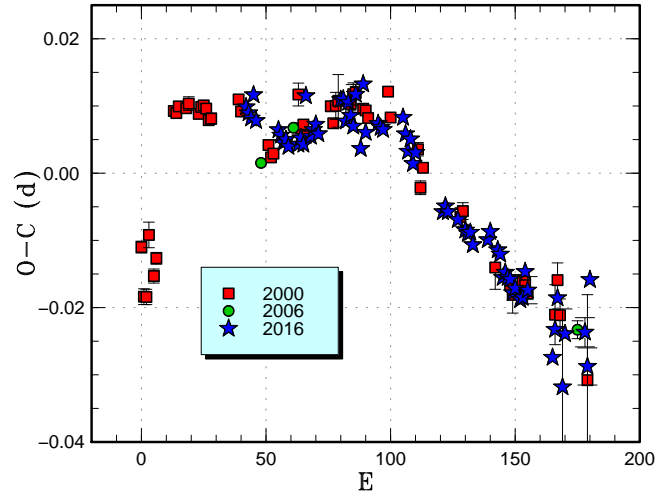


Fig. 18. Comparison of $O - C$ diagrams of RZ Leo between different superoutbursts. A period of 0.07865 d was used to draw this figure. Approximate cycle counts (E) after the start of the appearance of ordinary superhumps. Since starts of the 2006 and 2016 outbursts were not constrained, we shifted the $O - C$ diagram of these outbursts to best fit the better-recorded 2000 one. We had to shift 48 and 42 cycles for the 2006 and 2016 outbursts, respectively.

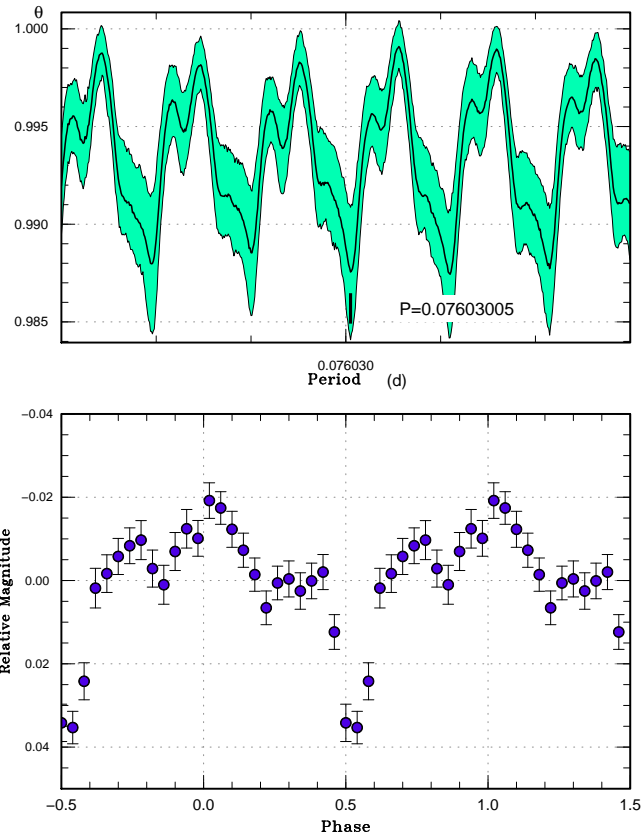


Fig. 19. Orbital variations in RZ Leo during superoutbursts (2000–2016). (Upper:) PDM analysis. (Lower:) Phase-averaged profile.

Table 18. Superhump maxima of RZ Leo (2016)

E	max*	error	$O - C^\dagger$	N^\ddagger	E	max*	error	$O - C^\dagger$	N^\ddagger
0	57419.5256	0.0004	-0.0055	98	66	57424.7117	0.0003	0.0079	60
1	57419.6033	0.0005	-0.0061	121	67	57424.7867	0.0005	0.0045	74
2	57419.6812	0.0003	-0.0066	161	68	57424.8670	0.0003	0.0064	97
3	57419.7633	0.0007	-0.0028	46	79	57425.7233	0.0006	0.0006	33
4	57419.8381	0.0004	-0.0064	37	80	57425.8028	0.0005	0.0018	39
13	57420.5446	0.0002	-0.0053	144	81	57425.8806	0.0011	0.0012	18
14	57420.6225	0.0002	-0.0058	136	85	57426.1940	0.0003	0.0011	125
15	57420.7000	0.0003	-0.0067	177	88	57426.4284	0.0002	0.0004	159
16	57420.7791	0.0003	-0.0059	79	89	57426.5066	0.0002	0.0002	233
17	57420.8567	0.0006	-0.0067	31	90	57426.5854	0.0003	0.0006	176
21	57421.1717	0.0002	-0.0052	129	91	57426.6622	0.0003	-0.0010	78
22	57421.2513	0.0005	-0.0040	106	97	57427.1348	0.0004	0.0014	145
23	57421.3289	0.0003	-0.0047	107	98	57427.2147	0.0012	0.0029	64
24	57421.4148	0.0009	0.0028	47	101	57427.4479	0.0006	0.0010	67
26	57421.5661	0.0003	-0.0027	71	102	57427.5260	0.0006	0.0007	66
27	57421.6457	0.0006	-0.0014	85	103	57427.6011	0.0008	-0.0025	60
28	57421.7252	0.0009	-0.0004	79	104	57427.6806	0.0008	-0.0015	88
29	57421.8024	0.0012	-0.0015	91	105	57427.7584	0.0006	-0.0020	34
38	57422.5153	0.0005	0.0061	58	106	57427.8368	0.0008	-0.0020	75
39	57422.5941	0.0004	0.0064	67	107	57427.9135	0.0005	-0.0037	140
40	57422.6694	0.0004	0.0034	87	108	57427.9928	0.0007	-0.0028	103
41	57422.7509	0.0003	0.0065	101	110	57428.1484	0.0004	-0.0039	185
42	57422.8276	0.0002	0.0048	119	111	57428.2274	0.0007	-0.0033	56
43	57422.9046	0.0002	0.0035	85	112	57428.3099	0.0011	0.0008	55
44	57422.9880	0.0015	0.0085	20	113	57428.3858	0.0020	-0.0017	28
46	57423.1373	0.0010	0.0010	99	123	57429.1622	0.0012	-0.0089	44
47	57423.2255	0.0008	0.0109	147	124	57429.2451	0.0009	-0.0045	44
48	57423.2970	0.0004	0.0039	146	125	57429.3284	0.0010	0.0005	45
53	57423.6915	0.0006	0.0066	36	127	57429.4724	0.0116	-0.0122	31
54	57423.7696	0.0005	0.0063	34	128	57429.5590	0.0008	-0.0040	94
55	57423.8480	0.0005	0.0063	37	136	57430.1884	0.0022	-0.0016	43
63	57424.4790	0.0004	0.0103	71	137	57430.2620	0.0028	-0.0064	44
64	57424.5552	0.0007	0.0081	66	138	57430.3536	0.0013	0.0068	40
65	57424.6312	0.0004	0.0058	80	-	-	-	-	-

*BJD-2400000.

†Against max = 2457419.5310 + 0.078375*E*.

‡Number of points used to determine the maximum.

tail (Kato et al. 2009). The 2012 superoutburst was also observed in Kato et al. (2013a).

The object is located in the Kepler field and two superoutbursts (2010 January–February and 2012 April–May) and one normal outburst (2013 January) were recorded during the Kepler mission. Although this target was also observed in short-cadence mode in limited epochs, all outbursts observed by Kepler were recorded in long-cadence mode, making detailed analysis of the superhump evolution difficult. Kato, Osaki (2013a) analyzed the Kepler long-cadence observations in 2010 using Markov-Chain Monte Carlo (MCMC)-based modeling of long-exposure (~ 29 min) sampling and derived an $O - C$ diagram. This analysis confirmed the results of ground-based photometry with higher time resolutions but frequent gaps (Kato et al. 2009). The particularly important point was that Kepler observation confirmed the superhump stages (A–C) and the lack of phase transition around the termination of the superoutburst. V585 Lyr was also unique among Kepler observations of dwarf novae: this object showed a rebrightening both in the 2000 and 2012 superoutbursts, though such rebrightenings are relatively common among other SU UMa/WZ Sge-type dwarf novae (cf. Kato et al. 2009; Kato 2015). There were “mini-rebrightenings” between the main superoutburst and the rebrightening (Kato, Osaki 2013a). Meyer, Meyer-Hofmeister (2015) interpreted these “mini-rebrightenings” as a result of reflection of cooling waves between the lower branch and the intermediate branch in the S-curve of the thermal equilibrium of the accretion disk. V585 Lyr was also the only object in the Kepler data in which no precursor outburst was associated with the superoutburst and a delay of development of superhumps was recorded. This was interpreted as a result of highly accumulated mass in the disk before the outbursts started (Kato, Osaki 2013a), corresponding to “case B” superoutburst (the mass stored in the disk before the superoutburst is large enough and the disk can remain at radius of the 3:1 resonance or beyond for some time before superhumps start to develop) discussed by Osaki, Meyer (2003).

The 2015 superoutburst was detected by the ASAS-SN team (vsnet-alert 18688). Subsequent observations detected superhumps (vsnet-alert 18698, 18722). The times of superhump maxima are listed in table 19. The final part of stage A and early part of stage B were observed (figure 20).

3.19 V2051 Ophiuchi

V2051 Oph was discovered as an emission-line object in outburst (Sanduleak 1972). Sanduleak (1972) suggested that this object to be a dwarf nova rather than a nova. Bond et al. (1977) listed this object as a candidate polar, although this list included various objects (EM Cyg: dwarf nova; V Sge: novalike variable; CL Sco, HK Sco: symbiotic stars) which are not currently considered to be related to polars. Angel et al. (1977)

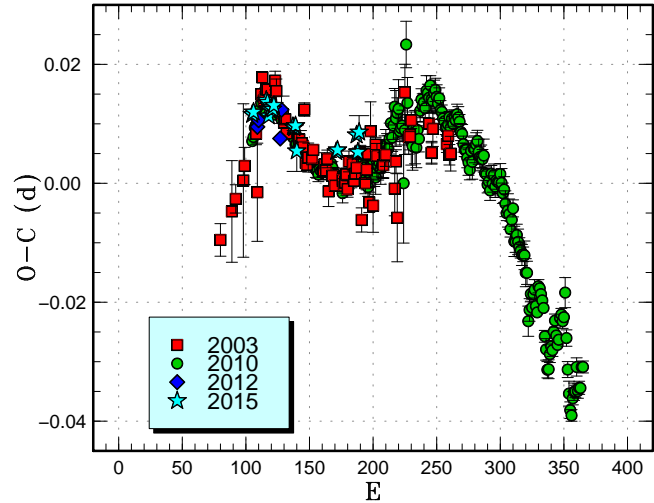


Fig. 20. Comparison of $O - C$ diagrams of V585 Lyr between different superoutbursts. The 2010 data refer to Kepler observations analyzed in Kato, Osaki (2013a). A period of 0.06045 d was used to draw this figure. Approximate cycle counts (E) after the start of the superoutburst were used. The starts of the 2010 and 2012 superoutbursts were well determined by the Kepler data. We had to shift 49 and 80 cycles for the 2003 and 2015 data, respectively, to obtain the best match with the 2010 data. These values suggest that the outbursts were missed for 3 d and 5 d for the 2003 and 2015 superoutbursts, respectively, or these superoutbursts had exceptionally smaller scales. Considering the limited visual monitoring, the first possibility looks more likely.

Table 19. Superhump maxima of V585 Lyr (2015)

E	max*	error	$O - C^\dagger$	N^\ddagger
0	57179.5047	0.0005	-0.0013	67
1	57179.5655	0.0007	-0.0008	60
11	57180.1720	0.0002	0.0020	55
12	57180.2321	0.0002	0.0017	67
13	57180.2903	0.0011	-0.0005	23
14	57180.3518	0.0002	0.0008	45
15	57180.4125	0.0004	0.0011	84
16	57180.4728	0.0002	0.0009	124
17	57180.5338	0.0003	0.0017	94
32	57181.4370	0.0006	-0.0006	52
33	57181.4973	0.0005	-0.0008	67
34	57181.5581	0.0005	-0.0003	67
35	57181.6143	0.0034	-0.0045	24
66	57183.4881	0.0007	-0.0020	67
67	57183.5489	0.0006	-0.0016	67
82	57184.4581	0.0010	0.0021	66
83	57184.5157	0.0010	-0.0007	66
84	57184.5795	0.0028	0.0028	36

*BJD-2400000.

† Against max = 2457179.5060 + 0.060366 E .

‡ Number of points used to determine the maximum.

reported that this object is an eclipsing system with a period of 96 min. Angel et al. (1977) also reported strong Balmer, HeI and HeII emission lines. Bond (2004) confirmed this spectroscopic finding. After a suggestion of similarity with HT Cas (Patterson 1980), this object started to be monitored by amateur astronomers in 1980. Secure outburst detections were not made in the 1980s. F. Bateson, Royal Astronomical Society of New Zealand, reported only limited number of outbursts up to 1997 (only reaching 13.0–13.5 mag and without evidence for superoutbursts: vsnet-chat 546; see also Warner, Cropper 1983). This object was considered to be too faint for amateur telescopes (cf. citation in Warner, O’Donoghue 1987).

The history of classification of this object had long been confusing. Warner, Cropper (1983) obtained high-speed photometry and found eclipse profiles were highly variable. Warner, Cropper (1983) suggested that this object is similar to other SU UMa-type eclipsing dwarf novae Z Cha, OY Car and HT Cas. The analysis of flickering suggested a possibility that the inner region of the disk may be truncated as in polars (Warner, Cropper 1983). A spectroscopic study by Cook, Brunt (1983) suggested that the white dwarf is eclipsed. Wenzel (1984) surveyed about 400 Sonneberg plates with limiting magnitudes of 11.5–13 mag and found no major outburst. Wenzel (1984) considered this finding to be compatible with a polar rather than a high-amplitude dwarf nova. Watts et al. (1986) reported detailed spectrophotometric analysis and suggested the similarity of the disk structure to that of OY Car. Warner, O’Donoghue (1987) reported high-speed photometry and the reconstructed eclipse map did not show evidence of a well-established accretion disk. Warner, O’Donoghue (1987) suggested that this object is a low-field polar based on these observations.

In 1997, several faint outbursts were recorded by R. Stubbings: 13.9 mag on June 27 (vsnet-alert 1019), 13.6 mag on August 7 (vsnet-obs 6643, vsnet-alert 1129) and 14.2 mag on September 24 (vsnet-obs 7540, vsnet-alert 1239). There was another outburst on 1998 March 27 at 13.6 mag (vsnet-alert 1600). On 1998 March 18, there was a bright outburst reaching 11.9 mag (the outburst started one day before) (vsnet-alert 1796). CCD observations by L. T. Jensen revealed humps and eclipses (vsnet-alert 1814). Observations by S. Kiyota identified these humps as superhumps (vsnet-alert 1819). Upon detection announcement of this superoutburst, B. Warner wrote: The eclipse centered on a “superhump” shown on your Web page is just the enhanced orbital hump that appears during outburst (vsnet-alert 1833). T. Kato reported that superhump signatures were present in observations by S. Kiyota and Osaka Kyoiku U. team and pointed out that B. Warner actually recorded the fading part of a superoutburst in Warner, O’Donoghue (1987), during which an apparent superhump was recorded only one night (vsnet-alert 1835). J. Patterson’s team also reported the identification of the observed humps as superhumps (vsnet-alert 1859).

The result by S. Kiyota was published in Kiyota, Kato (1998).

Another superoutburst was recorded in 1999 July–August (vsnet-alert 3284, 3308, 3315, 3330, 3347). There was also a rebrightening (vsnet-alert 3354). After this outburst, there was no doubt about the SU UMa-type classification of this object [see also Vrielmann, Offutt (2000); Vrielmann, Offutt (2003); Papadaki et al. (2008)]. Kato et al. (2001) reported a supercycle of 227 d and the recurrence time of normal outbursts of 45 d. In our series of papers, the 1999, 2003 and 2009 superoutbursts were analyzed in Kato et al. (2009), the 2010 one was reported in Kato et al. (2010). Despite that the recent observations suggest that this object is an ordinary SU UMa-type dwarf nova, there has been an argument using eclipse maps that outbursts in this system have properties different from what the disk-instability model suggests (Baptista et al. 2007; Andrade, Baptista 2014; Wojcikiewicz, Baptista 2014). Baptista (2012) suggested that dwarf novae have two groups, the one which can be understood in the framework of the disk instability model and the other which can only be explained in terms of the mass-transfer instability model. Baptista (2012) claimed that V2051 Oph belongs to the latter group.

In addition to above references, this object has been thoroughly investigated since it is fairly close and has received much attention from the early times: eclipse analysis (Baptista et al. 1998; Vrielmann et al. 2002; Papadaki et al. 2008), flickering (Bruch 2000; Baptista, Bortoletto 2004), spectroscopy (Steehgs et al. 2001; Saito, Baptista 2006; Longa-Peña et al. 2015), and secular variation of the orbital period (Echevarria, Alvarez 1993; Baptista et al. 2003).

The 2015 superoutburst was detected by R. Stubbings (vsnet-alert 18650). The outburst was detected on May 21 and reached a peak brightness of 11.9 mag on May 23. The object faded rather quickly and it was already around 14 mag when observations of superhumps were performed (vsnet-alert 18675). During the past superoutbursts, the object was mostly around 13 mag or fainter when CCD time-resolved observations were performed despite that the peak visual magnitude reached 12 or even brighter. The short duration of the brightness peak may have the reason why past plate collections and visual monitoring failed to record relatively frequent superoutbursts. Such a short peak of the superoutburst may be a result of a high inclination and would deserve a further study.

The times of superhump maxima in 2015 are listed in table 20. We possibly detected stage B and initial part of stage C by comparison with other superoutbursts of this object (figure 21).

The object was observed after the superoutburst and the superhump signal with a period of 0.06373(2) d was detected up to the next normal outburst (BJD 2457186, June 13). If we assume a disk radius of $0.35 \pm 0.04a$, where a is the binary separation, for the post-superoutburst state of an ordinary SU UMa-type dwarf nova (Kato, Osaki 2013b), the mass ratio is estimated

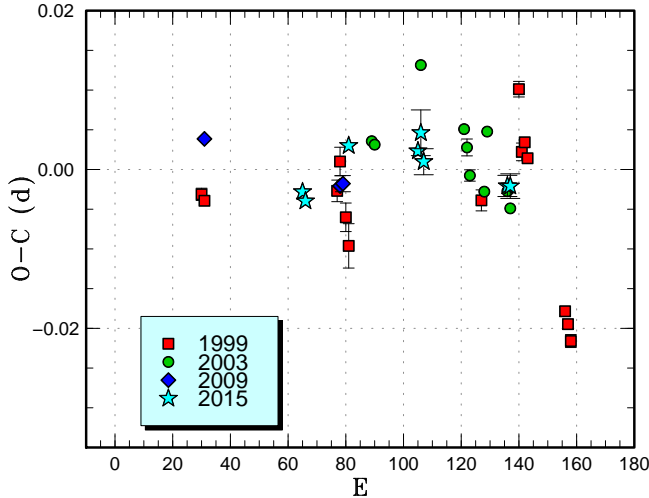


Fig. 21. Comparison of $O - C$ diagrams of V2051 Oph between different superoutbursts. A period of 0.06430 d was used to draw this figure. Approximate cycle counts (E) after the start of the superoutburst were used.

to be $q=0.11(3)$. Although this value is smaller than $q=0.19(3)$ (Baptista et al. 1998), who obtained the value from eclipse observations, and $q=0.18(5)$ (Longa-Peña et al. 2015) by Doppler-tomography, our smaller value for a short- P_{orb} object appears to fit more comfortably on the evolutionary diagram (e.g. figure 5 in Kato, Osaki 2013b, see also figure 160 in this paper). Since eclipse light curves in this system were very variable (Warner, O’Donoghue 1987) and ingress/egress features of the hot spot are difficult to define (Baptista et al. 1998), determination of q from eclipse observations would suffer intrinsic uncertainties. Our new value using post-superoutburst superhumps would be treated as a new measurement of q with comparable significance.

We have also updated the eclipse ephemeris by using MCMC analysis (Kato et al. 2013a) of the eclipse observations of our 1999–2015 data:

$$\text{Min}(\text{BJD}) = 2453189.48679(1) + 0.0624278552(2)E. \quad (1)$$

The epoch refers to the center of the entire observation.

3.20 V368 Pegasi

V368 Peg is a dwarf nova (Antipin Var 63) discovered by Antipin (1999). The SU UMA-type nature was identified by J. Pietz during the 1999 superoutburst (vsnet-alert 3317). The 2000, 2005 and 2006 superoutbursts were studied in Kato et al. (2009) and the 2009 superoutburst was reported in Kato et al. (2010).

The 2015 superoutburst was visually detected by P. Schmeer on September 14 (vsnet-alert 19063). This superoutburst was also detected by C. Chiselbrook (AAVSO) on the same night. Single-night observations on September 17 recorded

Table 20. Superhump maxima of V2051 Oph (2015)

E	max*	error	$O - C^\dagger$	phase ‡	N^\S
0	57168.1880	0.0006	-0.0024	0.78	36
1	57168.2511	0.0009	-0.0035	0.79	59
16	57169.2226	0.0009	0.0033	0.35	99
40	57170.7651	0.0010	0.0023	0.06	18
41	57170.8317	0.0029	0.0046	0.13	15
42	57170.8924	0.0016	0.0009	0.10	10
71	57172.7540	0.0013	-0.0025	0.92	10
72	57172.8183	0.0015	-0.0026	0.95	11

*BJD-2400000.

† Against max = 2457168.1904 + 0.064313 E .

‡ Orbital phase.

§ Number of points used to determine the maximum.

two superhumps maxima: BJD 2457283.3273(3) ($N=76$) and 2457283.3969(4) ($N=64$).

3.21 V650 Pegasi

This dwarf nova is an SU UMA-type dwarf nova selected by P. Wils (cf. Shears et al. 2011). The object was formerly referred to as ASAS J224349+0809.5. For more history, see Kato et al. (2014a).

The 2015 outburst was detected by the ASAS-SN team on September 5 (cf. vsnet-alert 19032). Superhumps were soon detected (vsnet-alert 19034, 19059, 19066, 19069). The times of superhumps maxima are listed in table 21. Although stage A was not recorded, stages B and C were clearly detected (figure 22).

3.22 PU Persei

PU Per was discovered as a dwarf nova (=S 9727) by Hoffmeister (1967), who detected two outbursts. Romano, Minello (1976) also detected two outbursts. Both Hoffmeister (1967) and Romano, Minello (1976) recorded short and long outbursts. Busch et al. (1979) recorded further two long outbursts. Bruch et al. (1987) detected another outburst. The presence of two types of outbursts and the large outburst amplitude made PU Per an excellent candidate for an SU UMA-type dwarf nova. Kato, Nogami (1995) observed a normal outburst in 1995 October and Kato, Matsumoto (1999a) finally detected superhumps during the 1998 September outburst. The 2009 superoutburst was reported in Kato et al. (2009).

The 2015 outburst was detected by E. Muylaert by CCD observations on October 3 (cf. vsnet-alert 19114). Superhumps were detected (vsnet-alert 19124, 19130, 19144). The times of superhump maxima are listed in table 22. A comparison with the 2009 data suggests that we only recorded stage C super-

Table 21. Superhump maxima of V650 Peg (2015)

E	max*	error	$O - C^\dagger$	N^\ddagger	E	max*	error	$O - C^\dagger$	N^\ddagger
0	57273.0768	0.0004	-0.0068	90	108	57280.6157	0.0017	0.0095	22
1	57273.1544	0.0003	0.0012	140	109	57280.6846	0.0017	0.0087	26
2	57273.2197	0.0003	-0.0032	139	110	57280.7551	0.0016	0.0095	25
3	57273.2897	0.0004	-0.0029	144	123	57281.6617	0.0009	0.0106	26
4	57273.3606	0.0001	-0.0016	183	124	57281.7316	0.0010	0.0109	23
5	57273.4292	0.0001	-0.0027	289	125	57281.8064	0.0026	0.0160	10
6	57273.4999	0.0002	-0.0017	167	135	57282.4955	0.0005	0.0087	91
7	57273.5676	0.0009	-0.0036	43	136	57282.5676	0.0012	0.0111	34
43	57276.0738	0.0004	-0.0049	69	137	57282.6343	0.0012	0.0081	25
44	57276.1430	0.0004	-0.0054	77	138	57282.7038	0.0010	0.0079	24
45	57276.2140	0.0004	-0.0041	51	139	57282.7700	0.0015	0.0045	24
52	57276.6977	0.0029	-0.0080	11	146	57283.2634	0.0070	0.0104	104
53	57276.7718	0.0009	-0.0035	22	147	57283.3247	0.0004	0.0020	189
54	57276.8380	0.0010	-0.0069	22	148	57283.3936	0.0005	0.0013	125
56	57276.9791	0.0005	-0.0051	74	151	57283.6012	0.0033	-0.0001	12
57	57277.0498	0.0005	-0.0041	77	152	57283.6711	0.0018	0.0001	26
58	57277.1192	0.0004	-0.0043	77	165	57284.5772	0.0017	0.0007	25
59	57277.1874	0.0005	-0.0058	77	166	57284.6471	0.0027	0.0010	50
80	57278.6593	0.0012	0.0034	20	180	57285.6141	0.0020	-0.0072	19
81	57278.7278	0.0012	0.0022	29	195	57286.6530	0.0014	-0.0131	26
82	57278.7947	0.0015	-0.0005	23	196	57286.7246	0.0035	-0.0112	25
94	57279.6419	0.0014	0.0109	25	209	57287.6224	0.0018	-0.0189	24
95	57279.7087	0.0017	0.0080	27	210	57287.6859	0.0035	-0.0250	26
96	57279.7744	0.0016	0.0040	29	-	-	-	-	-

*BJD-2400000.

 \dagger Against max = 2457273.0836 + 0.069654*E*. \ddagger Number of points used to determine the maximum.

humps (figure 23).

3.23 QY Persei

QY Per was discovered as a dwarf nova (=S 9178) by Hoffmeister (1966). Pinto, Romano (1976) reported another outburst at a photographic magnitude of 13.7 on 1971 September 21. The object has been renowned for its low frequency of outbursts and the 1989 October outburst was reported by Rosino, Candeo (1989). Although there was an outburst in 1994 October, it faded rather quickly. The next confirmed outburst occurred in 1999 December and superhumps were detected (Kato et al. 2009). Contrary to the expectation as a WZ Sge-type dwarf nova, the superhump period was long (~ 0.0786 d). The object was considered to be a long-period system resembling WZ Sge-type dwarf novae, although no early superhumps have been detected (Kato 2015). The next confirmed outburst (superoutburst) occurred in 2005 September, which was not well observed (Kato et al. 2009).

The 2015 outburst was detected by M. Hiraga at an unfiltered

CCD magnitude of 14.7 on November 14 (vsnet-alert 19263). The object was fainter than 16.2 two days before. Subsequent observations detected superhumps (vsnet-alert 19267, 19281). The times of superhump maxima are listed in table 23. The early appearance of superhumps after the start of the outbursts (figure 24) suggest that the object is less likely a WZ Sge-type dwarf nova. Since the 2015 outburst was much fainter than the 1999 outburst, there remains a possibility that the object shows superoutbursts of different extent as in the WZ Sge-type object AL Com (Kimura et al. 2016a).

3.24 TY Piscium

For the history of this well-known SU UMa-type object, see Kato et al. (2014a). The 2015 superoutburst was visually detected by E. Muylaert at a magnitude of 12.2 on October 29. Our observations covered the later part of the outburst and recorded superhumps in table 24. A comparison of $O - C$ diagrams of TY Psc between different superoutbursts is given in figure 25.

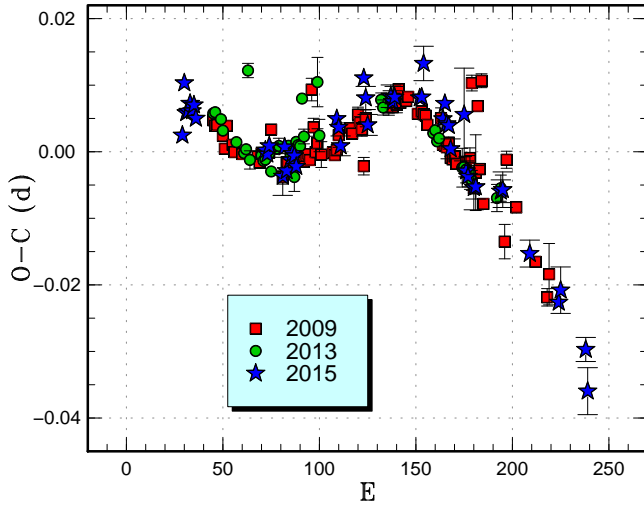


Fig. 22. Comparison of $O - C$ diagrams of V650 Peg between different superoutbursts. A period of 0.06975 d was used to draw this figure. Approximate cycle counts (E) after the start of the superoutburst were used. In Kato et al. (2014a), cycles were counted since the detection of the outbursts, on the contrary to the description in Kato et al. (2014a). The starts of the outbursts were not known at the time of Kato et al. (2014a). The start of the 2015 outburst is much better defined and we shifted the other outbursts to fit the 2015 one.

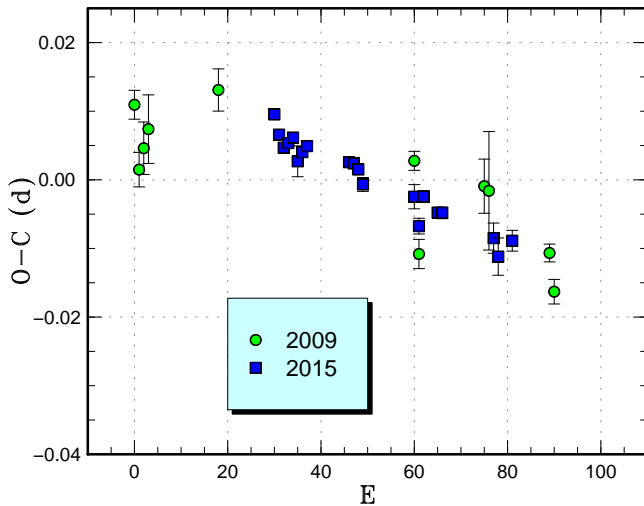


Fig. 23. Comparison of $O - C$ diagrams of PU Per between different superoutbursts. A period of 0.06831 d was used to draw this figure. Approximate cycle counts (E) after the start of the observation were used. Since starts of neither outbursts were constrained, we shifted the $O - C$ diagram of the 2015 outburst to best fit the better-recorded 2009 one.

Table 22. Superhump maxima of PU Per (2015)

E	max*	error	$O - C^\dagger$	N^\ddagger
0	57301.0557	0.0007	0.0027	64
1	57301.1211	0.0007	0.0001	73
2	57301.1875	0.0007	-0.0015	72
3	57301.2565	0.0007	-0.0005	69
4	57301.3256	0.0008	0.0007	68
5	57301.3904	0.0022	-0.0025	71
6	57301.4601	0.0005	-0.0008	132
7	57301.5293	0.0006	0.0004	132
16	57302.1417	0.0006	0.0011	71
17	57302.2098	0.0004	0.0012	218
18	57302.2773	0.0004	0.0007	213
19	57302.3434	0.0010	-0.0011	148
30	57303.0930	0.0018	0.0008	60
31	57303.1570	0.0011	-0.0032	75
32	57303.2297	0.0009	0.0015	146
35	57303.4323	0.0007	0.0001	178
36	57303.5005	0.0008	0.0004	126
47	57304.2482	0.0022	0.0004	127
48	57304.3139	0.0027	-0.0019	146
51	57304.5211	0.0015	0.0014	59

*BJD-2400000.

† Against max = 2457301.0530 + 0.067975 E .

‡ Number of points used to determine the maximum.

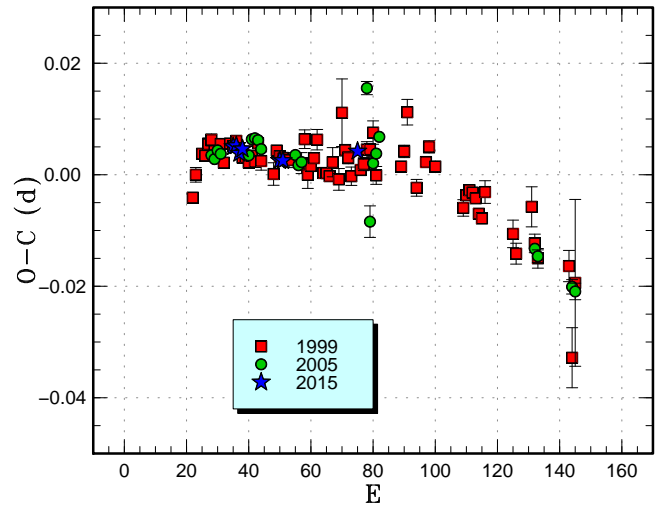


Fig. 24. Comparison of $O - C$ diagrams of QY Per between different superoutbursts. A period of 0.07862 d was used to draw this figure. Approximate cycle counts (E) after the start of the superoutburst were used. Since the start of the 2015 superoutburst was not well constrained, we shifted the $O - C$ diagram to best fit the others.

Table 23. Superhump maxima of QY Per (2015)

E	max*	error	$O - C^\dagger$	N^\ddagger
0	57343.2396	0.0005	0.0007	70
1	57343.3184	0.0004	0.0009	87
2	57343.3956	0.0005	-0.0004	87
3	57343.4750	0.0005	0.0004	65
15	57344.4164	0.0005	-0.0013	58
16	57344.4950	0.0008	-0.0013	68
40	57346.3836	0.0005	0.0010	57

*BJD-2400000.

†Against max = 2457343.2389 + 0.078593E.

‡Number of points used to determine the maximum.

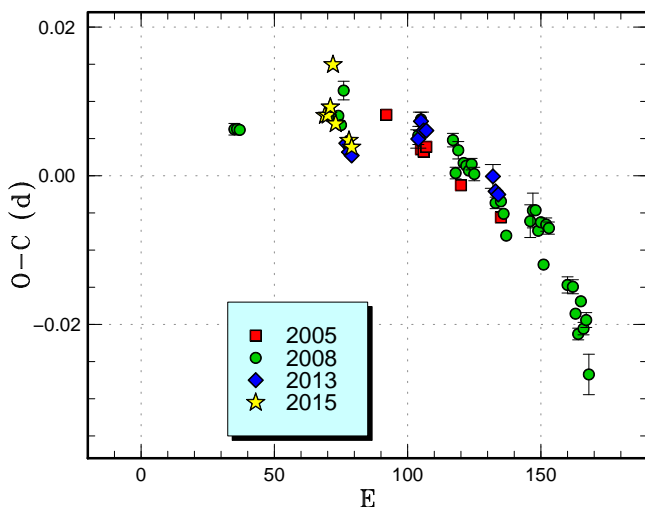


Fig. 25. Comparison of $O - C$ diagrams of TY Psc between different superoutbursts. A period of 0.07066 d was used to draw this figure. Approximate cycle counts (E) after the start of the superoutburst were used. Since the start of the 2013 superoutburst was not well constrained, we shifted the $O - C$ diagram to best fit the others.

Table 24. Superhump maxima of TY Psc (2015)

E	max*	error	$O - C^\dagger$	N^\ddagger
0	57330.2711	0.0004	-0.0022	225
1	57330.3418	0.0004	-0.0016	225
2	57330.4136	0.0004	0.0000	146
3	57330.4899	0.0009	0.0063	39
4	57330.5526	0.0006	-0.0011	54
9	57330.9037	0.0008	-0.0005	88
10	57330.9734	0.0005	-0.0008	131

*BJD-2400000.

†Against max = 2457330.2734 + 0.070093E.

‡Number of points used to determine the maximum.

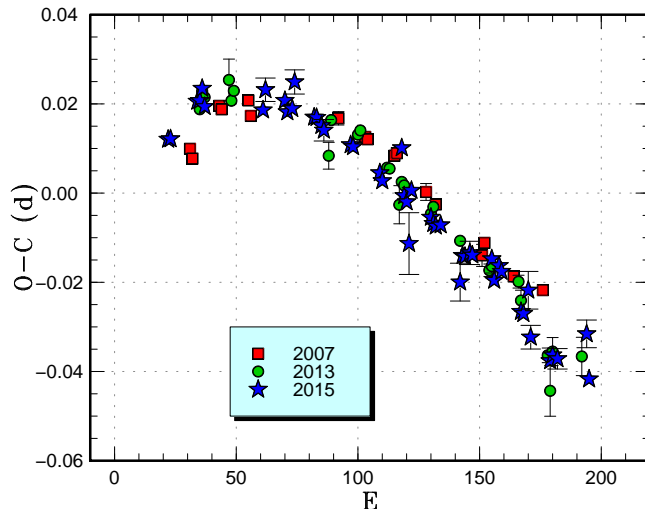


Fig. 26. Comparison of $O - C$ diagrams of V493 Ser between different superoutbursts. A period of 0.08300 d was used to draw this figure. Approximate cycle counts (E) after the start of the superoutburst were used. Since the start of the 2013 superoutburst was not well constrained, we shifted the $O - C$ diagram to best fit the better-recorded 2007 one.

3.25 V493 Serpentis

This object (=SDSS J155644.24-000950.2) was selected as a dwarf nova by SDSS (Szkody et al. 2002). The SU UMA-type nature was confirmed during the 2006 and 2007 superoutbursts (Kato et al. 2009). See Kato et al. (2014b) for more history. The 2015 superoutburst was detected by the ASAS-SN team in its early phase (vsnet-alert 18666). Subsequent observations indeed recorded stage A superhumps (vsnet-alert 18673, 18683) and later development (vsnet-alert 18721). The times of superhump maxima are listed in table 25. Although transitions between stages were rather smooth, we adopted stage classifications listed in table 3 referring to the well-recorded observation in Kato et al. (2009) (figure 26). The resultant $e^* = 0.0449(13)$ for stage A superhumps corresponds to $q = 0.129(5)$, which is in good agreement with $q = 0.136(6)$ using the 2007 observation (Kato, Osaki 2013b).

3.26 V1212 Tauri

V1212 Tau was discovered as an eruptive object near M45 (Parsamyan et al. 1983). See Kato et al. (2012) and Kato et al. (2014b) for more history. The 2016 superoutburst was detected on February 2 at $V = 15.91$ by the ASAS-SN team. The superoutburst was also detected by M. Moriyama on February 7 at an unfiltered CCD magnitude of 15.6 (vsnet-alert 19462, 19465). Only single-night observations on February 8 were obtained and two superhumps were recorded: BJD 2457427.0376(10) ($N = 103$) and 2457427.1028(28) ($N = 52$).

Table 25. Superhump maxima of V493 Ser (2015)

E	max*	error	$O - C^\dagger$	N^\ddagger	E	max*	error	$O - C^\dagger$	N^\ddagger
0	57171.3874	0.0003	-0.0203	85	100	57179.6859	0.0009	0.0060	25
1	57171.4706	0.0004	-0.0198	61	108	57180.3447	0.0010	0.0030	61
12	57172.3931	0.0002	-0.0072	85	109	57180.4264	0.0004	0.0020	84
13	57172.4763	0.0002	-0.0067	85	110	57180.5089	0.0004	0.0018	67
14	57172.5622	0.0006	-0.0036	38	112	57180.6754	0.0008	0.0028	18
15	57172.6412	0.0010	-0.0073	17	120	57181.3274	0.0042	-0.0070	44
39	57174.6348	0.0010	0.0010	16	121	57181.4164	0.0004	-0.0006	84
40	57174.7225	0.0026	0.0059	10	122	57181.4993	0.0005	-0.0005	83
48	57175.3849	0.0004	0.0065	62	124	57181.6663	0.0026	0.0011	20
49	57175.4654	0.0004	0.0044	60	125	57181.7489	0.0013	0.0010	18
51	57175.6324	0.0009	0.0059	20	133	57182.4129	0.0009	0.0031	69
52	57175.7214	0.0027	0.0122	10	134	57182.4912	0.0005	-0.0013	85
60	57176.3783	0.0004	0.0073	80	136	57182.6606	0.0019	0.0028	20
61	57176.4614	0.0003	0.0076	85	137	57182.7424	0.0016	0.0018	22
63	57176.6258	0.0017	0.0066	20	145	57183.3983	0.0005	-0.0041	84
64	57176.7078	0.0024	0.0059	12	146	57183.4809	0.0006	-0.0042	85
75	57177.6186	0.0013	0.0068	17	148	57183.6523	0.0042	0.0018	19
76	57177.7013	0.0012	0.0067	13	149	57183.7249	0.0027	-0.0084	19
87	57178.6095	0.0016	0.0051	13	157	57184.3844	0.0012	-0.0106	45
88	57178.6909	0.0007	0.0037	21	158	57184.4688	0.0009	-0.0090	45
96	57179.3631	0.0011	0.0141	43	160	57184.6342	0.0023	-0.0091	19
97	57179.4354	0.0003	0.0037	85	172	57185.6370	0.0031	0.0011	18
98	57179.5171	0.0011	0.0027	39	173	57185.7099	0.0017	-0.0087	20
99	57179.5909	0.0069	-0.0063	16	-	-	-	-	-

*BJD-2400000.

 \dagger Against max = 2457171.4077 + 0.082722*E*. \ddagger Number of points used to determine the maximum.

3.27 KK Telescopii

KK Tel was discovered as a dwarf nova by Hoffmeister (1963b). Howell et al. (1991) performed time-resolved photometry in quiescence and recorded a period of 0.084 d. The SU UMa-type nature was clarified during the 2002 superoutburst Kato et al. (2003b). Kato et al. (2003b) noticed an exceptionally large period decrease of superhumps, and was considered to be a prototypical SU UMa-type dwarf nova with a large period decrease and this result was often referred for comparison [cf. MN Dra (Nogami et al. 2003); KS UMa (Olech et al. 2003); V419 Lyr (Rutkowski et al. 2007)]. This detection of a large period decrease was before the establishment of the common pattern of period variations (stages A–C, Kato et al. 2009), and it has been clarified that the large period decrease in KK Tel was likely a result of stage A–B transition.

The 2015 superoutburst was detected by the ASAS-SN team on June 9 (cf. vsnet-alert 18713). Subsequent observations detected superhumps (vsnet-alert 18719, 18732, 18801). The times of superhump maxima are listed in table 26. The max-

ima up to $E=19$ were stage A superhumps (figure 27). Since the 2015 observation started 2 d later than the initial outburst detection, it took ~ 60 cycles for this object to develop stage B superhumps. It was not probably by chance that stage A superhumps in this system were well recorded both in 2002 and 2015, but it was likely a result of relatively long-lasting stage A in this system. In Kato et al. (2014a) and Kato et al. (2016b), we proposed that systems having q close to the stability border of the 3:1 resonance show slow evolution of superhumps (see also subsection 4.4). This is also probably the case for KK Tel and V419 Lyr. It is also worth noting that the epoch of the peak amplitude was earlier than the flattening of the $O - C$ diagram (pure stage B superhumps; figure 27). This tendency was also seen in the long-period system V1006 Cyg with a long duration of stage A (Kato et al. 2016b).

Since the period of stage A superhumps is well determined for KK Tel, precise determination of the orbital period will lead to a measurement of q , providing a test for this hypothesis.

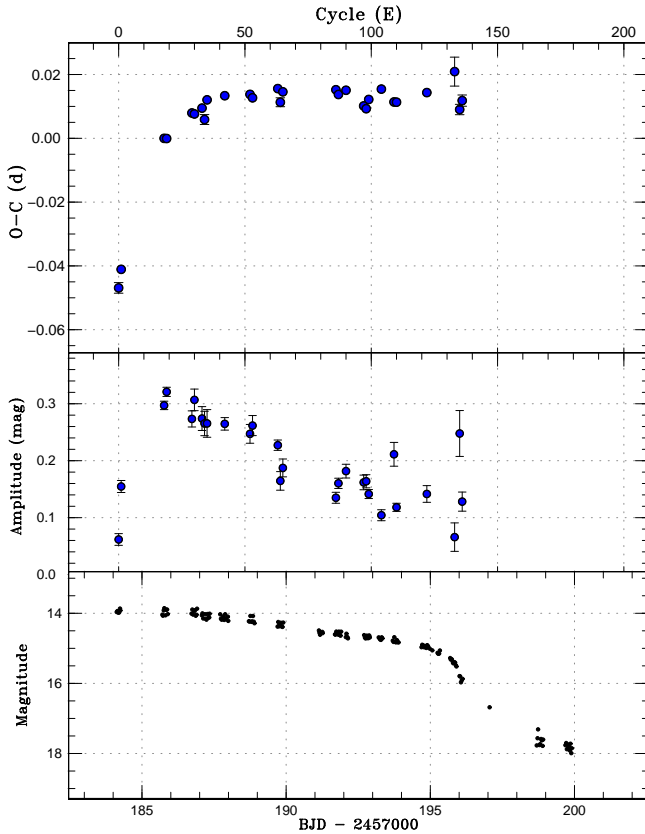


Fig. 27. $O - C$ diagram of superhumps in KK Tel (2015). (Upper:) $O - C$ diagram. We used a period of 0.08761 d for calculating the $O - C$ residuals. The superhump maxima up to $E = 19$ are stage A superhumps. (Middle:) Amplitudes of superhumps. The amplitudes were small around $E = 0$. It is worth noting that the epoch of the peak amplitude was earlier than the flattening of the $O - C$ diagram (pure stage B superhumps). (Lower:) Light curve. The data were binned to 0.029 d. The initial outburst detection was on BJD 2457182.7, 3 d before the start of our observation. It took 4 d for this object to fully develop stage B superhumps.

3.28 CI Ursae Majoris

This object was discovered by Goranskij (1972) and was confirmed to be an SU UMa-type dwarf nova by Nogami, Kato (1997). See Kato et al. (2014b) for more history. The 2016 outburst was detected at an unfiltered CCD magnitude of 14.4 on March 14 by M. Hiraga (vsnet-alert 19626). The outburst did not receive special attention since it faded rather quickly. The outburst, however, turned out to be a precursor based on the ASAS-SN observations (vsnet-alert 19626). Only single-night observations were obtained yielding the superhump maxima in table 27.

3.29 KS Ursae Majoris

KS UMa was originally discovered as an emission-line object (=SBS1017+533) (Balayan 1997). The SU UMa-type nature was confirmed during the 1998 outburst. Olech et al. (2003)

Table 26. Superhump maxima of KK Tel (2015)

E	max*	error	$O - C^\dagger$	N^\ddagger
0	57184.1440	0.0017	-0.0392	53
1	57184.2375	0.0009	-0.0336	34
18	57185.7679	0.0003	0.0038	20
19	57185.8554	0.0003	0.0035	26
29	57186.7396	0.0006	0.0093	31
30	57186.8269	0.0006	0.0088	19
33	57187.0915	0.0007	0.0100	41
34	57187.1755	0.0015	0.0062	31
35	57187.2693	0.0013	0.0121	42
42	57187.8839	0.0004	0.0119	25
52	57188.7604	0.0008	0.0102	37
53	57188.8469	0.0008	0.0089	26
63	57189.7259	0.0004	0.0096	50
64	57189.8093	0.0014	0.0051	15
65	57189.9001	0.0011	0.0082	19
86	57191.7406	0.0008	0.0043	27
87	57191.8267	0.0006	0.0026	38
90	57192.0909	0.0006	0.0033	48
97	57192.6992	0.0012	-0.0032	18
98	57192.7860	0.0007	-0.0043	19
99	57192.8765	0.0006	-0.0016	49
104	57193.3178	0.0011	0.0006	43
109	57193.7518	0.0013	-0.0045	17
110	57193.8394	0.0006	-0.0048	40
122	57194.8937	0.0011	-0.0044	38
133	57195.8640	0.0045	-0.0002	31
135	57196.0273	0.0016	-0.0125	44
136	57196.1177	0.0018	-0.0099	39

*BJD-2400000.

†Against max = 2457184.1833 + 0.087826E.

‡Number of points used to determine the maximum.

Table 27. Superhump maxima of CI UMa (2016)

E	max*	error	$O - C^\dagger$	N^\ddagger
0	57470.6381	0.0042	-0.0017	44
1	57470.7042	0.0017	0.0012	27
2	57470.7665	0.0019	0.0001	17
3	57470.8314	0.0021	0.0018	23
4	57470.8925	0.0037	-0.0004	26
5	57470.9551	0.0105	-0.0011	19

*BJD-2400000.

†Against max = 2457470.6398 + 0.063283E.

‡Number of points used to determine the maximum.

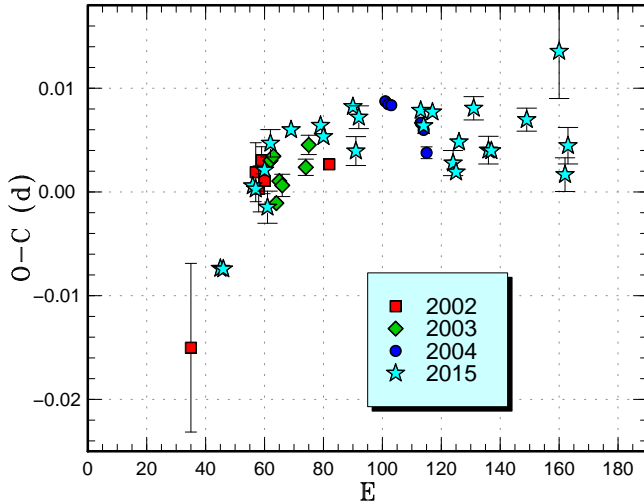


Fig. 28. Comparison of $O - C$ diagrams of KK Tel between different superoutbursts. A period of 0.08761 d was used to draw this figure. Approximate cycle counts (E) after the start of the superoutburst were used. In contrast to the diagram in Kato et al. (2009), the epochs were shifted by 24, 30 and 20 cycles for the 2002, 2003 and 2004 superoutbursts, respectively, to best match the 2015 result. These values suggests that either the true starts of the 2002–2004 superoutbursts were missed by 2–3 d, or the 2015 superoutburst started earlier than the others (such as a form of a precursor outburst).

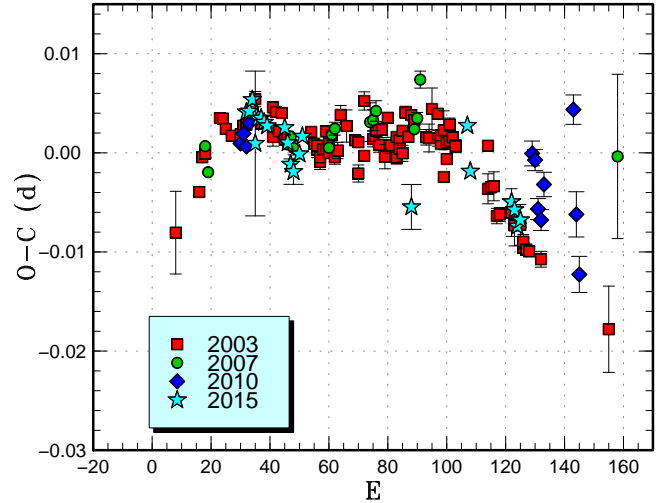


Fig. 29. Comparison of $O - C$ diagrams of KS UMa between different superoutbursts. A period of 0.07019 d was used to draw this figure. Approximate cycle counts (E) after the start of the superoutburst were used. Since the 2003 superoutburst was very well recorded, we shifted the others to fit the 2003 one. We had to shift 18, 30 and 32 cycles for the 2007, 2010 and 2015 data, respectively. Note that this treatment is different from the corresponding figure in Kato et al. (2009).

studied the 2003 superoutburst in detail. For more history, see Kato et al. (2009).

The 2015 superoutburst was detected by K. Hirosawa at $V=13.0$ on December 6. Subsequent observations detected superhumps (vsnet-alert 19330). The times of superhump maxima are listed in table 28. A comparison of $O - C$ diagrams suggests that we observed stage B (initial part) and stage C with a long gap in the observation between them.

3.30 MR Ursae Majoris

This object is a well-known SU UMa-type dwarf nova. See Kato et al. (2014b) for the history. The 2015 March superoutburst had a precursor outburst on March 7 (visually detected by E. Muylaert, vsnet-alert 18426). We observed on one night during the fading part of the precursor outburst and obtained two superhump maxima: BJD 2457091.4918(3) ($N=72$) and 2457091.5573(5) ($N=72$). Although these superhumps most likely correspond to stage A superhumps, the period was not meaningfully determined.

Recent outbursts of this object are listed in table 29. Although observations up to 2005 inferred a supercycle of approximately a year, recent observations suggest that the supercycles varied considerably and they can be as short as ~ 260 d.

Table 28. Superhump maxima of KS UMa (2015)

E	max*	error	$O - C^\dagger$	N^\ddagger
0	57364.2167	0.0002	0.0011	76
1	57364.2870	0.0003	0.0013	75
2	57364.3584	0.0007	0.0026	30
3	57364.4241	0.0073	-0.0018	34
4	57364.4968	0.0005	0.0008	89
5	57364.5671	0.0004	0.0010	94
6	57364.6368	0.0004	0.0006	94
7	57364.7067	0.0004	0.0004	93
13	57365.1276	0.0005	0.0007	52
14	57365.1963	0.0004	-0.0007	175
15	57365.2643	0.0005	-0.0028	181
16	57365.3337	0.0013	-0.0034	60
18	57365.4759	0.0003	-0.0015	75
19	57365.5479	0.0004	0.0004	69
56	57368.1378	0.0023	-0.0034	12
75	57369.4796	0.0007	0.0065	131
76	57369.5452	0.0007	0.0020	124
90	57370.5248	0.0008	0.0002	77
91	57370.5941	0.0005	-0.0005	77
92	57370.6627	0.0005	-0.0021	77
93	57370.7335	0.0007	-0.0014	55

*BJD-2400000.

† Against max = 2457364.2156 + 0.070100E.

‡ Number of points used to determine the maximum.

Table 29. List of recent outbursts of MR UMa

Year	Month	max*	magnitude	type	source
2002	3	52341	12.7	super	VSNET, AAVSO, Kato et al. (2009)
2003	3	52711	12.8	super	VSNET, AAVSO, Kato et al. (2009)
2004	3	53084	13.2	super	VSNET, AAVSO
2005	3	53440	12.9	super	VSNET, AAVSO
2005	4	53474	15.3	normal	AAVSO
2006	5	53870	12.8	super	VSNET, AAVSO
2006	11	54058	13.1 [†]	?	VSNET
2007	4	54205	12.5	super	VSNET, AAVSO, Kato et al. (2009)
2008	2	54503	12.7	super	VSNET, AAVSO
2008	6	54627	12.9	normal	VSNET, AAVSO
2009	4	54948	13.2	normal	VSNET, AAVSO
2010	4	55303	12.7	super	VSNET, AAVSO, Kato et al. (2010)
2011	5	55684	12.9	normal	VSNET, AAVSO
2012	6	56090	13.2	super	VSNET, AAVSO, Kato et al. (2013a)
2013	3	56354	13.2	super	VSNET, AAVSO, Kato et al. (2014b)
2013	11	56610	12.8	super?	AAVSO
2014	2	56708	13.3 [‡]	normal	AAVSO
2014	4	56770	13.5	normal	VSNET, AAVSO
2015	3	57094	12.8 [§]	super	VSNET, AAVSO, this paper

*JD–2400000.

[†]Single visual observation.[‡]Single CCD observation.[§]Refers to the main superoutburst.

3.31 NSV 2026

3.31.1 Introduction

This object was discovered as a variable star (=HV 6907) by Hoffleit (1935). The exact coordinates were given by Webbink et al. (2002). The object was identified to be a dwarf nova by a detection of an outburst by CRTS Mount Lemmon survey (=MLS101214:052959+184810) in 2010 (vsnet-alert 12503). It has been monitored for outbursts since then. Several outbursts were recorded by BAAVSS/AAVSO observers (since 2012) and by the MISA0 project (two outbursts in 2011 and one in 2012). There is an X-ray counterpart 1RXS J052954.9+184817. There were two past relatively long outbursts in 2012 February–March and 2014 February. Although time-resolved photometry was undertaken, no convincing superhumps were detected.¹²

3.31.2 2015 Superoutburst

The 2015 November bright outburst was detected by J. Shears on November 8 at an unfiltered CCD magnitude of 13.6 (vsnet-outburst 18873).¹³ This outburst turned out to be a superoutburst by the detection of superhumps (vsnet-alert 19258; figure 30). The times of superhump maxima are listed in table

Table 30. Superhump maxima of NSV 2026 (2015)

E	max*	error	$O - C^{\dagger}$	N^{\ddagger}
0	57335.4992	0.0004	–0.0002	90
1	57335.5709	0.0003	0.0017	91
42	57338.4311	0.0012	–0.0011	74
43	57338.5012	0.0009	–0.0008	93
44	57338.5715	0.0008	–0.0003	93
45	57338.6411	0.0009	–0.0005	77
46	57338.7098	0.0006	–0.0017	68
85	57341.4378	0.0014	0.0030	55
86	57341.5083	0.0009	0.0037	60
100	57342.4811	0.0015	–0.0011	34
101	57342.5511	0.0010	–0.0009	34
102	57342.6203	0.0008	–0.0016	34

*BJD–2400000.

[†]Against max = 2457335.4994 + 0.069829*E*.[‡]Number of points used to determine the maximum.¹²<<http://www.britastro.org/vss/NSV2026.pdf>>.¹³See also <<http://www.britastro.org/vss/NSV2026.pdf>> for the BAAVSS campaign.

30. Although there was an apparent stage transition (vsnet-alert 19282), we gave a globally averaged period due to insufficient observations.

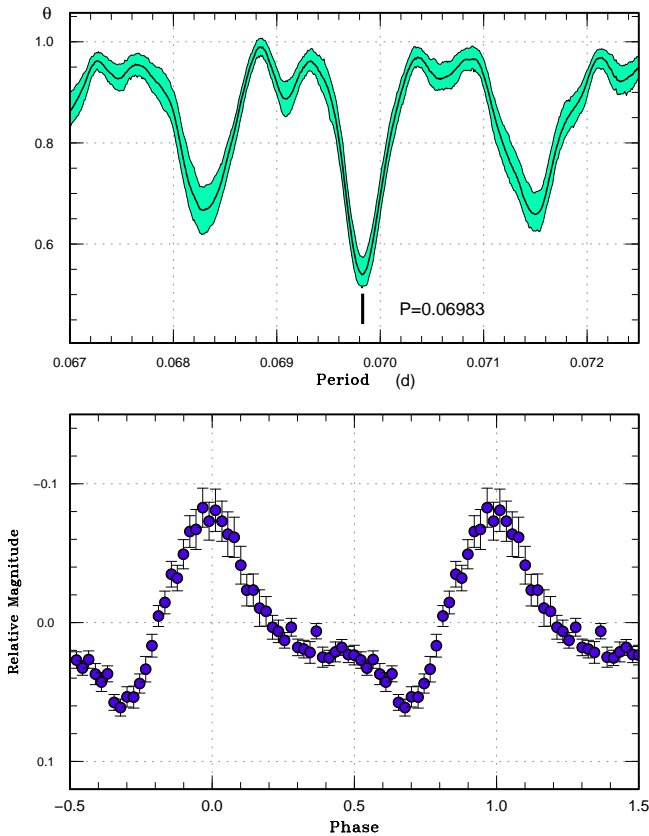


Fig. 30. Superhumps in NSV 2026 (2015). (Upper): PDM analysis. (Lower): Phase-averaged profile.

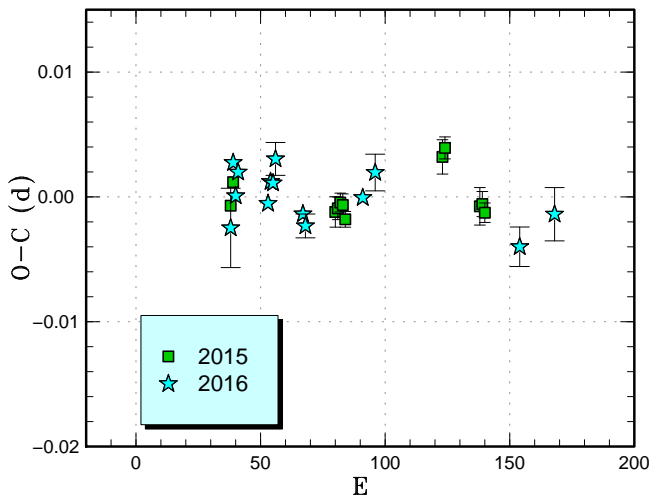


Fig. 31. Comparison of $O - C$ diagrams of NSV 2026 between different superoutbursts. A period of 0.06982 d was used to draw this figure. Approximate cycle counts (E) after the starts of the outbursts were used. The start of the 2016 outburst refers to the precursor outburst. Since the start of the 2015 outburst was not well constrained, the $O - C$ curve was shifted as in the 2016 one.

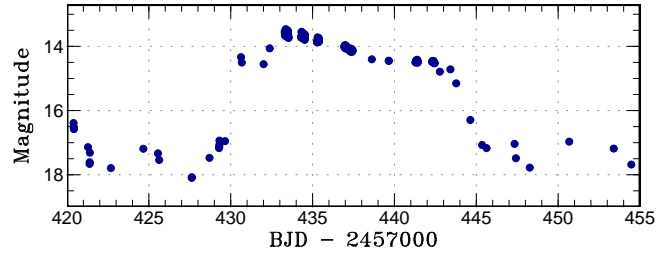


Fig. 32. Light curve of the superoutburst of NSV 2026 (2016). The data were binned to 0.01 d. The initial precursor part of the outburst and subsequent rise to the superoutburst maximum are clearly depicted. The widths of the light curve mainly reflect the amplitudes of superhumps.

Table 31. Superhump maxima of NSV 2026 (2016)

E	max*	error	$O - C^\dagger$	N^\ddagger
0	57433.2811	0.0032	-0.0033	54
1	57433.3561	0.0002	0.0019	187
2	57433.4233	0.0002	-0.0007	286
3	57433.4950	0.0002	0.0012	159
15	57434.3303	0.0005	-0.0010	78
16	57434.4019	0.0002	0.0008	197
17	57434.4716	0.0004	0.0007	145
18	57434.5433	0.0013	0.0026	33
29	57435.3070	0.0005	-0.0015	104
30	57435.3758	0.0010	-0.0024	57
53	57436.9839	0.0007	0.0004	145
58	57437.3351	0.0015	0.0025	66
116	57441.3787	0.0016	-0.0020	50
130	57442.3588	0.0021	0.0009	196

*BJD-2400000.

† Against max = 2457433.2844 + 0.069795 E .

‡ Number of points used to determine the maximum.

3.31.3 2016 Superoutburst

The 2016 superoutburst was detected by J. Shears on February 12 at an unfiltered CCD magnitude of 14.4 (BAAVSS alert 4308). Subsequent observations detected superhumps (vsnet-alert 19485, 19498, 19509). The outburst started with a precursor (figure 32). The times of superhump maxima are listed in table 31. Although the initial part of the data ($E \leq 58$) most likely refers to stage B, we gave a globally averaged period since the observations were not sufficient to determine P_{dot} for stage B. A comparison of the $O - C$ diagrams (figure 31) suggests that the later parts of 2015 and 2016 observations were likely stage C.

3.31.4 Interpretation

Although the 2012 and 2014 outbursts were not very well observed, the lack of prominent superhumps would suggest that these outbursts may have been long, normal outbursts as seen

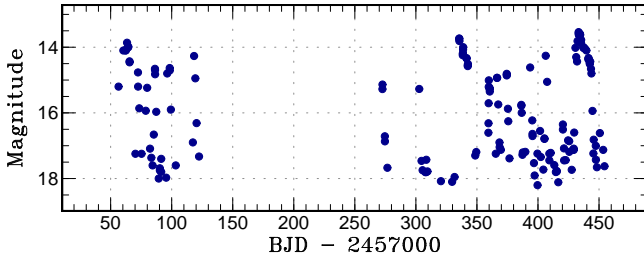


Fig. 33. Long-term curve of NSV 2026 from AAVSO observations. The data were binned to 0.1 d.

in TU Men (Warner 1995b; Bateson et al. 2000), V1006 Cyg (Kato et al. 2016b) and potentially NY Ser (Pavlenko et al. 2014). The big difference between NSV 2026 and these objects is the orbital period – TU Men, V1006 Cyg and NY Ser have long orbital periods in or above the period gap, while NSV 2026 is not. If the presence of long normal outbursts is due to the difficulty in attaining the 3:1 resonance, it would be easy to understand why most objects showing this behavior have long- P_{orb} and the case of NSV 2026 might require another explanation. Since superhump amplitudes became significantly smaller in the 2016 superoutburst in the late phase, it may just have been that the 2012 and 2014 observations did not record the phases with large-amplitude superhumps. Confirmation of superhumps in every long outburst of NSV 2026 would be a task to check these possibilities.

AAVSO observations of this object show a relatively regular supercycle pattern: normal outbursts with recurrence time of 6–14 d and the supercycle length of ~ 95 d (figure 33). As judged from this light curve, NSV 2026 looks like to be a fairly normal SU UMa-type dwarf nova with frequent outbursts.

3.32 ASASSN-13ah

This object was detected as a transient on 2013 April 23 by the ASAS-SN team (Shappee et al. 2013). The object was confirmed to be a dwarf nova in outburst by spectroscopy (Shappee et al. 2013). Although there were observations during the 2015 outburst (cf. vsnet-alert 18619) by KU team, the observations were insufficient to confirm superhumps.

The 2016 outburst was detected by the ASAS-SN team on February 11 at $V=16.4$. Subsequent observations detected superhumps (vsnet-alert 19480, 19497; figure 34). The times of superhump maxima are listed in table 32.

3.33 ASASSN-13ak

This object was detected as a transient at $V=15.4$ on 2013 May 23 by the ASAS-SN team (Stanek et al. 2013). The MASTER network also detected this outburst (Shurpakov et al. 2013). There is an X-ray counterpart (1RXS J174827.1+505053).

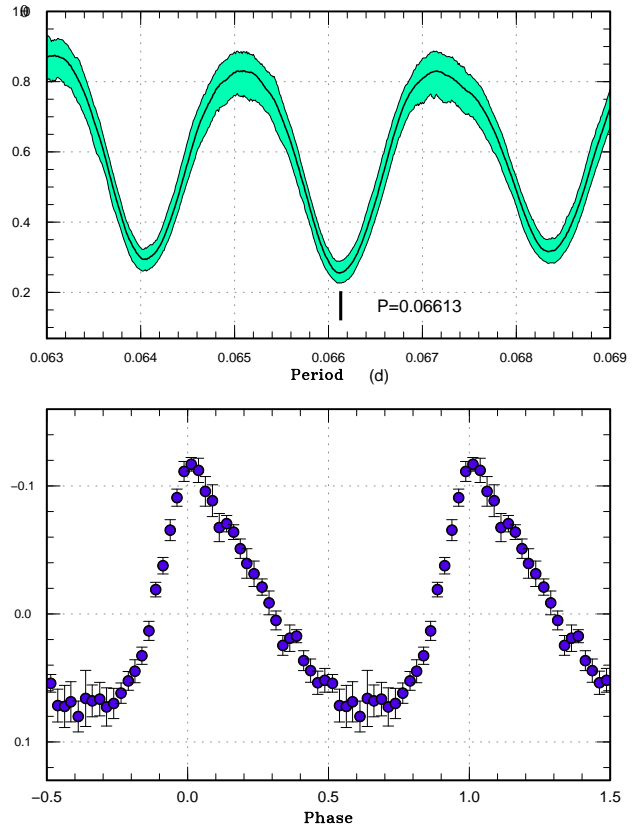


Fig. 34. Superhumps in ASASSN-13ah (2016). (Upper): PDM analysis. The alias selection was based on $O - C$ analysis. (Lower): Phase-averaged profile.

Table 32. Superhump maxima of ASASSN-13ah (2016)

E	max*	error	$O - C^\dagger$	N^\ddagger
0	57431.5184	0.0004	0.0006	67
1	57431.5839	0.0003	-0.0001	65
2	57431.6495	0.0003	-0.0006	67
3	57431.7162	0.0004	0.0000	62
31	57433.5679	0.0007	-0.0003	62
32	57433.6340	0.0010	-0.0003	56
33	57433.7011	0.0011	0.0006	64

*BJD-2400000.

† Against max = 2457431.5178 + 0.066141E.

‡ Number of points used to determine the maximum.

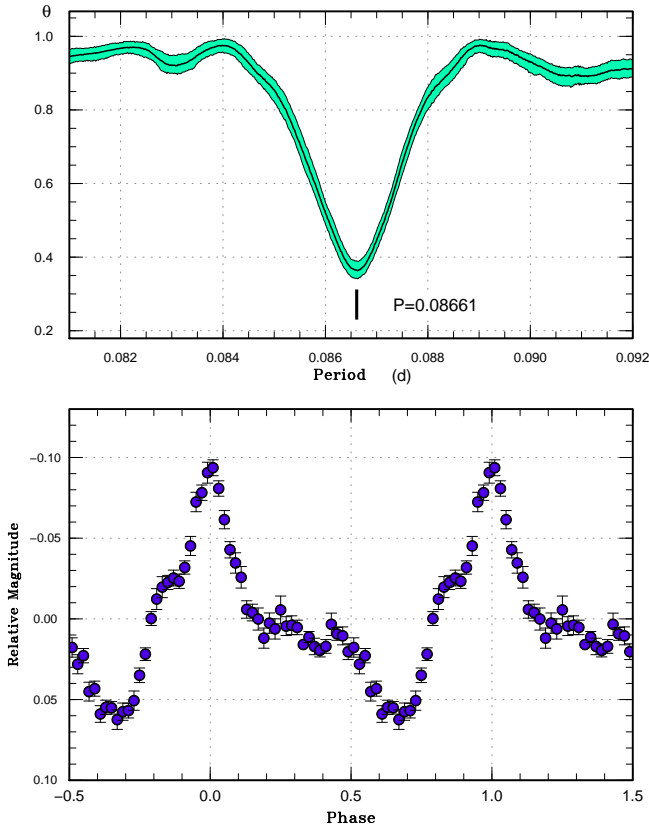


Fig. 35. Superhumps in ASASSN-13ak (2015). (Upper): PDM analysis. (Lower): Phase-averaged profile.

There have been five outbursts (including the 2015 one) in the CRTS data. The SDSS colors suggested a short orbital period (vsnet-alert 15742)

The 2015 outburst was detected by E. Muylaert on May 8 at an unfiltered CCD magnitude of 15.1 (vsnet-alert 18607). This object was confirmed to be an SU UMA-type dwarf nova by the detection of superhumps (vsnet-alert 18612, 18613, 18615, 18624; figure 35). The times of superhump maxima are listed in table 33. The superhump stage is unknown.

3.34 ASASSN-13az

This object was detected as a transient at $V=14.4$ on 2013 July 1 by the ASAS-SN team (vsnet-alert 15892). Although the object was identified with a 20.8 mag (B_J) star in the USNO-B1.0 catalog, this object was later found to be unrelated by spectroscopy (cf. vsnet-alert 19555). Although there was a 14.858 mag detection close to the ASAS-SN position in URAT1 catalog (Zacharias et al. 2015), the identification is unclear. The object may have been recorded in outburst. If this identification is confirmed, the coordinates are $18^{\text{h}}42^{\text{m}}58^{\text{s}}.21, +73^{\circ}42'28''.4$.

The 2016 outburst was detected by the ASAS-SN team on March 1 at $V=14.42$. Subsequent observations detected

Table 33. Superhump maxima of ASASSN-13ak (2015)

E	max*	error	$O - C^\dagger$	N^\ddagger
0	57154.6695	0.0005	0.0001	63
9	57155.4500	0.0003	0.0007	187
10	57155.5365	0.0003	0.0005	195
11	57155.6226	0.0003	-0.0001	114
18	57156.2282	0.0003	-0.0010	181
20	57156.3995	0.0012	-0.0030	56
21	57156.4901	0.0009	0.0009	77
22	57156.5767	0.0009	0.0009	73
32	57157.4444	0.0008	0.0020	62
33	57157.5289	0.0005	-0.0002	84
34	57157.6148	0.0006	-0.0009	71

*BJD-2400000.

† Against max = 2457154.6694 + 0.086655 E .

‡ Number of points used to determine the maximum.

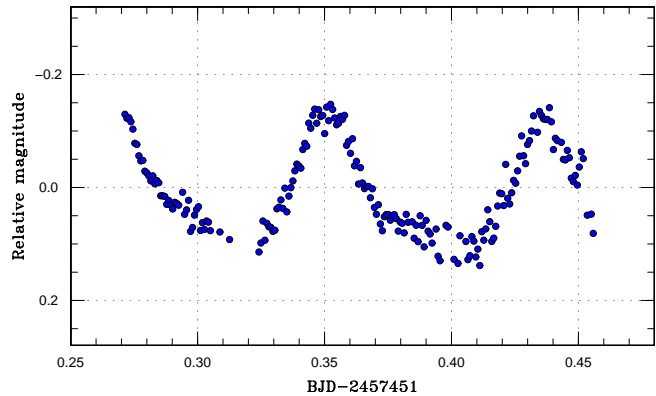


Fig. 36. Superhumps in ASASSN-13az (2016).

superhumps (vsnet-alert 19554; figure 36). Two superhump maxima were recorded: BJD 2457451.3514(3) ($N=77$) and 2457451.4374(5) ($N=61$). The best superhump period with the PDM method is 0.0843(3) d.

3.35 ASASSN-14ca

This object was detected as a transient at $V=15.5$ on 2014 June 7 by the ASAS-SN team (Davis et al. 2014). The object was initially reported as an unusual long-lived transient from a red source. Davis et al. (2014) also reported an outburst in 2005 July in the CRTS data, which lasted at least for 6 d. Upon this report, Cao, Kulkarni (2014) examined the PTF/iPTF archival data and found another brightening in 2009 November, which lasted at least for 15 d. Cao, Kulkarni (2014) reported that the color temperature is consistent with a Mira star. Prieto et al. (2014) reported a spectrum taken on June 9 and it had a strong blue continuum, Balmer lines in absorption, $H\alpha$ line in double-

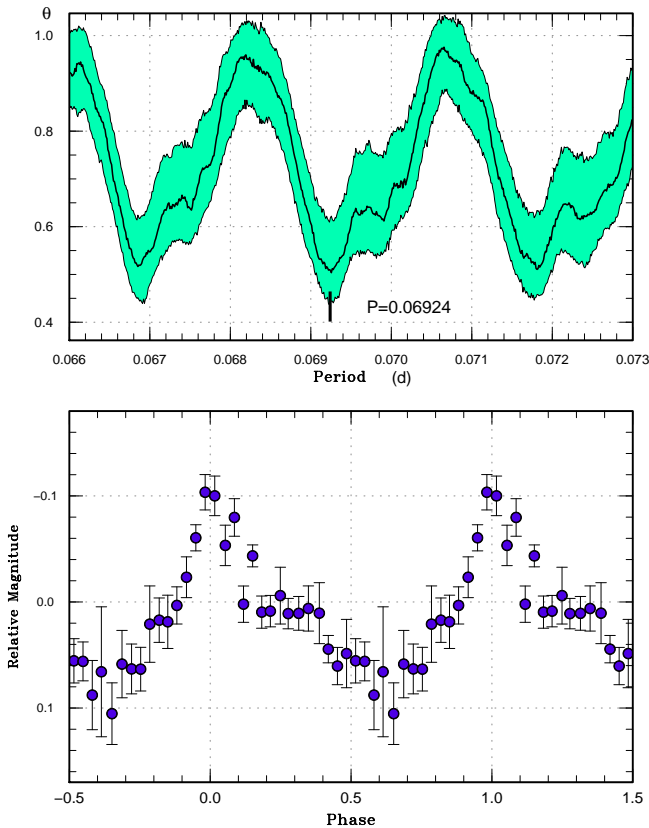


Fig. 37. Superhumps in ASASSN-14ca (2015). (Upper): PDM analysis. The alias selection was based on the $O - C$ analysis. (Lower): Phase-averaged profile.

Table 34. Superhump maxima of ASASSN-14ca (2015)

E	max*	error	$O - C^\dagger$	N^\ddagger
0	57219.5689	0.0009	-0.0000	50
28	57221.5070	0.0017	0.0002	64
29	57221.5758	0.0011	-0.0002	59

*BJD-2400000.

† Against max = 2457219.5689 + 0.069210*E*.

‡ Number of points used to determine the maximum.

peaked emission and HeII 468.6nm in emission. The object was confirmed to be a dwarf nova in outburst. The object was independently suggested to be a dwarf nova (vsnet-alert 17369) and D. Denisenko detected an outburst in 2009 November in the MASTER network observations, the same one reported in Cao, Kulkarni (2014). The $g=20.6$ SDSS counterpart may be an unrelated unresolved red star.

The 2015 outburst was detected by the ASAS-SN team on July 7 at $V=15.53$ (cf. vsnet-alert 18833). Subsequent observations detected superhumps (vsnet-alert 18852; figure 37). The times of superhump maxima are listed in table 34. The alias selection was based on the $O - C$ analysis of the second night.

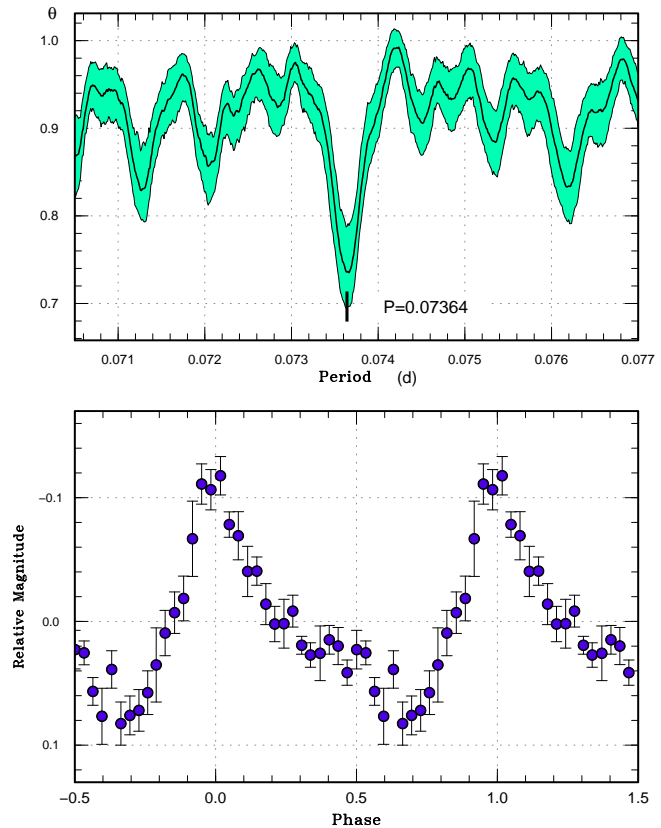


Fig. 38. Superhumps in ASASSN-14dh (2015). (Upper): PDM analysis. (Lower): Phase-averaged profile.

3.36 ASASSN-14dh

This object was detected as a transient at $V=15.93$ on 2014 June 27 by the ASAS-SN team. There were past known outbursts in the CRTS data and ASAS-3 data (see also vsnet-alert 17424, 18823).

The 2015 outburst was detected by ASSN-SN on July 2 at $V=13.3$. Subsequent observations detected superhumps (vsnet-alert 18840, 18842; figure 38). The times of superhump maxima are listed in table 35. The maxima for $E \leq 89$ corresponds to superhumps after the rapid fading. This outburst was observed only during the late phase and we probably observed only stage C superhumps.

3.37 ASASSN-14fz

This object was detected as a transient at $V=15.18$ on 2014 August 20 by the ASAS-SN team. The light curve of the 2014 outburst was suggestive of an SU UMa-type precursor outburst (vsnet-alert 17647).

The 2015 outburst was detected by the ASAS-SN team on May 27 at $V=14.21$. Subsequent observations detected superhumps (vsnet-alert 18672, 18685; figure 39). The times of su-

Table 35. Superhump maxima of ASASSN-14dh (2015)

E	max*	error	$O - C^\dagger$	N^\ddagger
0	57212.2003	0.0003	0.0016	153
1	57212.2739	0.0003	0.0015	151
28	57214.2575	0.0024	-0.0029	88
35	57214.7765	0.0009	0.0007	28
36	57214.8489	0.0008	-0.0005	30
49	57215.8065	0.0006	-0.0002	44
50	57215.8824	0.0010	0.0021	24
62	57216.7595	0.0017	-0.0043	29
63	57216.8343	0.0012	-0.0031	40
64	57216.9116	0.0017	0.0005	12
89	57218.7578	0.0072	0.0060	31
90	57218.8289	0.0026	0.0035	40
91	57218.8942	0.0064	-0.0048	20

*BJD-2400000.

 † Against max = 2457212.1988 + 0.073629 E . ‡ Number of points used to determine the maximum.**Table 36.** Superhump maxima of ASASSN-14fz (2015)

E	max*	error	$O - C^\dagger$	N^\ddagger
0	57171.7282	0.0043	-0.0063	9
1	57171.8107	0.0005	-0.0020	15
13	57172.7518	0.0013	0.0019	14
26	57173.7685	0.0007	0.0034	17
39	57174.7837	0.0008	0.0033	17
52	57175.7996	0.0023	0.0040	11
64	57176.7362	0.0021	0.0034	13
77	57177.7435	0.0024	-0.0045	17
90	57178.7621	0.0017	-0.0012	18
103	57179.7765	0.0016	-0.0020	17

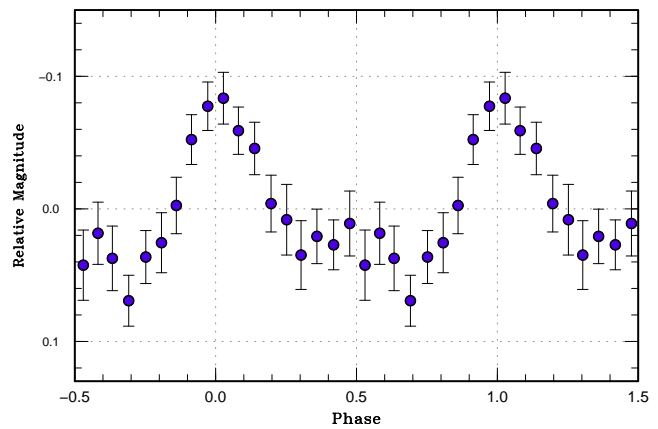
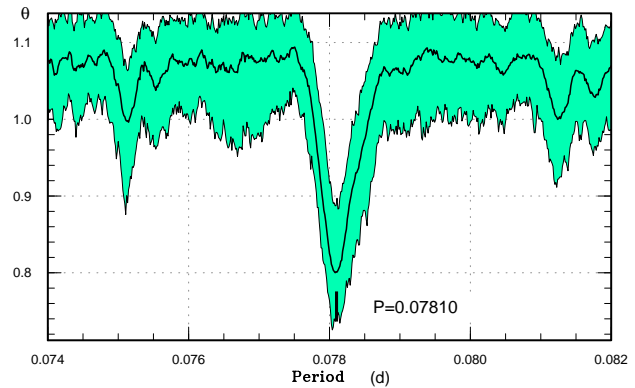
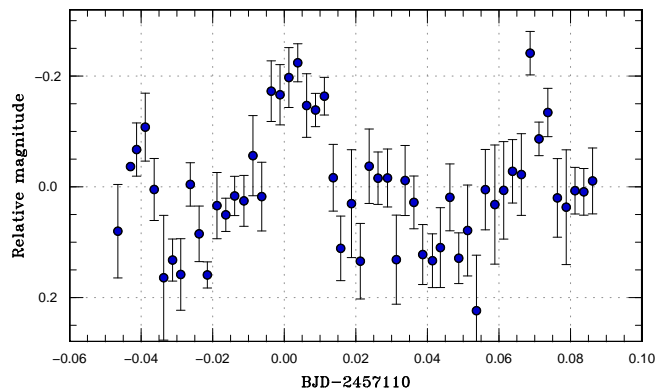
*BJD-2400000.

 † Against max = 2457171.7345 + 0.078097 E . ‡ Number of points used to determine the maximum.

perhump maxima are listed in table 36. The epochs $E \leq 1$ correspond to stage A superhumps. It was not clear whether there was a stage transition in the later part of the outburst, and we listed a global P_{dot} in table 3.

3.38 ASASSN-14le

This object was detected as a transient at $V=16.4$ on 2014 November 29 by the ASAS-SN team. Observations on December 5 detected superhumps (figure 40). The times of maxima are BJD 2456997.0031(12) ($N=135$) and 2456997.0719(20) ($N=113$). The superhump period was estimated to be 0.068(1) d using these times of maxima and with the PDM method.

**Fig. 39.** Superhumps in ASASSN-14fz during the plateau phase (2015). (Upper): PDM analysis. (Lower): Phase-averaged profile.**Fig. 40.** Superhumps in ASASSN-14le (2014). The data were binned to 0.0025 d.

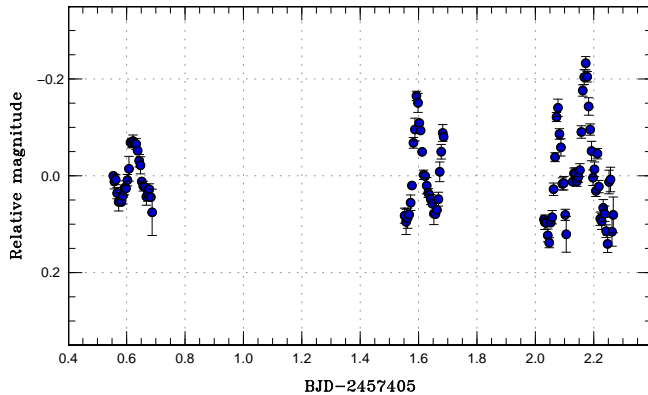


Fig. 41. Growing superhumps in ASASSN-15cl (2016). The data were binned to 0.005 d.

3.39 ASASSN-15cl

This object was detected as a transient at $V=13.9$ on 2015 February 1 by the ASAS-SN team. The object was found to be already in outburst at $V=14.8$ on January 31. There were three past outbursts reaching $V=13.3$ in the ASAS-3 data (cf. vsnet-alert 18256). Although the 2015 outburst was observed on two nights by S. Kiyota, no definite superhump signal was detected.

The 2016 outburst was detected by the ASAS-SN team at $V=13.8$ on January 17 (vsnet-alert 19421). Subsequent observations detected long-period superhumps (vsnet-alert 19427, 19431). The superhumps were still growing (see also figure 41) and the period then dramatically shortened (vsnet-alert 19431, 19436, 19442). The times of superhump maxima are listed in table 37. The behavior was very similar to another long- P_{orb} system V1006 Cyg (Kato et al. 2016b) and we identified $E \leq 22$ to be stage A superhumps (figure 43). The sharp decrease in the period was likely due to stage B to C transition around $E=33$. The periods given in table 3 refers to these period identifications. The mean profile excluding stage A superhumps is shown in figure 42.

Kato et al. (2016b) discussed that the long duration of the growing stage of superhumps in a long- P_{orb} system reflects the slow growth rate of the 3:1 resonance when the mass ratio is close to the stability limit of the 3:1 resonance (see also subsection 4.4). Yet another example ASASSN-15cl also supports that this mechanism is likely working in many long- P_{orb} systems. Future determination of the orbital period in this system will allow the measurement of q using the period of stage A superhumps in this study. Such a measurement will test the hypothesis whether the system has a borderline q .

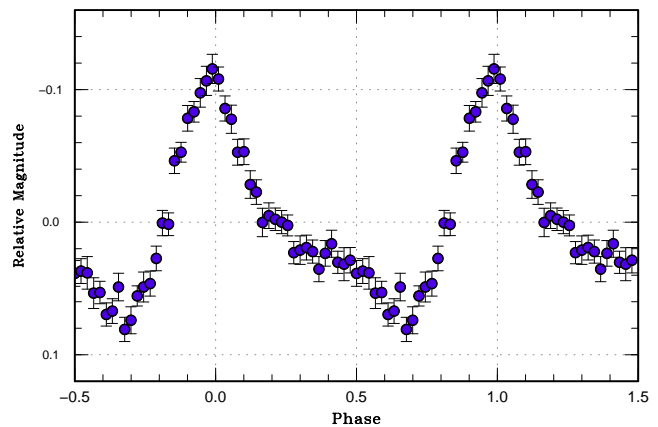
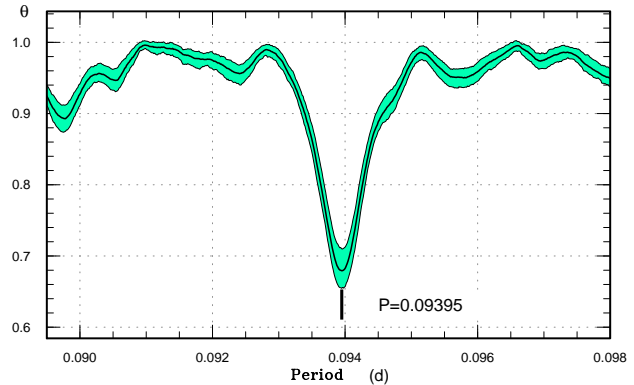


Fig. 42. Superhumps in ASASSN-15cl (2016). The data after BJD 2457407.5 (excluding stage A) were used. (Upper): PDM analysis. (Lower): Phase-averaged profile.

3.40 ASASSN-15cy

This object was detected as a transient at $V=14.6$ on 2015 February 16 by the ASAS-SN team. The coordinates are $08^{\text{h}} 11^{\text{m}} 50^{\text{s}}.53$, $-12^{\circ} 27' 51''.5$ (based on S. Kiyota's image on February 20, UCAC4 reference stars). There is no quiescent counterpart in available catalogs.

Up to February 20, the object showed only little variations. On February 22 (6 d after the initial detection), it showed prominent superhumps with a very short (~ 0.050 d) period (vsnet-alert 18326, 18327). There were long gaps in the observation and the next continuous run was on February 28. There was only one superhump detection on February 26. Using the period determined from the continuous run on February 22 and the single epoch on February 26, we have tried several possible periods and obtained the smallest $O - C$ scatter using a period of 0.04996 d up to February 28. The cycle counts and $O - C$ values assuming this period is shown in table 38. The mean superhump profile is shown in figure 44. We should note, however, this choice may not be correct, particularly if there was strong period variation when there were gaps in the observation. The times for $E \geq 161$ were uncertain since the amplitudes of

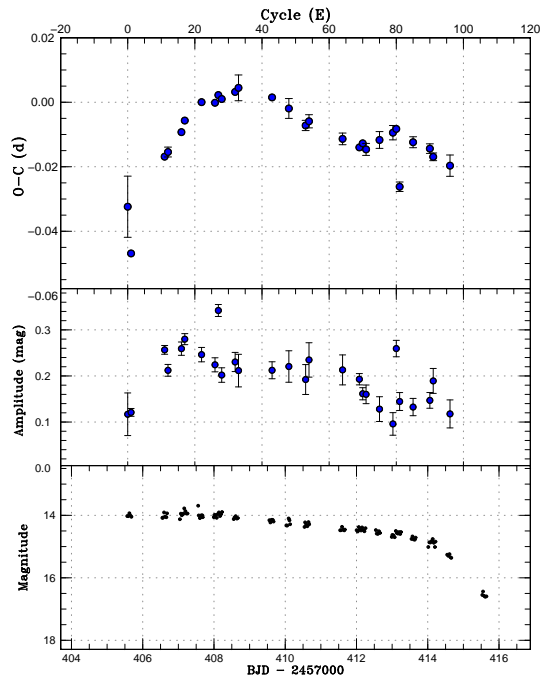


Fig. 43. $O - C$ diagram of superhumps in ASASSN-15cl (2016). (Upper:) $O - C$ diagram. We used a period of 0.09423 d for calculating the $O - C$ residuals. The superhump maxima up to $E=22$ are stage A superhumps, maxima between $E=22$ and $E=33$ are identified as stage B superhumps. After this, the period decreased to a constant one (stage C superhumps). (Middle:) Amplitudes of superhumps. The amplitudes were small around $E = 0$. (Lower:) Light curve. The data were binned to 0.031 d.

superhumps were already small (~ 0.07 mag) and the object already faded close to 16 mag. The phase jump between $E = 122$ and $E = 161$ was too large to be identified as stage B-C transition. Although there may have been a true phase jump, the conclusion is unclear due to the poor quality of the data around these epochs.

The resultant superhump period suggests that this object belong to EI Psc-type objects with compact secondaries having an evolved core (cf. T. Ohshima et al. in preparation). Since the quiescent brightness is below the limit of photographic surveys, the outburst amplitude is likely larger than 6 mag. This object shares properties with CSS J174033.5+414756 ($P_{\text{orb}}=0.04505$ d, outburst amplitude ~ 6.7 mag; Kato et al. 2014b; Kato et al. 2015a; T. Ohshima et al. in preparation; Prieto et al. 2013; Nesci et al. 2013), which is classified as a WZ Sge-type object in Kato (2015). Although a period of 0.0494(2) d was inferred from the observations on the first two nights (cf. vsnet-alert 18327), this period is uncertain due to the low amplitude (less than 0.02 mag) and limited coverage.

3.41 ASASSN-15dh

This object was detected as a transient at $V=15.2$ on 2015 February 12 by the ASAS-SN team. There was another outburst

Table 37. Superhump maxima of ASASSN-15cl (2016)

E	max*	error	$O - C^\dagger$	N^\ddagger
0	57405.5459	0.0095	-0.0218	21
1	57405.6256	0.0008	-0.0363	44
11	57406.5979	0.0004	-0.0063	47
12	57406.6936	0.0015	-0.0048	19
16	57407.0767	0.0006	0.0014	150
17	57407.1745	0.0005	0.0050	176
22	57407.6513	0.0007	0.0107	30
26	57408.0281	0.0008	0.0105	167
27	57408.1247	0.0005	0.0129	164
28	57408.2177	0.0010	0.0117	117
32	57408.5968	0.0010	0.0139	28
33	57408.6923	0.0040	0.0152	11
43	57409.6316	0.0010	0.0122	32
48	57410.0993	0.0031	0.0088	106
53	57410.5652	0.0016	0.0036	27
54	57410.6608	0.0020	0.0049	23
64	57411.5976	0.0018	-0.0006	32
69	57412.0661	0.0007	-0.0032	220
70	57412.1616	0.0010	-0.0019	161
71	57412.2539	0.0019	-0.0038	73
75	57412.6338	0.0026	-0.0009	33
79	57413.0130	0.0022	0.0014	130
80	57413.1084	0.0009	0.0026	156
81	57413.1847	0.0015	-0.0153	173
85	57413.5754	0.0017	-0.0015	30
90	57414.0446	0.0015	-0.0035	175
91	57414.1363	0.0012	-0.0060	132
96	57414.6047	0.0033	-0.0087	31

*BJD-2400000.

† Against max = 2457405.5677 + 0.094226E.

‡ Number of points used to determine the maximum.

on October 29 at $V=15.03$ detected by the ASAS-SN team (see also vsnet-alert 19228). Subsequent observations detected superhumps (vsnet-alert 19218, 19228; figure 45). The times of superhump maxima are listed in table 39. There was probably a stage transition at around $E=11$. We were not able to determine the type of transition. In table 3, we listed a global value.

3.42 ASASSN-15dp

This object was detected as a transient at $V=14.1$ on 2015 February 22 by the ASAS-SN team. The object was recorded in outburst in 1989 at a red magnitude of 15.2 in GSC 2.3 (GSC2.3NCCX024953). The quiescent magnitude was 19.4(4) (green magnitude, Initial Gaia Source List).

Early observations soon detected superhumps (vsnet-alert 18350). It soon became apparent that early observations

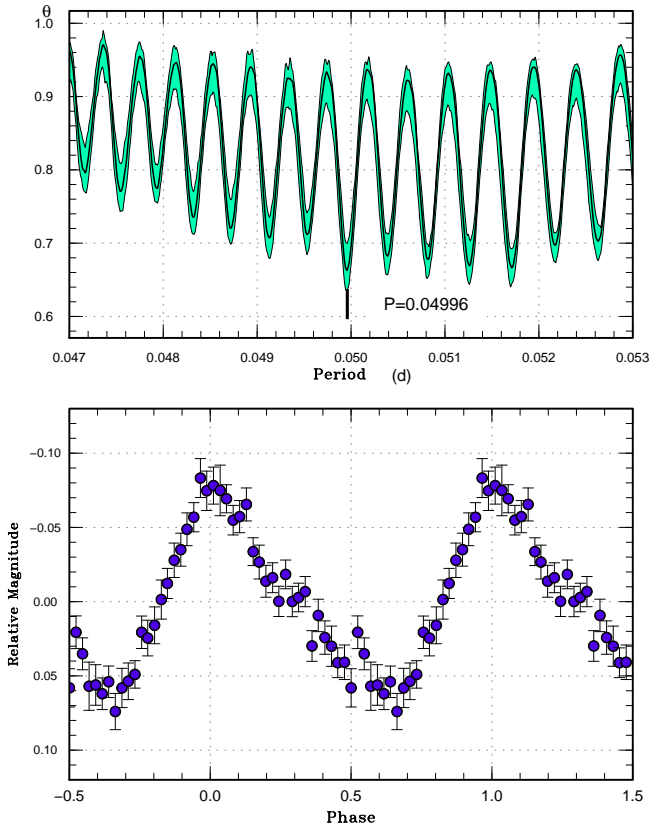


Fig. 44. Superhumps in ASASSN-15cy between BJD 2457076 and 2457083 (2015). (Upper): PDM analysis. The alias selection was based on the continuous data on BJD 2457076 and the selection of the cycle counts to minimize the scatter in the $O - C$ diagram. (Lower): Phase-averaged profile.

Table 38. Superhump maxima of ASASSN-15cy (2015)

E	max*	error	$O - C^\dagger$	N^\ddagger
0	57076.3205	0.0019	-0.0024	61
1	57076.3693	0.0004	-0.0034	115
2	57076.4190	0.0004	-0.0035	114
3	57076.4685	0.0004	-0.0038	115
4	57076.5188	0.0004	-0.0033	115
5	57076.5670	0.0018	-0.0048	55
66	57079.6148	0.0007	0.0063	13
86	57080.6117	0.0016	0.0076	12
120	57082.3159	0.0018	0.0193	115
121	57082.3637	0.0009	0.0172	115
122	57082.4132	0.0013	0.0170	114
161	57084.3262	0.0019	-0.0115	115
162	57084.3724	0.0024	-0.0151	115
163	57084.4177	0.0025	-0.0195	113

*BJD-2400000.

† Against max = 2457076.3230 + 0.049781E.

‡ Number of points used to determine the maximum.

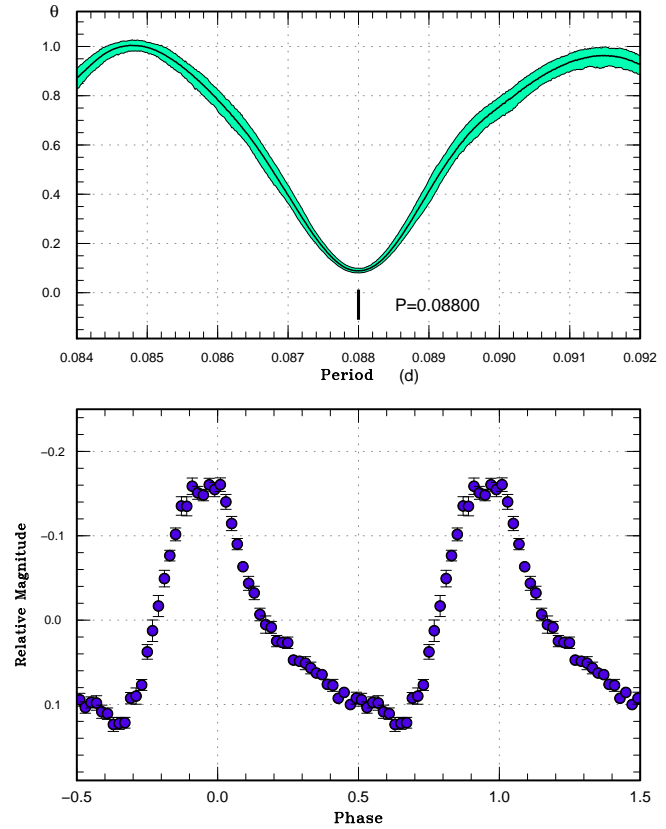


Fig. 45. Superhumps in ASASSN-15dh (2015). (Upper): PDM analysis. (Lower): Phase-averaged profile.

Table 39. Superhump maxima of ASASSN-15dh (2015)

E	max*	error	$O - C^\dagger$	N^\ddagger
0	57328.2626	0.0003	-0.0014	78
1	57328.3508	0.0003	-0.0012	77
2	57328.4407	0.0003	0.0007	79
3	57328.5281	0.0004	0.0001	81
11	57329.2343	0.0007	0.0022	52
12	57329.3226	0.0003	0.0024	81
18	57329.8467	0.0003	-0.0015	74
19	57329.9348	0.0004	-0.0014	88

*BJD-2400000.

† Against max = 2457328.2639 + 0.088014E.

‡ Number of points used to determine the maximum.

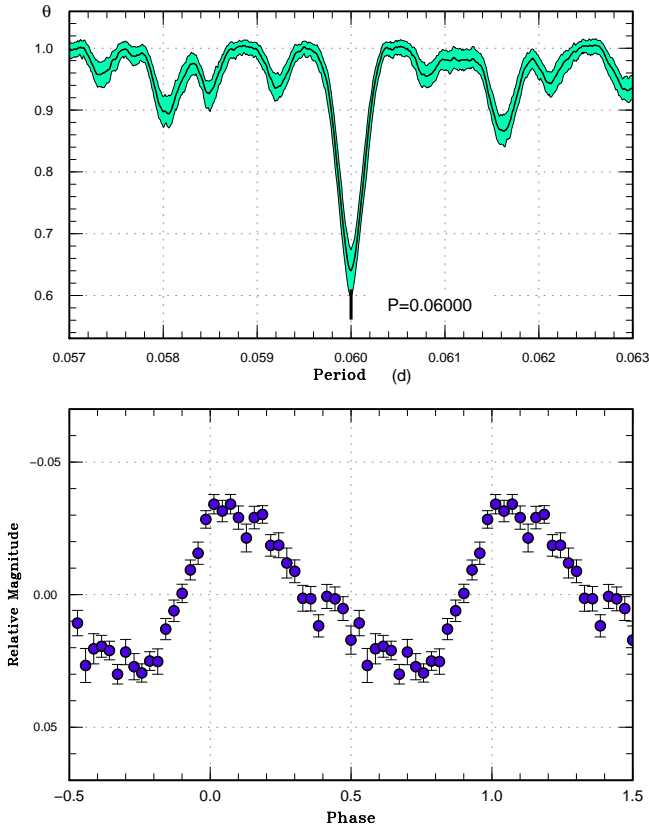


Fig. 46. Superhumps in ASASSN-15dp after BJD 2457084 (2015). (Upper): PDM analysis. (Lower): Phase-averaged profile.

recorded the final part of the precursor outburst with a relatively rapid fading, and stage A superhumps were observed on the first two nights (vsnet-alert 18363, 18417). Figure 46 shows the profile of stage B superhumps. The times of superhump maxima are listed in table 40. The maxima for $E \leq 24$ correspond to stage A superhumps. There was no observed transition to stage C superhumps.

The object entered the rapid fading stage on March 11, 17 d after the initial outburst detection. It took ~ 8 d to develop stage B superhumps, which is relatively long. It was also somewhat unusual that the fading part of the precursor outburst was observed even 5 d after the initial detection. The lack of stage C superhumps and small P_{dot} are usual characteristics of WZ Sge-type dwarf novae (Kato 2015). Since the system has a relatively long superhump period, there could even be a chance of a candidate period bouncer, if our measurement of P_{dot} is correct. Since the present observations lacks the earliest data and post-outburst data, this object should require further observation on the next outburst occasion.

Table 40. Superhump maxima of ASASSN-15dp (2015)

E	max*	error	$O - C^\dagger$	N^\ddagger
0	57081.3059	0.0013	-0.0242	61
1	57081.3670	0.0019	-0.0233	61
2	57081.4320	0.0013	-0.0185	61
23	57082.7238	0.0014	0.0093	61
24	57082.7780	0.0029	0.0034	30
49	57084.2959	0.0003	0.0165	54
50	57084.3580	0.0004	0.0185	44
66	57085.3171	0.0009	0.0145	64
67	57085.3733	0.0011	0.0106	67
84	57086.3971	0.0012	0.0112	51
115	57088.2596	0.0008	0.0078	91
116	57088.3171	0.0006	0.0052	186
117	57088.3781	0.0007	0.0059	170
132	57089.2793	0.0008	0.0043	62
133	57089.3371	0.0016	0.0020	59
134	57089.3971	0.0017	0.0018	61
150	57090.3488	0.0009	-0.0096	42
151	57090.4124	0.0009	-0.0061	58
165	57091.2587	0.0012	-0.0025	61
166	57091.3161	0.0010	-0.0053	62
167	57091.3789	0.0013	-0.0027	62
199	57093.2971	0.0018	-0.0105	61
200	57093.3595	0.0031	-0.0083	61

*BJD-2400000.

† Against max = 2457081.3276 + 0.060201E.

‡ Number of points used to determine the maximum.

3.43 ASASSN-15dr

This object was detected as a transient at $V=14.9$ on 2015 February 22 by the ASAS-SN team. On February 28, the object started to show growing superhumps (vsnet-alert 18366). Stable superhumps were observed later (vsnet-alert 18384; figure 47). The times of superhump maxima are listed in table 41. Although the times for $E \leq 2$ apparently correspond to stage A superhumps, the period of stage A superhump could not be determined due to the lack of the data. The photometric quality for this object was not good enough due to its faintness (16.3 mag on February 26, which was much fainter than the ASAS-SN report).

3.44 ASASSN-15ea

This object was detected as a transient at $V=16.1$ on 2015 February 25 by the ASAS-SN team. There was one previous outburst reaching 14.15 mag on 2006 October 4 in the CRTS data. Although T. Vanmunster reported the detection of superhumps (vsnet-alert 18357), this period was later rejected (vsnet-alert 18373).

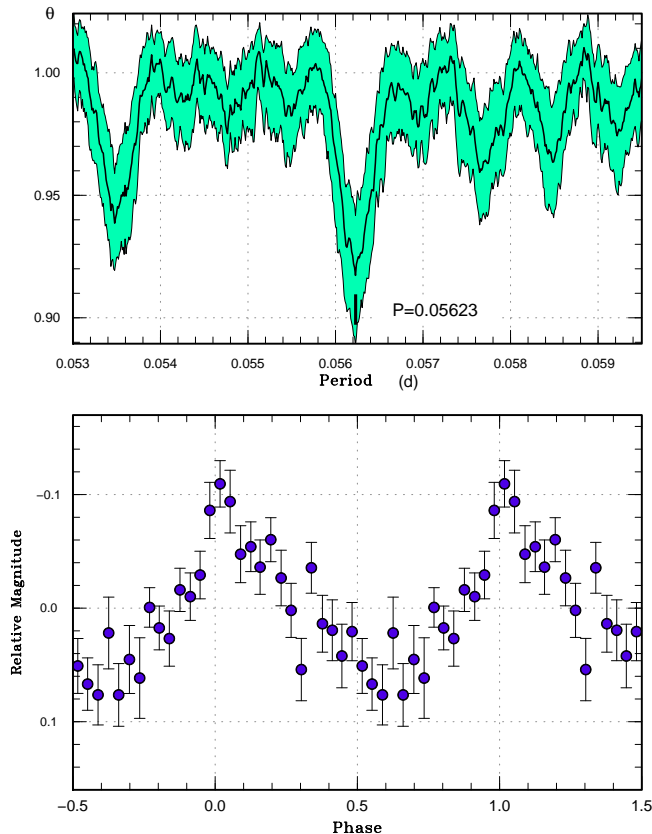


Fig. 47. Superhumps in ASASSN-15dr between BJD 2457082 and 2457087 (2015). (Upper): PDM analysis. (Lower): Phase-averaged profile.

Although individual superhumps maxima were difficult to determine due to the poor coverage (we do not give a table of superhump maxima), a PDM analysis yielded a strong signal of superhumps (figure 48). Although the best period is 0.09522(8) d, one-day aliases are still possible. If this period is confirmed, the object is located on the lower edge of the period gap.

3.45 ASASSN-15ee

This object was detected as a transient at $V=12.6$ on 2015 March 2 by the ASAS-SN team. The outburst amplitude exceeded 7 mag, and was considered to be a good candidate for a WZ Sge-type dwarf nova (vsnet-alert 18364). The object initially faded rather rapidly without strong modulations (vsnet-alert 18381). Ordinary superhump started to appear on March 8, 6 d after the initial detection and reached a peak amplitude of 0.17 mag within 1 d. The superhumps started to decay slowly (vsnet-alert 18392, 18394, 18415, 18423, 18428, 18437; figure 49) The times of superhump maxima are listed in table 42. The epochs $E \leq 14$ likely correspond to stage A superhumps since the amplitudes grew up to $E = 14$ (figure 50). The epoch for $E \geq 200$ probably correspond to stage C superhumps. There

Table 41. Superhump maxima of ASASSN-15dr (2015)

E	max*	error	$O - C^\dagger$	N^\ddagger
0	57082.2958	0.0021	-0.0146	129
1	57082.3476	0.0030	-0.0196	130
2	57082.4085	0.0038	-0.0155	130
24	57083.6840	0.0020	0.0107	15
25	57083.7430	0.0015	0.0129	17
26	57083.8002	0.0012	0.0133	22
27	57083.8568	0.0011	0.0132	22
40	57084.5919	0.0053	0.0100	12
43	57084.7647	0.0022	0.0125	20
44	57084.8134	0.0023	0.0044	21
45	57084.8727	0.0016	0.0069	16
59	57085.6680	0.0065	0.0072	13
60	57085.7189	0.0012	0.0014	15
61	57085.7724	0.0017	-0.0020	17
62	57085.8234	0.0104	-0.0078	15
76	57086.6181	0.0042	-0.0080	14
77	57086.6746	0.0033	-0.0084	19
78	57086.7369	0.0037	-0.0028	25
79	57086.7883	0.0086	-0.0083	29
80	57086.8477	0.0063	-0.0057	28

*BJD-2400000.

† Against max = 2457082.3104 + 0.056786E.

‡ Number of points used to determine the maximum.

was no strong indication of early superhumps before the development of ordinary superhumps.

Although the outburst amplitude is large, the object is probably not an extreme WZ Sge-type dwarf nova since the growth of superhumps is quick and the P_{dot} for stage B superhumps is large [$+8.1(1.2) \times 10^{-5}$]. The inclination of this object is probably low, as suggested from the lack of early superhumps, which would have made the outburst amplitude larger.

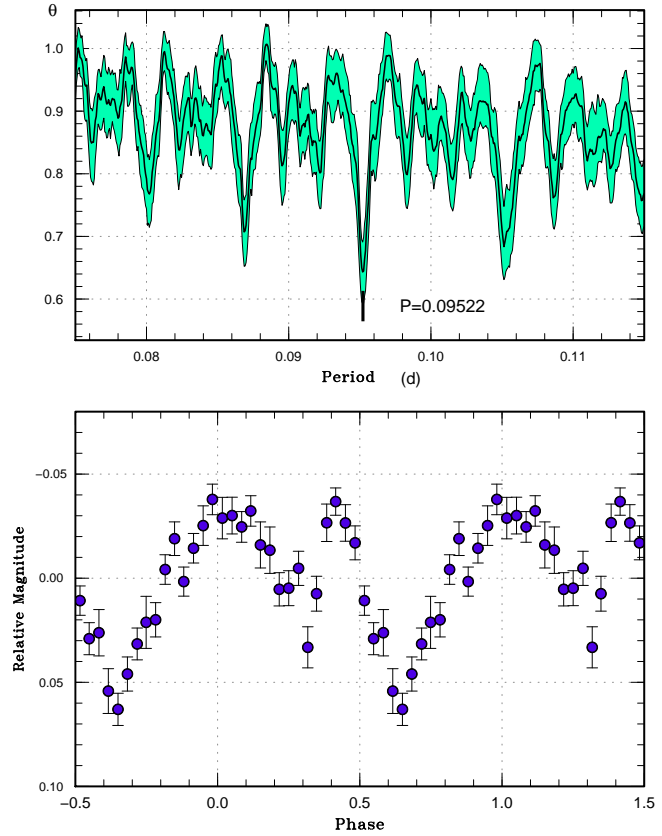
3.46 ASASSN-15eh

This object was detected as a transient at $V=15.6$ on 2015 March 3 by the ASAS-SN team. The object was apparent detected during a precursor outburst, and the SU UMa-type nature was suspected (vsnet-alert 18380). Superhump were subsequently detected (vsnet-alert 18391, 18393; figure 51). The times of superhump maxima are listed in table 43. Although there may have been a stage transition between the second and the final night, we listed the mean value in table 3 due to the lack of the data.

Table 42. Superhump maxima of ASASSN-15ee (2015)

E	max*	error	$O - C^\dagger$	N^\ddagger
0	57089.5560	0.0008	-0.0115	12
1	57089.6130	0.0015	-0.0116	13
13	57090.3099	0.0003	0.0002	132
14	57090.3657	0.0003	-0.0010	131
15	57090.4268	0.0007	0.0030	62
17	57090.5384	0.0005	0.0004	12
18	57090.5976	0.0008	0.0025	12
19	57090.6541	0.0011	0.0019	13
30	57091.2809	0.0002	0.0007	132
31	57091.3374	0.0002	0.0002	132
32	57091.3940	0.0003	-0.0004	132
33	57091.4482	0.0019	-0.0033	30
52	57092.5336	0.0006	-0.0026	17
53	57092.5940	0.0007	0.0008	18
54	57092.6498	0.0015	-0.0005	18
66	57093.3340	0.0005	-0.0013	132
67	57093.3914	0.0005	-0.0010	131
70	57093.5607	0.0009	-0.0030	15
71	57093.6188	0.0009	-0.0020	17
87	57094.5356	0.0010	0.0013	19
88	57094.5925	0.0010	0.0011	17
89	57094.6470	0.0012	-0.0014	17
105	57095.5685	0.0028	0.0067	15
106	57095.6201	0.0016	0.0012	16
118	57096.3134	0.0011	0.0094	132
119	57096.3683	0.0011	0.0072	131
120	57096.4242	0.0018	0.0060	88
130	57097.0003	0.0014	0.0112	48
131	57097.0554	0.0009	0.0093	65
200	57100.9730	0.0021	-0.0122	30
287	57105.9418	0.0018	-0.0102	65
288	57106.0081	0.0017	-0.0010	31

*BJD-2400000.

 † Against max = 2457089.5675 + 0.057089*E*. ‡ Number of points used to determine the maximum.**Fig. 48.** Superhumps in ASASSN-15ea (2015). (Upper): PDM analysis. (Lower): Phase-averaged profile.**Table 43.** Superhump maxima of ASASSN-15eh (2015)

E	max*	error	$O - C^\dagger$	N^\ddagger
0	57088.4648	0.0008	-0.0014	178
1	57088.5504	0.0011	-0.0015	197
2	57088.6375	0.0012	-0.0001	132
24	57090.5234	0.0008	0.0012	198
25	57090.6117	0.0008	0.0039	196
59	57093.5196	0.0009	-0.0008	197
60	57093.6049	0.0009	-0.0013	165

*BJD-2400000.

 † Against max = 2457088.4662 + 0.085665*E*. ‡ Number of points used to determine the maximum.

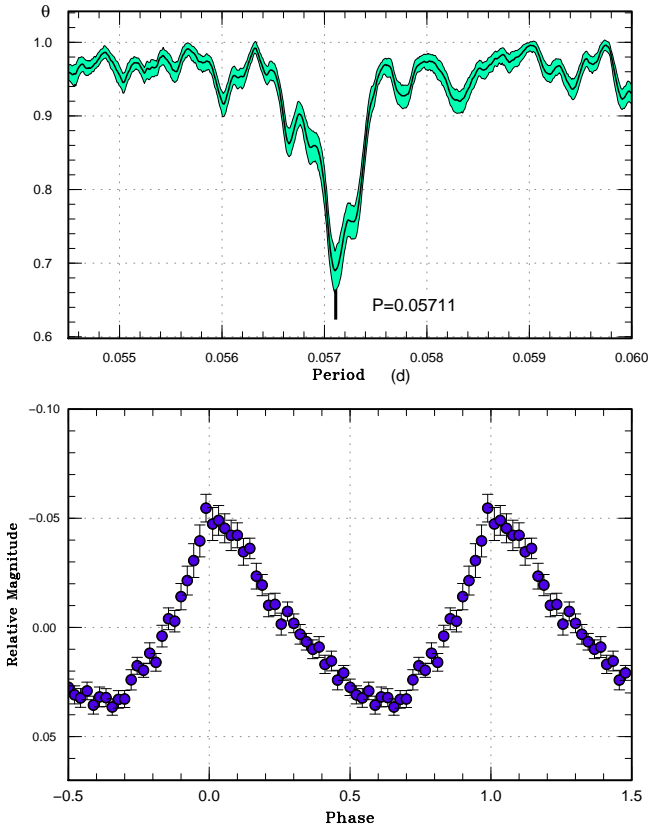


Fig. 49. Superhumps in ASASSN-15ee (2015). (Upper): PDM analysis. (Lower): Phase-averaged profile.

3.47 ASASSN-15ev

This object was detected as a transient at $V=15.1$ on 2015 March 16 by the ASAS-SN team. The object has an X-ray counterpart 1SXPS J073819.6–825039. Subsequent observations detected superhumps (vsnet-alert 18465, 18482; figure 52). The times of superhump maxima are listed in table 44. The superhump period in table 3 was determined with the PDM method. The object started fading rapidly on March 26–27, ~ 10 d after the outburst detection. The upper limit of the duration of the plateau phase was 13 d, which is relatively short for an SU UMa-type dwarf nova with this superhump period.

3.48 ASASSN-15fo

This object was detected as a transient at $V=15.4$ on 2015 March 19 by the ASAS-SN team. It further brightened to $V=14.7$ on March 20. Subsequent observations detected superhumps (vsnet-alert 18498). The superhumps were clearly seen only on the first night of our observations (figure 53). Although there were observations on later nights, they did not yield a meaningful superhump signal due to the faintness of the object (fainter than 16 mag after March 31). We restricted our analysis

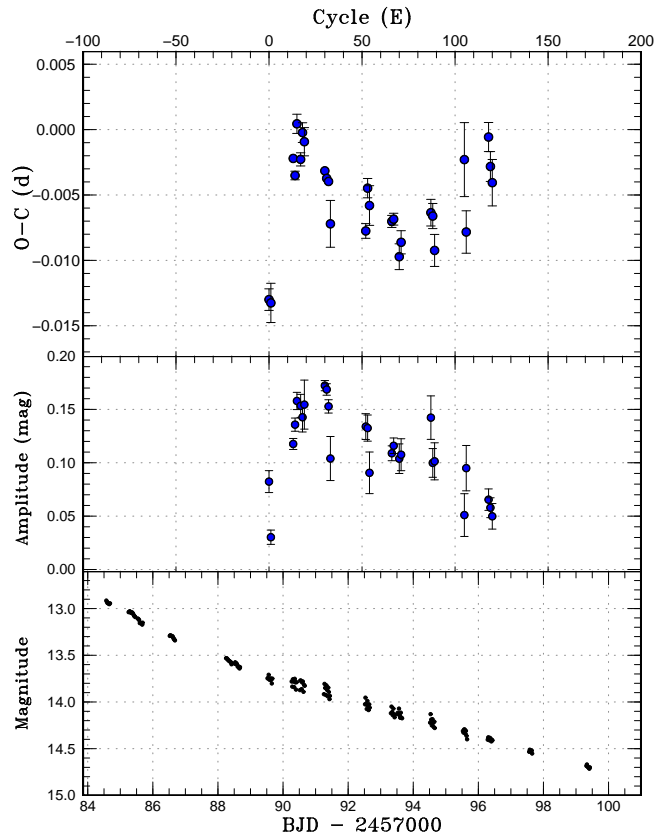


Fig. 50. $O - C$ diagram of superhumps in ASASSN-15ee (2015). (Upper:) $O - C$ diagram. We used a period of 0.05716 d for calculating the $O - C$ residuals. (Middle:) Amplitudes of superhumps. (Lower:) Light curve. The data were binned to 0.019 d.

Table 44. Superhump maxima of ASASSN-15ev (2015)

E	max*	error	$O - C^\dagger$	N^\ddagger
0	57100.2449	0.0022	-0.0016	79
1	57100.3036	0.0006	-0.0008	134
2	57100.3661	0.0024	0.0037	77
3	57100.4191	0.0006	-0.0013	133
18	57101.2933	0.0014	0.0035	109
19	57101.3448	0.0012	-0.0029	99
20	57101.4052	0.0009	-0.0005	61

*BJD-2400000.

† Against max = 2457100.2465 + 0.057961E.

‡ Number of points used to determine the maximum.

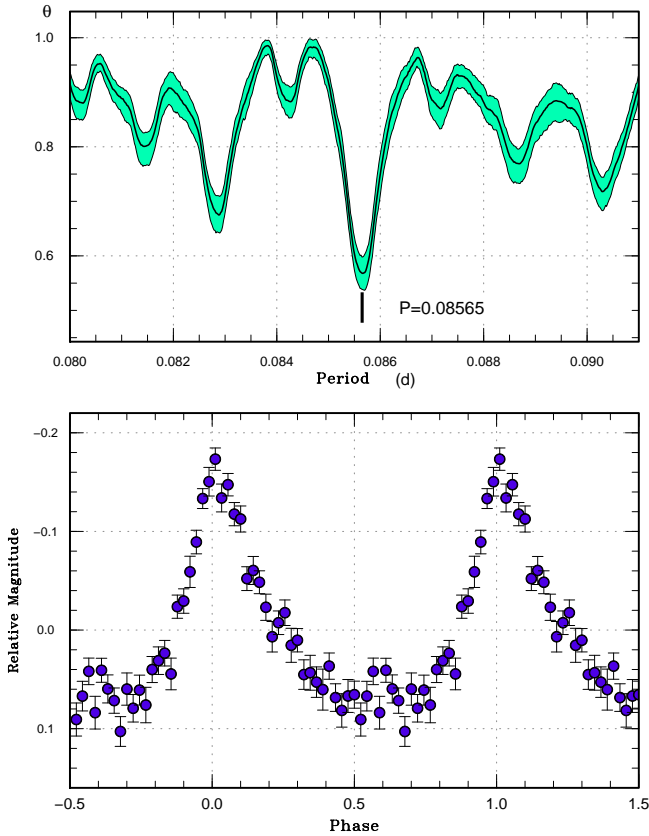


Fig. 51. Superhumps in ASASSN-15eh (2015). (Upper): PDM analysis. (Lower): Phase-averaged profile.

Table 45. Superhump maxima of ASASSN-15fo (2015)

E	max*	error	$O - C^\dagger$	N^\ddagger
0	57110.3405	0.0012	0.0037	97
1	57110.3927	0.0008	-0.0045	145
2	57110.4549	0.0017	-0.0025	145
3	57110.5215	0.0018	0.0038	135
4	57110.5776	0.0018	-0.0005	144

*BJD-2400000.

† Against max = 2457110.3368 + 0.060301 E .

‡ Number of points used to determine the maximum.

to the first-night observation. The times of superhump maxima are listed in table 45. The period given in table 3 is by the PDM analysis. The object started fading rapidly on April 4, giving 16 d for the duration of the superoutburst.

3.49 ASASSN-15fu

This object was detected as a transient at $V=15.6$ on 2015 March 27 by the ASAS-SN team. Superhumps were immediately detected (vsnet-alert 18503, 18506, 18522; figure 54). The times of superhump maxima are listed in table 46. Although

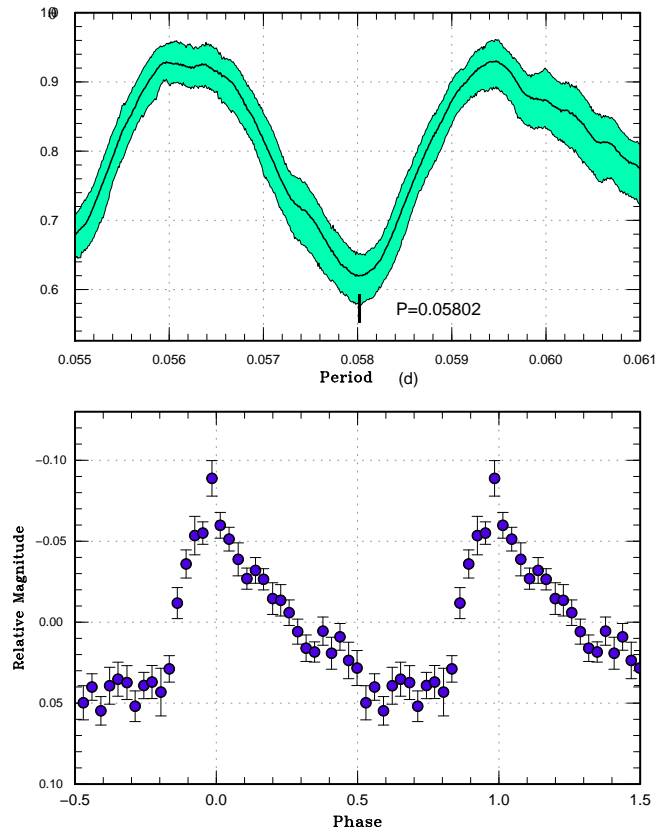


Fig. 52. Superhumps in ASASSN-15ev during the plateau phase (2015). (Upper): PDM analysis. (Lower): Phase-averaged profile.

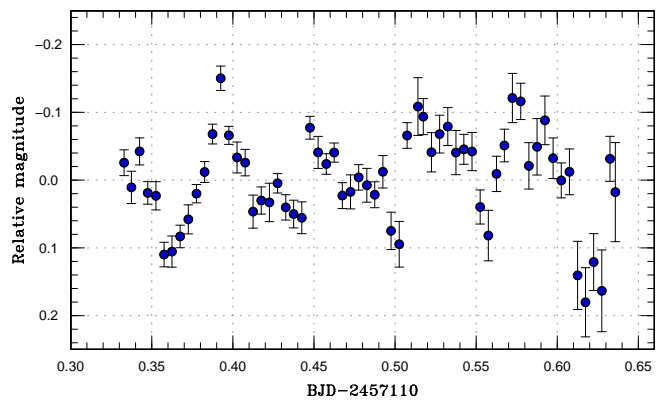


Fig. 53. Superhumps in ASASSN-15fo (2015). The data were binned to 0.005 d.

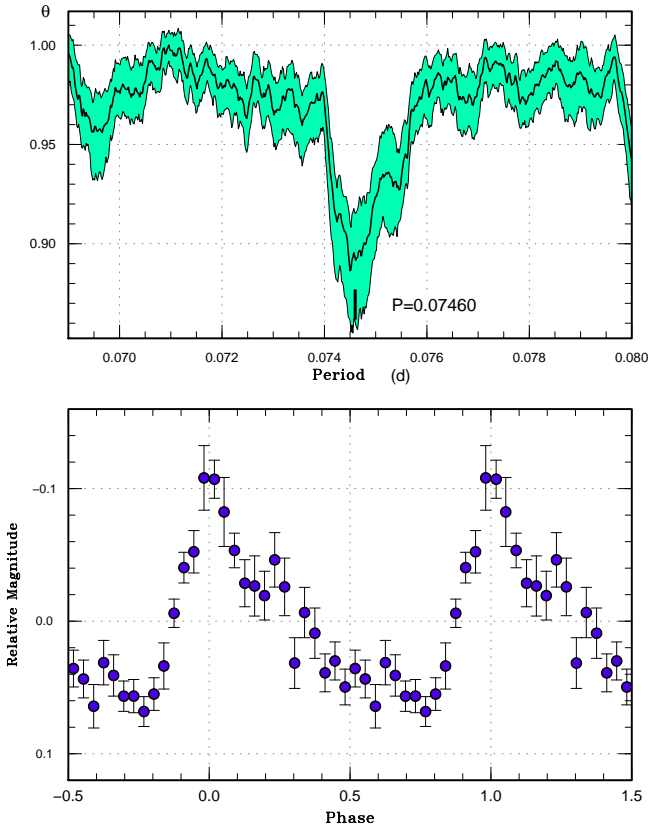


Fig. 54. Superhumps in ASASSN-15fu (2015). (Upper): PDM analysis. (Lower): Phase-averaged profile.

there was a stage B-C transition in the later part of the observation, the period of stage C superhumps (table 3) was uncertain due to the limited quality of the observation.

3.50 ASASSN-15gf

This object was detected as a transient at $V=15.2$ on 2015 April 2 by the ASAS-SN team. There is an $r=21.5$ mag counterpart in IPHAS DR2. Subsequent observations detected superhumps (vsnet-alert 18520, 18525). Due to the shortness of the runs, there were many equally acceptable one-day aliases by the PDM analysis (figure 55). We have chosen the one which give the smallest $O - C$ scatter (table 47). We should note that other one-day aliases are still possible. In table 3, we gave the period selected by the $O - C$ method and refined by the PDM analysis.

3.51 ASASSN-15gh

This object was detected as a transient at $V=14.6$ on 2015 April 1 by the ASAS-SN team. No quiescent counterpart was recorded. Before April 9, there was little indication of hump-like variations. On April 10, superhumps became apparent. Since the object had very low signal-to-noise due to the faint-

Table 46. Superhump maxima of ASASSN-15fu (2015)

E	max*	error	$O - C^\dagger$	N^\ddagger
0	57111.2945	0.0013	-0.0027	121
1	57111.3692	0.0007	-0.0027	172
2	57111.4465	0.0008	0.0001	173
3	57111.5189	0.0007	-0.0021	173
4	57111.5984	0.0030	0.0028	71
13	57112.2661	0.0010	-0.0006	152
14	57112.3396	0.0010	-0.0016	172
15	57112.4145	0.0012	-0.0013	162
43	57114.5155	0.0011	0.0118	38
44	57114.5813	0.0034	0.0030	35
57	57115.5566	0.0029	0.0089	44
70	57116.5070	0.0051	-0.0100	16
71	57116.5860	0.0031	-0.0056	19

*BJD-2400000.

† Against max = 2457111.2973 + 0.074568E.

‡ Number of points used to determine the maximum.

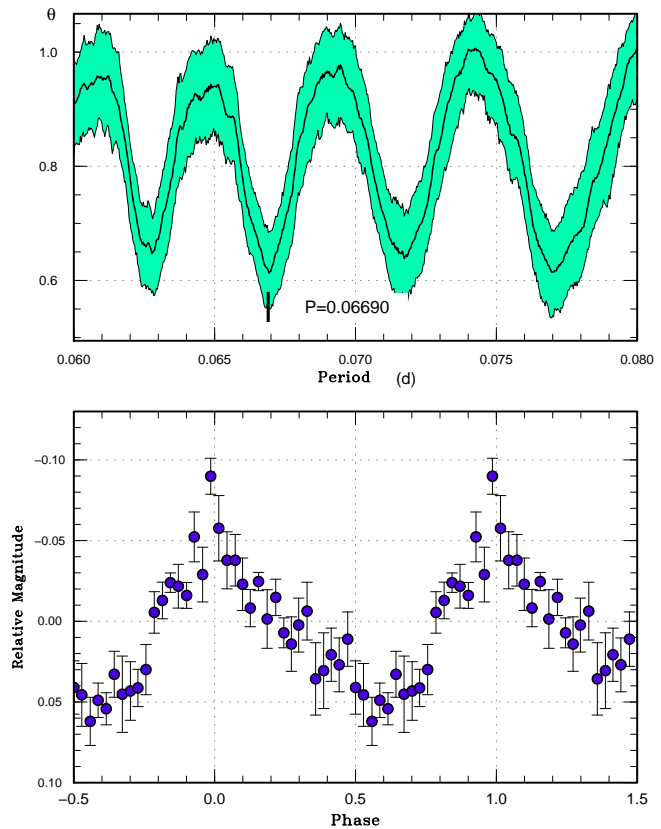


Fig. 55. Superhumps in ASASSN-15gf (2015). (Upper): PDM analysis of the first two nights. The alias selection was based on the $O - C$ analysis. The other one-day aliases are still possible. (Lower): Phase-averaged profile.

Table 47. Superhump maxima of ASASSN-15gf (2015)

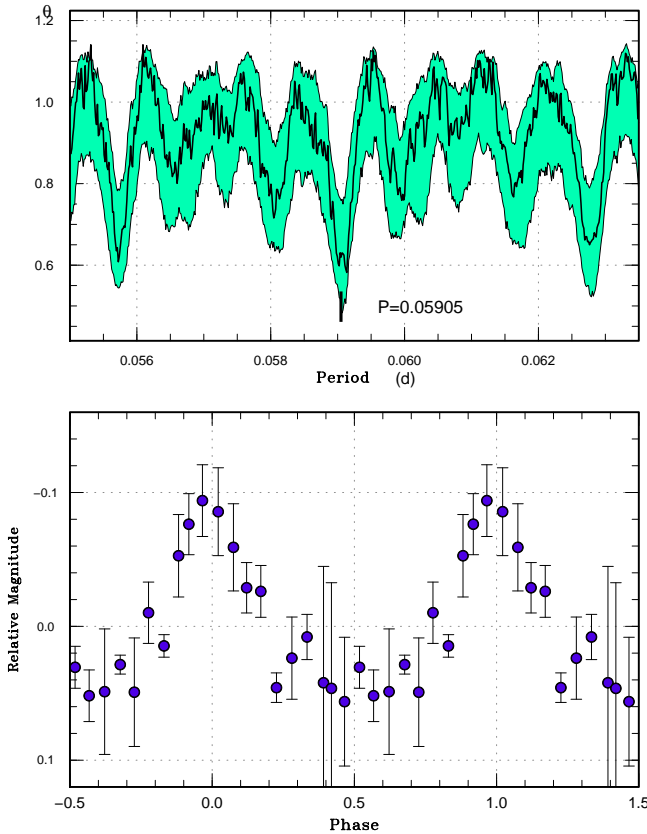
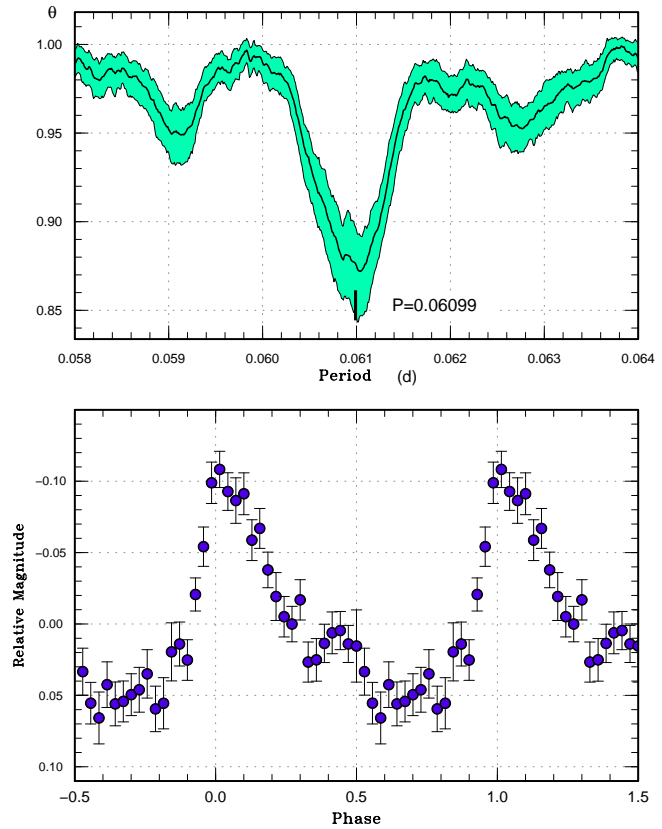
E	max*	error	$O - C^\dagger$	N^\ddagger
0	57118.3250	0.0010	0.0007	96
1	57118.3904	0.0017	-0.0008	67
15	57119.3282	0.0009	0.0001	58

*BJD-2400000.

 † Against max = 2457118.3243 + 0.066928*E*. ‡ Number of points used to determine the maximum.**Table 48.** Superhump maxima of ASASSN-15gh (2015)

E	max*	error	$O - C^\dagger$	N^\ddagger
0	57122.8319	0.0015	0.0006	15
1	57122.8894	0.0021	-0.0009	14
51	57125.8444	0.0013	0.0015	13
68	57126.8457	0.0022	-0.0011	13

*BJD-2400000.

 † Against max = 2457122.8313 + 0.059050*E*. ‡ Number of points used to determine the maximum.**Fig. 56.** Superhumps in ASASSN-15gh (2015). (Upper): PDM analysis for the interval BJD 2457122–2457127 when superhumps were most clearly visible. The alias selection was based on the $O - C$ analysis. The other one-day aliases are still possible. (Lower): Phase-averaged profile.**Fig. 57.** Superhumps in ASASSN-15gi (2015). (Upper): PDM analysis. (Lower): Phase-averaged profile.

ness (the object was already at 16.2 mag on April 10; it was only 15.5 mag on April 4 and the ASAS-SN detection magnitude may have been too bright), only the data between April 10 and 14 (BJD 2457122–2457127) were used to determine superhumps. Among the potential aliases, we selected the one which minimizes the scatter in the $O - C$ diagram (figure 56). Other possibilities still remain. The times of superhump maxima are listed in table 48. In table 3, we gave the period selected by the $O - C$ method and refined by the PDM analysis.

3.52 ASASSN-15gi

This object was detected as a transient at $V=15.4$ on 2015 April 1 by the ASAS-SN team. Subsequent observations detected superhumps (vsnet-alert 18521, 18529; figure 57). The times of superhump maxima are listed in table 49. The $O - C$ data indicate the presence of stage B-C transition around $E=65$. At the time of observation on April 4, the object was at 15.8 mag. The initial report on the ASAS-SN Transients page ($V=14.6$) was probably erroneous.

Table 49. Superhump maxima of ASASSN-15gi (2015)

E	max*	error	$O - C^\dagger$	N^\ddagger
0	57116.5035	0.0016	0.0018	15
1	57116.5586	0.0023	-0.0042	17
2	57116.6204	0.0010	-0.0035	15
17	57117.5374	0.0016	-0.0037	22
18	57117.5978	0.0014	-0.0044	23
33	57118.5149	0.0018	-0.0044	20
34	57118.5794	0.0021	-0.0011	23
64	57120.4192	0.0021	0.0045	141
65	57120.4873	0.0040	0.0115	146
66	57120.5380	0.0053	0.0010	56
78	57121.2742	0.0013	0.0035	80
79	57121.3386	0.0006	0.0067	141
80	57121.3990	0.0008	0.0060	140
88	57121.8799	0.0035	-0.0022	15
94	57122.2509	0.0007	0.0019	141
95	57122.3140	0.0007	0.0039	140
96	57122.3739	0.0009	0.0026	141
97	57122.4354	0.0011	0.0031	141
99	57122.5539	0.0034	-0.0008	23
100	57122.6164	0.0016	0.0006	15
128	57124.3175	0.0023	-0.0102	139
129	57124.3846	0.0016	-0.0042	141
130	57124.4416	0.0031	-0.0084	141

*BJD-2400000.

† Against max = 2457116.5017 + 0.061141*E*.

‡ Number of points used to determine the maximum.

3.53 ASASSN-15gn

This object was detected as a transient at $V=14.2$ on 2015 April 3 by the ASAS-SN team (vsnet-alert 18518). The likely quiescent counterpart was recorded very faint (22.4 mag on J plate). The object initially did not show strong short-term variations. On April 14 (11 d after the outburst detection), it started to show superhumps (vsnet-alert 18546, 18548, 18550, 18556, 18559; figure 58). On April 25, it started to fade rapidly (figure 59). The times of superhump maxima are listed in table 50. Although it was initially suggested that superhumps in this systems grew slowly (vsnet-alert 18550), the $O - C$ data would indicate that stage A superhumps were likely only recorded for the initial night when superhumps started to appear. In table 3, we listed a period of stage A superhumps with an assumption that $E=18$ corresponds to the end of stage A. There was some indication of stage C after $E=112$.

This object has a large outburst amplitude, a long superhump period, a long waiting time before the appearance of superhumps and a small P_{dot} . These features are suggestive of a period bouncer (cf. Kato 2015). The small amplitude of su-

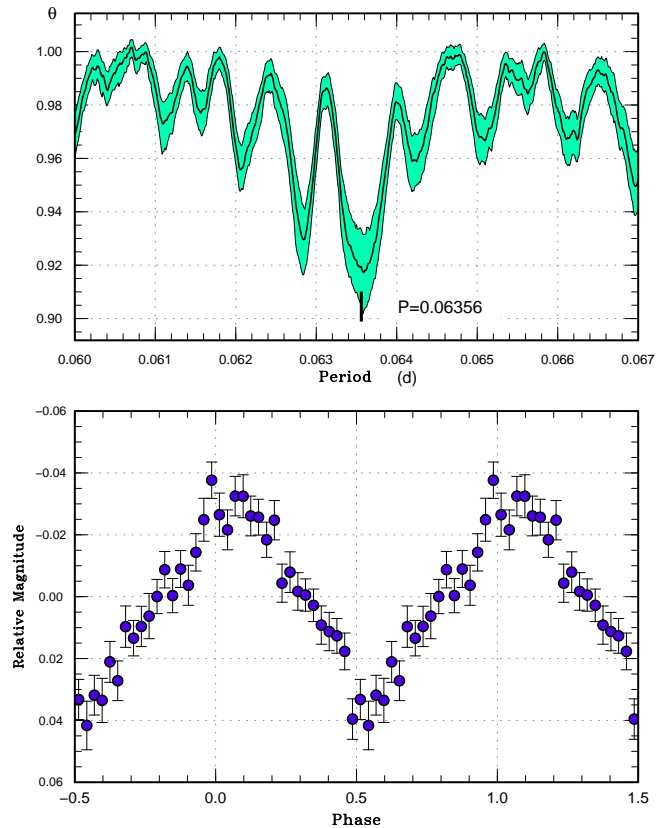


Fig. 58. Ordinary superhumps in ASASSN-15gn (2015). (Upper): PDM analysis. (Lower): Phase-averaged profile.

perhumps is also suggestive of a small tidal effect and the superhump profile is more symmetric than in other SU UMa-type dwarf novae (figure 58). The growth time of superhumps, however, is short, which is not compatible with a small q if this object is a period bouncer. It may be possible either that the growing stage of superhumps was not well recorded due to the faintness of the object (15.5 mag at the time of emergence of superhumps) and low sampling rates on some nights or that the stage identification is not correct and the entire superhumps are stage A superhumps. The either possibility is not ruled out because superhumps were close to the detection limit and the data were not so densely obtained. The small amplitude and relatively symmetric profile of the superhumps may suggest that the outburst terminated before superhump developed fully. Since the behavior of superhumps is known to be complex in period bouncers (cf. C. Nakata et al. in preparation, Kato 2015), this possibility may deserve consideration.

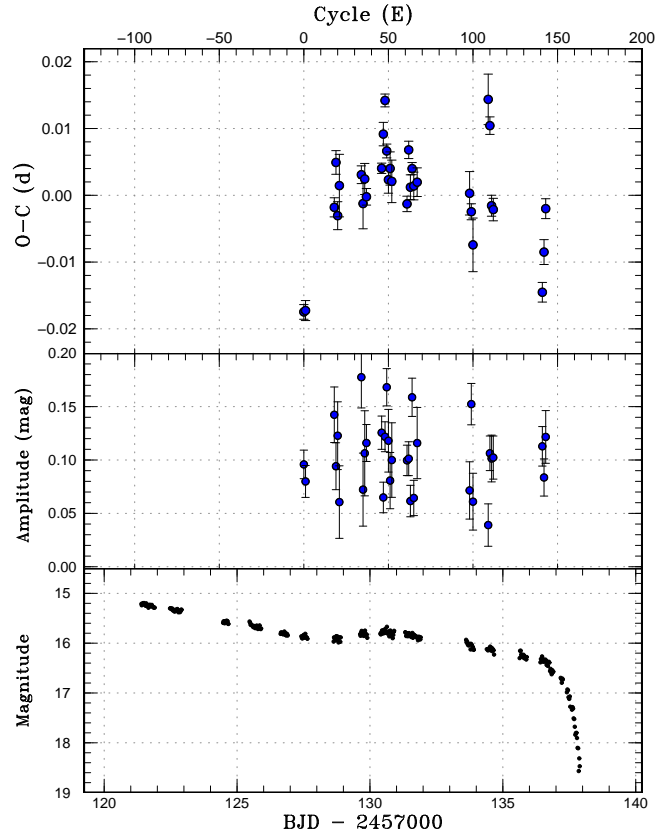
3.54 ASASSN-15gq

This object was detected as a transient at $V=15.4$ on 2015 April 10 by the ASAS-SN team. There is a $g=21.6$ mag SDSS object (SDSS J101510.86+812418.7) $1''.5$ distant from this position.

Table 50. Superhump maxima of ASASSN-15gn (2015)

E	max*	error	$O - C^\dagger$	N^\ddagger
0	57127.4945	0.0011	-0.0179	146
1	57127.5584	0.0015	-0.0177	147
18	57128.6557	0.0014	-0.0022	17
19	57128.7261	0.0018	0.0045	17
20	57128.7817	0.0021	-0.0035	15
21	57128.8499	0.0047	0.0010	16
34	57129.6788	0.0013	0.0027	17
35	57129.7382	0.0038	-0.0017	17
36	57129.8055	0.0023	0.0020	13
37	57129.8665	0.0012	-0.0006	17
46	57130.4435	0.0008	0.0036	114
47	57130.5122	0.0018	0.0088	147
48	57130.5809	0.0010	0.0138	127
49	57130.6370	0.0010	0.0062	75
50	57130.6963	0.0020	0.0019	17
51	57130.7617	0.0025	0.0036	15
52	57130.8234	0.0032	0.0017	14
61	57131.3927	0.0012	-0.0017	147
62	57131.4645	0.0013	0.0064	145
63	57131.5225	0.0019	0.0008	146
64	57131.5890	0.0009	0.0036	147
65	57131.6500	0.0021	0.0010	162
67	57131.7778	0.0021	0.0015	15
98	57133.7490	0.0033	-0.0001	18
99	57133.8099	0.0012	-0.0029	15
100	57133.8686	0.0040	-0.0079	17
109	57134.4631	0.0038	0.0139	126
110	57134.5228	0.0013	0.0100	147
111	57134.5745	0.0016	-0.0020	146
112	57134.6375	0.0017	-0.0026	147
141	57136.4707	0.0015	-0.0150	146
142	57136.5404	0.0019	-0.0090	147
143	57136.6105	0.0015	-0.0025	151

*BJD-2400000.

 † Against max = 2457127.5124 + 0.063640E. ‡ Number of points used to determine the maximum.**Fig. 59.** $O - C$ diagram of superhumps in ASASSN-15gn (2015). (Upper:) $O - C$ diagram. We used a period of 0.06364 d for calculating the $O - C$ residuals. (Middle:) Amplitudes of superhumps. (Lower:) Light curve. The data were binned to 0.021 d.

This SDSS object is less likely the quiescent counterpart since it has colors (e.g. $u - g = 0.76$) unlike a CV.

The object initially showed double-wave modulations (vsnet-alert 18526, 18528, 18531, 18539), which we identify to be early superhumps (figure 60). The object is thus identified as a WZ Sge-type dwarf nova. Later the object showed fully developed ordinary superhumps (vsnet-alert 18549, 18558, 18593; figure 61). The times of maxima of ordinary superhumps are listed in table 51. The times for $E \leq 1$ are clearly of stage A superhumps. There is a suggestion for stage B-C transition after $E=120$. In table 3, we listed a period of stage A superhumps with an assumption that $E=15$ corresponds to the end of stage A. This fractional superhump excess [$\epsilon^* = 0.038(2)$] corresponds to $q=0.107(8)$. Although we could not observe the termination of stage A superhumps, the above value is likely close to the actual value since if stage A terminated much earlier than $E=15$, the value of ϵ^* should be larger, which will give an unacceptably large q for a WZ Sge-type object.

Considering the large positive P_{dot} for stage B superhumps, the presence of stage C superhumps, the relatively long orbital period and the short duration of stage A, this object is probably a

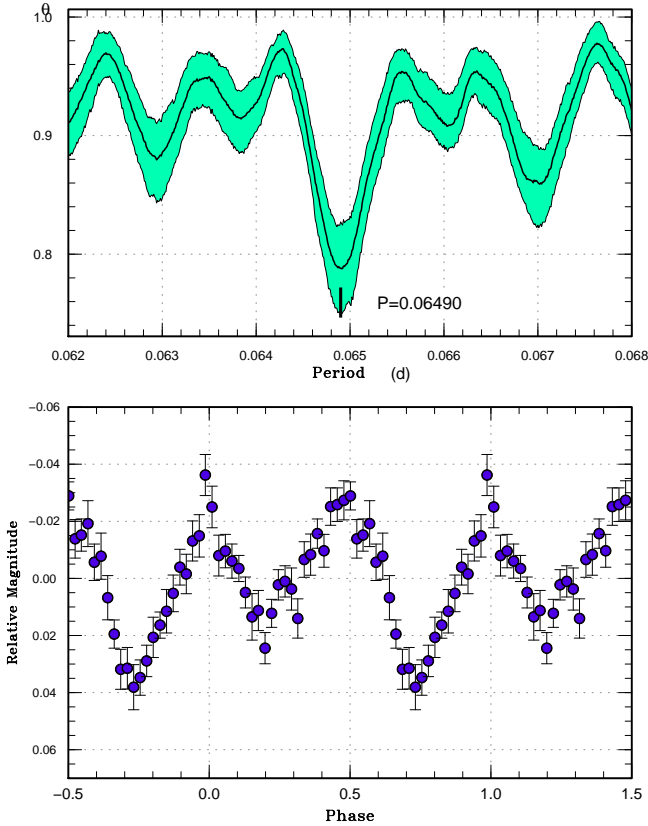


Fig. 60. Early superhumps in ASASSN-15gq (2015). (Upper): PDM analysis. (Lower): Phase-averaged profile.

borderline WZ Sge/SU UMa-type object rather than an extreme WZ Sge-type object (cf. Kato 2015).

3.55 ASASSN-15gs

This object was detected as a transient at $V=15.7$ on 2015 April 8 by the ASAS-SN team. There is an X-ray counterpart (1SXPS J135917.3–375242). The object was observed on one night and superhumps were detected (vsnet-alert 18541, figure 62). The times of superhump maxima are listed in table 52. The best period with the PDM method was 0.0719(8) d.

3.56 ASASSN-15hd

This object was detected as a transient at $V=14.0$ on 2015 April 15 by the ASAS-SN team (vsnet-alert 18547). The large outburst amplitude inferred from the faint ($g=21.4$ – 21.9 mag) SDSS counterpart already suggested a WZ Sge-type object.

The object initially showed large-amplitude (0.3 mag) variations which resembled ordinary superhumps, but they gradually became double-wave modulations characteristic to early superhumps (vsnet-alert 18552, 18555, 18557, 18573; figure 63). The object then showed ordinary superhumps (vsnet-alert

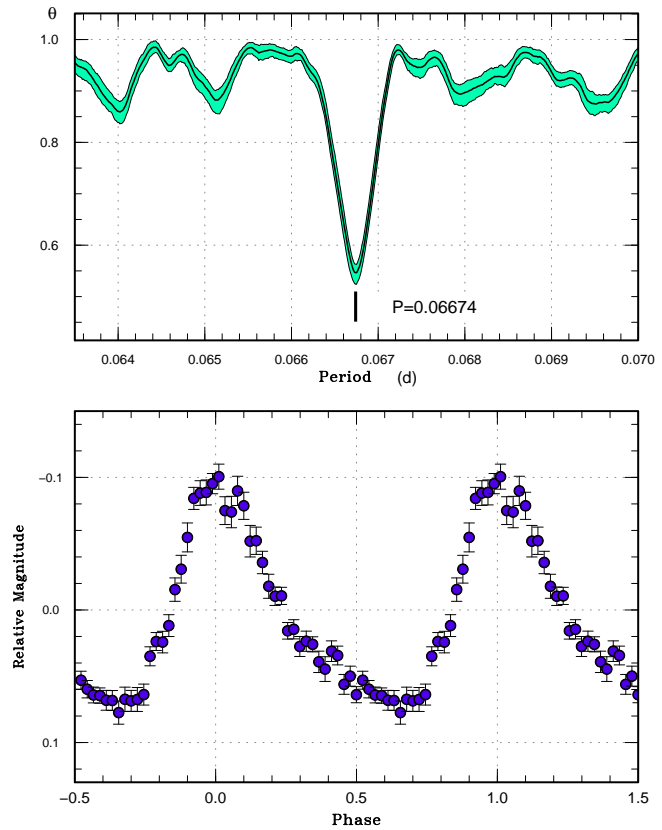


Fig. 61. Ordinary superhumps in ASASSN-15gq (2015). (Upper): PDM analysis. (Lower): Phase-averaged profile.

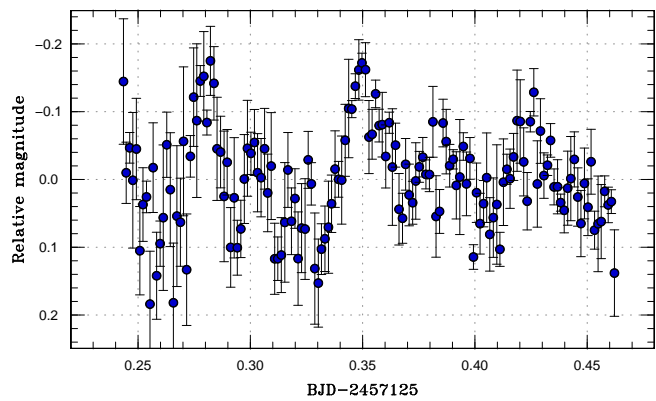


Fig. 62. Superhumps in ASASSN-15gs (2015). The data were binned to 0.0015 d.

Table 51. Superhump maxima of ASASSN-15gq (2015)

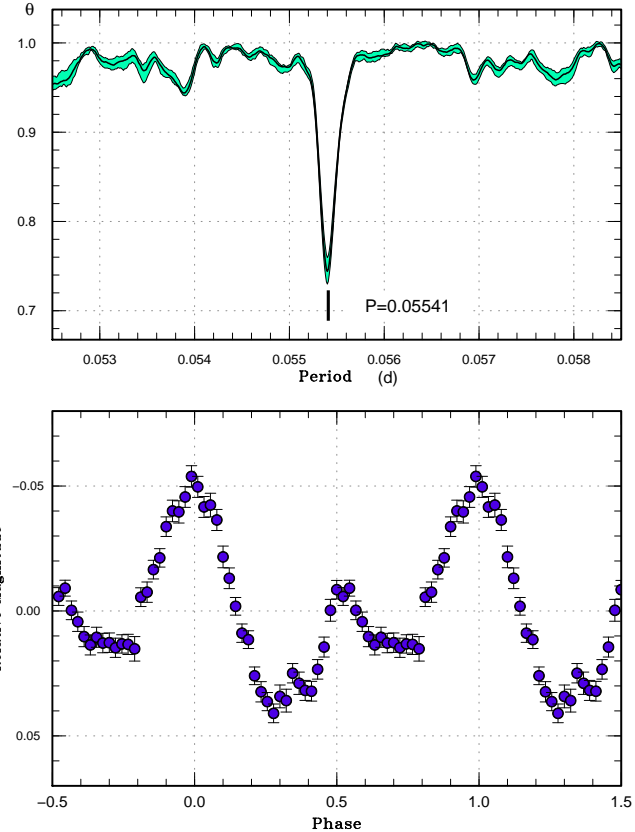
E	max*	error	$O - C^\dagger$	N^\ddagger
0	57127.3844	0.0012	-0.0022	67
1	57127.4489	0.0008	-0.0046	63
15	57128.3953	0.0005	0.0069	95
16	57128.4610	0.0004	0.0058	114
17	57128.5292	0.0008	0.0072	63
18	57128.5953	0.0005	0.0065	57
45	57130.3917	0.0004	-0.0003	62
46	57130.4578	0.0004	-0.0009	51
60	57131.3893	0.0004	-0.0044	98
61	57131.4569	0.0004	-0.0035	122
62	57131.5233	0.0006	-0.0040	56
65	57131.7224	0.0019	-0.0052	86
66	57131.7922	0.0007	-0.0022	104
75	57132.3904	0.0004	-0.0050	61
76	57132.4575	0.0006	-0.0048	51
90	57133.3939	0.0005	-0.0033	128
91	57133.4619	0.0007	-0.0021	116
105	57134.3994	0.0013	0.0004	86
106	57134.4647	0.0008	-0.0010	92
120	57135.4089	0.0008	0.0081	45
134	57136.3392	0.0012	0.0035	29
135	57136.4076	0.0008	0.0051	45

*BJD-2400000.

 † Against max = 2457127.3867 + 0.066784*E*. ‡ Number of points used to determine the maximum.**Table 52.** Superhump maxima of ASASSN-15gs (2015)

E	max*	error	$O - C^\dagger$	N^\ddagger
1	57125.2821	0.0018	-0.0009	165
2	57125.3529	0.0009	-0.0020	165
3	57125.4264	0.0018	-0.0004	166

*BJD-2400000.

 † Against max = 2457125.2818 + 0.072165*E*. ‡ Number of points used to determine the maximum.**Fig. 63.** Early superhumps in ASASSN-15hd (2015). (Upper): PDM analysis. (Lower): Phase-averaged profile.

18582, 18585, 18594, 18604, 18609; figure 64). The times of superhump maxima are listed in table 53. There was a clear transition from stage A to B around $E=22$. There was no strong indication of transition to stage C (figure 65).

The ϵ^* of 0.028(4) for stage A superhumps corresponds to $q=0.076(12)$. This relatively low q value appears to be consistent with the small P_{dot} of stage B superhumps (cf. Kato 2015). There was one post-superoutburst rebrightening (figure 65). We cannot, however, exclude the possibility of more rebrightenings since the object was not well observed after the superoutburst.

The object is notable for its initially large amplitude of early superhumps and the singly-peaked “saw-tooth” profile at the beginning (figure 65). The mean amplitude of early superhumps of 0.09 mag implies that ASASSN-15hd belongs to a group of WZ Sge-type objects with largest amplitudes of early superhumps (Kato 2015). The initial “saw-tooth”-like profile was also recorded in V455 And (cf. Kato 2015). Since the large amplitude of early superhumps strongly suggests a high orbital inclination, the common presence of the “saw-tooth”-like profile in this system and an eclipsing system V455 And suggests that this feature is seen only in high-inclination systems.

Table 53. Superhump maxima of ASASSN-15hd (2015)

E	max*	error	$O - C^\dagger$	N^\ddagger	E	max*	error	$O - C^\dagger$	N^\ddagger
0	57139.1728	0.0029	-0.0089	64	77	57143.5007	0.0009	-0.0019	51
1	57139.2179	0.0023	-0.0199	88	78	57143.5557	0.0011	-0.0029	51
17	57140.1378	0.0012	0.0021	24	79	57143.6119	0.0008	-0.0029	50
18	57140.1954	0.0004	0.0036	42	89	57144.1736	0.0016	-0.0024	55
19	57140.2456	0.0028	-0.0023	17	98	57144.6879	0.0022	0.0069	37
22	57140.4238	0.0008	0.0076	32	99	57144.7338	0.0013	-0.0033	56
23	57140.4787	0.0009	0.0064	31	100	57144.7911	0.0009	-0.0021	51
24	57140.5387	0.0017	0.0102	16	101	57144.8459	0.0012	-0.0034	57
41	57141.4882	0.0022	0.0057	25	160	57148.1526	0.0018	-0.0076	39
42	57141.5412	0.0004	0.0027	52	166	57148.4916	0.0022	-0.0052	38
43	57141.5961	0.0005	0.0015	43	167	57148.5533	0.0027	0.0004	37
44	57141.6531	0.0003	0.0023	50	168	57148.6039	0.0013	-0.0051	22
45	57141.7082	0.0005	0.0014	55	182	57149.3930	0.0013	-0.0016	35
46	57141.7654	0.0006	0.0024	56	183	57149.4521	0.0012	0.0013	34
47	57141.8247	0.0018	0.0056	13	184	57149.5083	0.0011	0.0014	78
48	57141.8770	0.0011	0.0018	30	185	57149.5630	0.0011	-0.0001	72
54	57142.2127	0.0004	0.0008	25	186	57149.6157	0.0010	-0.0034	60
55	57142.2687	0.0004	0.0006	25	187	57149.6808	0.0041	0.0055	19
58	57142.4382	0.0030	0.0018	30	217	57151.3577	0.0008	-0.0010	30
59	57142.4920	0.0018	-0.0005	27	218	57151.4157	0.0010	0.0009	23
60	57142.5511	0.0010	0.0025	32	250	57153.2062	0.0022	-0.0043	42
61	57142.6055	0.0012	0.0007	40	262	57153.8904	0.0015	0.0065	92
62	57142.6602	0.0007	-0.0006	30	270	57154.3285	0.0019	-0.0044	30
71	57143.1641	0.0011	-0.0018	87	271	57154.3933	0.0023	0.0044	31
72	57143.2194	0.0015	-0.0026	87	272	57154.4447	0.0020	-0.0004	30
75	57143.3899	0.0009	-0.0005	53	273	57154.5065	0.0010	0.0054	30
76	57143.4432	0.0007	-0.0033	45	-	-	-	-	-

*BJD-2400000.

†Against max = 2457139.1817 + 0.056115*E*.

‡Number of points used to determine the maximum.

3.57 ASASSN-15hl

This object was detected as a transient at $V=16.2$ on 2015 April 19 by the ASAS-SN team. Superhumps (figure 67) were soon detected (vsnet-alert 18568). The times of superhump maxima are listed in table 54. The superhump stage is unknown.

3.58 ASASSN-15hm

This object was detected as a transient at $V=13.6$ on 2015 April 18 by the ASAS-SN team (vsnet-alert 18563). On April 26 (8 d after the outburst detection), this object started to show superhumps (vsnet-alert 18578, 18587; figure 68). The times of superhump maxima are listed in table 55. The $O - C$ values clearly indicate that stage B started relatively late (around $E=34$). The slow evolution of superhumps suggests a relatively low q , although it was impossible to determine the q value from stage A superhump due to the lack of information about the or-

Table 54. Superhump maxima of ASASSN-15hl (2015)

E	max*	error	$O - C^\dagger$	N^\ddagger
0	57134.2526	0.0010	-0.0007	116
1	57134.3197	0.0007	-0.0016	147
44	57137.2457	0.0012	0.0028	157
45	57137.3114	0.0015	0.0005	126
74	57139.2854	0.0017	0.0040	156
88	57140.2276	0.0013	-0.0050	123
89	57140.3006	0.0030	0.0000	124

*BJD-2400000.

†Against max = 2457134.2533 + 0.067947*E*.

‡Number of points used to determine the maximum.

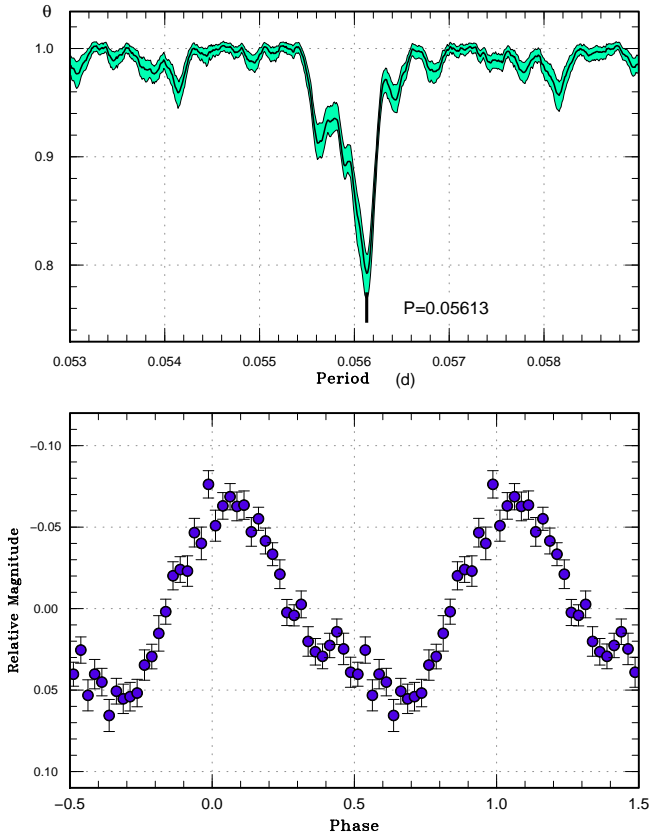


Fig. 64. Ordinary superhumps in ASASSN-15hd (2015). (Upper): PDM analysis. (Lower): Phase-averaged profile.

bit period. Although the large outburst amplitude suggests a WZ Sge-type object, we do not have evidence for it.

3.59 ASASSN-15hn

This object was detected as a transient at $V=12.9$ on 2015 April 17 by the ASAS-SN team (vsnet-alert 18564). The quiescent counterpart was very faint (21.9 mag in GSC 2.3.2 on J plate) and the large outburst amplitude suggested a WZ Sge-type dwarf nova. Ordinary superhumps started to appear on April 30–May 1 (13–14 d after the outburst detection, vsnet-alert 18592, 18599, 18605, 18610; figure 70). The object started to fade rapidly on May 11, 24 d after the outburst detection. The times of superhump maxima are listed in table 56. Stage A lasted nearly 30 cycles (figure 69), which implies a small q (Kato 2015).

There was no indication of early superhumps before the appearance of ordinary superhumps. The upper limit for the amplitude of early superhumps was 0.005 mag, probably suggesting a low orbital inclination. Although this object did not show early superhumps, all the observed features suggest the WZ Sge-type classification: long duration (13–14 d) before the appearance of ordinary superhumps, long duration of stage A

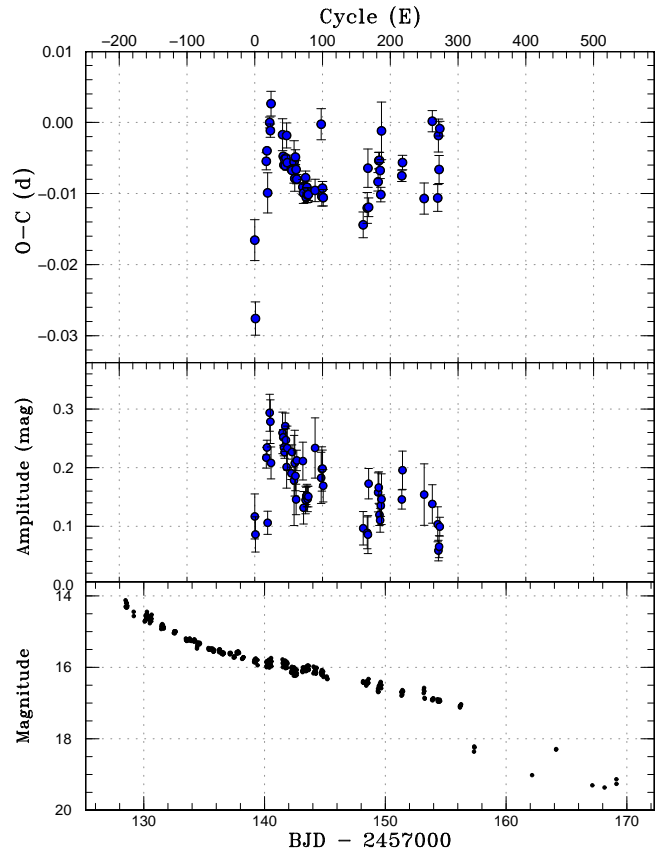


Fig. 65. $O - C$ diagram of superhumps in ASASSN-15hd (2015). (Upper:) $O - C$ diagram. We used a period of 0.05611 d for calculating the $O - C$ residuals. (Middle:) Amplitudes of superhumps. (Lower:) Light curve. The data were binned to 0.019 d.

(~ 30 cycles), small P_{dot} for stage B superhumps, low amplitude of superhumps and the lack of stage C superhumps. The empirical relation between P_{dot} for stage B superhumps and q (equation 6 in Kato 2015) gives a q of 0.058(9). Since the object has a relatively long superhump period, this estimated q would place it in a region of period bouncers. The apparent large outburst amplitude would favor this interpretation. Ordinary superhumps started to appear at 14.7 mag. Although quiescent magnitude is highly uncertain, the “amplitude” when ordinary superhumps appear (7.2 mag) is also in the region of period bouncers (see figure 23 of Kato 2015).

3.60 ASASSN-15ia

This object was detected as a transient at $V=15.3$ on 2015 April 25 by the ASAS-SN team. The object faded to $V=15.6$ on April 26 and brightened to $V=15.3$ on April 27, suggesting a precursor outburst. Superhumps were detected in observations starting 4 d after the outburst detection (figure 71). The times of superhump maxima are listed in table 57. Both stages B and C were recorded. The early part of stage B was not observed. The rapid

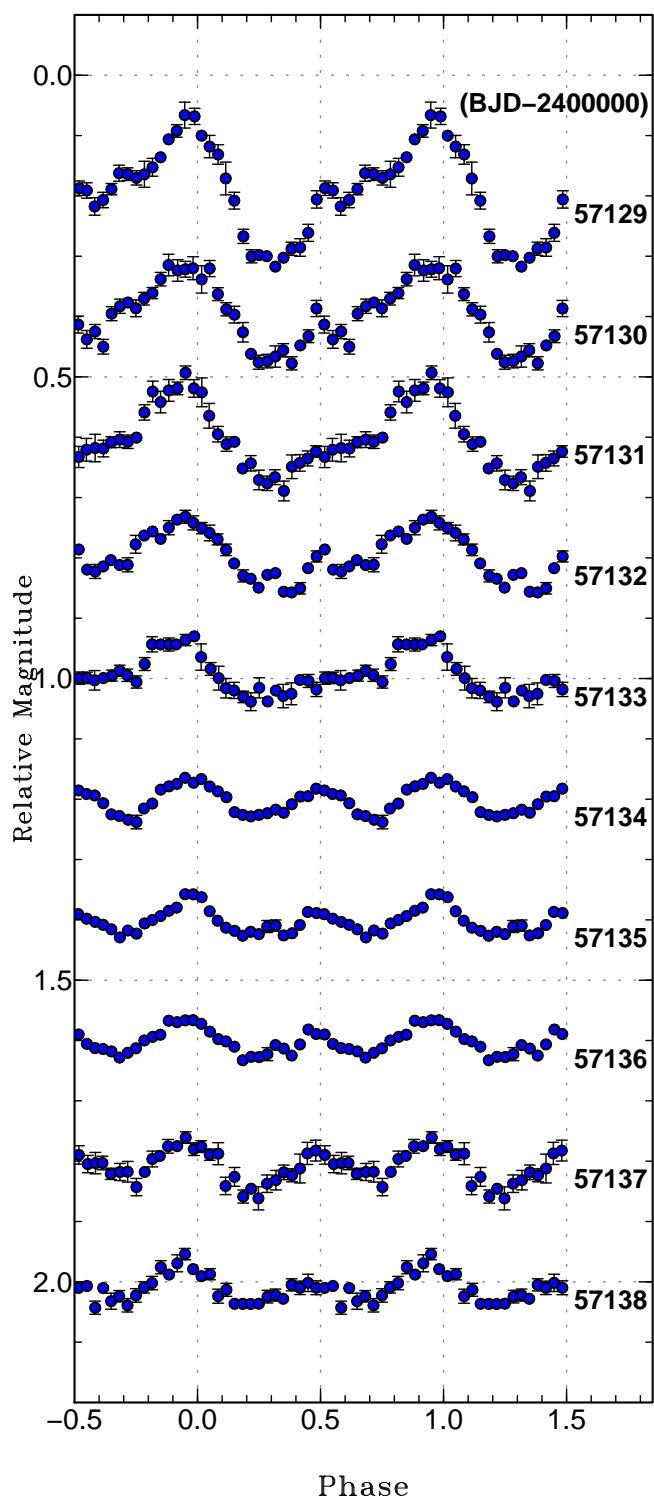


Fig. 66. Evolution of profile of early superhumps in ASASSN-15hd (2015). A period of 0.055410 d was used to draw this figure.

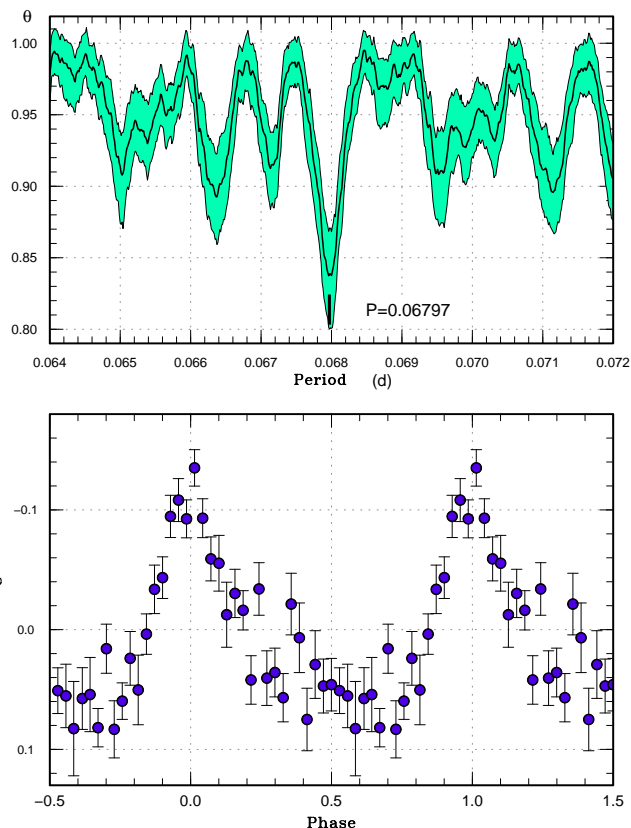


Fig. 67. Superhumps in ASASSN-15hl (2015). (Upper): PDM analysis. (Lower): Phase-averaged profile.

Table 55. Superhump maxima of ASASSN-15hm (2015)

E	max*	error	$O - C^\dagger$	N^\ddagger
0	57138.5846	0.0010	-0.0089	15
9	57139.0952	0.0028	-0.0042	85
16	57139.4893	0.0054	-0.0037	8
17	57139.5550	0.0004	0.0057	19
25	57139.9984	0.0059	-0.0006	53
26	57140.0586	0.0013	0.0034	101
34	57140.5112	0.0013	0.0062	17
35	57140.5667	0.0009	0.0056	19
52	57141.5179	0.0021	0.0010	19
53	57141.5761	0.0020	0.0030	16
70	57142.5275	0.0029	-0.0013	18
71	57142.5879	0.0061	0.0029	12
88	57143.5334	0.0030	-0.0074	15
105	57144.4941	0.0015	-0.0024	13
106	57144.5528	0.0036	0.0002	23
159	57147.5328	0.0023	0.0005	19

*BJD-2400000.

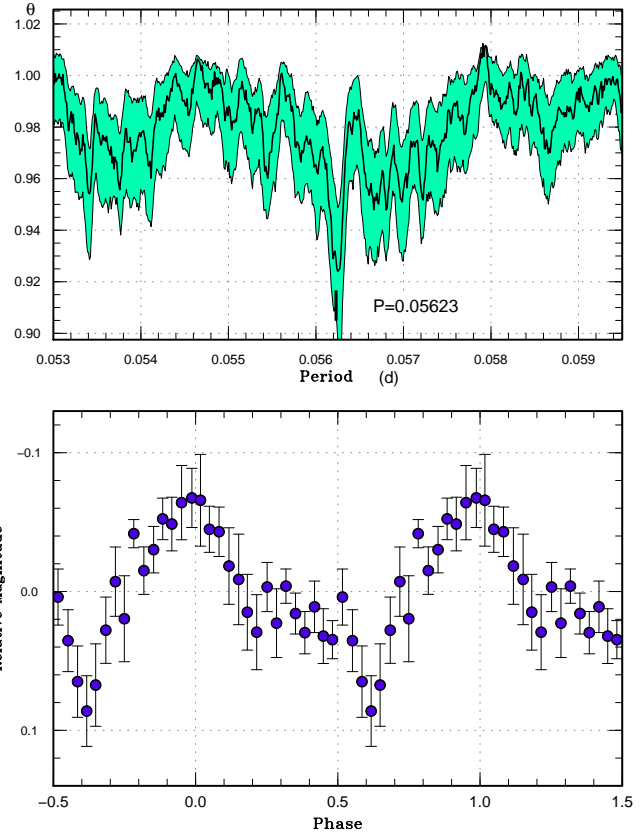
† Against max = 2457138.5935 + 0.056219E.

‡ Number of points used to determine the maximum.

Table 56. Superhump maxima of ASASSN-15hn (2015)

E	max*	error	$O - C^\dagger$	N^\ddagger
0	57143.5085	0.0014	-0.0266	15
1	57143.5639	0.0024	-0.0331	17
2	57143.6414	0.0009	-0.0176	90
16	57144.5255	0.0013	-0.0009	23
27	57145.2176	0.0007	0.0097	111
28	57145.2770	0.0006	0.0071	143
29	57145.3395	0.0008	0.0077	143
32	57145.5297	0.0018	0.0119	24
48	57146.5174	0.0016	0.0084	23
49	57146.5767	0.0033	0.0057	13
60	57147.2616	0.0008	0.0091	142
61	57147.3220	0.0010	0.0076	142
62	57147.3837	0.0043	0.0073	36
64	57147.5088	0.0013	0.0085	18
65	57147.5676	0.0020	0.0053	20
70	57147.8739	0.0007	0.0018	20
78	57148.3742	0.0005	0.0065	83
80	57148.4987	0.0024	0.0071	16
81	57148.5594	0.0014	0.0058	21
92	57149.2376	0.0007	0.0025	143
93	57149.3001	0.0007	0.0031	143
94	57149.3601	0.0011	0.0011	154
113	57150.5343	0.0025	-0.0019	21
119	57150.9078	0.0007	-0.0002	22
120	57150.9654	0.0041	-0.0045	56
125	57151.2816	0.0021	0.0020	54
126	57151.3381	0.0012	-0.0036	143
129	57151.5315	0.0018	0.0040	20
145	57152.5217	0.0036	0.0029	20
161	57153.5129	0.0019	0.0028	20
162	57153.5634	0.0050	-0.0087	16
167	57153.8665	0.0056	-0.0153	12
177	57154.4998	0.0032	-0.0016	23
178	57154.5495	0.0037	-0.0138	25

*BJD-2400000.

 † Against max = 2457143.5351 + 0.061957E. ‡ Number of points used to determine the maximum.**Fig. 68.** Superhumps in ASASSN-15hm (2015). (Upper): PDM analysis. (Lower): Phase-averaged profile.

fading from the superoutburst plateau apparently took place on May 7. The total duration of the superoutburst was 11 d.

3.61 ASASSN-15ie

This object was detected as a transient at $V=14.0$ on 2015 May 4 by the ASAS-SN team. On May 9 (5 d after the outburst detection), superhumps started to appear (vsnet-alert 18606, 18611, 18616, 18634; figure 72). The times of superhump maxima are listed in table 58. The maxima for $E \leq 2$ recorded stage A superhumps. Although there were observations, the times of maxima between $E=138$ and $E=222$ could not be determined due to the low amplitudes of superhumps and the faintness (16.2 mag) of the object. The maxima around $E=223$ correspond to stage B-C transition, when superhump again became apparent and the object slightly brightened. The object started fading rapidly on May 25 and the total duration of the superoutburst was 20 d.

Although the apparent large outburst amplitude, the short delay before the appearance of superhumps and the presence of stage C make this object less likely an extreme WZ Sge-type object.

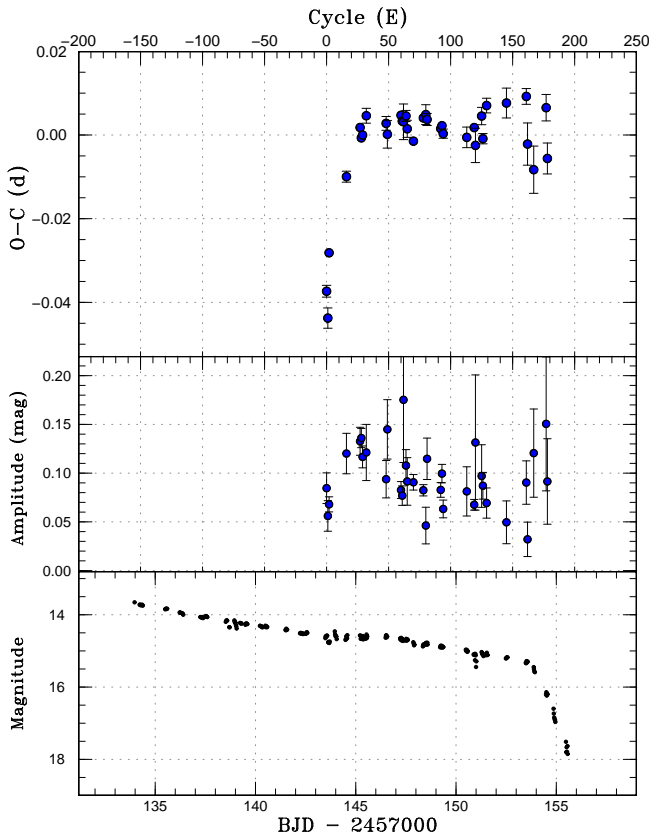


Fig. 69. $O - C$ diagram of superhumps in ASASSN-15hn (2015). (Upper:) $O - C$ diagram. We used a period of 0.06185 d for calculating the $O - C$ residuals. (Middle:) Amplitudes of superhumps. (Lower:) Light curve. The data were binned to 0.021 d.

Table 57. Superhump maxima of ASASSN-15ia (2015)

E	max*	error	$O - C^\dagger$	N^\ddagger
0	57141.8193	0.0012	-0.0008	22
1	57141.8864	0.0013	-0.0037	19
14	57142.7982	0.0014	-0.0025	21
15	57142.8698	0.0010	-0.0009	23
28	57143.7852	0.0017	0.0039	18
29	57143.8562	0.0016	0.0048	18
42	57144.7618	0.0018	-0.0001	18
43	57144.8377	0.0011	0.0058	23
44	57144.9031	0.0016	0.0011	12
57	57145.8078	0.0017	-0.0047	19
58	57145.8838	0.0030	0.0012	18
71	57146.7892	0.0018	-0.0040	27
72	57146.8631	0.0064	-0.0001	29

*BJD-2400000.

† Against max = 2457141.8201 + 0.070043E.

‡ Number of points used to determine the maximum.

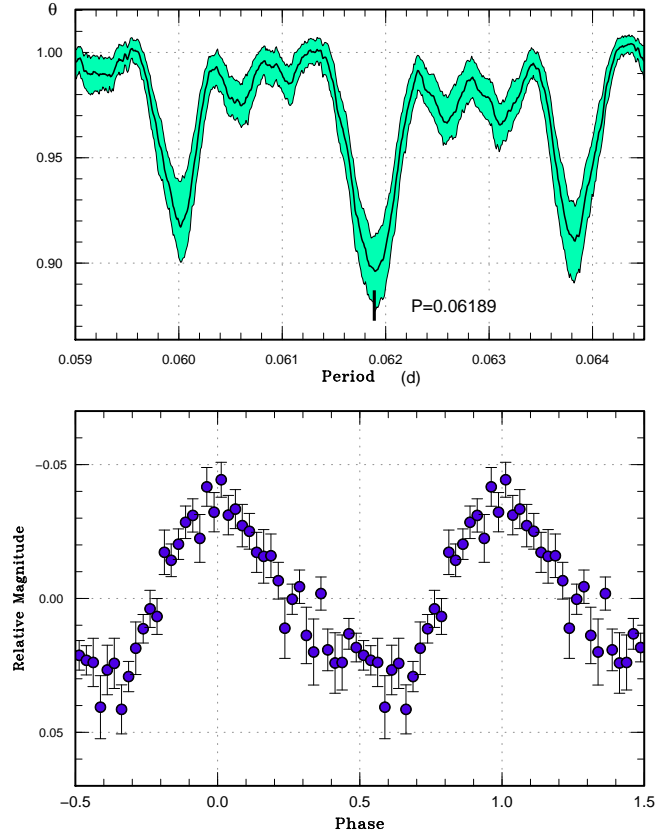


Fig. 70. Ordinary superhumps in ASASSN-15hn during the plateau phase (2015). (Upper:) PDM analysis. (Lower:) Phase-averaged profile.

3.62 ASASSN-15iv

This object was detected as a transient at $V=15.8$ on 2015 May 11 by the ASAS-SN team. Superhumps were present already 2 d after the outburst detection (vsnet-alert 18614, 18643; figure 73). The times of superhump maxima are listed in table 59. There was clear stage B-C transition around $E=88$. The object started fading rapidly between May 23 and 25. The total duration of the superoutburst was about 13 d.

3.63 ASASSN-15iz

This object was detected as a transient at $V=16.7$ on 2015 May 11 by the ASAS-SN team. It was initially suspected that this object could be identified with a cataloged high proper motion object (cf. vsnet-alert 18620). This high proper motion, however, was found to be spurious by examination of archival plates (B. Skiff, vsnet-alert 18623). The object showed large-amplitude superhumps (vsnet-alert 18626, 18644; figure 74). The times of superhump maxima are listed in table 60. In this table, we adopted a period [0.08140(6) d] which appears to give the smallest scatter in the $O - C$ diagram. Other longer one-day aliases [particularly 0.08863(7) d] are still possible, and the

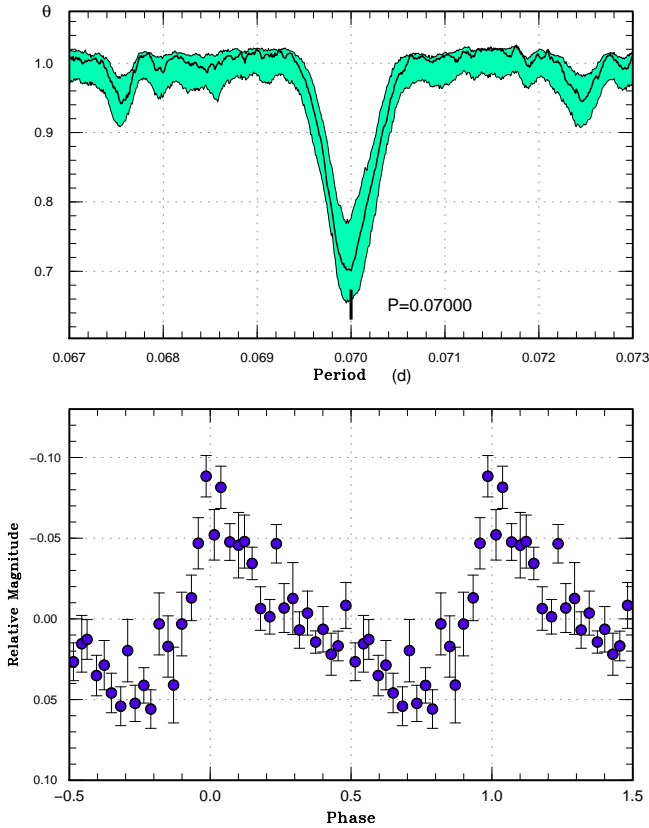


Fig. 71. Superhumps in ASASSN-15ia during the plateau phase (2015). (Upper): PDM analysis. (Lower): Phase-averaged profile.

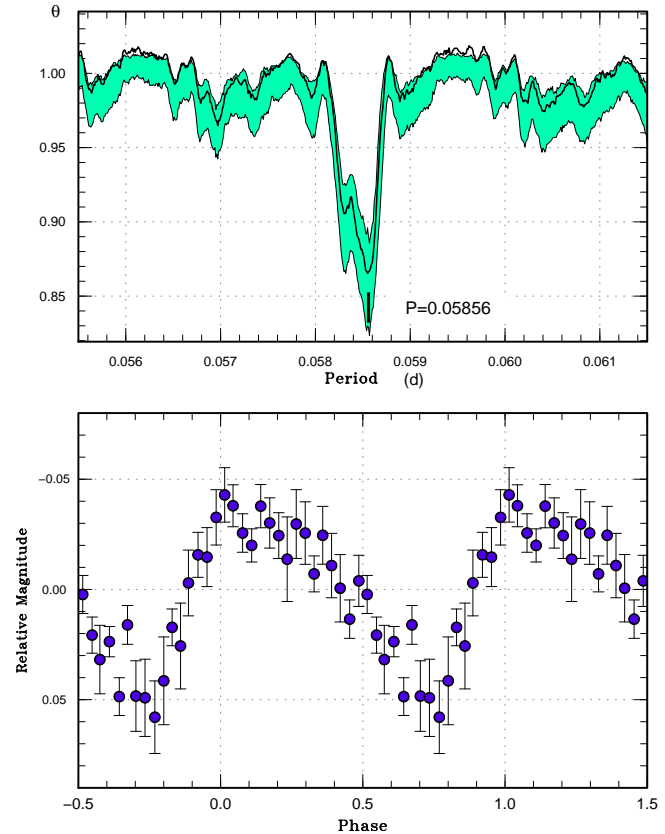


Fig. 72. Superhumps in ASASSN-15ie (2015). (Upper): PDM analysis. (Lower): Phase-averaged profile.

cycle numbers in this table may be subject to correction.

3.64 ASASSN-15jj

This object was detected as a transient at $V=14.5$ on 2015 May 16 by the ASAS-SN team. Superhumps were already present on May 19 and were continuously observed (vsnet-alert 18637, 18642, 18655; figure 75). The times of superhump maxima are listed in table 61. The $O-C$ diagram shows a clear pattern of stages B and C. The large positive P_{dot} [$+8.1(0.6) \times 10^{-5}$] is typical for this superhump period.

3.65 ASASSN-15kf

This object was detected as a transient at $V=15.0$ on 2015 May 27 by the ASAS-SN team. Subsequent observations detected very short-period superhumps [period 0.0192(1) d, figure 76], making this object a likely AM CVn-type object (vsnet-alert 18669). The superhumps were clearly detected only on this night, and the object faded after a 6 d gap in observation. The times of superhumps maxima are listed in table 62. The period given in table 3 refers to the one determined with the PDM method.

The object then showed (probably damping) oscillations (vsnet-alert 18712, 18724; figure 77), which are characteristic to AM CVn-type superoutbursts (cf. Levitan et al. 2015, Kato et al. 2004a, Nogami et al. 2004, Kato et al. 2013a, Kato et al. 2014b). During this phase, there were weak variations with a period of 0.01906(1) d, which may be late stage superhumps or the orbital variation (figure 78).

3.66 ASASSN-15kh

This object was detected as a transient at $V=13.2$ on 2015 June 1 by the ASAS-SN team. No quiescent counterpart is known. Emerging (ordinary) superhumps were observed on June 14 (13 d after the outburst detection, vsnet-alert 18734, 18758, 18799; figure 79). The times of superhump maxima are listed in table 63. The $O-C$ diagram shows clear stages A and B. Stage A lasted for 43 cycles and there was no indication of stage C (figure 80). The object started fading rapidly on June 27, 26 d after the outburst detection.

The amplitude of early superhumps was below the limit (0.01 mag) of our detection although the long duration before the appearance of stage A superhumps (figure 80) strongly suggests that the 2:1 resonance was working.

Table 58. Superhump maxima of ASASSN-15ie (2015)

E	max*	error	$O - C^\dagger$	N^\ddagger
0	57151.7387	0.0010	0.0070	15
1	57151.7990	0.0007	0.0087	15
2	57151.8578	0.0012	0.0089	13
35	57153.7938	0.0011	0.0121	19
52	57154.7765	0.0007	-0.0009	16
53	57154.8370	0.0010	0.0009	16
69	57155.7686	0.0007	-0.0046	16
70	57155.8261	0.0008	-0.0056	15
71	57155.8853	0.0010	-0.0050	16
86	57156.7624	0.0008	-0.0065	23
87	57156.8225	0.0007	-0.0049	20
88	57156.8801	0.0012	-0.0059	17
103	57157.7586	0.0011	-0.0060	28
104	57157.8169	0.0013	-0.0063	27
105	57157.8766	0.0015	-0.0051	18
120	57158.7574	0.0008	-0.0029	28
121	57158.8150	0.0013	-0.0039	27
122	57158.8727	0.0020	-0.0048	19
137	57159.7568	0.0015	0.0007	17
138	57159.8168	0.0027	0.0022	14
222	57164.7413	0.0017	0.0066	15
223	57164.8031	0.0022	0.0099	15
224	57164.8565	0.0016	0.0047	8
240	57165.7930	0.0024	0.0041	14
241	57165.8442	0.0022	-0.0033	11

*BJD-2400000.

†Against max = 2457151.7317 + 0.058572*E*.

‡Number of points used to determine the maximum.

The small P_{dot} [$+1.2(1.6) \times 10^{-5}$] suggests that the object has a small q . The empirical relation between P_{dot} for stage B superhumps and q (equation 6 in Kato 2015) gives a q of 0.065(9). Combined with the long duration of stage A superhumps, low amplitude of superhumps (probably reflecting the small tidal torque) and the long superhump period, this object is a good candidate for the period bouncer. The brightness when superhump appeared was 14.9 mag. Kato (2015) has shown that quiescent brightness is 6.4 and 7.2 mag (in average) fainter in WZ Sge-type objects and period bouncers, respectively. The expected quiescent brightness is 21.3 and 22.1 mag, respectively, and it is not a surprise that there was no previous detection of the quiescent counterpart.

3.67 ASASSN-15le

This object was detected as a transient at $V=14.9$ on 2015 June 12 by the ASAS-SN team. There is a $V=14.9$ mag star $5''$ from this position. There is a GALEX counterpart with an NUV mag-

Table 59. Superhump maxima of ASASSN-15iv (2015)

E	max*	error	$O - C^\dagger$	N^\ddagger
0	57155.6363	0.0014	0.0004	19
1	57155.7062	0.0013	0.0029	11
15	57156.6463	0.0011	-0.0003	21
30	57157.6545	0.0015	-0.0028	21
44	57158.5963	0.0022	-0.0044	13
45	57158.6608	0.0019	-0.0073	18
59	57159.6047	0.0040	-0.0067	12
60	57159.6701	0.0032	-0.0087	21
74	57160.6241	0.0044	0.0020	18
75	57160.6871	0.0031	-0.0024	13
87	57161.5077	0.0040	0.0096	16
88	57161.5715	0.0076	0.0060	11
89	57161.6393	0.0026	0.0065	19
102	57162.5164	0.0021	0.0075	16
103	57162.5818	0.0013	0.0056	11
104	57162.6512	0.0038	0.0076	17
117	57163.5209	0.0023	0.0014	15
118	57163.6024	0.0023	0.0154	12
119	57163.6494	0.0025	-0.0049	17
132	57164.5263	0.0074	-0.0040	14
134	57164.6588	0.0039	-0.0063	15
148	57165.6000	0.0033	-0.0084	14
149	57165.6671	0.0050	-0.0087	13

*BJD-2400000.

†Against max = 2457155.6359 + 0.067382*E*.

‡Number of points used to determine the maximum.

Table 60. Superhump maxima of ASASSN-15iz (2015)

E	max*	error	$O - C^\dagger$	N^\ddagger
0	57159.6872	0.0016	0.0013	16
12	57160.6601	0.0020	-0.0030	22
24	57161.6415	0.0014	0.0012	23
48	57163.5967	0.0037	0.0019	13
61	57164.6520	0.0031	-0.0014	17

*BJD-2400000.

†Against max = 2457159.6859 + 0.081434*E*.

‡Number of points used to determine the maximum.

Table 61. Superhump maxima of ASASSN-15jj (2015)

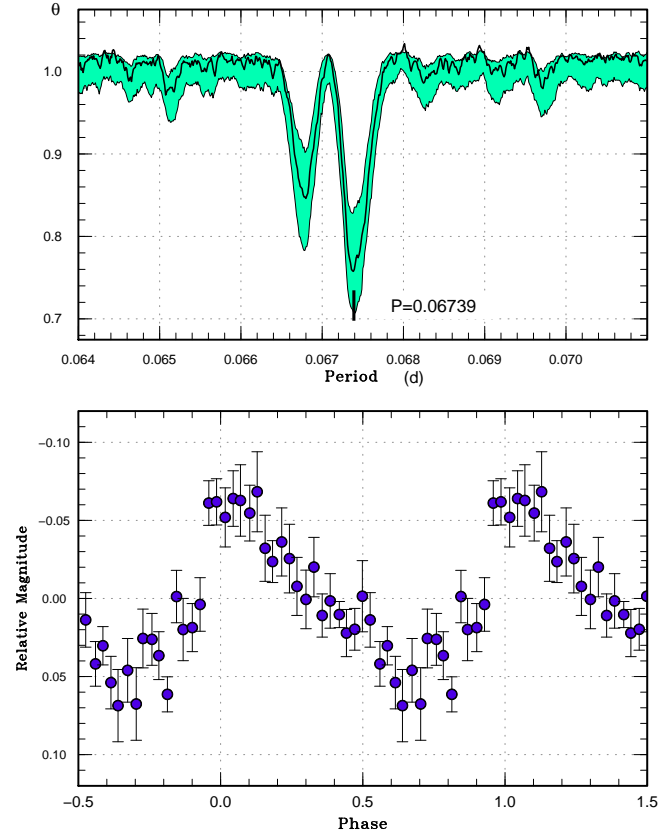
E	max*	error	$O - C^\dagger$	N^\ddagger
0	57161.7489	0.0006	0.0055	16
1	57161.8120	0.0007	0.0063	13
2	57161.8757	0.0007	0.0076	14
12	57162.4961	0.0021	0.0039	69
13	57162.5581	0.0004	0.0035	144
14	57162.6198	0.0005	0.0028	120
16	57162.7441	0.0008	0.0023	17
17	57162.8056	0.0011	0.0013	14
18	57162.8688	0.0008	0.0022	16
32	57163.7402	0.0008	-0.0001	16
33	57163.8002	0.0007	-0.0025	15
34	57163.8631	0.0010	-0.0019	16
48	57164.7341	0.0008	-0.0046	16
49	57164.7990	0.0021	-0.0021	14
50	57164.8590	0.0010	-0.0045	15
64	57165.7303	0.0008	-0.0069	15
65	57165.7932	0.0014	-0.0064	15
66	57165.8536	0.0011	-0.0084	16
80	57166.7314	0.0015	-0.0042	13
81	57166.7860	0.0043	-0.0120	15
82	57166.8542	0.0076	-0.0062	17
96	57167.7288	0.0022	-0.0053	21
97	57167.7961	0.0069	-0.0003	21
144	57170.7385	0.0021	0.0091	20
145	57170.7985	0.0015	0.0066	20
146	57170.8587	0.0018	0.0044	17
161	57171.7954	0.0018	0.0052	14
162	57171.8605	0.0009	0.0078	24
178	57172.8551	0.0059	0.0040	17
194	57173.8510	0.0030	0.0014	16
209	57174.7771	0.0016	-0.0085	14

*BJD-2400000.

 † Against max = 2457161.7433 + 0.062403 E . ‡ Number of points used to determine the maximum.**Table 62.** Superhump maxima of ASASSN-15kf (2015)

E	max*	error	$O - C^\dagger$	N^\ddagger
0	57170.3198	0.0003	0.0004	44
1	57170.3380	0.0003	-0.0007	45
2	57170.3584	0.0003	0.0003	44
3	57170.3773	0.0003	0.0000	44

*BJD-2400000.

 † Against max = 2457170.3195 + 0.019272 E . ‡ Number of points used to determine the maximum.**Fig. 73.** Superhumps in ASASSN-15iv (2015). (Upper): PDM analysis. The apparent signal around 0.0668 d was most likely an artefact produced by a combination of stage B and C superhumps and observational intervals. This signal did not appear when we analyzed the segments of stage B and C individually. (Lower): Phase-averaged profile.

nitude of 19.5(1). There was at least one long outburst reaching $V=13.6$ in 2007 October in the ASAS-3 data. Superhumps were soon detected (vsnet-alert 18736, 18746; figure 81). Although there were observations after BJD 2457193, we could not detect a confident superhump signal on later nights, probably due to the contamination by the nearby star. We only listed superhump maxima for the initial three nights in table 64.

3.68 ASASSN-15lt

This object was detected as a transient at $V=13.8$ on 2015 June 21 by the ASAS-SN team. The object soon developed superhumps (vsnet-alert 18797; figure 82). The early evolution (3 d after the outburst detection, less than 7 d after the outburst maximum even considering the observational gap in the ASAS-SN data) of superhumps apparently excludes the possibility of a WZ Sge-type object. The times of superhump maxima are listed in table 65. There was an apparent stage A-B transition around $E=50$. The maxima after $E=188$ were likely stage C superhumps, which were associated with the small brightening of the

Table 63. Superhump maxima of ASASSN-15kh (2015)

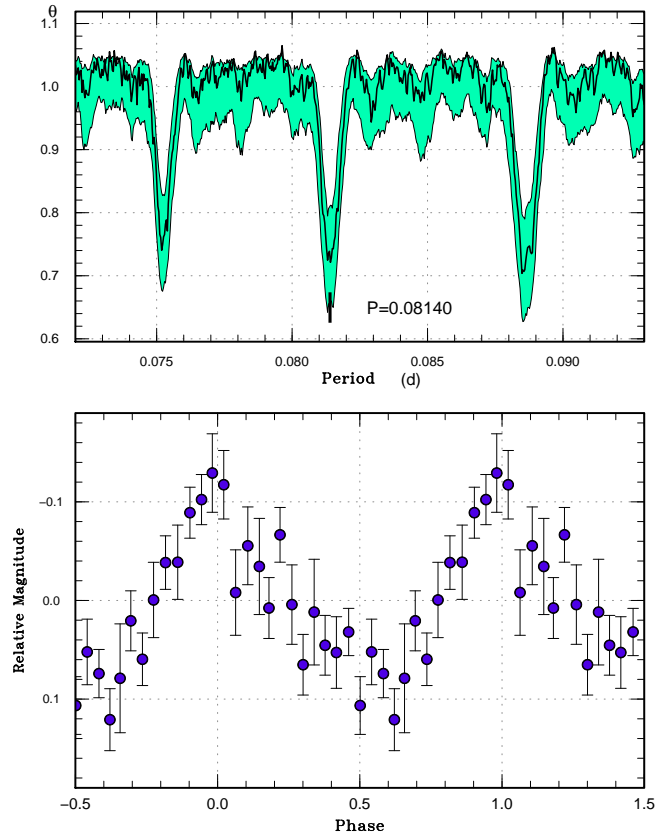
E	max*	error	$O - C^\dagger$	N^\ddagger
0	57187.8600	0.0026	-0.0167	36
1	57187.9206	0.0024	-0.0169	38
6	57188.2301	0.0014	-0.0111	137
7	57188.2896	0.0014	-0.0124	138
8	57188.3522	0.0026	-0.0105	118
11	57188.5377	0.0016	-0.0073	16
27	57189.5237	0.0009	0.0067	15
43	57190.5055	0.0014	0.0166	13
55	57191.2303	0.0007	0.0124	140
56	57191.2916	0.0010	0.0129	139
59	57191.4718	0.0011	0.0109	11
60	57191.5344	0.0017	0.0127	16
68	57192.0203	0.0024	0.0127	21
72	57192.2591	0.0006	0.0085	139
73	57192.3194	0.0006	0.0080	139
76	57192.5032	0.0011	0.0096	13
85	57193.0508	0.0042	0.0104	26
88	57193.2272	0.0008	0.0046	138
93	57193.5305	0.0010	0.0042	16
109	57194.4902	0.0020	-0.0081	14
125	57195.4634	0.0114	-0.0069	10
126	57195.5238	0.0013	-0.0073	17
138	57196.2522	0.0017	-0.0078	138
139	57196.3123	0.0015	-0.0085	94
175	57198.4910	0.0014	-0.0167	13

*BJD-2400000.

 † Against max = 2457187.8767 + 0.060748 E . ‡ Number of points used to determine the maximum.**Table 64.** Superhump maxima of ASASSN-15le (2015)

E	max*	error	$O - C^\dagger$	N^\ddagger
0	57189.4670	0.0008	0.0020	57
13	57190.4796	0.0006	0.0006	73
14	57190.5532	0.0007	-0.0037	59
41	57192.6640	0.0044	0.0011	18
42	57192.7411	0.0024	0.0001	21
43	57192.8189	0.0035	-0.0001	27

*BJD-2400000.

 † Against max = 2457189.4650 + 0.078000 E . ‡ Number of points used to determine the maximum.**Fig. 74.** Superhumps in ASASSN-15iz (2015). (Upper): PDM analysis. The alias selection was based on the $O - C$ analysis. The other one-day aliases [particularly 0.08863(7) d] are still possible. (Lower): Phase-averaged profile.

object. Due to the observational gap, the P_{dot} for stage B superhumps could not be determined. We adopted the period of stage A superhumps determined from the maxima $E \leq 17$.

3.69 ASASSN-15mb

This object was detected as a transient at $V=13.0$ on 2015 June 30 by the ASAS-SN team. There is an likely X-ray counterpart 1RXS J025246.3-395853. There was a past outburst in 2009, which was initially detected at $V=12.74$ by ASAS-3 on October 31, and was observed at 14.2 mag (unfiltered CCD) by CRTS on November 18 (vsnet-alert 18818, 18821).

During the 2015 outburst, superhumps were detected (vsnet-alert 18838, 18843). Due to the short nightly observations, we could not detect many superhumps. The data, however, showed periodic signals in different segments by PDM analysis (figures 83, 84). Since the $O - C$ analysis is not helpful in identifying the alias, we selected the strongest signal in the PDM analysis and assigned the cycle counts (table 66). The maxima for $E \leq 173$ were recorded in the post-superoutburst phase. Since there was significant brightening during the superoutburst

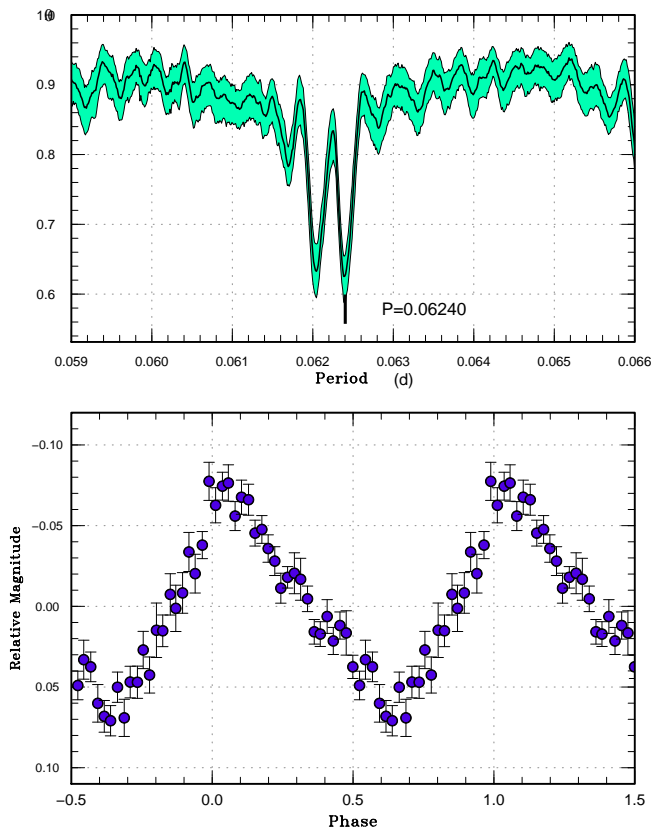


Fig. 75. Superhumps in ASASSN-15jj (2015). (Upper): PDM analysis. The apparent signal around 0.0620 d was most likely an artefact produced by a combination of the effect of strongly varying superhump periods and observational intervals rather than the signal of stage C superhumps. (Lower): Phase-averaged profile.

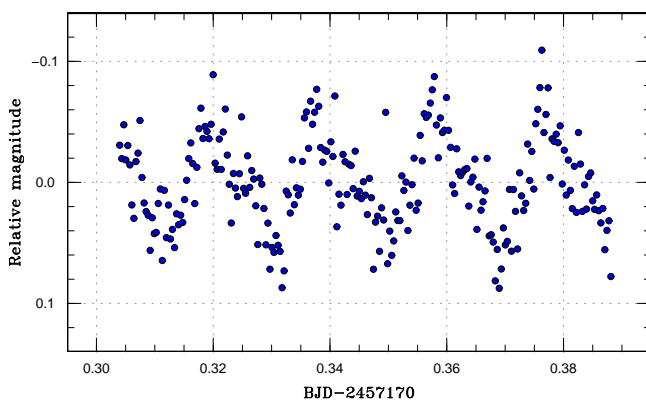


Fig. 76. Superhumps in ASASSN-15kf (2015). This object is likely an AM CVn-type system.

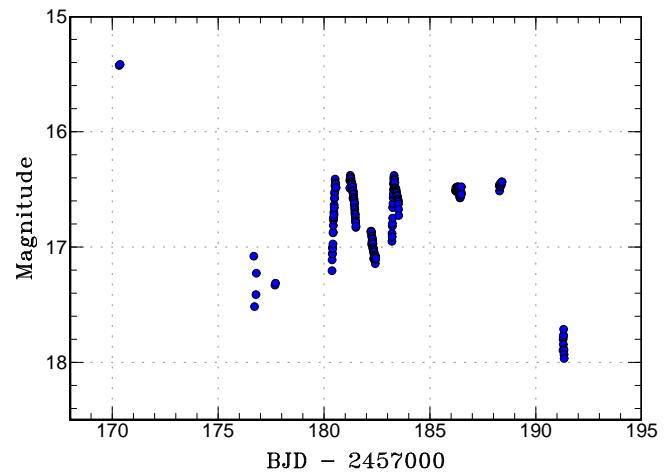


Fig. 77. Outburst light curve of ASASSN-15kf (2015). The data for BJD 2457176–2457178 were binned to 0.05 d. The other data were binned to 0.0064 d.

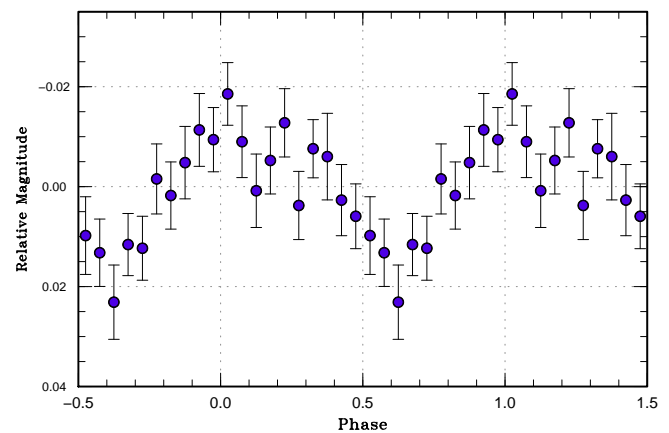
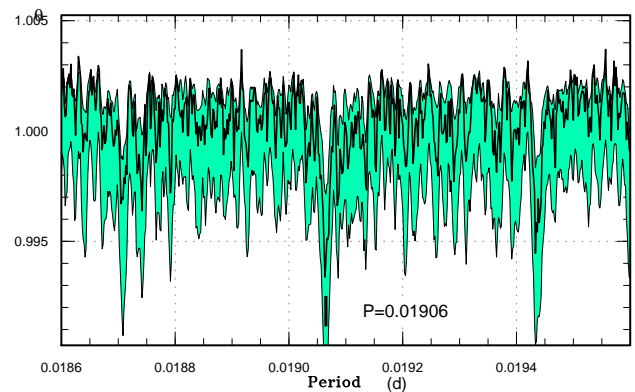


Fig. 78. Late-stage variations in ASASSN-15kf (2015). (Upper): PDM analysis. (Lower): Phase-averaged profile.

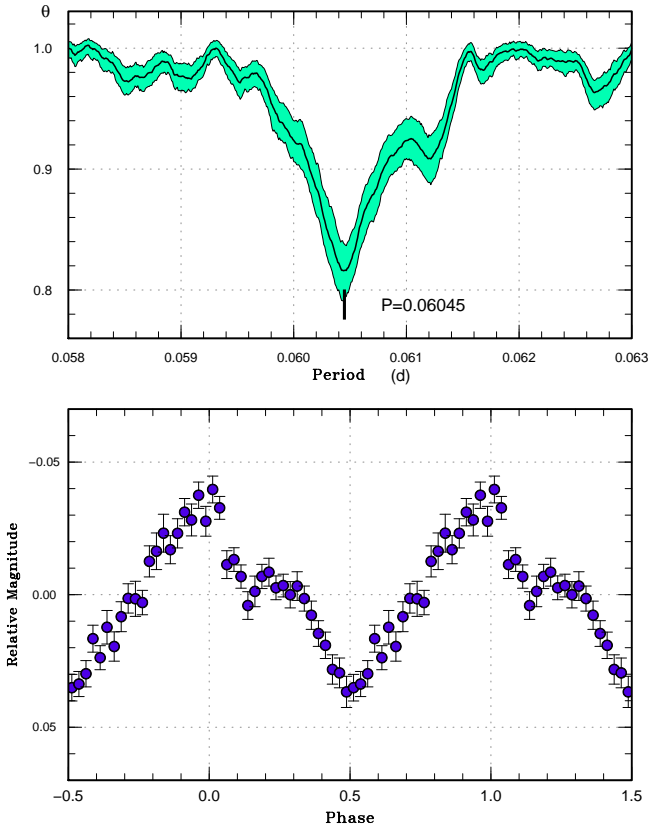


Fig. 79. Superhumps in ASASSN-15kh (2015). (Upper): PDM analysis. (Lower): Phase-averaged profile.

plateau around BJD 2457217, the maxima after this can be attributed to stage C superhumps. We included $E=43$ to stage C in table 3 based on the continuity of the $O - C$ curve. There remain possibilities of other one-day aliases.

The superoutburst lasted at least 19 d (but less than 23 d). The object showed a post-superoutburst rebrightening on July 29, 11 d after the rapid fading from the superoutburst plateau. The second observation during the 2009 outburst likely detected the rapidly fading part or a rebrightening.

3.70 ASASSN-15mt

This object was detected as a transient at $V=13.7$ on 2015 July 18 by the ASAS-SN team (Simonian et al. 2015). The object has a strong UV excess in quiescence. ($U - g = -0.74$, Greiss et al. 2012).

Subsequent observations immediately detected superhumps (vsnet-alert 18878, 18882, 18890; figure 85). The times of superhump maxima are listed in table 67. After $E=42$, there was significant reduction of the superhump amplitudes and we identified this epoch to be stage B-C transition. As is usual for a system with a long superhump period, the transition is not sharp as in short-period systems. The object started fading rapidly on

Table 65. Superhump maxima of ASASSN-15lt (2015)

E	max*	error	$O - C^\dagger$	N^\ddagger
0	57197.8197	0.0026	-0.0328	18
1	57197.8748	0.0015	-0.0375	23
16	57198.8121	0.0009	0.0022	17
17	57198.8711	0.0009	0.0015	23
33	57199.8364	0.0012	0.0093	20
34	57199.8983	0.0007	0.0113	20
49	57200.7980	0.0011	0.0135	23
50	57200.8585	0.0006	0.0142	36
58	57201.3360	0.0008	0.0129	28
66	57201.8077	0.0012	0.0059	24
67	57201.8675	0.0017	0.0059	29
71	57202.1063	0.0007	0.0053	37
188	57209.1090	0.0008	0.0070	37
189	57209.1701	0.0010	0.0082	34
204	57210.0625	0.0015	0.0031	29
205	57210.1235	0.0010	0.0043	32
222	57211.1390	0.0008	0.0025	32
223	57211.1929	0.0006	-0.0034	35
233	57211.7859	0.0016	-0.0088	26
234	57211.8503	0.0023	-0.0043	30
250	57212.8038	0.0021	-0.0082	31
251	57212.8602	0.0015	-0.0116	25
266	57213.7687	0.0046	-0.0007	23

*BJD-2400000.

†Against max = 2457197.8524 + 0.059838E.

‡Number of points used to determine the maximum.

Table 66. Superhump maxima of ASASSN-15mb (2015)

E	max*	error	$O - C^\dagger$	N^\ddagger
0	57212.8860	0.0011	-0.0217	18
43	57215.8791	0.0015	0.0059	23
86	57218.8477	0.0021	0.0091	17
101	57219.8807	0.0021	0.0076	29
115	57220.8560	0.0025	0.0174	20
173	57224.8420	0.0017	0.0036	30
202	57226.8329	0.0013	-0.0055	35
203	57226.8910	0.0022	-0.0163	38

*BJD-2400000.

†Against max = 2457212.9078 + 0.068964E.

‡Number of points used to determine the maximum.

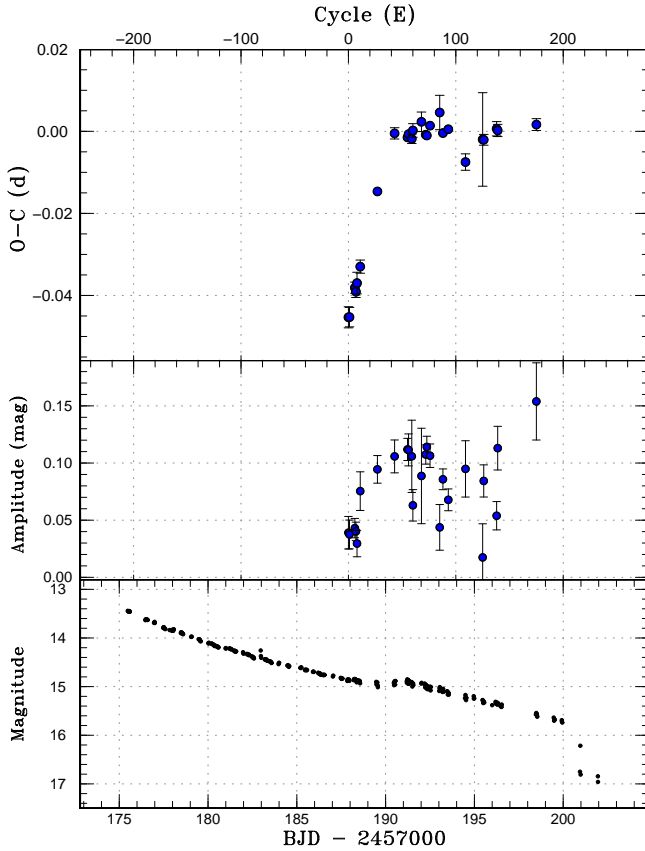


Fig. 80. $O - C$ diagram of superhumps in ASASSN-15kh (2015). (Upper:) $O - C$ diagram. We used a period of 0.06048 d for calculating the $O - C$ residuals. (Middle:) Amplitudes of superhumps. (Lower:) Light curve. The data were binned to 0.020 d.

July 28–29, and the duration of the superoutburst was at least 11 d (but shorter than 16 d).

3.71 ASASSN-15na

This object was detected as a transient at $V=14.8$ on 2015 July 20 by the ASAS-SN team. Double-wave modulations were immediately detected (vsnet-alert 18884). The object was initially suspected as an AM CVn-type dwarf nova (cf. vsnet-alert 18910), which was incorrect due to the mistaken identity of a non-existent rapid fading (cf. vsnet-alert 18923). The object showed growth of superhumps associated with the brightening of the system (vsnet-alert 18923, 18933; figure 86).

The times of superhump maxima after the development of superhumps are listed in table 68. Although there were modulations before these epochs, we have not been able to determine the individual maxima due to the poor statistics (due to the faintness of the object). The epoch $E=174$ probably corresponds to a stage C superhump. The cycle count between $E=111$ and $E=174$ is somewhat ambiguous. Using the data between BJD 2457231.6 and 2457233.8, a period of 0.06491(12) d was ob-

Table 67. Superhump maxima of ASASSN-15mt (2015)

E	max*	error	$O - C^\dagger$	N^\ddagger
0	57225.0985	0.0004	-0.0036	116
1	57225.1739	0.0004	-0.0043	140
2	57225.2493	0.0005	-0.0051	140
19	57226.5482	0.0004	-0.0003	131
29	57227.3108	0.0005	0.0010	43
30	57227.3878	0.0006	0.0018	49
31	57227.4647	0.0006	0.0026	29
42	57228.3007	0.0015	0.0011	22
43	57228.3782	0.0004	0.0026	45
44	57228.4553	0.0003	0.0035	45
45	57228.5315	0.0003	0.0036	35
48	57228.7580	0.0003	0.0016	215
52	57229.0632	0.0006	0.0023	111
53	57229.1350	0.0011	-0.0020	180
54	57229.2118	0.0010	-0.0013	139
55	57229.2925	0.0014	0.0032	66
56	57229.3684	0.0004	0.0030	44
57	57229.4432	0.0006	0.0017	45
58	57229.5179	0.0004	0.0003	43
64	57229.9772	0.0014	0.0028	82
65	57230.0540	0.0006	0.0034	231
66	57230.1272	0.0007	0.0006	191
67	57230.2009	0.0011	-0.0019	139
68	57230.2674	0.0063	-0.0115	81
69	57230.3554	0.0011	0.0003	27
70	57230.4316	0.0007	0.0004	44
71	57230.5084	0.0004	0.0011	46
83	57231.4217	0.0014	0.0008	29
84	57231.5024	0.0007	0.0053	43
95	57232.3306	0.0009	-0.0039	42
96	57232.4061	0.0017	-0.0045	38
97	57232.4818	0.0015	-0.0049	45

*BJD-2400000.

† Against max = 2457225.1021 + 0.076131E.

‡ Number of points used to determine the maximum.

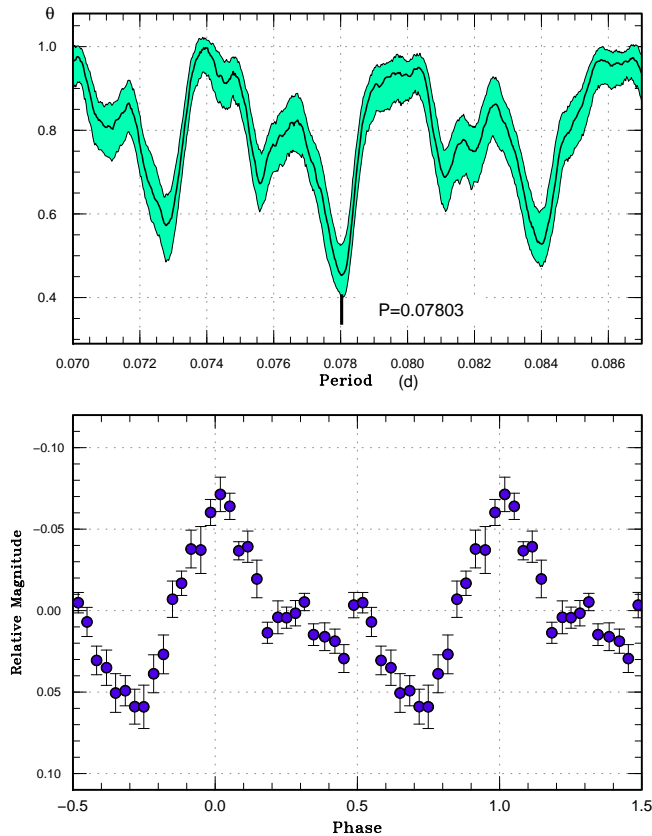


Fig. 81. Superhumps in ASASSN-15le for the first three nights (BJD 2457189–2457193) (2015). (Upper): PDM analysis. The alias selection was the most likely one based on the $O - C$ analysis. (Lower): Phase-averaged profile.

tained, which we identified to be the period of stage A superhumps. The data before BJD 2457231.5 were well expressed by a shorter period of 0.06297(2) d, which we identified to be the period of early superhumps (figure 87). By using these periods, we have obtained $q=0.081(5)$.

Although the orbital period (approximated by the period of early superhumps) is much longer than the period minimum, the object does not have a very low q , which is expected for a period bouncer. The short duration of stage A and large amplitude of superhumps (figure 86) are also consistent with a high q (Kato 2015). The system may be similar to WZ Sge-type dwarf novae with multiple rebrightenings (MASTER OT J211258.65+242145.4, MASTER OT J203749.39+552210.3; Nakata et al. 2013).

3.72 ASASSN-15ni

This object was detected as a transient at $V=12.9$ on 2015 July 28 by the ASAS-SN team (Dong et al. 2015). The dwarf nova-type nature was spectroscopically confirmed (Berardi 2015).

Although no clear superhumps were visible before August

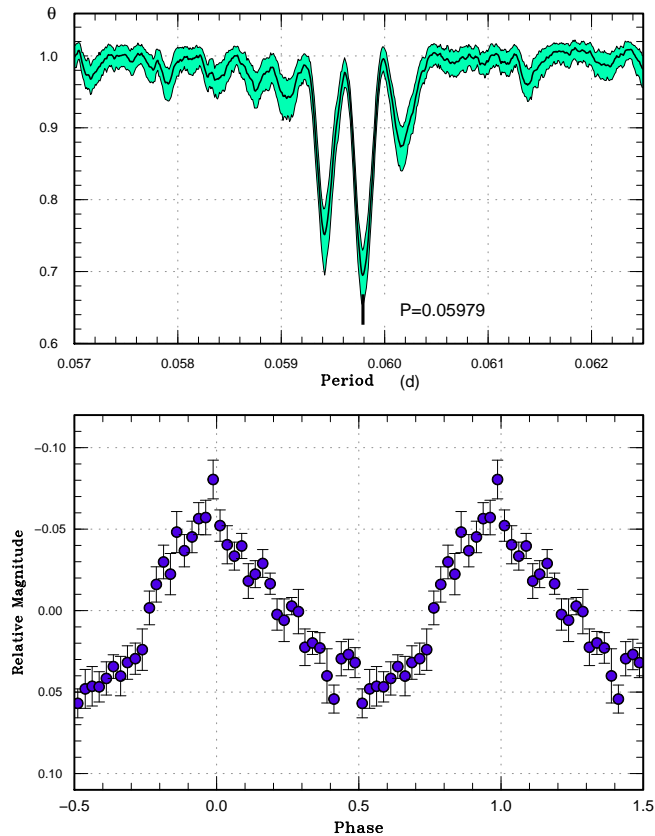


Fig. 82. Superhumps in ASASSN-15lt (2015). (Upper): PDM analysis. (Lower): Phase-averaged profile.

7 (10 d after the outburst detection), ordinary superhumps appeared (vsnet-alert 18945, 18950, 18959, 18968, 18976; figure 88). The times of superhump maxima are listed in table 69. Clear stages A and B can be recognized. Stage A lasted at least 26 cycles. A retrospective analysis of the early data detected low-amplitude double-wave early superhumps (figure 89) confirming the WZ Sge-type classification. The period of early superhump with the PDM method is 0.05517(4) d. The fractional superhump excess $\epsilon^*=0.027(2)$ of stage A corresponds to $q=0.074(2)$. The low value of q is consistent with the long duration of stage A, relatively small P_{dot} and low amplitude of ordinary superhumps.

3.73 ASASSN-15nl

This object was detected as a transient at $V=14.1$ on 2015 August 1 by the ASAS-SN team. The object was found to be already bright ($V=13.3$) on July 29. Although no superhump-like modulations were recorded in our early observations, the object showed superhumps on August 9 (vsnet-alert 18958, 18966; figure 90). Since there was a gap in the observation between August 5 and 9, we could not determine when superhumps started to appear but it took more than 7 d to develop super-

Table 69. Superhump maxima of ASASSN-15ni (2015)

E	max*	error	$O - C^\dagger$	N^\ddagger	E	max*	error	$O - C^\dagger$	N^\ddagger
0	57241.5578	0.0013	-0.0152	54	86	57246.3778	0.0004	-0.0002	29
9	57242.0711	0.0004	-0.0047	120	87	57246.4340	0.0008	0.0002	134
10	57242.1227	0.0004	-0.0090	119	88	57246.4893	0.0007	-0.0005	135
13	57242.3053	0.0035	0.0060	17	89	57246.5451	0.0004	-0.0005	90
14	57242.3528	0.0004	-0.0024	55	90	57246.5988	0.0021	-0.0027	26
15	57242.4116	0.0005	0.0005	76	104	57247.3815	0.0011	-0.0022	27
16	57242.4655	0.0004	-0.0015	96	105	57247.4353	0.0006	-0.0043	50
17	57242.5225	0.0004	-0.0003	56	106	57247.4934	0.0007	-0.0021	58
18	57242.5811	0.0005	0.0025	55	107	57247.5451	0.0016	-0.0062	51
26	57243.0327	0.0003	0.0070	64	122	57248.3867	0.0010	-0.0027	28
32	57243.3684	0.0003	0.0075	56	123	57248.4434	0.0011	-0.0019	27
33	57243.4229	0.0003	0.0062	54	124	57248.4983	0.0011	-0.0029	29
44	57244.0334	0.0011	0.0020	38	134	57249.0532	0.0014	-0.0067	31
45	57244.0903	0.0007	0.0031	45	135	57249.1132	0.0004	-0.0025	100
49	57244.3122	0.0003	0.0015	42	139	57249.3467	0.0031	0.0075	22
50	57244.3689	0.0003	0.0023	55	140	57249.3927	0.0016	-0.0024	25
51	57244.4252	0.0003	0.0027	58	141	57249.4490	0.0006	-0.0019	28
52	57244.4806	0.0007	0.0022	82	142	57249.5104	0.0032	0.0036	17
53	57244.5363	0.0008	0.0021	75	152	57250.0641	0.0012	-0.0014	144
54	57244.5937	0.0022	0.0036	9	153	57250.1208	0.0005	-0.0006	113
64	57245.1502	0.0002	0.0014	105	154	57250.1784	0.0007	0.0011	85
65	57245.2057	0.0005	0.0010	119	157	57250.3434	0.0013	-0.0015	28
67	57245.3167	0.0007	0.0003	20	158	57250.3997	0.0009	-0.0011	30
68	57245.3717	0.0006	-0.0006	67	159	57250.4554	0.0021	-0.0013	25
69	57245.4302	0.0005	0.0021	85	160	57250.5106	0.0013	-0.0020	26
70	57245.4857	0.0005	0.0017	76	175	57251.3568	0.0024	0.0062	22
71	57245.5408	0.0018	0.0009	14	176	57251.4103	0.0031	0.0039	29
80	57246.0407	0.0022	-0.0020	49	177	57251.4603	0.0015	-0.0021	27
81	57246.0979	0.0008	-0.0007	76	190	57252.1870	0.0020	-0.0016	51
82	57246.1594	0.0021	0.0049	28	205	57253.0315	0.0050	0.0047	14
85	57246.3210	0.0005	-0.0012	24	-	-	-	-	-

*BJD-2400000.

 \dagger Against max = 2457241.5730 + 0.055872E. \ddagger Number of points used to determine the maximum.

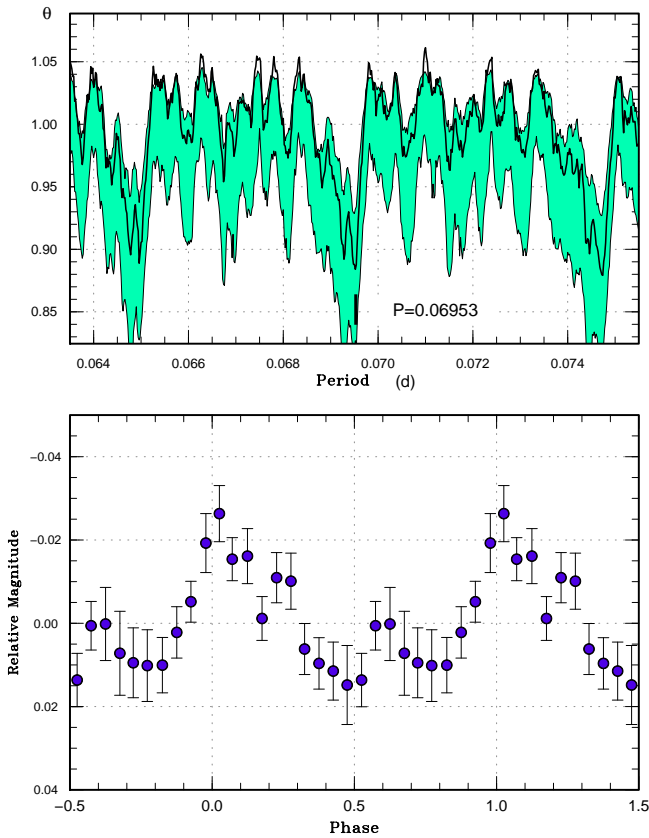


Fig. 83. Superhumps in ASASSN-15mb during the plateau phase (2015). (Upper): PDM analysis. (Lower): Phase-averaged profile.

humps. The times of superhump maxima are listed in table 70.

3.74 ASASSN-15ob

This object was detected as a transient at $V=15.2$ on 2015 August 9 by the ASAS-SN team. There were previous outbursts in the CRTS data. Subsequent observations detected superhumps (vsnet-alert 18975, 18982, 18991; figure 91). The times of superhump maxima are listed in table 71.

3.75 ASASSN-15oj

This object was detected as a transient at $V=13.8$ on 2015 August 15 by the ASAS-SN team. There were four previous outbursts in the CRTS data. Subsequent observations detected superhumps (vsnet-alert 19007; figure 92). The times of superhump maxima are listed in table 72. This table is based on a candidate period. Other aliases [0.07203(1) d, 0.07764(1) d] are also viable.

Table 68. Superhump maxima of ASASSN-15na (2015)

E	max*	error	$O - C^\dagger$	N^\ddagger
0	57234.6800	0.0017	-0.0041	16
1	57234.7438	0.0013	-0.0039	24
9	57235.2544	0.0009	-0.0022	146
10	57235.3208	0.0009	0.0006	143
11	57235.3826	0.0007	-0.0012	146
12	57235.4460	0.0006	-0.0014	146
13	57235.5114	0.0011	0.0004	97
16	57235.6973	0.0008	-0.0045	24
17	57235.7603	0.0014	-0.0052	24
25	57236.2735	0.0010	-0.0009	147
26	57236.3380	0.0006	0.0000	147
27	57236.4012	0.0012	-0.0004	133
32	57236.7144	0.0024	-0.0053	14
47	57237.6768	0.0022	0.0030	11
48	57237.7390	0.0021	0.0015	14
56	57238.2528	0.0023	0.0064	128
57	57238.3102	0.0012	0.0002	147
58	57238.3777	0.0055	0.0040	133
59	57238.4457	0.0033	0.0085	65
63	57238.6917	0.0027	0.0000	14
64	57238.7601	0.0019	0.0048	14
79	57239.6989	0.0036	-0.0106	18
80	57239.7748	0.0053	0.0016	11
95	57240.7301	0.0042	0.0028	17
110	57241.6970	0.0016	0.0155	18
111	57241.7580	0.0030	0.0128	15
174	57245.7304	0.0019	-0.0224	26

*BJD-2400000.

†Against max = 2457234.6841 + 0.063613E.

‡Number of points used to determine the maximum.

Table 70. Superhump maxima of ASASSN-15nl (2015)

E	max*	error	$O - C^\dagger$	N^\ddagger
0	57244.3661	0.0006	0.0006	33
1	57244.4252	0.0008	-0.0004	33
16	57245.3269	0.0005	-0.0002	48
32	57246.2848	0.0043	-0.0038	13
33	57246.3524	0.0006	0.0038	44

*BJD-2400000.

†Against max = 2457244.3655 + 0.060095E.

‡Number of points used to determine the maximum.

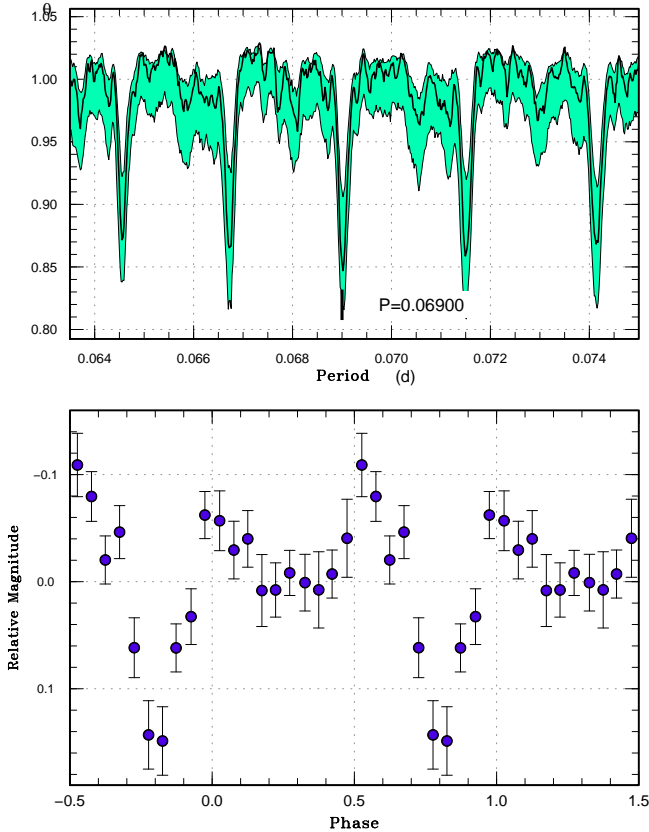


Fig. 84. Superhumps in ASASSN-15mb during the post-superoutburst phase (BJD 2457222–2457232) (2015). (Upper): PDM analysis. (Lower): Phase-averaged profile.

Table 71. Superhump maxima of ASASSN-15ob (2015)

E	max*	error	$O - C^\dagger$	N^\ddagger
0	57247.5669	0.0008	0.0047	19
16	57248.5307	0.0040	0.0002	11
17	57248.5921	0.0028	0.0010	15
29	57249.3127	0.0012	-0.0047	83
33	57249.5580	0.0008	-0.0015	19
45	57250.2821	0.0009	-0.0037	32
83	57252.5897	0.0021	0.0040	12

*BJD-2400000.

† Against max = 2457247.5622 + 0.060525 E .

‡ Number of points used to determine the maximum.

Table 72. Superhump maxima of ASASSN-15oj (2015)

E	max*	error	$O - C^\dagger$	N^\ddagger
0	57259.2591	0.0010	-0.0006	154
14	57260.2143	0.0016	0.0083	99
15	57260.2658	0.0011	-0.0077	155

*BJD-2400000.

† Against max = 2457259.2596 + 0.067596 E .

‡ Number of points used to determine the maximum.

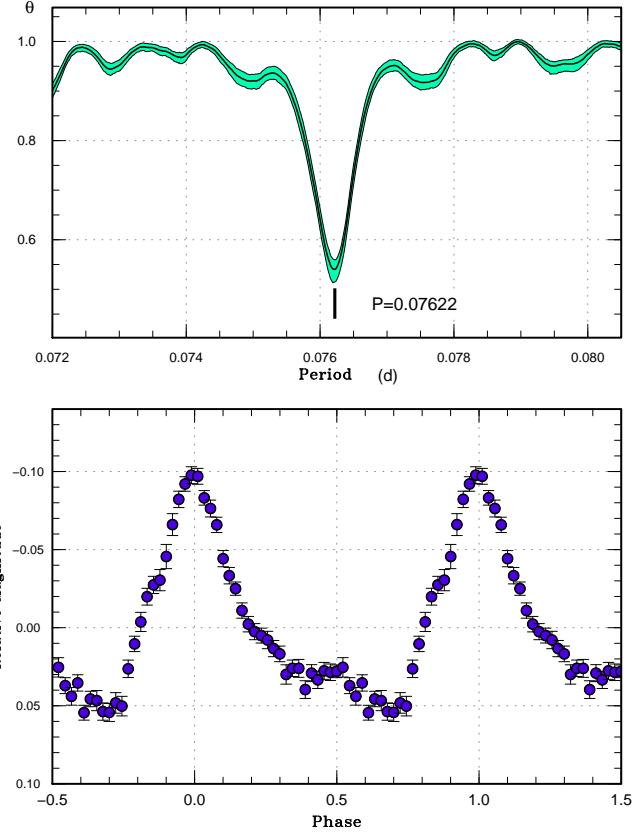


Fig. 85. Superhumps in ASASSN-15mt during the superoutburst plateau (2015). (Upper): PDM analysis. (Lower): Phase-averaged profile.

3.76 ASASSN-15ok

This object was detected as a transient at $V=13.7$ on 2015 August 15 by the ASAS-SN team. There was at least one well-recorded outburst (2008 February) in ASAS-3 data (vsnet-alert 18980). Although the object was initially suspected to be an SS Cyg-type due to the relatively bright counterpart in 2MASS (vsnet-alert 18980), the 2MASS colors are consistent (such as $J - K \sim 0$) with those of an outbursting dwarf nova. The object was accidentally in outburst in 2MASS scans. Subsequent observations detected superhumps (vsnet-alert 18987, 18994, 19008; figure 93). The times of superhump maxima are listed in table 73. The observations apparently covered the later phase of the superoutburst (the object faded rapidly 9 d after the initial observation) and the maxima for $E \geq 25$ likely represent stage C superhumps. The maxima $E < 25$ were likely the final phase of stage B superhumps.

3.77 ASASSN-15pi

This object was detected as a transient at $V=16.4$ on 2015 September 8 by the ASAS-SN team. The object was already $V=16.1$ on September 5 (ASAS-SN data). There is no known

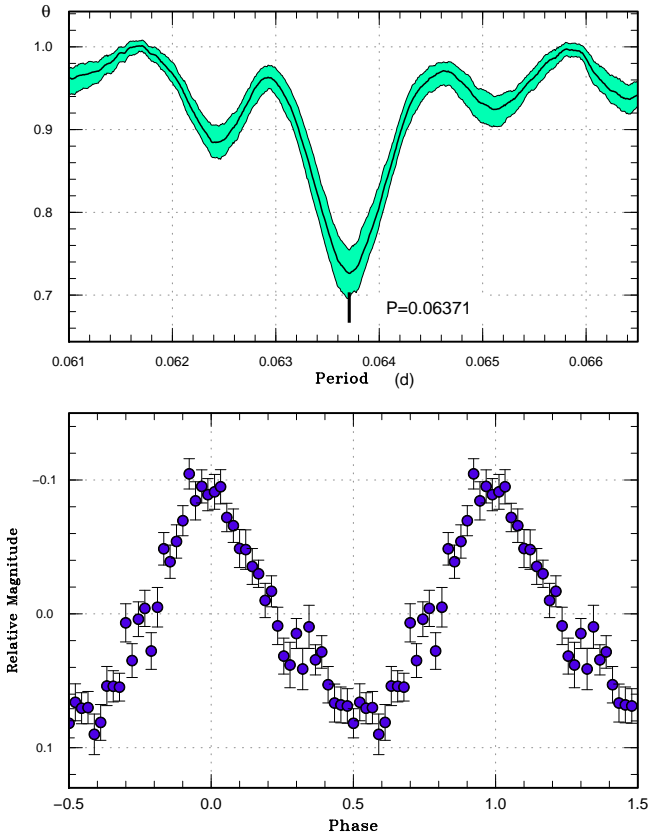


Fig. 86. Superhumps in ASASSN-15na (2015). (Upper): PDM analysis of the segment BJD 2457234–2457242. (Lower): Phase-averaged profile.

quiescent counterpart. Superhumps were detected on single-night observation on September 10 (vsnet-alert 19046; figure 94). The best period determined by the PDM method is 0.0785(2) d. The times of superhump maxima are listed in table 74.

3.78 ASASSN-15pu

This object was detected as a transient at $V=13.7$ on 2015 September 18 by the ASAS-SN team (Stanek et al. 2015). There is a $B_j=22.1$ mag counterpart in GSC 2.3.2. The large outburst amplitude already suggested a WZ Sge-type dwarf nova (Stanek et al. 2015). Early superhumps were immediately recorded (vsnet-alert 19074; the period was corrected in vsnet-alert 19095; figure 95), Ordinary superhumps started to grow on September 28 (vsnet-alert 19095, 19125). The times of superhump maxima are listed in table 75. The maxima for $E \leq 18$ correspond to stage A superhumps. The ϵ^* for stage A superhumps [0.028(5)] corresponds to $q=0.074(16)$.

Table 73. Superhump maxima of ASASSN-15ok (2015)

E	max*	error	$O - C^\dagger$	N^\ddagger
0	57251.8177	0.0006	-0.0068	29
1	57251.8954	0.0008	-0.0076	23
12	57252.7606	0.0013	-0.0065	20
25	57253.7910	0.0007	0.0027	30
26	57253.8680	0.0008	0.0012	30
38	57254.8116	0.0008	0.0021	32
39	57254.8906	0.0008	0.0026	26
46	57255.4404	0.0003	0.0025	175
47	57255.5206	0.0003	0.0042	182
48	57255.5980	0.0003	0.0030	181
51	57255.8345	0.0008	0.0039	23
58	57256.3828	0.0004	0.0023	128
59	57256.4624	0.0003	0.0034	181
60	57256.5401	0.0003	0.0025	181
61	57256.6189	0.0003	0.0027	181
76	57257.7925	0.0015	-0.0019	25
77	57257.8716	0.0015	-0.0013	25
89	57258.8191	0.0027	0.0036	25
90	57258.8946	0.0032	0.0005	16
96	57259.3696	0.0009	0.0042	181
97	57259.4450	0.0013	0.0011	182
98	57259.5276	0.0008	0.0051	135
102	57259.8361	0.0024	-0.0006	24
109	57260.3840	0.0028	-0.0026	181
110	57260.4631	0.0021	-0.0020	181
111	57260.5349	0.0035	-0.0088	181
115	57260.8485	0.0050	-0.0093	22

*BJD–2400000.

†Against max = 2457251.8245 + 0.078551E.

‡Number of points used to determine the maximum.

Table 74. Superhump maxima of ASASSN-15pi (2015)

E	max*	error	$O - C^\dagger$	N^\ddagger
0	57276.3205	0.0008	-0.0006	36
1	57276.4000	0.0007	0.0006	51
2	57276.4784	0.0006	0.0007	50
3	57276.5548	0.0009	-0.0012	51
4	57276.6346	0.0007	0.0003	45

*BJD–2400000.

†Against max = 2457276.3211 + 0.078307E.

‡Number of points used to determine the maximum.

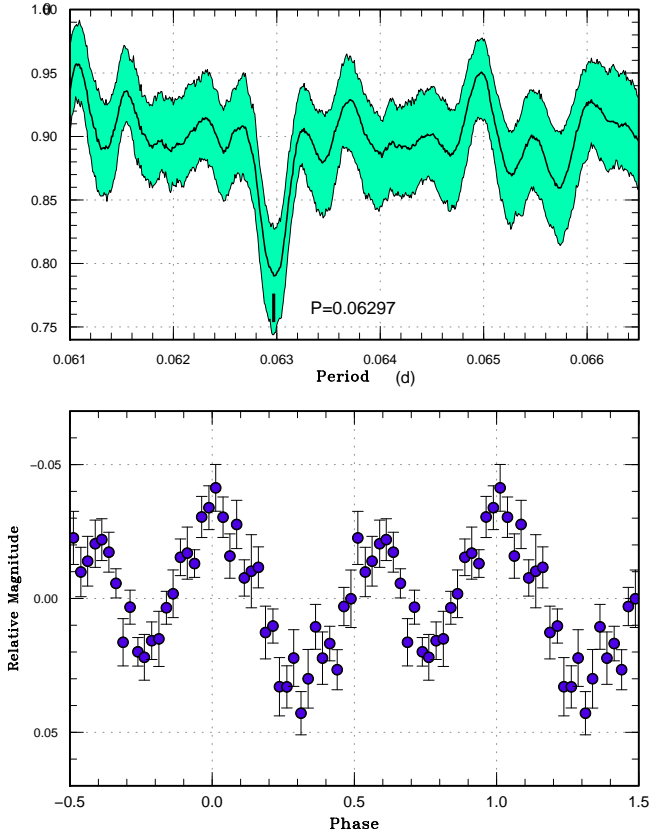


Fig. 87. Early superhumps in ASASSN-15na (2015). (Upper): PDM analysis. (Lower): Phase-averaged profile.

3.79 ASASSN-15qe

This object was detected as a transient at $V=15.0$ on 2015 October 2 by the ASAS-SN team. The object was found to be rising at $V=16.3$ on October 1. There is a $B_j=21.2$ mag counterpart in GSC 2.3.2. Subsequent observations detected superhumps (vsnet-alert 19112, 19131; figure 97). The times of superhump maxima are listed in table 76. Due to the gap in the observation between $E=62$ and $E=175$, the cycle count between them is uncertain. We used maxima for $E \leq 62$ for determining the period in table 3.

3.80 ASASSN-15ql

This object was detected as a transient at $V=15.4$ on 2015 October 4 by the ASAS-SN team. The object was found to be already bright at $V=14.8$ on September 30. Although the observation on October 8 suggested the presence of superhumps (vsnet-alert 19141; figure 98), the object was already rapidly fading 4 d later, and no confirmatory observations were obtained.

Table 75. Superhump maxima of ASASSN-15pu (2015)

E	max*	error	$O - C^\dagger$	N^\ddagger
0	57293.0992	0.0029	-0.0064	21
1	57293.1490	0.0023	-0.0149	36
16	57294.0433	0.0013	0.0048	25
17	57294.1001	0.0014	0.0033	37
18	57294.1605	0.0015	0.0054	36
34	57295.0918	0.0010	0.0038	36
35	57295.1552	0.0016	0.0089	36
69	57297.1285	0.0016	-0.0003	36
70	57297.1919	0.0035	0.0048	17
84	57298.0006	0.0007	-0.0028	23
86	57298.1174	0.0015	-0.0026	37
87	57298.1786	0.0014	0.0004	30
103	57299.1129	0.0013	0.0017	37
104	57299.1685	0.0018	-0.0010	30
106	57299.2841	0.0012	-0.0020	134
107	57299.3435	0.0012	-0.0009	134
108	57299.4008	0.0025	-0.0019	135
109	57299.4589	0.0053	-0.0021	54
123	57300.2816	0.0017	0.0043	135
124	57300.3375	0.0017	0.0019	134
125	57300.3929	0.0021	-0.0011	134
141	57301.3274	0.0018	0.0006	134
142	57301.3884	0.0051	0.0033	60
146	57301.6112	0.0042	-0.0072	27

*BJD-2400000.

† Against max = $2457293.1056 + 0.058307E$.

‡ Number of points used to determine the maximum.

Table 76. Superhump maxima of ASASSN-15qe (2015)

E	max*	error	$O - C^\dagger$	N^\ddagger
0	57299.3882	0.0002	0.0015	54
1	57299.4498	0.0003	0.0019	57
42	57301.9524	0.0005	-0.0017	88
43	57302.0165	0.0003	0.0013	171
44	57302.0747	0.0002	-0.0017	229
45	57302.1361	0.0004	-0.0014	129
59	57302.9929	0.0007	-0.0004	101
60	57303.0546	0.0005	0.0002	131
61	57303.1160	0.0004	0.0004	131
62	57303.1751	0.0014	-0.0015	63
175	57310.0869	0.0023	0.0027	99
176	57310.1439	0.0016	-0.0014	129

*BJD-2400000.

† Against max = $2457299.3867 + 0.061128E$.

‡ Number of points used to determine the maximum.

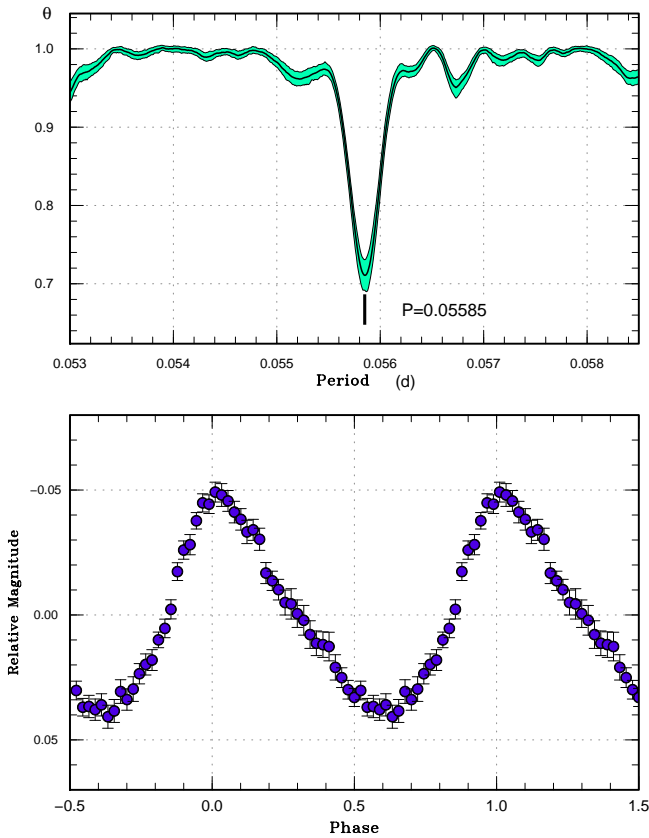


Fig. 88. Superhumps in ASASSN-15ni (2015). (Upper): PDM analysis of the segment BJD 2457241–2457254. (Lower): Phase-averaged profile.

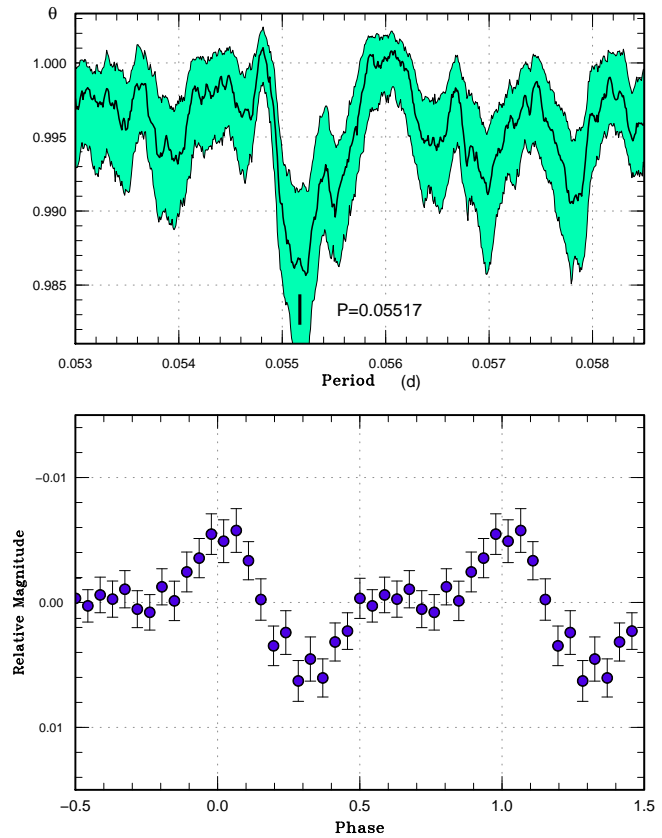


Fig. 89. Early superhumps in ASASSN-15ni (2015). (Upper): PDM analysis. (Lower): Phase-averaged profile.

3.81 ASASSN-15qo

This object was detected as a transient at $V=15.2$ on 2015 October 7 by the ASAS-SN team. Observations on October 8 detected modulations (vsnet-alert 19142; figure 99). The data, however, on later nights were fragmentary and not conclusive. As judged from the large outburst amplitude and the profile of the humps (slower rise), we consider that these modulations were early superhumps and the object is likely a WZ Sge-type dwarf nova. The period determined from the single-night observations is 0.062(1) d, which is long for a WZ Sge-type dwarf nova.

3.82 ASASSN-15qq

This object was detected as a transient at $V=16.2$ on 2015 October 7 by the ASAS-SN team. The object was found to be already bright at $V=15.7$ on October 4. Superhumps were immediately detected (vsnet-alert 19152, 19163, 19171; figure 100). The times of superhump maxima are listed in table 77. The stage of superhumps was not clear. It is possible that the data are a combination of stages B and C, since the outburst detection was not made early enough. In table 3, we gave a

globally averaged value.

3.83 ASASSN-15rf

This object was detected as a transient at $V=15.7$ on 2015 October 13 by the ASAS-SN team. Although observations on the initial night (October 16, figure 101) detected likely superhumps, we could not detect a significant signal on four nights since October 22, probably due to the low signal-to-noise ratio.

3.84 ASASSN-15rj

This object was detected as a transient at $V=16.0$ on 2015 October 14 by the ASAS-SN team. Subsequent observations detected superhumps (vsnet-alert 19168, 19174; figure 102). The times of superhump maxima are listed in table 78. The mean superhump period with the PDM method is 0.09255(4) d.

3.85 ASASSN-15ro

This object was detected as a transient at $V=15.5$ on 2015 October 18 by the ASAS-SN team. Subsequent observations detected superhumps (vsnet-alert 19181, 19185). The times of

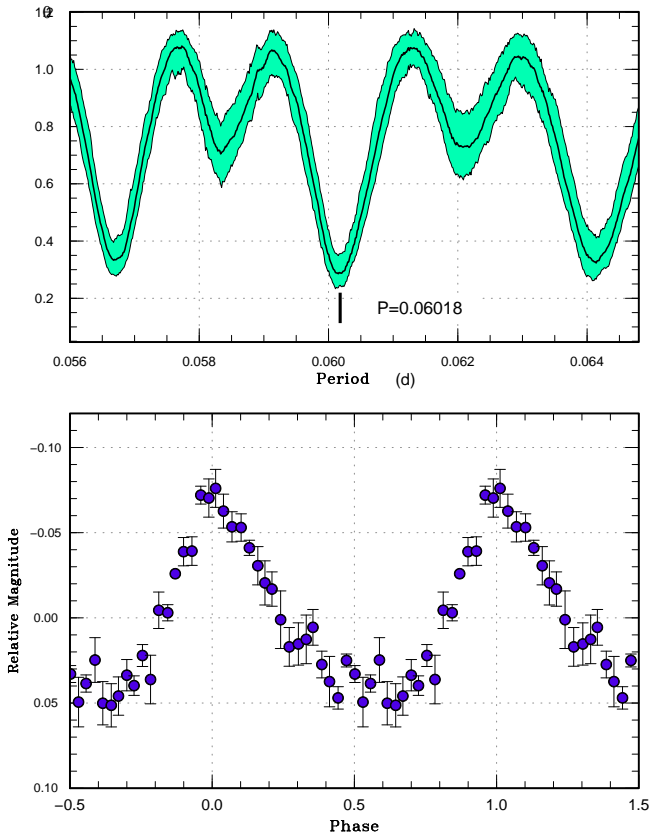


Fig. 90. Superhumps in ASASSN-15nl (2015). (Upper): PDM analysis of the segment after BJD 2457244. The alias selection was based on $O - C$ analysis of two nights. (Lower): Phase-averaged profile.

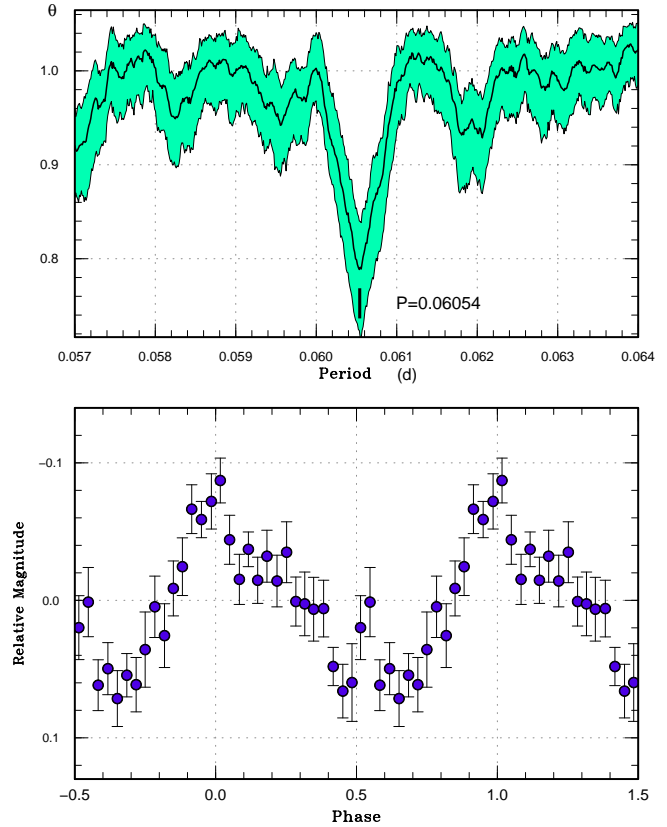


Fig. 91. Superhumps in ASASSN-15ob (2015). (Upper): PDM analysis. (Lower): Phase-averaged profile.

Table 77. Superhump maxima of ASASSN-15qq (2015)

E	max*	error	$O - C^\dagger$	N^\ddagger
0	57305.4081	0.0010	-0.0012	178
1	57305.4876	0.0016	0.0011	112
11	57306.2561	0.0007	-0.0017	138
12	57306.3352	0.0008	0.0003	112
25	57307.3363	0.0010	-0.0013	178
26	57307.4128	0.0013	-0.0019	142
29	57307.6452	0.0019	-0.0009	19
30	57307.7278	0.0038	0.0045	9
37	57308.2654	0.0009	0.0023	149
39	57308.4183	0.0009	0.0009	159
42	57308.6502	0.0025	0.0013	19
55	57309.6499	0.0034	-0.0016	26
68	57310.6507	0.0045	-0.0035	26
81	57311.6587	0.0028	0.0018	22

*BJD-2400000.

† Against max = 2457305.4093 + 0.077131E.

‡ Number of points used to determine the maximum.

Table 78. Superhump maxima of ASASSN-15rj (2015)

E	max*	error	$O - C^\dagger$	N^\ddagger
0	57311.1576	0.0003	-0.0001	186
1	57311.2493	0.0003	-0.0009	179
11	57312.1768	0.0007	0.0019	255
12	57312.2679	0.0005	0.0006	305
13	57312.3609	0.0009	0.0012	86
14	57312.4541	0.0011	0.0019	34
15	57312.5400	0.0017	-0.0046	34

*BJD-2400000.

† Against max = 2457311.1577 + 0.092463E.

‡ Number of points used to determine the maximum.

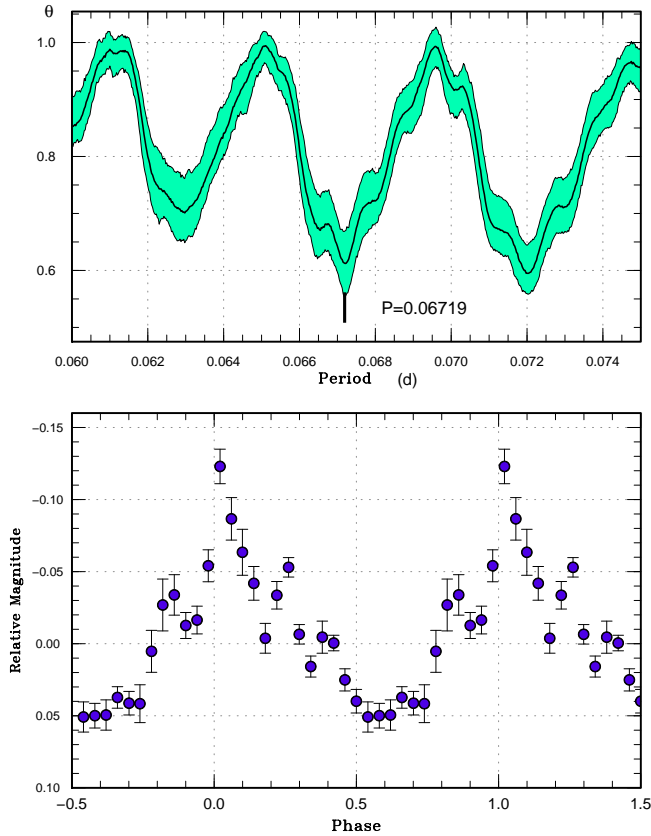


Fig. 92. Superhumps in ASASSN-15oj (2015). (Upper): PDM analysis. The alias selection was to minimize the $O - C$ scatter. Other aliases are also viable. (Lower): Phase-averaged profile.

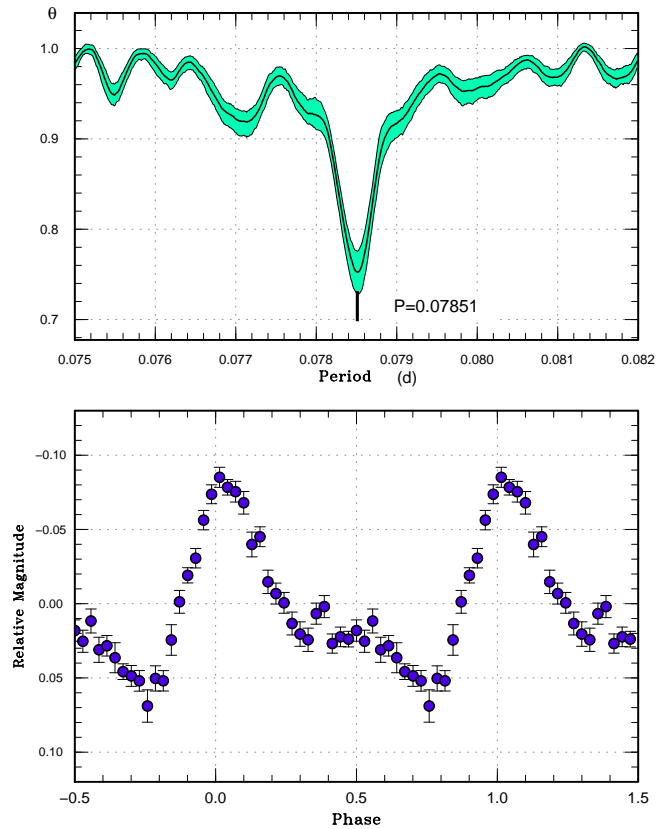


Fig. 93. Superhumps in ASASSN-15ok (2015). (Upper): PDM analysis. (Lower): Phase-averaged profile.

superhump maxima are listed in table 79. The large superhump amplitudes suggest that we observed stage B superhumps.

3.86 ASASSN-15rr

This object was detected as a transient at $V=14.6$ on 2015 October 17 by the ASAS-SN team (the detection announcement was after the observation on October 21 at $V=15.3$). The quiescent counterpart is very faint ($B_j=22.0$) and the large outburst amplitude received attention. Subsequent observations detected superhumps (vsnet-alert 19196). Due to the shortness of the observing runs and the gap in the observation, there remained possibilities of aliases. The times of superhump maxima are listed in table 80 with an assumption of one of the aliases which gives the smallest absolute $O - C$ values.

3.87 ASASSN-15rs

This object was detected as a transient at $V=14.5$ on 2015 October 21 by the ASAS-SN team. The object was also cataloged as an $H\alpha$ emission-line object IPHAS J044633.68+485755.6 (Drew et al. 2005). Subsequent observa-

Table 79. Superhump maxima of ASASSN-15ro (2015)

E	max*	error	$O - C^\dagger$	N^\ddagger
0	57316.0134	0.0033	-0.0005	37
1	57316.0885	0.0002	0.0016	148
2	57316.1596	0.0004	-0.0002	141
3	57316.2336	0.0005	0.0009	130
4	57316.3065	0.0006	0.0009	124
15	57317.1006	0.0031	-0.0070	72
16	57317.1802	0.0005	-0.0003	127
17	57317.2508	0.0005	-0.0026	140
18	57317.3322	0.0008	0.0058	105
27	57317.9833	0.0006	0.0008	127
28	57318.0539	0.0007	-0.0015	137
29	57318.1306	0.0017	0.0022	41

*BJD-2400000.

† Against max = 2457316.0140 + 0.072909E.

‡ Number of points used to determine the maximum.

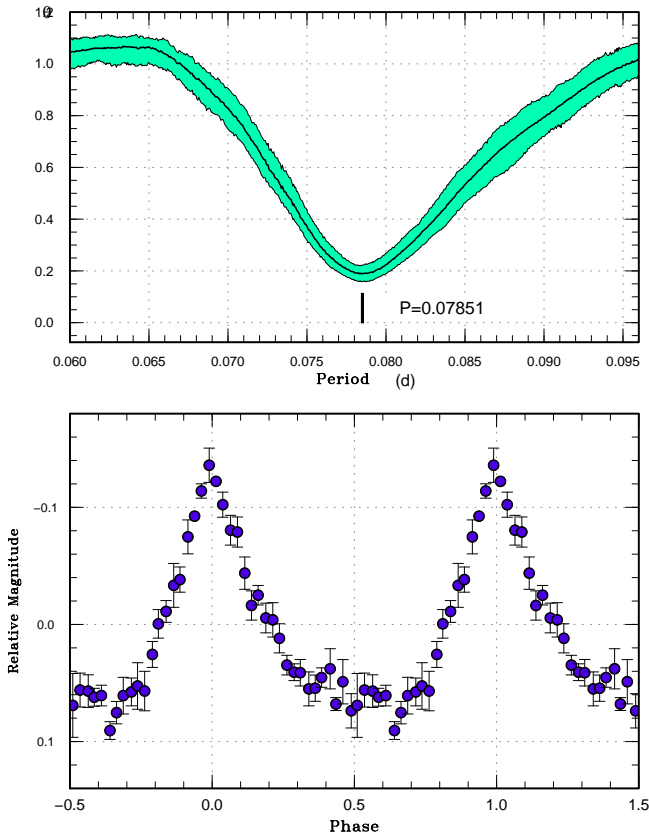


Fig. 94. Superhumps in ASASSN-15pi (2015). (Upper): PDM analysis. (Lower): Phase-averaged profile.

Table 80. Superhump maxima of ASASSN-15rr (2015)

E	max*	error	$O - C^\dagger$	N^\ddagger
0	57318.2426	0.0031	0.0043	69
1	57318.2911	0.0010	-0.0022	66
37	57320.2687	0.0010	-0.0024	115
38	57320.3242	0.0020	-0.0018	126
73	57322.2527	0.0022	0.0038	73
74	57322.3025	0.0023	-0.0013	127
75	57322.3584	0.0027	-0.0003	106

*BJD-2400000.

† Against max = 2457318.2384 + 0.054938 E .

‡ Number of points used to determine the maximum.

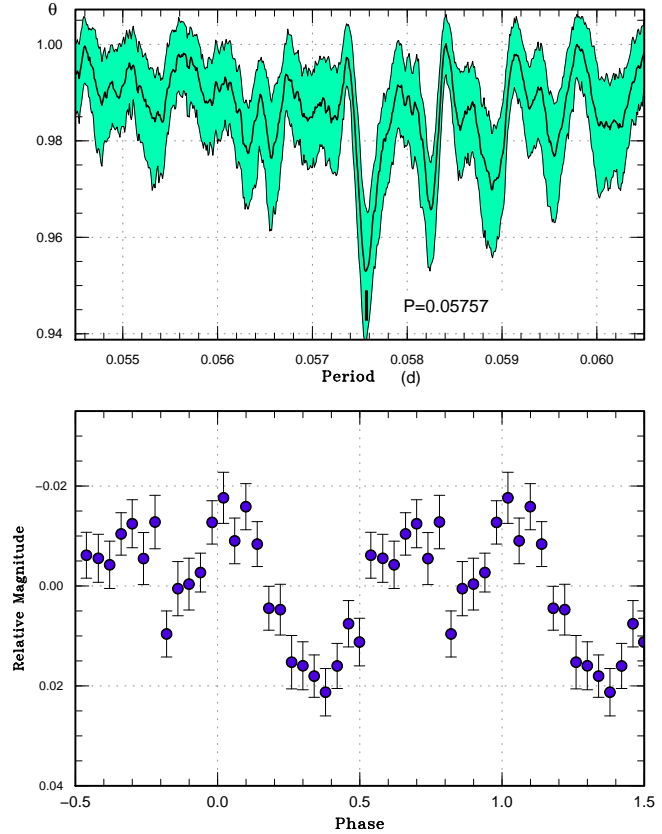


Fig. 95. Early superhumps in ASASSN-15pu (2015). (Upper): PDM analysis. (Lower): Phase-averaged profile.

tions detected long-period superhumps (vsnet-alert 19195; figure 105). The times of superhump maxima are listed in table 81. Due to the gap in the observation, the cycle count between $E=22$ and $E=92$ is somewhat uncertain. Since the superhump period of this system is long, the superhump period may have strongly decreased during the observation (Kato et al. 2009; Kato et al. 2016b; see also subsection 4.4). We restricted the period analysis for $E \leq 22$ in table 3 and figure 105).

3.88 ASASSN-15ry

This object was detected as a transient at $V=15.9$ on 2015 October 22 by the ASAS-SN team (the detection announcement was after the observation on October 24 at $V=15.3$). The object was also independently detected by S. Ueda (TCP J05285567+3618388) on October 24 at an unfiltered CCD magnitude of 14.2.¹⁴ (Our observations suggest that this estimate was too bright by ~ 1 mag). The object was also cataloged as an $H\alpha$ emission-line object IPHAS2 J052855.67+361839.0 (Barentsen et al. 2014). Subsequent observations detected superhumps (vsnet-alert 19193; figure 106). Only single-night

¹⁴<<http://www.cbat.eps.harvard.edu/unconf/followups/J05285567+3618388.html>>.

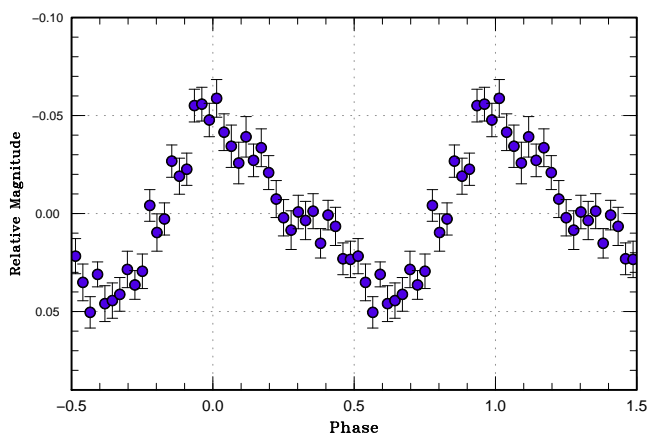
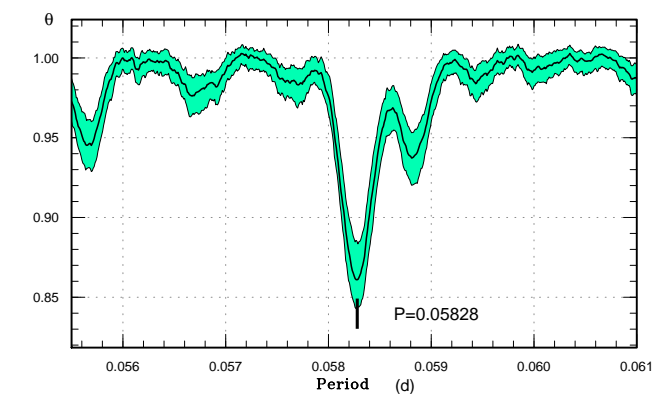


Fig. 96. Ordinary superhumps in ASASSN-15pu (2015). (Upper): PDM analysis. (Lower): Phase-averaged profile.

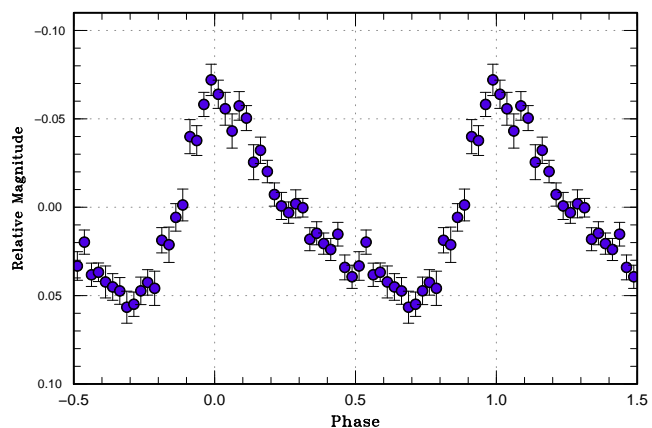
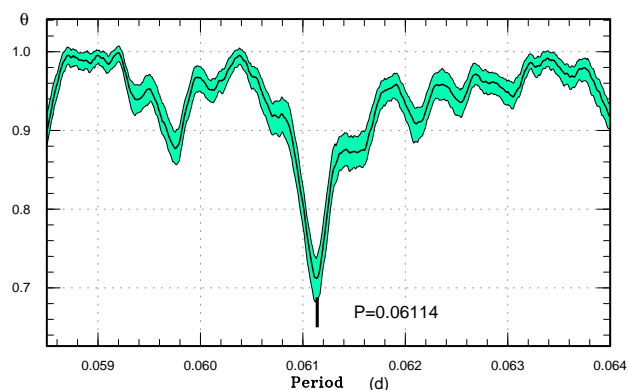


Fig. 97. Ordinary superhumps in ASASSN-15qe (2015). (Upper): PDM analysis. (Lower): Phase-averaged profile.

Table 81. Superhump maxima of ASASSN-15rs (2015)

E	max*	error	$O - C^\dagger$	N^\ddagger
0	57318.2008	0.0003	-0.0018	197
1	57318.2951	0.0004	-0.0049	195
12	57319.3681	0.0009	-0.0035	104
13	57319.4651	0.0008	-0.0040	107
14	57319.5678	0.0013	0.0012	69
20	57320.1560	0.0010	0.0049	182
21	57320.2473	0.0007	-0.0013	109
22	57320.3579	0.0036	0.0119	36
92	57327.1743	0.0017	0.0084	80
93	57327.2523	0.0014	-0.0110	93

*BJD-2400000.

† Against max = 2457318.2026 + 0.097427E.

‡ Number of points used to determine the maximum.

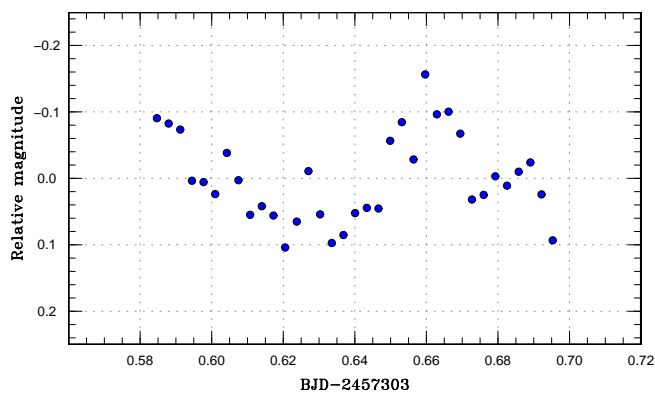


Fig. 98. Likely superhumps in ASASSN-15ql (2015).

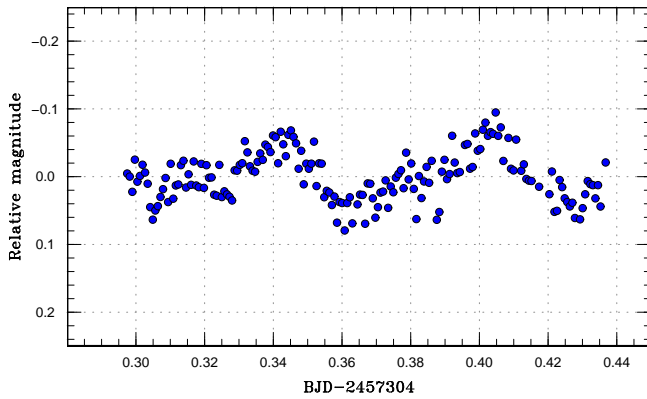


Fig. 99. Likely early superhumps in ASASSN-15qo (2015).

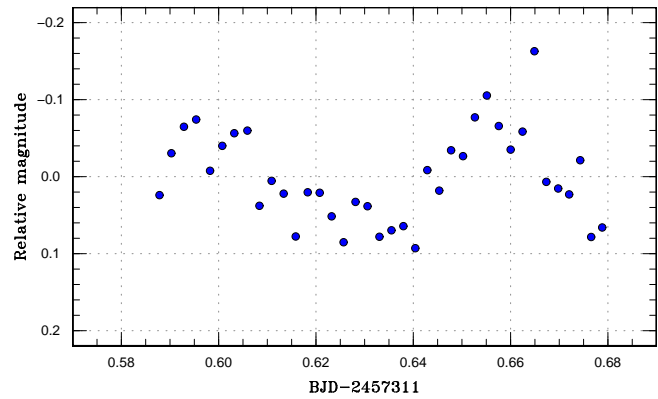


Fig. 101. Likely superhumps in ASASSN-15f (2015).

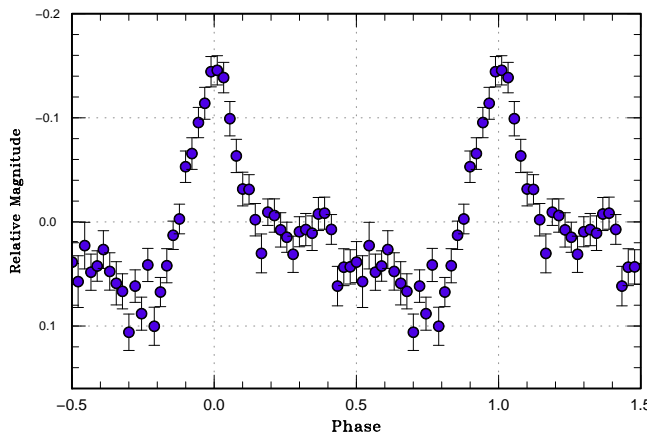
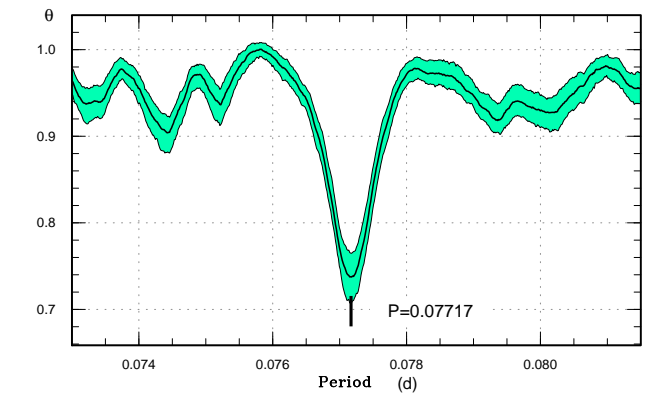


Fig. 100. Superhumps in ASASSN-15qq (2015). (Upper): PDM analysis. (Lower): Phase-averaged profile.

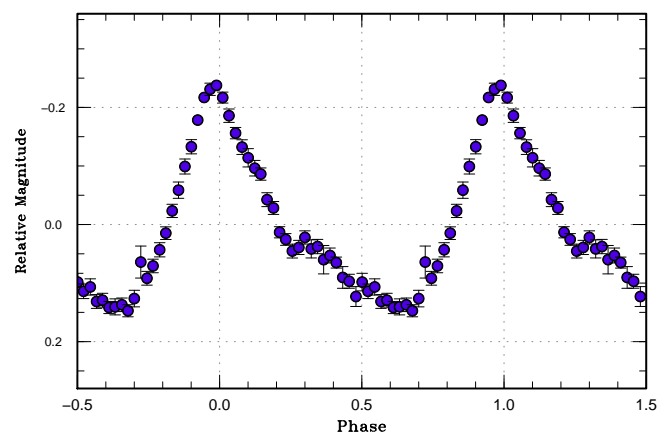
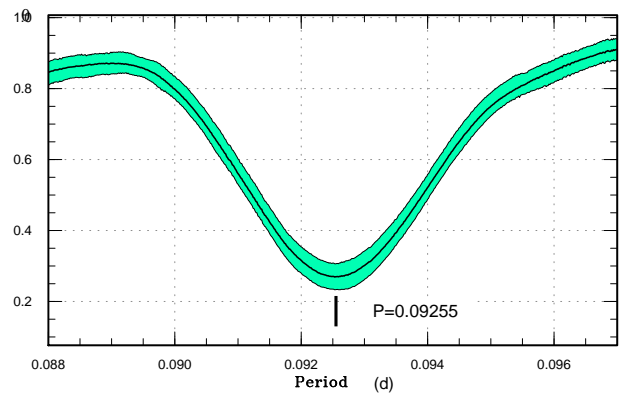


Fig. 102. Superhumps in ASASSN-15rj (2015). (Upper): PDM analysis. (Lower): Phase-averaged profile.

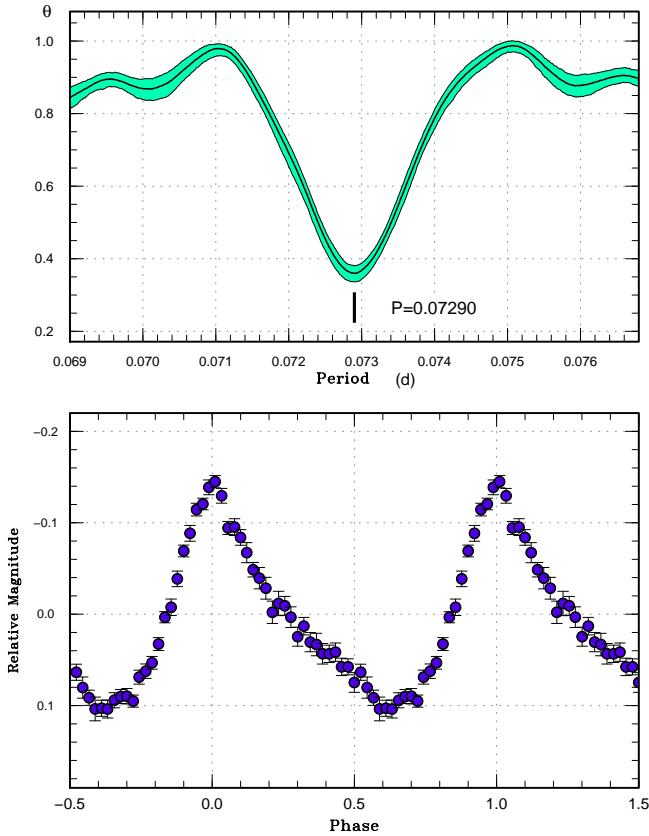


Fig. 103. Superhumps in ASASSN-15ro (2015). (Upper): PDM analysis. (Lower): Phase-averaged profile.

Table 82. Superhump maxima of ASASSN-15ry (2015)

E	max*	error	$O - C^\dagger$	N^\ddagger
0	57321.1181	0.0008	-0.0004	170
1	57321.1811	0.0005	0.0011	282
2	57321.2405	0.0006	-0.0009	228
3	57321.3032	0.0007	0.0003	198

*BJD-2400000.

† Against max = 2457321.1185 + 0.061469E.

‡ Number of points used to determine the maximum.

observations are available and the times of superhump maxima are listed in table 82. The superhump period given in table 3 is based on the PDM analysis.

3.89 ASASSN-15sc

This object was detected as a transient at $V=14.6$ on 2015 October 24 by the ASAS-SN team. The object was still rising at $V=16.2$ on October 22. Although there is a 19.9-mag star $5''$ distant in the Initial Gaia Source List, this object appears too bright and too red for the quiescent counterpart. Time-resolved photometry started on October 28. There were no periodic mod-

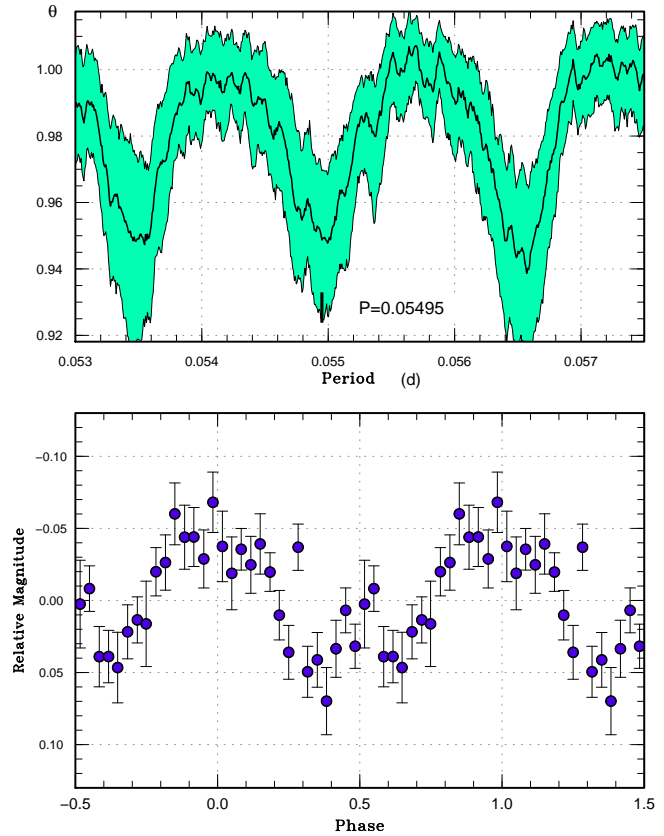


Fig. 104. Superhumps in ASASSN-15rr (2015). (Upper): PDM analysis. The alias selection was based on $O - C$ analysis. The other aliases, particularly 0.05653(4) d, are also viable. (Lower): Phase-averaged profile.

ulations on the first two night. Growing likely superhumps were detected on October 30 and further observations confirmed superhumps (vsnet-alert 19215, 19217, 19219, 19226, 19236, 19238, 19249, 19277; figure 107). The times of superhump maxima are listed in table 83. The $O - C$ data clearly indicate the stages A-B-C with a strongly positive P_{dot} typical for this short superhump period. Although stage C was present, the short duration of stage C (typical for a short-period system) made it difficult to determine the period of stage C superhumps.

3.90 ASASSN-15sd

This object was detected as a transient at $V=14.8$ on 2015 October 27 by the ASAS-SN team. Subsequent observations detected superhumps (vsnet-alert 19210; figure 108). The object rapidly faded on November 5. The times of superhump maxima are listed in table 84. The lack of a significantly positive P_{dot} expected for this superhump period suggests that we only observed stage C superhumps. The duration of the superoutburst plateau was shorter than 11 d, considering the negative observation in the ASAS-SN data on October 24. The development of superhumps and the duration of the superoutburst may

Table 83. Superhump maxima of ASASSN-15sc (2015)

E	max*	error	$O - C^\dagger$	N^\ddagger	E	max*	error	$O - C^\dagger$	N^\ddagger
0	57326.3985	0.0014	-0.0058	66	79	57330.9645	0.0029	-0.0025	50
1	57326.4508	0.0027	-0.0112	74	80	57331.0211	0.0017	-0.0037	57
15	57327.2772	0.0007	0.0066	45	81	57331.0776	0.0018	-0.0049	56
16	57327.3350	0.0004	0.0066	56	82	57331.1348	0.0011	-0.0055	57
17	57327.3937	0.0004	0.0076	56	83	57331.1934	0.0012	-0.0047	81
18	57327.4508	0.0005	0.0069	74	84	57331.2499	0.0011	-0.0059	87
19	57327.5100	0.0004	0.0084	115	85	57331.3072	0.0009	-0.0063	36
20	57327.5681	0.0002	0.0088	106	86	57331.3687	0.0007	-0.0026	30
21	57327.6274	0.0004	0.0103	41	87	57331.4236	0.0007	-0.0055	30
33	57328.3181	0.0004	0.0079	86	88	57331.4825	0.0007	-0.0043	31
34	57328.3737	0.0003	0.0057	86	89	57331.5392	0.0006	-0.0054	31
41	57328.7773	0.0002	0.0050	99	90	57331.5954	0.0009	-0.0070	31
42	57328.8341	0.0002	0.0041	116	101	57332.2317	0.0013	-0.0060	30
43	57328.8916	0.0003	0.0038	115	102	57332.2918	0.0008	-0.0036	31
44	57328.9488	0.0003	0.0032	110	103	57332.3485	0.0009	-0.0046	19
47	57329.1212	0.0011	0.0024	53	104	57332.4047	0.0011	-0.0062	30
48	57329.1774	0.0011	0.0008	114	105	57332.4633	0.0007	-0.0054	31
49	57329.2375	0.0010	0.0031	126	124	57333.5615	0.0009	-0.0046	54
50	57329.2929	0.0010	0.0008	90	125	57333.6189	0.0011	-0.0049	54
51	57329.3502	0.0008	0.0004	88	126	57333.6779	0.0010	-0.0037	54
52	57329.4094	0.0007	0.0018	31	139	57334.4304	0.0010	-0.0020	54
56	57329.6383	0.0004	-0.0003	60	140	57334.4860	0.0013	-0.0042	31
57	57329.6966	0.0004	0.0002	61	158	57335.5288	0.0015	-0.0010	54
58	57329.7536	0.0003	-0.0005	61	159	57335.5895	0.0021	0.0020	31
59	57329.8123	0.0004	0.0004	41	207	57338.3652	0.0016	0.0053	189
62	57329.9841	0.0016	-0.0011	65	208	57338.4269	0.0013	0.0092	106
63	57330.0436	0.0010	0.0007	66	262	57341.5460	0.0015	0.0095	54
64	57330.1011	0.0013	0.0004	66	263	57341.6033	0.0027	0.0090	44
65	57330.1548	0.0015	-0.0037	91	269	57341.9350	0.0041	-0.0058	54
66	57330.2129	0.0006	-0.0032	261	270	57341.9970	0.0059	-0.0015	57
67	57330.2732	0.0011	-0.0007	261	278	57342.4586	0.0108	-0.0020	19
69	57330.3890	0.0013	-0.0004	26	279	57342.5236	0.0016	0.0052	53
70	57330.4480	0.0009	0.0008	31	280	57342.5801	0.0014	0.0039	54

*BJD-2400000.

 † Against max = 2457326.4042 + 0.057757E. ‡ Number of points used to determine the maximum.

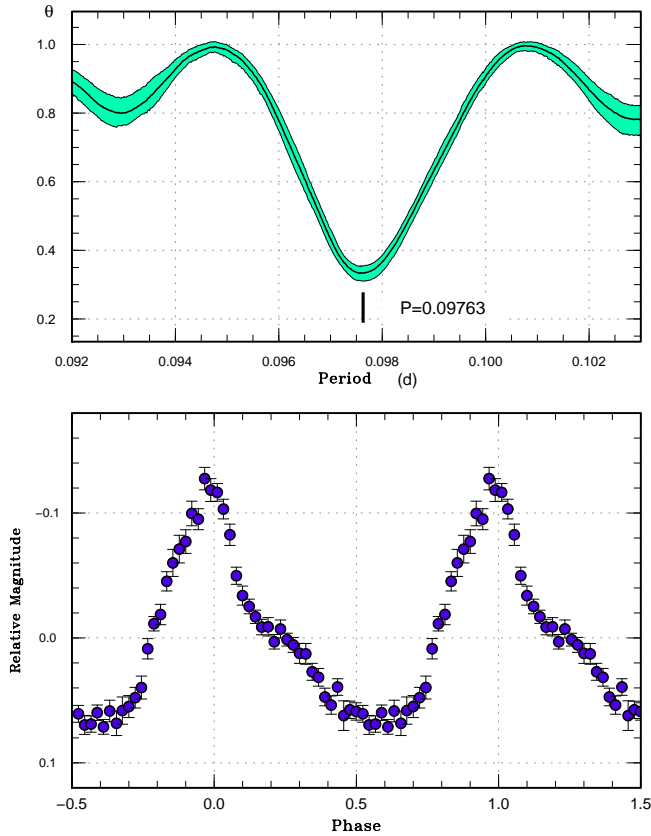


Fig. 105. Superhumps in ASASSN-15rs (2015). (Upper): PDM analysis before BJD 2457321. (Lower): Phase-averaged profile.

be somewhat atypical for this superhump period and further observations are needed to understand the object better.

3.91 ASASSN-15se

This object was detected as a transient at $V=13.04$ on 2015 October 25 by the ASAS-SN team. The outburst announcement was after $V=13.46$ observation on October 28 (vsnet-alert 19208). No superhumps were detected on October 28 and 29. Growing superhumps were detected on October 31 (vsnet-alert 19216). Further data confirmed the superhumps (vsnet-alert 19220, 19227; the period given in vsnet-alert 19227 was in error due to the confusion with ASASSN-15sc; figure 109). The times of superhump maxima are listed in table 85. Although $E=0$ corresponded a stage A superhump, we could not determine the period of stage A superhumps. The object showed at least two rebrightenings on November 15 (vsnet-alert 19286) and November 20–22 (vsnet-alert 19294) (figure 110). It is not clear whether the type of the rebrightenings is type A/B (multiple rebrightenings with small amplitudes) or type B (discrete multiple rebrightenings) in Kato (2015). Since the superhump period is relatively long, this object may belong to WZ Sge-type dwarf novae with multiple rebrightenings as described by

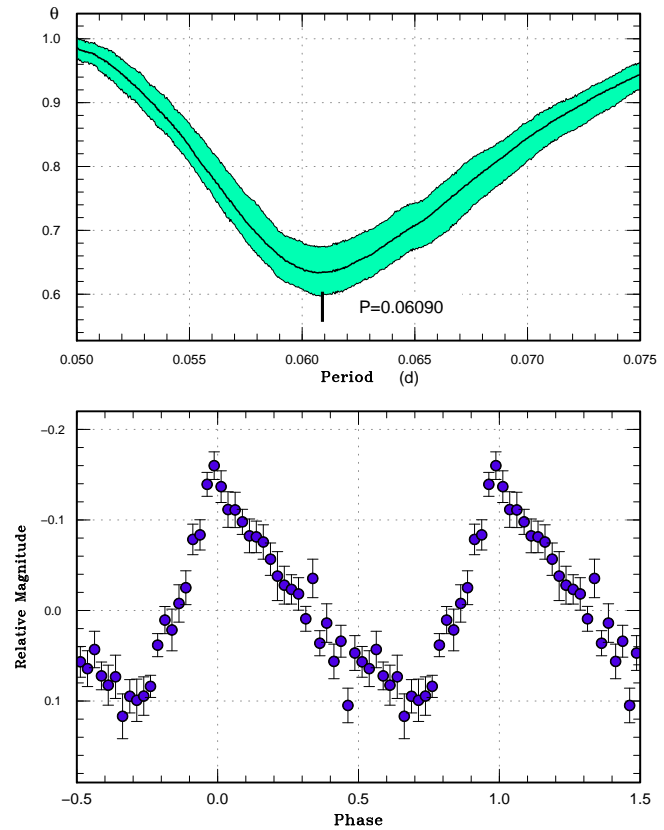


Fig. 106. Superhumps in ASASSN-15ry (2015). (Upper): PDM analysis. (Lower): Phase-averaged profile.

Table 84. Superhump maxima of ASASSN-15sd (2015)

E	max*	error	$O - C^\dagger$	N^\ddagger
0	57324.2650	0.0003	-0.0000	129
1	57324.3366	0.0010	0.0027	94
2	57324.4052	0.0004	0.0024	154
19	57325.5669	0.0059	-0.0071	18
20	57325.6434	0.0020	0.0005	19
34	57326.6089	0.0008	0.0015	40
48	57327.5692	0.0017	-0.0027	29
49	57327.6426	0.0025	0.0018	14
63	57328.6043	0.0011	-0.0010	41
92	57330.6048	0.0038	0.0016	42
93	57330.6724	0.0163	0.0002	14

*BJD-2400000.

† Against max = 2457324.2650 + 0.068894E.

‡ Number of points used to determine the maximum.

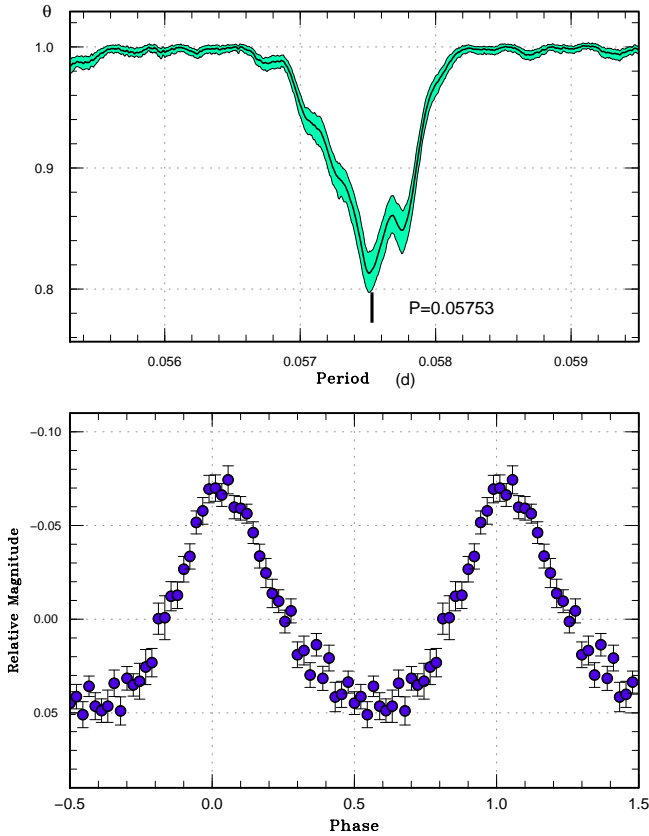


Fig. 107. Superhumps in ASASSN-15sc (2015). (Upper): PDM analysis. (Lower): Phase-averaged profile.

Table 85. Superhump maxima of ASASSN-15se (2015)

E	max*	error	$O - C^\dagger$	N^\ddagger
0	57326.6294	0.0004	-0.0093	59
10	57327.2759	0.0004	0.0029	114
16	57327.6582	0.0004	0.0046	97
17	57327.7206	0.0004	0.0036	84
32	57328.6708	0.0004	0.0023	57
56	57330.1932	0.0016	0.0025	35
57	57330.2509	0.0005	-0.0033	46
58	57330.3144	0.0007	-0.0032	27

*BJD-2400000.

† Against max = 2457326.6387 + 0.063430 E .

‡ Number of points used to determine the maximum.

Nakata et al. (2014).

3.92 ASASSN-15sl

This object was detected as a transient at $V=15.0$ on 2015 November 3 by the ASAS-SN team. The object soon turned out to be a deeply eclipsing SU UMa-type dwarf nova (vsnet-alert 19254, 19259, 19264, 19278, 19279; figure 111). The

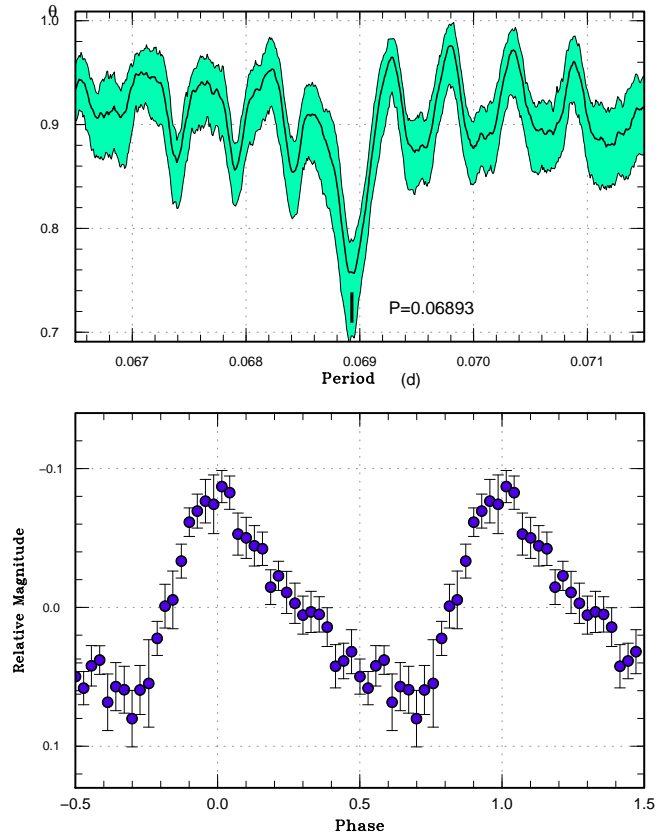


Fig. 108. Superhumps in ASASSN-15sd (2015). (Upper): PDM analysis. (Lower): Phase-averaged profile.

eclipse ephemeris was determined by using MCMC analysis (Kato et al. 2013a) of the observations:

$$\text{Min(BJD)} = 2457341.23671(7) + 0.0870484(7)E. \quad (2)$$

This ephemeris is not intended for long-term prediction of eclipses. The epoch refers to the center of the observation. The times of superhump maxima outside the eclipses are listed in table 86. Although the superhump stage is unknown, we should note that most of our observations were in the later phase of the superoutburst. These superhumps may be mostly stage C superhumps.

3.93 ASASSN-15sn

This object was detected as a transient at $V=15.4$ on 2015 November 4 by the ASAS-SN team. The object was in outburst at $g=15.57$ in the Kepler Input Catalog. The object was recorded at $g=20.85$ and $U=19.94$ in quiescence in the Extended Kepler-INT Survey (Greiss et al. 2012). Subsequent observations detected superhumps (vsnet-alert 19247, 19257; figure 112). The times of superhump maxima are listed in table 87. Since we observed the relatively late stage of the superoutburst, the break in the $O - C$ diagram around $E=27$ probably reflects stage B-C

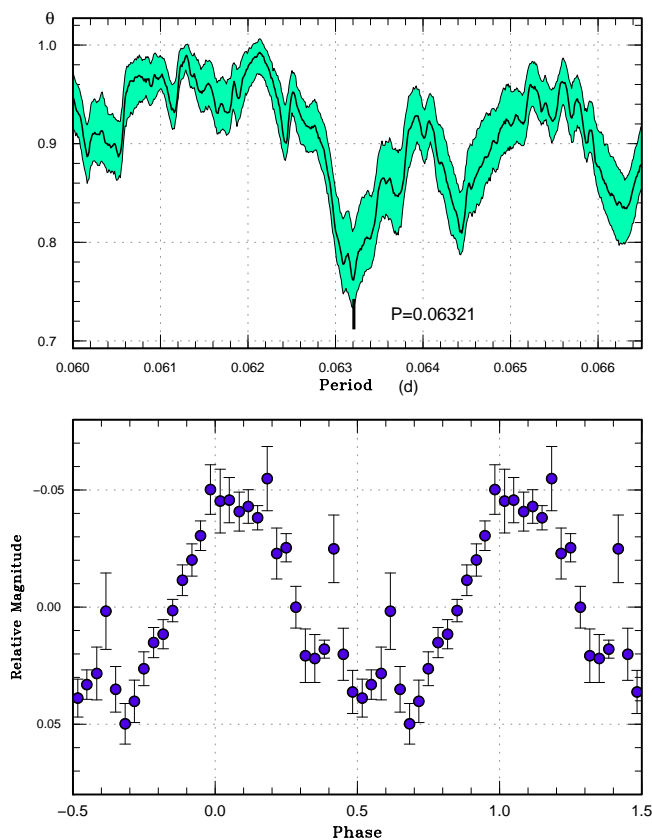


Fig. 109. Superhumps in ASASSN-15se (2015). (Upper): PDM analysis. (Lower): Phase-averaged profile.

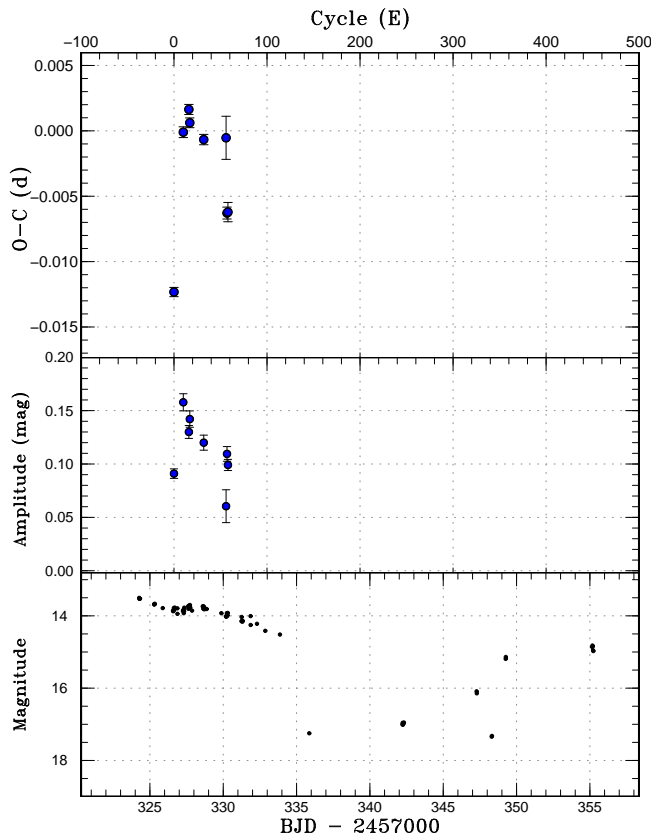


Fig. 110. $O - C$ diagram of superhumps in ASASSN-15se (2015). (Upper:) $O - C$ diagram. We used a period of 0.06343 d for calculating the $O - C$ residuals. (Middle:) Amplitudes of superhumps. (Lower:) Light curve. The data were binned to 0.021 d.

transition. We gave a global value in table 87.

Table 86. Superhump maxima of ASASSN-15sl (2015)

E	max*	error	$O - C^\dagger$	phase [‡]	N^\S
0	57335.5707	0.0014	0.0058	0.91	33
43	57339.4808	0.0015	0.0002	0.83	41
44	57339.5707	0.0073	-0.0010	0.86	29
54	57340.4768	0.0002	-0.0055	0.27	443
55	57340.5659	0.0002	-0.0076	0.29	430
72	57342.1247	0.0041	0.0032	0.20	62
73	57342.2111	0.0067	-0.0015	0.19	70
76	57342.4854	0.0004	-0.0004	0.34	253
97	57344.4050	0.0006	0.0069	0.40	131

*BJD-2400000.

[†]Against max = 2457335.5649 + 0.091065E.

[‡]Orbital phase.

[§]Number of points used to determine the maximum.

3.94 ASASSN-15sp

This object was detected as a transient at $V=13.9$ on 2015 November 8 by the ASAS-SN team. There is an X-ray counterpart 1RXS J075806.5-572239. There was an outburst on 2008 January 26-28 reaching $V=14.02$ detected by ASAS-3 (vsnet-alert 19246). There were double-humped variations on November 9 (vsnet-alert 19252), which developed into full superhumps on November 12 (vsnet-alert 19256, 19260, 19280; figure 113). The initial variation probably reflected growing phase superhumps (part of stage A). The times of superhump maxima are listed in table 88. The maxima for $E \leq 1$ correspond to stage A superhumps. Due to the gap in the observation before $E=33$, we could not determine the period of stage A superhumps. The P_{dot} was positive, as is expected for this superhump period. Although there were observations after $E=138$, we could not determine individual times of maxima. A PDM analysis of the data between BJD 2457345 and 2457352 (late part of the plateau phase with slight brightening) yielded a

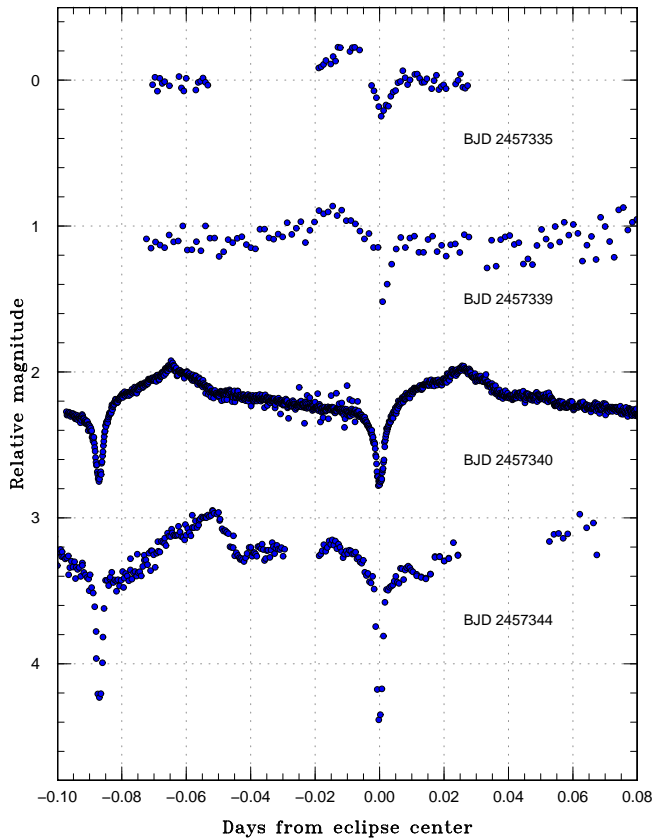


Fig. 111. Light curve of ASASSN-15sl. Superposition of superhumps and eclipses is well visible.

Table 87. Superhump maxima of ASASSN-15sn (2015)

E	max*	error	$O - C^\dagger$	N^\ddagger
0	57335.2699	0.0018	-0.0030	65
1	57335.3348	0.0015	-0.0028	65
2	57335.3997	0.0019	-0.0026	59
27	57337.0303	0.0012	0.0110	47
28	57337.0891	0.0049	0.0051	25
31	57337.2802	0.0008	0.0022	69
32	57337.3434	0.0014	0.0007	70
33	57337.4089	0.0012	0.0014	66
46	57338.2433	0.0015	-0.0050	70
47	57338.3121	0.0013	-0.0009	68
48	57338.3716	0.0011	-0.0061	68

*BJD-2400000.

† Against max = 2457335.2729 + 0.064684*E*.

‡ Number of points used to determine the maximum.

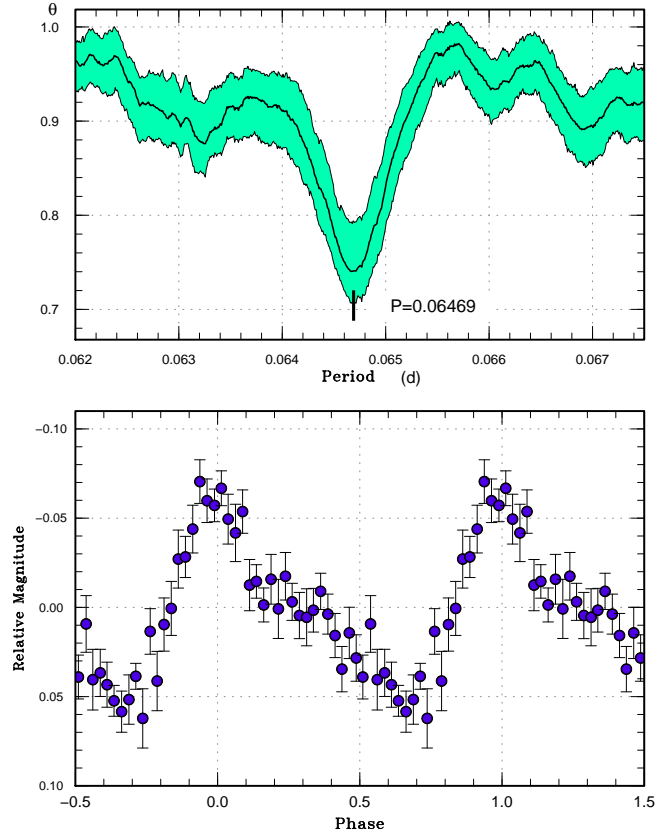


Fig. 112. Superhumps in ASASSN-15sn (2015). (Upper): PDM analysis. (Lower): Phase-averaged profile.

strong signal of 0.05829(4) d. This period is adopted as that of stage C superhumps in table 3.

3.95 ASASSN-15su

This object was detected as a transient at $V=15.0$ on 2015 November 15 by the ASAS-SN team. Previous outbursts were recorded in the CRTS data. Superhumps were immediately detected (vsnet-alert 19285). Although only one superhump maximum was measured at BJD 2457345.5947(6) ($N=57$), the period has been reasonably determined as 0.0670(3) d (figures 114, 115).

3.96 ASASSN-15sv

This object was detected as a transient at $V=15.8$ on 2015 November 16 by the ASAS-SN team. Superhumps were immediately detected (vsnet-alert 19284; figure 116). The long superhump period placed the object in the period gap. Two superhump maxima were recorded: BJD 2457345.3086(9) ($N=52$) and 2457345.3998(9) ($N=72$). The superhump period is 0.091(1) d.

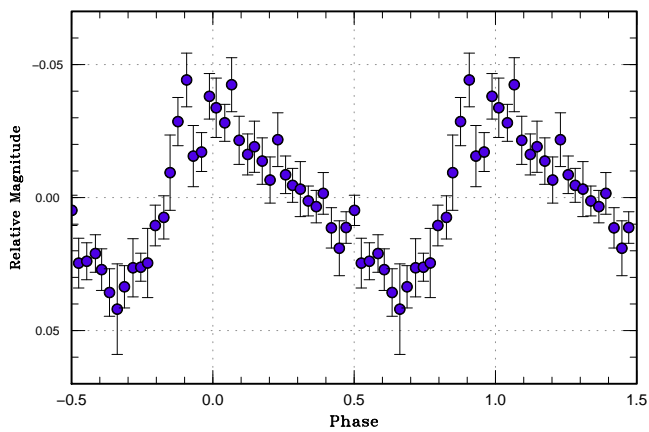
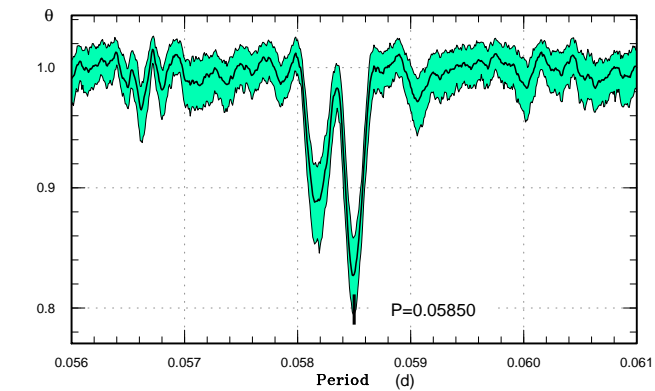


Fig. 113. Superhumps in ASASSN-15sp during the plateau phase (2015). (Upper): PDM analysis. (Lower): Phase-averaged profile.

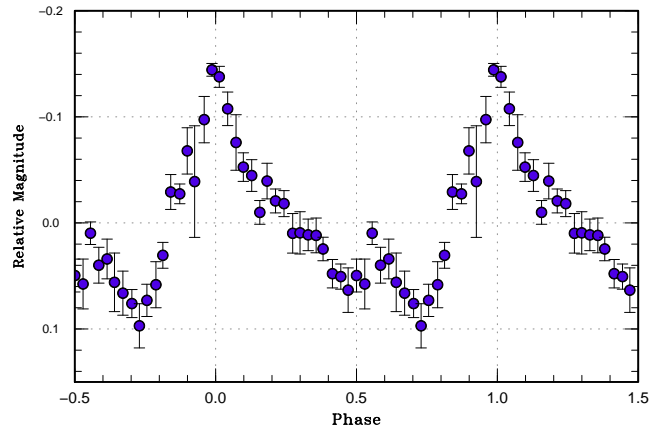
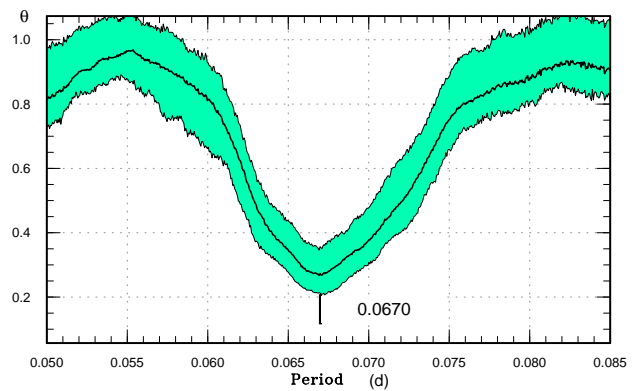


Fig. 115. Superhumps in ASASSN-15su (2015). (Upper): PDM analysis. (Lower): Phase-averaged profile.

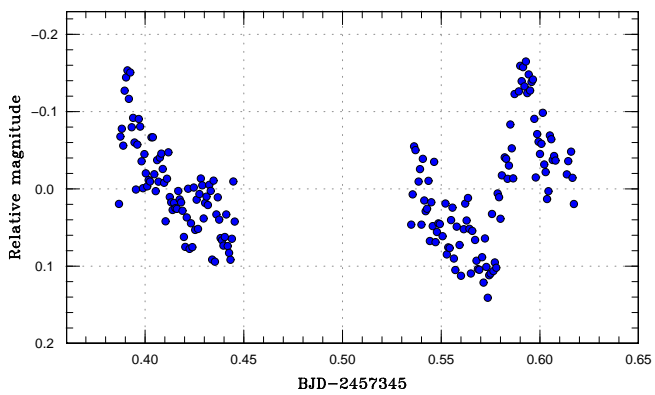


Fig. 114. Superhumps in ASASSN-15sv (2015).

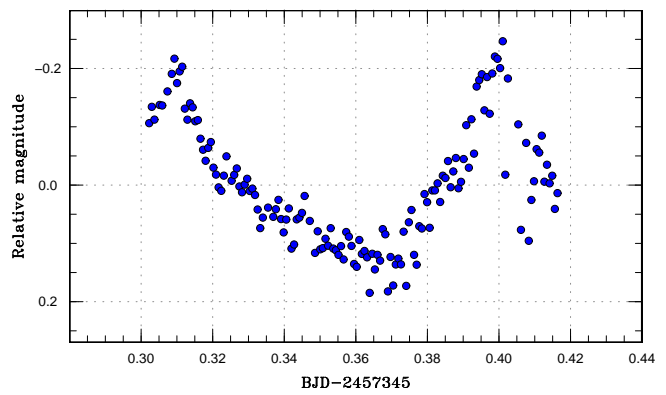


Fig. 116. Superhumps in ASASSN-15sv (2015).

Table 88. Superhump maxima of ASASSN-15sp (2015)

E	max*	error	$O - C^\dagger$	N^\ddagger
0	57336.7419	0.0025	-0.0168	18
1	57336.8110	0.0015	-0.0062	19
33	57338.6977	0.0005	0.0099	13
34	57338.7533	0.0006	0.0071	17
35	57338.8129	0.0004	0.0082	19
50	57339.6874	0.0019	0.0059	12
51	57339.7435	0.0005	0.0035	20
52	57339.8018	0.0006	0.0033	19
85	57341.7263	0.0006	-0.0013	20
86	57341.7847	0.0009	-0.0013	20
87	57341.8415	0.0016	-0.0029	11
102	57342.7182	0.0012	-0.0031	21
103	57342.7777	0.0009	-0.0020	19
104	57342.8366	0.0016	-0.0017	13
119	57343.7153	0.0010	0.0002	21
120	57343.7728	0.0023	-0.0007	19
121	57343.8295	0.0016	-0.0025	16
137	57344.7673	0.0020	0.0000	20
138	57344.8261	0.0018	0.0003	16

*BJD-2400000.

 † Against max = 2457336.7587 + 0.058457*E*. ‡ Number of points used to determine the maximum.**Table 89.** Superhump maxima of ASASSN-15ud (2015)

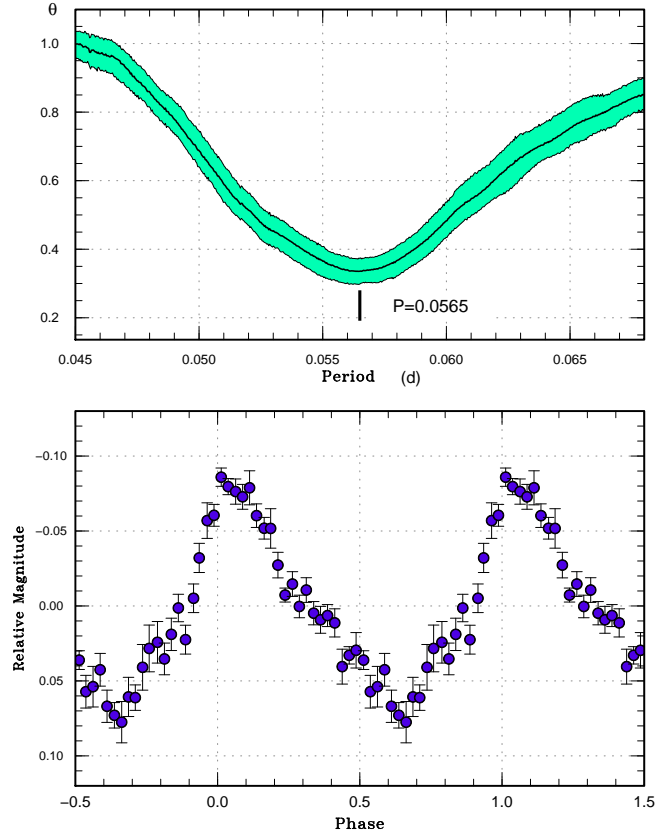
E	max*	error	$O - C^\dagger$	N^\ddagger
0	57374.1940	0.0005	0.0005	89
1	57374.2480	0.0006	-0.0015	95
2	57374.3070	0.0004	0.0015	108
3	57374.3611	0.0006	-0.0005	108

*BJD-2400000.

 † Against max = 2457374.1935 + 0.056030*E*. ‡ Number of points used to determine the maximum.

3.97 ASASSN-15ud

This object was detected as a large-amplitude transient at $V=15.3$ on 2015 December 14 by the ASAS-SN team. There is a $B_j=22.1$ mag counterpart in GSC 2.3.2. Single-night observations detected superhumps (vsnet-alert 19353; figure 117). The times of superhump maxima are listed in table 89. Although the outburst amplitude is large, the object is likely an ordinary SU UMa-type dwarf nova as judged from the early appearance of superhumps. The period given in table 3 is based on the PDM analysis.

**Fig. 117.** Superhumps in ASASSN-15ud (2015). (Upper): PDM analysis. (Lower): Phase-averaged profile.

3.98 ASASSN-15uj

This object was detected as a large-amplitude transient at $V=14.3$ on 2015 December 20 by the ASAS-SN team (cf. vsnet-alert 19352). Subsequent observations detected double-wave early superhumps (vsnet-alert 19359, 19361, 19368; figure 118) confirming the WZ Sge-type classification. The best period of early superhumps with the PDM method is 0.055266(7) d. The object then showed growing ordinary superhumps (vsnet-alert 19392; figure 119). The outburst lasted at least up to 2016 January 17 ($V=16.43$, part of the rebrightening phase?, ASAS-SN data). The times of superhump maxima are listed in table 90. The maxima for $E \leq 22$ correspond to stage A superhumps (figure 120). The measured $\epsilon^*=0.0243(13)$ for stage A superhumps corresponds to $q=0.064(4)$. The almost constant period of stage B superhumps is also consistent with this small q (cf. Kato 2015). The object is a WZ Sge-type dwarf nova likely in relatively evolved state.

3.99 ASASSN-15ux

This object was detected as a large-amplitude transient at $V=14.4$ on 2015 December 29 by the ASAS-SN team. No

Table 90. Superhump maxima of ASASSN-15uj (2015)

E	max*	error	$O - C^\dagger$	N^\ddagger	E	max*	error	$O - C^\dagger$	N^\ddagger
0	57386.5738	0.0038	-0.0117	14	84	57391.2865	0.0013	0.0061	75
1	57386.6264	0.0020	-0.0150	14	85	57391.3379	0.0006	0.0016	128
2	57386.6878	0.0031	-0.0095	14	86	57391.3937	0.0004	0.0015	128
18	57387.5930	0.0010	0.0015	12	87	57391.4475	0.0005	-0.0006	128
19	57387.6486	0.0012	0.0012	14	88	57391.5047	0.0006	0.0007	129
20	57387.7049	0.0014	0.0016	14	89	57391.5596	0.0009	-0.0003	140
21	57387.7605	0.0008	0.0013	19	90	57391.6210	0.0028	0.0052	13
22	57387.8179	0.0012	0.0028	20	91	57391.6753	0.0013	0.0036	12
35	57388.5473	0.0015	0.0056	12	92	57391.7240	0.0014	-0.0035	13
36	57388.6023	0.0012	0.0047	12	93	57391.7842	0.0014	0.0008	19
37	57388.6588	0.0017	0.0053	12	94	57391.8375	0.0018	-0.0019	16
38	57388.7128	0.0016	0.0034	11	107	57392.5657	0.0018	-0.0003	19
53	57389.5514	0.0009	0.0036	13	108	57392.6194	0.0022	-0.0024	14
54	57389.6064	0.0020	0.0027	13	109	57392.6725	0.0023	-0.0053	14
55	57389.6615	0.0020	0.0020	12	110	57392.7328	0.0017	-0.0008	14
56	57389.7199	0.0024	0.0045	13	111	57392.7862	0.0016	-0.0033	18
57	57389.7739	0.0019	0.0025	19	112	57392.8410	0.0033	-0.0044	14
58	57389.8270	0.0027	-0.0002	19	125	57393.5711	0.0016	-0.0009	15
67	57390.3330	0.0004	0.0027	128	126	57393.6230	0.0026	-0.0049	14
68	57390.3873	0.0004	0.0012	128	127	57393.6800	0.0031	-0.0038	13
69	57390.4448	0.0004	0.0028	128	128	57393.7377	0.0020	-0.0019	15
70	57390.5014	0.0006	0.0035	126	129	57393.7938	0.0020	-0.0018	19

*BJD-2400000.

 \dagger Against max = 2457386.5855 + 0.055892*E*. \ddagger Number of points used to determine the maximum.

quiescent counterpart is known. Subsequent observations detected early superhumps (these modulations were initially reported as superhumps) (vsnet-alert 19390, 19391, 19396; figure 121). The object started to show ordinary superhumps on 2016 January 12 (vsnet-alert 19409, 19411; figure 122). The large amplitude of early superhumps and the complex profile of individual superhumps suggested the presence of eclipses (vsnet-alert 19391, 19409). The eclipsing nature was confirmed by further observations (vsnet-alert 19423; figure 123).

The eclipse ephemeris was determined by using MCMC analysis (Kato et al. 2013a) of the observations after BJD 2457396.5 (when eclipses became apparent):

$$\text{Min(BJD)} = 2457400.82908(10) + 0.056109(2)E. \quad (3)$$

This ephemeris is not intended for long-term prediction of eclipses. The epoch refers to the center of the observations used. The period of early superhumps was 0.056091(4) d, 0.03% shorter than the orbital period. This value is in very good agreement with the other eclipsing WZ Sge-type dwarf novae (Kato 2015).

The times of superhump maxima determined from observations outside the eclipses are listed in table 91. Although hump

maxima for $E \leq 3$ looked like stage A superhumps, they may have been a transition phase from early superhumps to ordinary superhumps (e.g. WZ Sge, figure 126 in Kato et al. 2009), we have disregarded these maxima in determining the period of stage A superhumps. There also remains ambiguity in cycle counts between $E=3$ and $E=55$. The maxima for $E \geq 73$ are clearly stage B superhumps.

Although the object is very faint, the object is a rare WZ Sge-type dwarf nova with high amplitude of early superhumps (the mean amplitude of 0.38 mag is one of the largest, cf. Kato 2015) and eclipses. The object will deserve further detailed observations.

3.100 ASASSN-16af

This object was detected as a transient at $V=15.5$ on 2016 January 10 by the ASAS-SN team. Subsequent observations detected superhumps (vsnet-alert 19417, 19419, 19424; figure 124). The times of superhump maxima are listed in table 92. A positive P_{dot} typical for this superhump period was recorded.

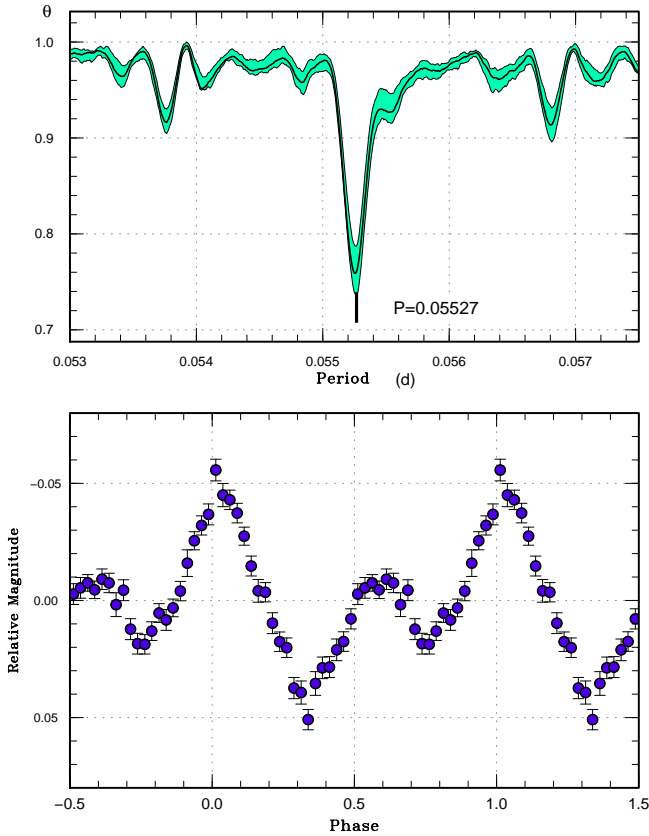


Fig. 118. Early superhumps in ASASSN-15uj (2015). (Upper): PDM analysis. (Lower): Phase-averaged profile.

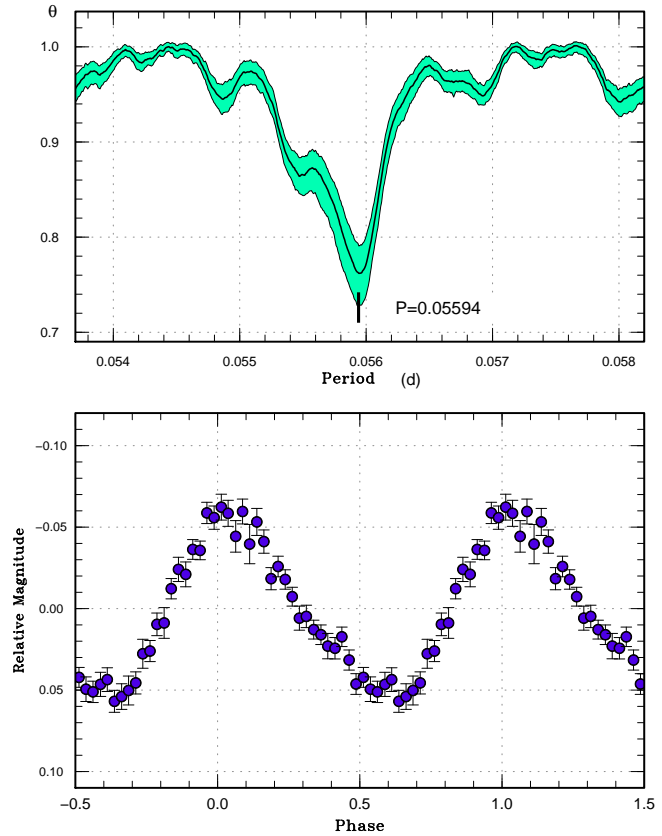


Fig. 119. Ordinary superhumps in ASASSN-15uj (2015). (Upper): PDM analysis. (Lower): Phase-averaged profile.

3.101 ASASSN-16ag

This object was detected as a transient at $V=16.2$ on 2016 January 11 by the ASAS-SN team. Although the observations on January 12.4–12.6 UT did not detect superhumps, superhumps were detected immediately after these observations (vsnet-alert 19407). Although these superhumps were possibly stage A superhumps, we could not determine the stage due to the lack of observations and the low signal-to-noise ratios caused by faintness of the object. In table 93, we list times of maxima using a period which reasonably expresses all the observations (see also figure 125). The object apparently has a low outburst amplitude (3.5 mag) for an SU UMa-type dwarf nova.

3.102 ASASSN-16ao

This object was detected as a transient at $V=16.1$ on 2016 January 13 by the ASAS-SN team. The outburst once faded below $V=18.0$ on January 16 (ASAS-SN data). The object was observed bright by B. Monard on January 19 when the object was at about 18.7 mag. These observations detected modulations attributable to superhumps (vsnet-alert 19433; figure 126). The identification, however, is not secure since the object was

not in very bright state (the identification of a precursor in vsnet-alert 19433 was probably incorrect). The best period from these observations was 0.0639(5) d. Further observations are needed to firmly characterize the nature of this object.

3.103 ASASSN-16aq

This object was detected as a transient at $V=15.1$ on 2016 January 17 by the ASAS-SN team. The large outburst amplitude suggested a possible WZ Sge-type dwarf nova (cf. vsnet-alert 19428). Superhump-type modulations were immediately recorded (vsnet-alert 19432; figure 127). Two superhump maxima were detected: BJD 2457407.7398(6) ($N=97$) and 2457415.7009(20) ($N=83$). Since there was a long gap of observations between these two maxima, we could not choose an unambiguous period. The light curve suggests that the period is relatively longer (longer than 0.08 d). This period is, however, too long for a WZ Sge-type dwarf nova and the object may be a kind of large-amplitude, long- P_{orb} SU UMa-type dwarf novae such as V1251 Cyg and RZ Leo (see Kato 2015).

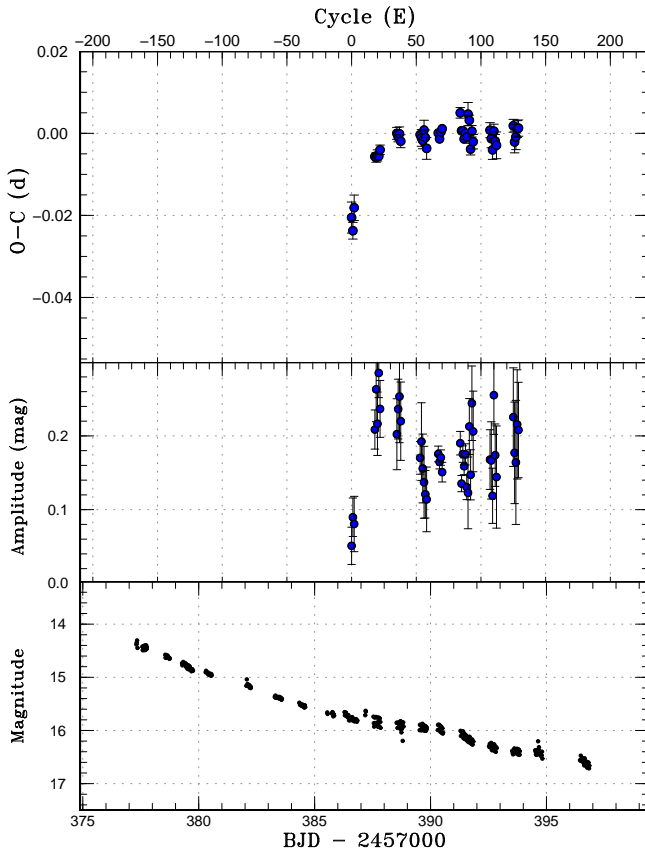


Fig. 120. $O - C$ diagram of superhumps in ASASSN-15uj (2015). (Upper:) $O - C$ diagram. We used a period of 0.05580 d for calculating the $O - C$ residuals. (Middle:) Amplitudes of superhumps. (Lower:) Light curve. The data were binned to 0.018 d.

3.104 ASASSN-16bh

This object was detected as a transient at $V=12.7$ on 2016 February 6 by the ASAS-SN team (Simonian et al. 2016). The object was suspected to be a WZ Sge-type dwarf nova based on the large (~ 8 mag) outburst amplitude. Early observations detected low-amplitude modulations, which were suspected to be early superhumps (vsnet-alert 19476, 19479). After the development of ordinary superhumps, the period of early superhumps was established (vsnet-alert 19513). In figure 128, we show the mean profile of early superhumps using the high-quality data from the southern hemisphere (MLF). The best period with the PDM method was 0.05346(2) d. It is noteworthy that the profile has three peaks (in contrast to two peaks in many WZ Sge-type dwarf novae, cf. Kato 2015) in one cycle.

Ordinary superhumps then appeared (vsnet-alert 19484, 19513, 19520, 19521; figure 129). The times of superhump maxima are listed in table 94. The maxima for $E \leq 15$ were very clearly stage A superhumps. After $E = 206$ (rapid fading phase), there was probably a phase jump. Similar phenomena were recorded in other WZ Sge-type dwarf novae (e.g. GW Lib:

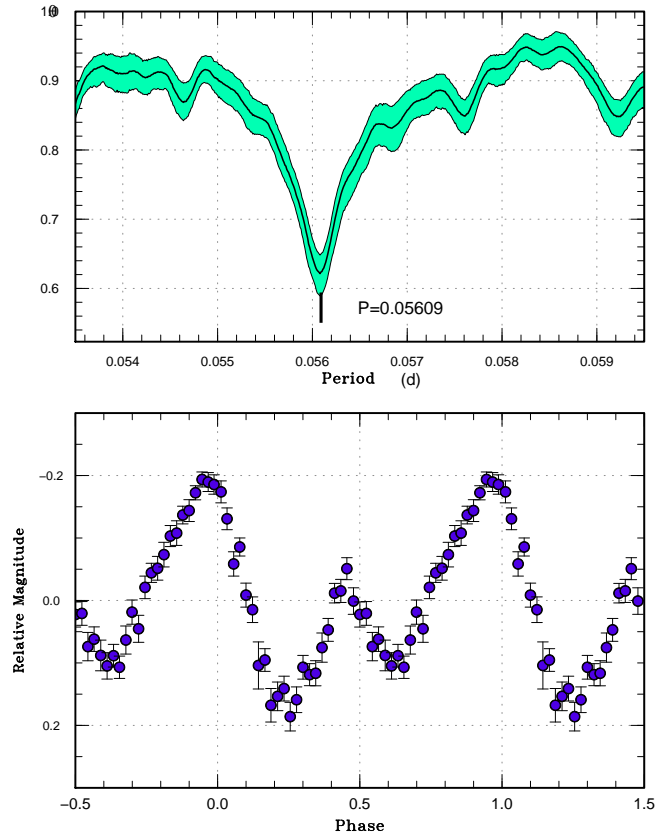


Fig. 121. Early superhumps in ASASSN-15ux (2015). The data before BJD 2457396 were used. (Upper): PDM analysis. (Lower): Phase-averaged profile.

figure 33 in Kato et al. 2009; FL Psc = ASAS J002511+1217.2: figure 34 in Kato et al. 2009; V355 UMa: figure 43 in Kato et al. 2012).

The object rapidly faded from the superoutburst plateau on February 25. This fading was actually a “dip” seen in many WZ Sge-type dwarf novae (Kato 2015) (see figure 130). The object brightened again on February 28 (vsnet-alert 19536) and this rebrightening was a plateau-type one without major fluctuations (vsnet-alert 19567). On March 9, the object rapidly faded from the rebrightening phase (vsnet-alert 19569). During the rebrightening phase, superhumps were present and grew in amplitudes (figure 130). The times of superhump maxima during the rebrightening phase are listed in table 95, although the data were rather noisy due to the faintness. The superhumps, however, were very apparent on March 6 (BJD 2457454), the final night before the rapid fading. The mean period of the superhumps during the rebrightening phase was determined to be 0.05389(3) d with the PDM method (figure 131).

The resultant ϵ^* for stage A superhumps was 0.0283(3), corresponding to $q=0.076(1)$. Using the relation between P_{dot} and q in equation (6) in Kato (2015), we can obtain $q=0.076(6)$, consistent with that from stage A superhumps.

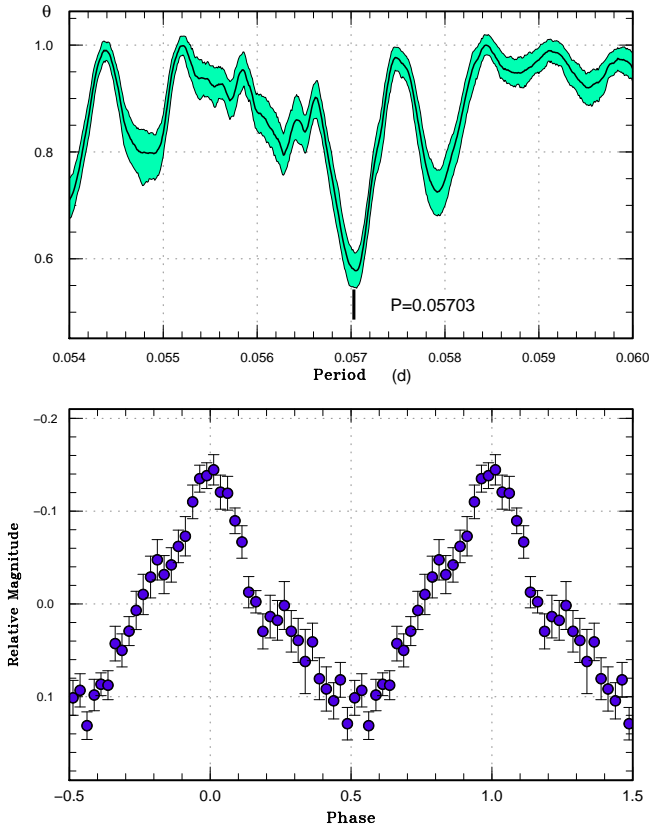


Fig. 122. Superhumps in ASASSN-15ux (2015). The data after BJD 2457400 were used. The averaged profile outside the eclipses is shown. The mean period and profile were likely affected by the beat phenomenon with the orbital variation. (Upper): PDM analysis. (Lower): Phase-averaged profile.

It took 7 d for this object from the outburst detection to the emergence of ordinary superhumps. This value is relatively short among WZ Sge-type dwarf novae, particularly among objects with type-A rebrightenings [see figure 18 in Kato (2015)]. Since the gap in the ASAS-SN data before the outburst detection was very short, this delay of appearance of superhumps should not exceed 9 d.

We can estimate the disk radius during the rebrightening using the superhump period as shown in subsection 4.3 in Kato, Osaki (2013b). The mean superhump period during the rebrightening phase gives ϵ^* of 0.0080(7). This value corresponds to a radius of $0.26(2)a$, where a is the binary separation, if we can ignore the pressure effect. This value is small compared to the values ($0.30a$ – $0.38a$) in post-outburst state of WZ Sge-type dwarf novae (Kato, Osaki 2013b). Although pressure effect may have reduced ϵ^* and give a systematically small disk radius, it is likely that the disk radius during the plateau-type rebrightening was indeed small.

The object resembles AL Com (cf. Patterson et al. 1996; Howell et al. 1996; Nogami et al. 1997; Kato et al. 1996a;

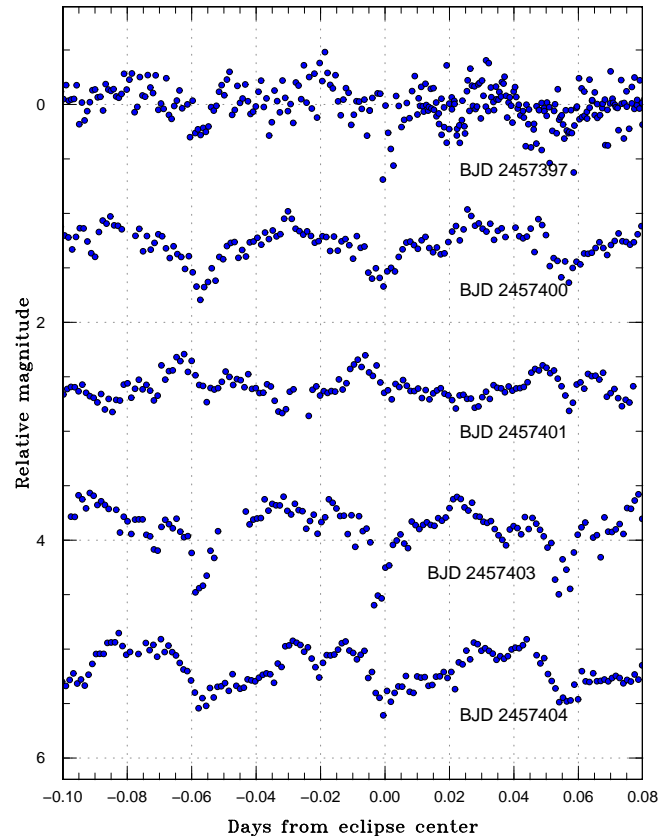


Fig. 123. Light curve of ASASSN-15ux after the appearance of the eclipses. Shallow eclipses with variable profiles were recorded.

Ishioka et al. 2002) in many respects. The apparent brightness may even qualify this object to be the southern counterpart of AL Com. Since the superoutbursts in AL Com appear to have some degree of diversity (cf. Uemura et al. 2008; Kimura et al. 2016a), further monitoring for outbursts and time-resolved photometry during each superoutburst will be rewarding. Photometry and spectroscopy in quiescence to determine the exact orbital period are also desired.

3.105 ASASSN-16bi

This object was detected as a transient on the rise from $V=15.2$ to $V=14.3$ on 2016 February 6 by the ASAS-SN team. The object was also detected by Gaia as Gaia16ads on February 13.¹⁵ Although an $R=20.6$ star was initially suggested to be the quiescent counterpart, it is $6''$ from the Gaia position and is unlikely the counterpart. The large outburst amplitude suggested a possible WZ Sge-type dwarf nova. Early observations detected double-wave early superhumps (vsnet-alert 19514; figure 132). The best period with the PDM method is 0.05814(5) d. Although emerging ordinary superhumps were detected (vsnet-

¹⁵<http://gsaweb.ast.cam.ac.uk/alerts/alert/Gaia16ads/>.

Table 94. Superhump maxima of ASASSN-16bh (2016)

E	max*	error	$O - C^\dagger$	N^\ddagger	E	max*	error	$O - C^\dagger$	N^\ddagger
0	57432.1129	0.0007	-0.0112	33	107	57437.9040	0.0006	-0.0022	53
1	57432.1641	0.0006	-0.0140	34	108	57437.9603	0.0015	-0.0000	18
2	57432.2192	0.0005	-0.0130	34	123	57438.7680	0.0069	-0.0028	28
3	57432.2733	0.0006	-0.0129	31	124	57438.8241	0.0006	-0.0009	54
13	57432.8255	0.0004	-0.0011	54	125	57438.8762	0.0007	-0.0028	53
14	57432.8808	0.0005	0.0002	54	126	57438.9298	0.0006	-0.0031	49
15	57432.9350	0.0005	0.0003	54	128	57439.0435	0.0011	0.0025	30
32	57433.8590	0.0003	0.0057	24	129	57439.0941	0.0006	-0.0010	34
36	57434.0753	0.0003	0.0058	19	130	57439.1480	0.0003	-0.0011	34
37	57434.1287	0.0003	0.0052	33	131	57439.2003	0.0005	-0.0029	34
38	57434.1836	0.0002	0.0061	33	132	57439.2559	0.0005	-0.0013	34
39	57434.2351	0.0004	0.0035	28	140	57439.6894	0.0019	-0.0001	25
44	57434.5040	0.0017	0.0022	28	141	57439.7420	0.0011	-0.0016	25
45	57434.5608	0.0019	0.0049	52	142	57439.7975	0.0008	-0.0001	79
46	57434.6145	0.0002	0.0046	120	143	57439.8492	0.0007	-0.0025	68
47	57434.6680	0.0010	0.0041	11	144	57439.9055	0.0006	-0.0002	66
48	57434.7223	0.0006	0.0043	17	148	57440.1215	0.0006	-0.0004	34
49	57434.7755	0.0007	0.0035	17	149	57440.1761	0.0008	0.0002	34
50	57434.8303	0.0006	0.0043	26	150	57440.2215	0.0013	-0.0084	29
51	57434.8841	0.0006	0.0040	22	151	57440.2807	0.0007	-0.0033	28
61	57435.4229	0.0012	0.0024	36	166	57441.0962	0.0009	0.0016	34
62	57435.4772	0.0004	0.0027	77	167	57441.1485	0.0012	-0.0001	31
63	57435.5322	0.0003	0.0037	92	168	57441.2042	0.0009	0.0016	31
64	57435.5850	0.0002	0.0024	124	169	57441.2567	0.0008	0.0001	34
65	57435.6386	0.0006	0.0020	66	173	57441.4744	0.0010	0.0016	125
68	57435.7994	0.0013	0.0007	40	174	57441.5274	0.0009	0.0005	125
69	57435.8544	0.0007	0.0016	64	175	57441.5820	0.0013	0.0011	124
73	57436.0711	0.0003	0.0022	33	176	57441.6356	0.0010	0.0007	93
74	57436.1242	0.0002	0.0012	33	183	57442.0098	0.0101	-0.0034	15
75	57436.1741	0.0010	-0.0029	67	184	57442.0721	0.0013	0.0049	34
76	57436.2326	0.0006	0.0016	108	185	57442.1254	0.0012	0.0041	34
77	57436.2871	0.0050	0.0020	29	186	57442.1782	0.0013	0.0028	34
87	57436.8274	0.0006	0.0019	54	188	57442.2853	0.0010	0.0019	25
88	57436.8793	0.0005	-0.0002	54	191	57442.4472	0.0008	0.0017	124
89	57436.9333	0.0006	-0.0003	52	192	57442.5020	0.0009	0.0025	121
91	57437.0411	0.0034	-0.0006	16	193	57442.5574	0.0011	0.0038	123
92	57437.0956	0.0004	-0.0001	33	194	57442.6100	0.0008	0.0023	124
93	57437.1485	0.0005	-0.0012	34	205	57443.2112	0.0011	0.0091	52
94	57437.2032	0.0003	-0.0005	120	206	57443.2620	0.0016	0.0059	52
95	57437.2576	0.0004	-0.0001	103	221	57444.0614	0.0019	-0.0053	34
96	57437.3123	0.0007	0.0004	46	222	57444.1167	0.0028	-0.0040	34
97	57437.3614	0.0018	-0.0045	17	223	57444.1685	0.0041	-0.0062	34
105	57437.7992	0.0008	0.0011	43	224	57444.2131	0.0040	-0.0157	28
106	57437.8507	0.0005	-0.0015	52	-	-	-	-	-

*BJD-2400000.

 † Against max = 2457432.1241 + 0.054039E. ‡ Number of points used to determine the maximum.

Table 91. Superhump maxima of ASASSN-15ux (2015)

E	max*	error	$O - C^\dagger$	phase‡	N^\S
0	57397.1599	0.0031	-0.0010	0.35	54
1	57397.2180	0.0022	0.0002	0.59	46
2	57397.2716	0.0027	-0.0033	0.41	101
3	57397.3300	0.0028	-0.0019	0.52	83
55	57400.3020	0.0030	0.0053	0.79	17
56	57400.3483	0.0017	-0.0054	0.41	37
57	57400.4049	0.0019	-0.0058	0.46	35
58	57400.4634	0.0010	-0.0043	0.27	38
59	57400.5249	0.0018	0.0002	0.37	33
60	57400.5787	0.0008	-0.0030	0.29	52
73	57401.3286	0.0008	0.0056	0.23	31
74	57401.3876	0.0012	0.0076	0.39	31
75	57401.4419	0.0008	0.0050	0.37	28
76	57401.4993	0.0011	0.0053	0.38	30
77	57401.5561	0.0012	0.0051	0.53	27
108	57403.3219	0.0023	0.0034	0.53	30
109	57403.3762	0.0009	0.0007	0.43	31
110	57403.4344	0.0023	0.0019	0.56	30
111	57403.4898	0.0009	0.0003	0.38	35
112	57403.5472	0.0013	0.0007	0.54	35
113	57403.6052	0.0013	0.0016	0.33	36
126	57404.3424	0.0009	-0.0024	0.27	33
127	57404.3987	0.0007	-0.0031	0.31	33
128	57404.4555	0.0014	-0.0033	0.40	36
129	57404.5128	0.0011	-0.0030	0.32	32
130	57404.5695	0.0011	-0.0033	0.30	34
131	57404.6271	0.0012	-0.0027	0.35	25

*BJD-2400000.

†Against max = 2457397.1609 + 0.057015*E*.

‡Orbital phase.

§Number of points used to determine the maximum.

alert 19519), the period was not well determined due to the faintness of the object. The only available superhumps maxima are BJD 2457437.2963(33) $N=39$ and 2457437.3571(8) $N=61$. The outburst light curve is shown in figure 133. The phase of early superhumps lasted at least for 6 d if it immediately started after the outburst detection. The entire duration of the superoutburst was 23 d.

3.106 ASASSN-16bu

This object was detected as a transient at $V=14.5$ on 2016 February 15 by the ASAS-SN team (vsnet-alert 19491). The large outburst amplitude suggested a possible WZ Sge-type dwarf nova (cf. vsnet-alert 19500). After nine nights, ordinary superhumps emerged (vsnet-alert 19525; figure 134). The

Table 92. Superhump maxima of ASASSN-16af (2016)

E	max*	error	$O - C^\dagger$	N^\ddagger
0	57401.4789	0.0013	0.0046	26
1	57401.5401	0.0006	0.0016	58
2	57401.6045	0.0009	0.0019	52
10	57402.1163	0.0010	-0.0000	51
11	57402.1816	0.0005	0.0011	111
12	57402.2446	0.0006	-0.0001	125
13	57402.3098	0.0007	0.0009	124
20	57402.7560	0.0010	-0.0023	22
21	57402.8215	0.0028	-0.0010	22
26	57403.1429	0.0012	-0.0006	104
27	57403.2050	0.0005	-0.0028	125
28	57403.2703	0.0006	-0.0017	97
29	57403.3340	0.0009	-0.0021	35
35	57403.7202	0.0009	-0.0012	19
36	57403.7852	0.0021	-0.0004	22
37	57403.8502	0.0025	0.0004	14
51	57404.7461	0.0019	-0.0026	20
52	57404.8113	0.0015	-0.0016	20
63	57405.5183	0.0017	-0.0008	60
64	57405.5788	0.0017	-0.0045	55
65	57405.6480	0.0014	0.0005	58
66	57405.7120	0.0062	0.0003	16
67	57405.7773	0.0035	0.0014	20
75	57406.2988	0.0028	0.0093	45

*BJD-2400000.

†Against max = 2457401.4743 + 0.064204*E*.

‡Number of points used to determine the maximum.

Table 93. Superhump maxima of ASASSN-16ag (2015)

E	max*	error	$O - C^\dagger$	N^\ddagger
0	57400.3447	0.0014	-0.0009	51
1	57400.4013	0.0019	-0.0028	54
2	57400.4598	0.0013	-0.0027	62
3	57400.5202	0.0012	-0.0008	53
17	57401.3369	0.0041	-0.0028	52
18	57401.4137	0.0024	0.0156	45
19	57401.4521	0.0049	-0.0045	31
34	57402.3342	0.0055	0.0004	63
44	57402.9099	0.0035	-0.0087	21
45	57402.9746	0.0036	-0.0025	47
46	57403.0445	0.0015	0.0090	58
47	57403.0882	0.0107	-0.0058	32
53	57403.4544	0.0014	0.0095	49
96	57405.9564	0.0044	-0.0031	54

*BJD-2400000.

†Against max = 2457400.3432 + 0.058596*E*.

‡Number of points used to determine the maximum.

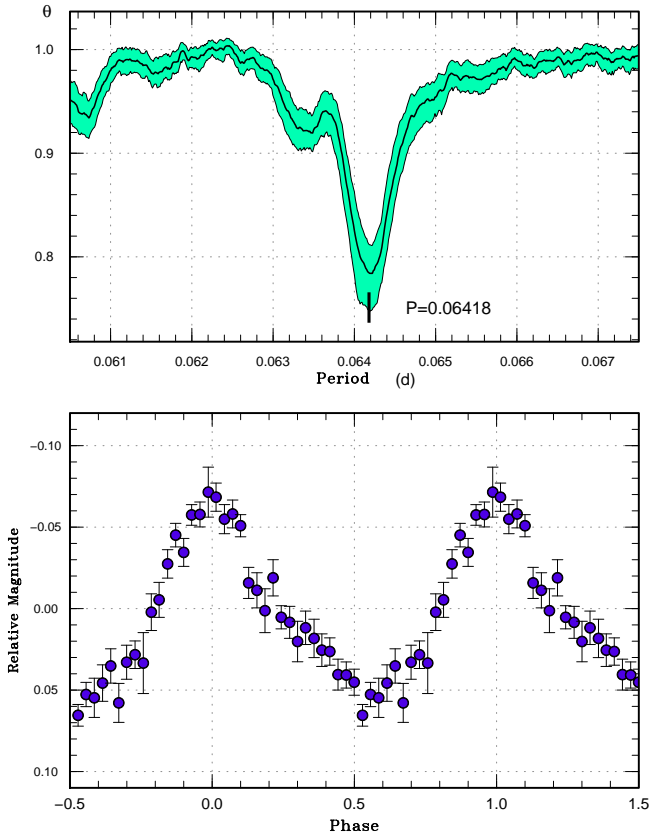


Fig. 124. Superhumps in ASASSN-16af (2016). (Upper): PDM analysis. (Lower): Phase-averaged profile.

times of superhump maxima are listed in table 96. The maxima for $E \leq 30$ are clearly stage A superhumps with growing amplitudes. An analysis of the earlier part of the observation yielded a weak signal of possible early superhumps (figure 135). The period with the PDM method was 0.05934(13) d. By using this period and the period of stage A superhumps, the value of $\epsilon^* = 0.037(4)$. This value corresponds to $q = 0.10(1)$. Since the periods of early superhumps and stage A superhumps were not very well determined, this q value needs to be treated with caution. The other features of the behavior, including the slow growth of ordinary superhumps and small amplitudes of superhumps, likely suggest a low q comparable to a period bouncer (Kato 2015).

3.107 ASASSN-16de

This object was detected as a transient at $V=14.5$ on 2016 March 17 by the ASAS-SN team (vsnet-alert 19491). The object was probably in outburst in USNO-A2.0 at $B=16.1$. A blue object is present in SDSS images, but it is not listed in Abazajian et al. 2009. Subsequent observations detected superhumps (vsnet-alert 19610; figure 136). This observation on the first night gave a period of 0.063(1) d (PDM method). The times

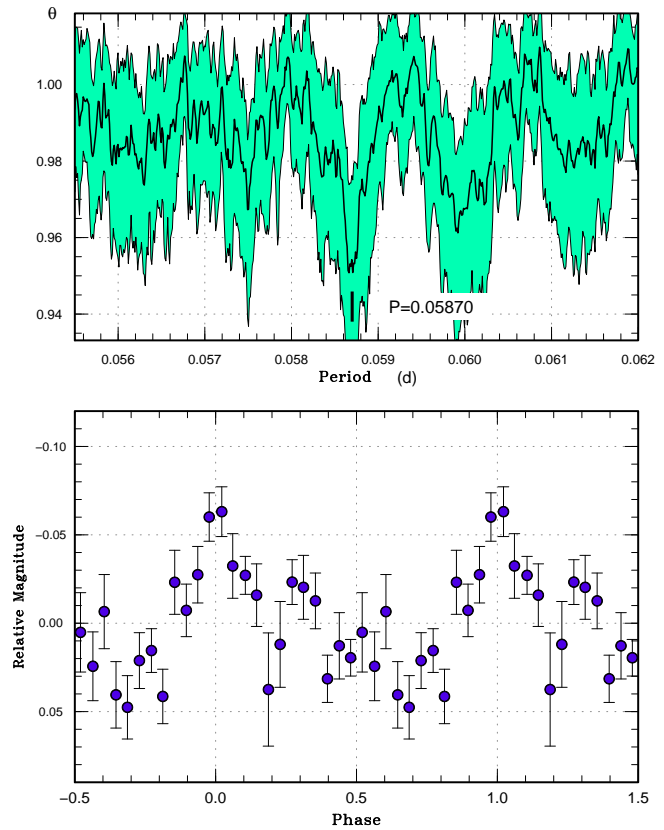


Fig. 125. Superhumps in ASASSN-16ag (2016). (Upper): PDM analysis. (Lower): Phase-averaged profile.

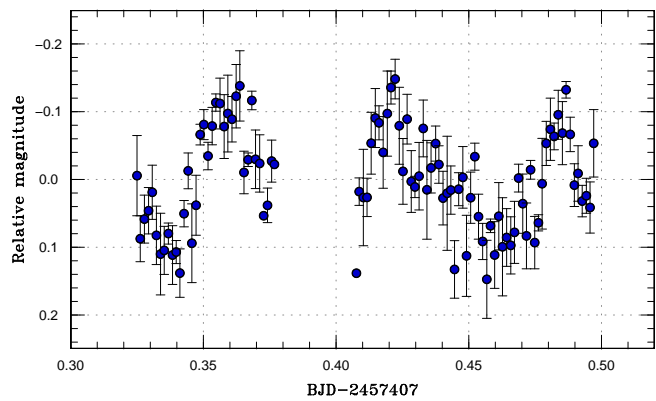


Fig. 126. Possible superhumps in ASASSN-16ao (2016). The data were binned to 0.0015 d.

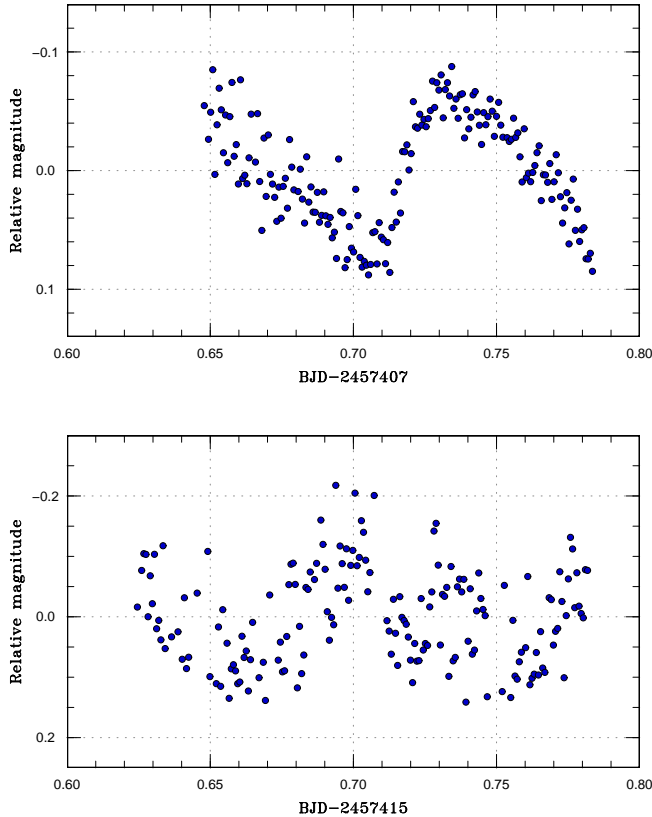


Fig. 127. Superhumps in ASASSN-16aq (2016).

of superhump maxima were BJD 2457465.6155(8) ($N=60$) and 2457465.6774(7) ($N=46$). Although the object was observed on five nights in the late stage of the superoutburst (6 d after the initial observation of superhumps), the superhump signal was too weak to determine the period. The object faded rapidly on March 28, 11 d after the outburst detection.

3.108 CRTS J081936.1+191540

This object (hereafter CRTS J081936) was confirmed to be an SU UMa-type dwarf nova on its outburst in 2013 (Kato et al. 2015a). Another superoutburst was detected on 2015 March 10 by the ASAS-SN team (vsnet-alert 18411). Two superhump maxima were measured: BJD 2457093.4786(13) ($N=85$) and 2457093.5492(18) ($N=79$).

3.109 CRTS J095926.4–160147

This object (=CSS110226:095926–160147, hereafter CRTS J095926) was detected as a transient by CRTS on 2011 February 26. Five outbursts were recorded in the CRTS data up to 2013 July.

The 2015 outburst was detected on May 14 by the ASAS-SN team (vsnet-alert 18622). Our observations starting after two

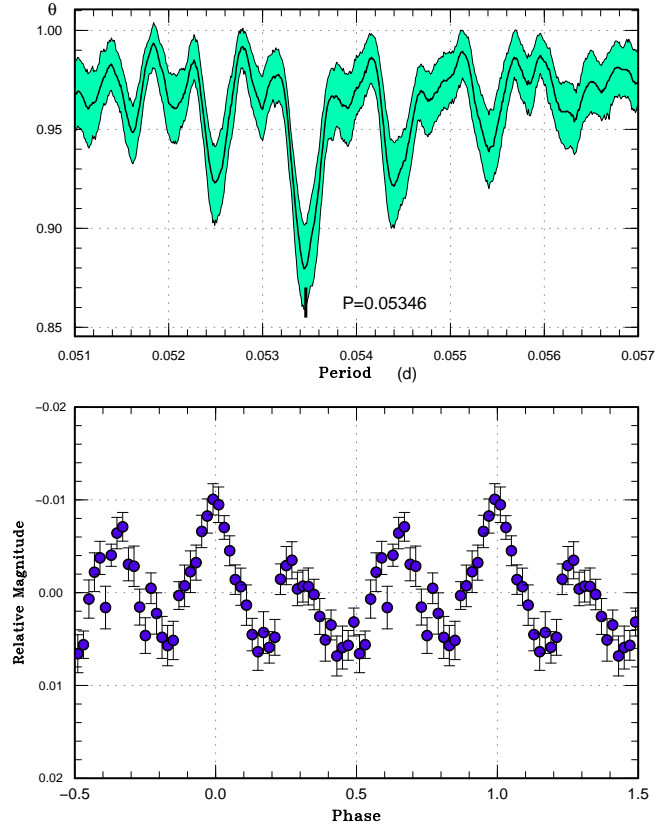


Fig. 128. Early superhumps in ASASSN-16bh (2016). The high-quality data by MLF before BJD 2457431 were used. (Upper): PDM analysis. (Lower): Phase-averaged profile.

nights detected superhumps (vsnet-alert 18628, 18633, 18648; figure 137). The times of superhump maxima are listed in table 97. Although it was initially difficult to distinguish one-day aliases due to the short observing time, observations at two different longitudes established the alias selection (vsnet-alert 18648). It is possible that maxima for $E \leq 12$ correspond to stage A superhumps since there was a large decrease in the period (by 1.5%) around $E=11$. If it is the case, stage A in this system likely lasted more than 3 d.

3.110 CRTS J120052.9–152620

This object (=CSS110205:120053–152620, hereafter CRTS J120052) was discovered by the CRTS on 2011 February 5. The 2011 superoutburst was observed only on two nights and the analysis was reported in Kato et al. (2012). Due to the lack of observations, there remained ambiguity in selecting the superhump period (Kato et al. 2012).

The 2016 superoutburst was detected by the ASAS-SN team at $V=13.78$ on March 14 (cf. vsnet-alert 19590). Subsequent observations detected superhumps (vsnet-alert 19609, 19618; figure 138). The times of superhump maxima are listed in table

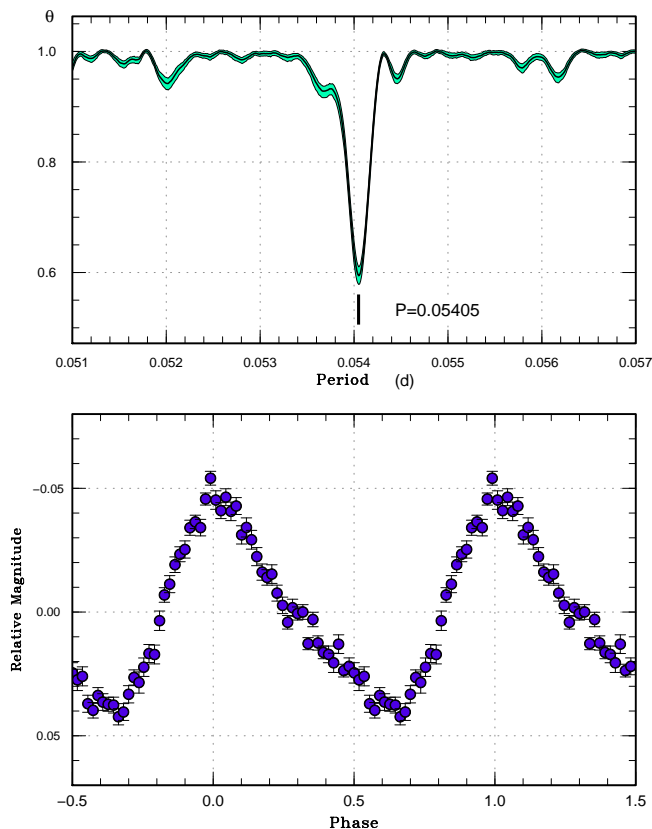


Fig. 129. Ordinary superhumps in ASASSN-16bh (2016). The data between BJD 2457432 and 2457444 were used. (Upper): PDM analysis. (Lower): Phase-averaged profile.

98. These observations recorded the relatively late phase of the superoutburst and these superhumps may be of stage C. In table 3, we gave a mean period.

Thanks to the new observation, it has become evident that an alias different from that reported in Kato et al. (2012) was the correct superhump period during the 2011 superoutburst (vsnet-alert 19618). The corrected period for the 2011 superoutburst based on this identification is 0.08882(3) d.

3.111 CRTS J163120.9+103134

This object (=CSS080505:163121+103134, hereafter CRTS J163120) was detected as a transient by CRTS on 2008 May 5. Refer to Kato et al. 2009 for the history. The 2008 and 2010 superoutbursts were reported in Kato et al. (2009) and Kato et al. (2010), respectively.

The 2015 superoutburst was detected by the ASAS-SN team (cf. vsnet-alert 18603) and superhumps were observed on single night (table 99). The period by the PDM method is listed in table 3.

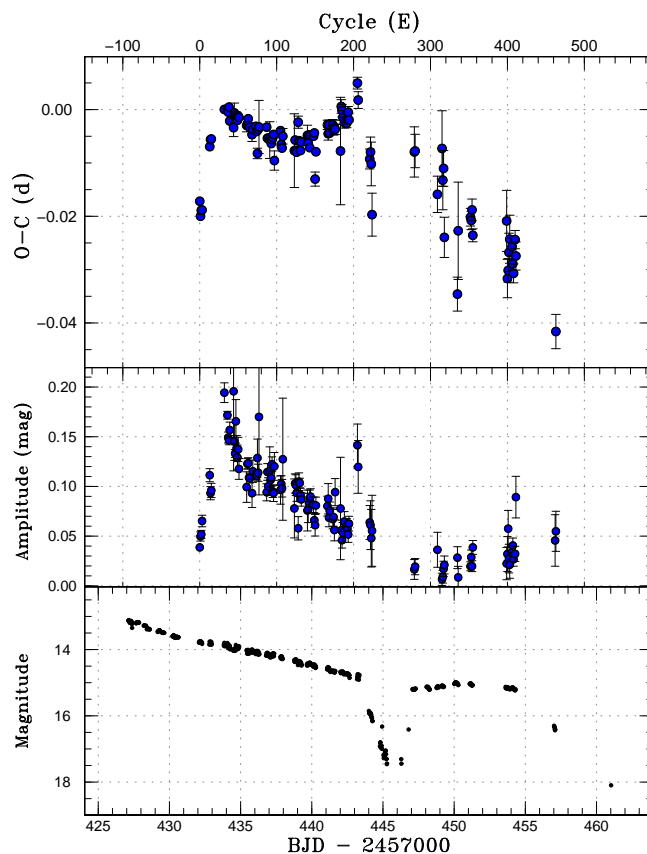


Fig. 130. $O - C$ diagram of superhumps in ASASSN-16bh (2016). (Upper:) $O - C$ diagram. We used a period of 0.05403 d for calculating the $O - C$ residuals. (Middle:) Amplitudes of superhumps. (Lower:) Light curve. The data were binned to 0.017 d.

3.112 CRTS J200331.3-284941

This object (=SSS100615:200331-284941, hereafter CRTS J200331) was discovered by CRTS Siding Spring Survey (SSS) on 2010 June 15. Since the 2010 outburst had a fading tail resembling those of WZ Sge-type dwarf novae (cf. vsnet-alert 18763), the object received special attention.

The 2015 outburst, the second known outburst of this object, was detected by the ASAS-SN team on June 20 at $V=14.84$. The initial observation revealed that this object is an eclipsing SU UMa-type (or WZ Sge-type) dwarf nova (vsnet-alert 18788). The eclipses became clearer as the outburst proceeded and we have obtained the eclipse ephemeris by using MCMC analysis (Kato et al. 2013a) of the present observations:

$$\text{Min(BJD)} = 2457200.79900(6) + 0.0587048(3)E. \quad (4)$$

This ephemeris is not intended for long-term prediction of eclipses.

The object showed growing superhumps up to June 26 (figure 139) and the object significantly brightened after this epoch. Before June 26 superhumps with a long period of 0.06058(2) d

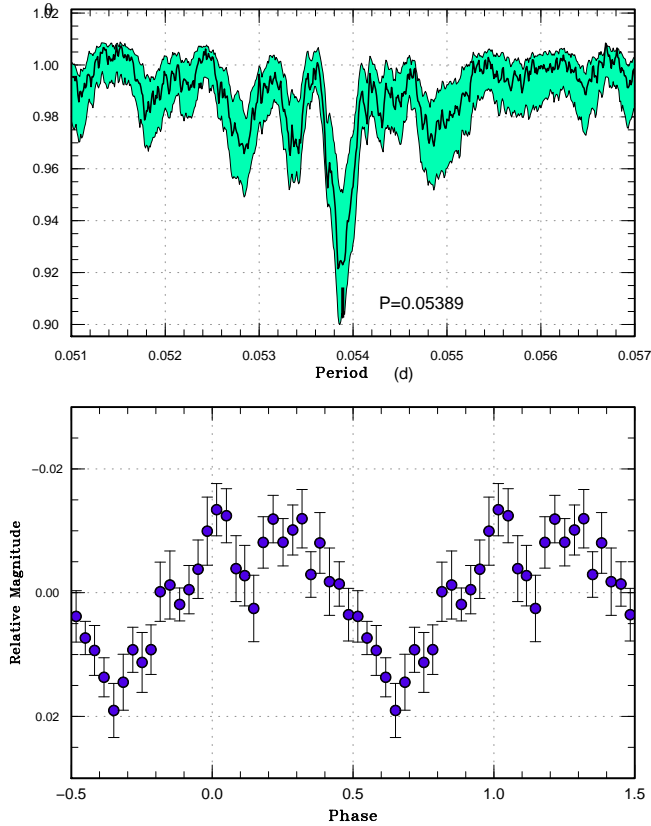


Fig. 131. Superhumps in ASASSN-16bh in the rebrightening phase (2016). (Upper): PDM analysis. (Lower): Phase-averaged profile.

were observed (note that the period reported in vsnet-alert 18798 referred to this period). We identified them to be stage A superhumps. On the three subsequent nights, stable superhumps were recorded, which we identified to be stage B superhumps. The times of superhump maxima are listed in table 100. The cycle count between $E=84$ and $E=250$ was ambiguous. The period of stage A superhumps corresponds to $q=0.084(1)$, which is close to those of WZ Sge-type dwarf novae (Kato 2015). The duration of stage A superhumps (more than 50 cycles) is also long, consistent with the small q . All the pieces of evidence suggest that this object is located near the borderline of SU UMa-type and WZ Sge-type objects. Since our initial observation started 3 d after the ASAS-SN detection and it was not clear whether there were early superhumps before this observation. We can, however, probably rule out the long-lasting (more than 10 d) phase of early superhumps seen in typical WZ Sge-type dwarf novae.

This object is probably the first one in which the period of stage A superhumps were sufficiently measured in a deeply eclipsing system. Determination of system parameters in quiescence using eclipse modeling in such a system would provide a direct test for our method of q determination using stage A superhumps (cf. Kato, Osaki 2013b).

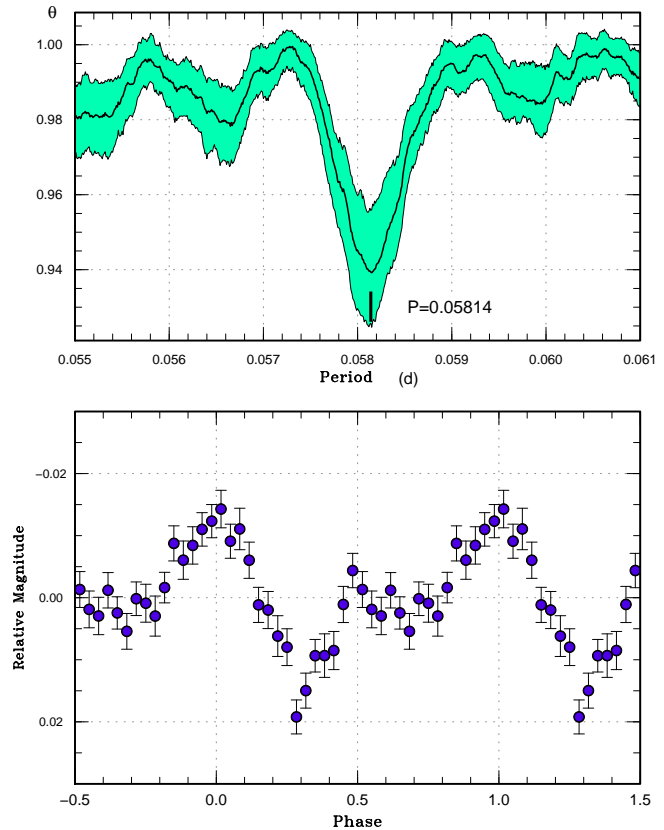


Fig. 132. Early superhumps in ASASSN-16bi (2016). The data before BJD 2457432 were used. (Upper): PDM analysis. (Lower): Phase-averaged profile.

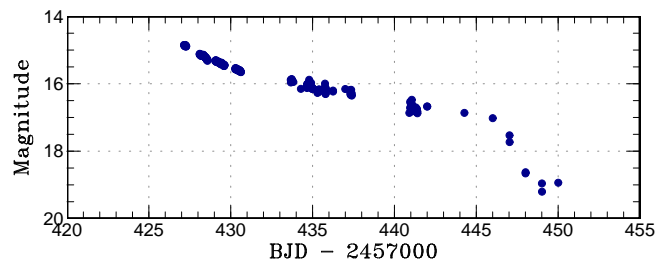


Fig. 133. Light curve of the superoutburst of ASASSN-16bi (2016). The data were binned to 0.01 d. The ASAS-SN detection corresponds to BJD 2457424.53.

Table 95. Superhump maxima of ASASSN-16bh in the rebrightening phase (2016)

E	max*	error	$O - C^\dagger$	N^\ddagger
0	57447.1965	0.0047	0.0000	22
1	57447.2507	0.0031	0.0004	26
30	57448.8094	0.0034	-0.0025	59
36	57449.1422	0.0071	0.0072	26
37	57449.1903	0.0056	0.0015	22
38	57449.2465	0.0034	0.0038	26
39	57449.2876	0.0038	-0.0089	18
56	57450.1955	0.0032	-0.0165	21
57	57450.2614	0.0091	-0.0044	26
73	57451.1284	0.0017	0.0011	26
74	57451.1818	0.0017	0.0006	22
75	57451.2379	0.0020	0.0028	26
76	57451.2871	0.0012	-0.0018	22
120	57453.6671	0.0057	0.0089	22
121	57453.7104	0.0036	-0.0017	22
122	57453.7659	0.0022	-0.0000	22
123	57453.8233	0.0036	0.0035	28
124	57453.8798	0.0045	0.0062	36
127	57454.0405	0.0016	0.0053	27
128	57454.0914	0.0013	0.0023	26
129	57454.1436	0.0018	0.0007	25
131	57454.2580	0.0017	0.0074	25
132	57454.3089	0.0026	0.0045	11
183	57457.0306	0.0045	-0.0201	26
184	57457.1043	0.0032	-0.0002	15

*BJD-2400000.

†Against max = 2457447.1964 + 0.053848*E*.

‡Number of points used to determine the maximum.

3.113 CRTS J212521.8-102627

This object (=CSS080927:212522-102627, hereafter CRTS J212521) was discovered by CRTS on 2008 September 27. There were at least 6 outbursts (up to 2013 September) in the CRTS data.

The 2015 outburst was detected by the ASAS-SN team on August 23 at a magnitude of $V=15.0$. Since the past outbursts recorded in the ASAS-SN data resembled superoutbursts, an SU UMa-type dwarf nova was suspected (vsnet-alert 19000). Observations soon recorded superhumps (vsnet-alert 19006, 19010; figure 140). The times of superhump maxima are listed in table 101. Although the basic superhump period was determined to be 0.0791(1) d from the observations on the first two nights, the cycle count is ambiguous between $E=26$ and $E=100$. The maxima for $E \geq 100$ may represent stage C superhumps. We listed a period only based on the initial two nights in table 3.

Table 96. Superhump maxima of ASASSN-16bu (2016)

E	max*	error	$O - C^\dagger$	N^\ddagger
0	57442.3543	0.0035	-0.0204	61
15	57443.2903	0.0010	0.0023	76
16	57443.3410	0.0008	-0.0079	120
17	57443.4056	0.0011	-0.0041	95
18	57443.4688	0.0016	-0.0019	58
27	57444.0286	0.0009	0.0099	136
28	57444.0843	0.0005	0.0047	190
29	57444.1454	0.0007	0.0049	111
30	57444.2070	0.0010	0.0057	63
42	57444.9445	0.0011	0.0124	65
43	57444.9985	0.0005	0.0056	67
44	57445.0632	0.0017	0.0094	125
45	57445.1138	0.0014	-0.0009	95
46	57445.1781	0.0016	0.0025	60
47	57445.2401	0.0018	0.0036	59
59	57445.9678	0.0018	0.0007	59
60	57446.0288	0.0015	0.0008	59
61	57446.0879	0.0022	-0.0010	60
62	57446.1501	0.0015	0.0003	58
63	57446.2038	0.0031	-0.0069	34
76	57446.9945	0.0009	-0.0078	65
77	57447.0606	0.0009	-0.0026	66
82	57447.3585	0.0006	-0.0091	57

*BJD-2400000.

†Against max = 2457442.3747 + 0.060889*E*.

‡Number of points used to determine the maximum.

Table 97. Superhump maxima of CRTS J095926 (2015)

E	max*	error	$O - C^\dagger$	N^\ddagger
0	57159.4812	0.0099	-0.0144	10
1	57159.5829	0.0011	-0.0024	11
11	57160.4845	0.0011	0.0028	18
12	57160.5800	0.0007	0.0087	12
23	57161.5658	0.0014	0.0084	11
34	57162.5467	0.0008	0.0032	16
41	57163.1710	0.0041	0.0001	29
42	57163.2616	0.0003	0.0010	207
43	57163.3509	0.0009	0.0006	103
45	57163.5295	0.0006	-0.0000	20
56	57164.5126	0.0010	-0.0030	18
67	57165.4966	0.0021	-0.0050	25

*BJD-2400000.

†Against max = 2457159.4956 + 0.089643*E*.

‡Number of points used to determine the maximum.

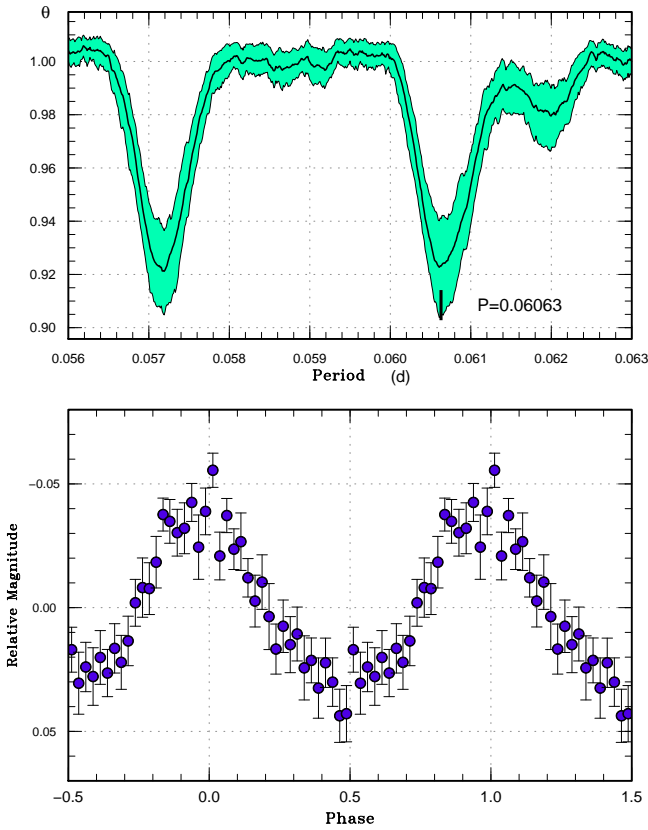


Fig. 134. Superhumps in ASASSN-16bu (2016). The data between BJD 2457441 and 2457450 were used. (Upper): PDM analysis. The true period was selected by $O - C$ analysis. (Lower): Phase-averaged profile.

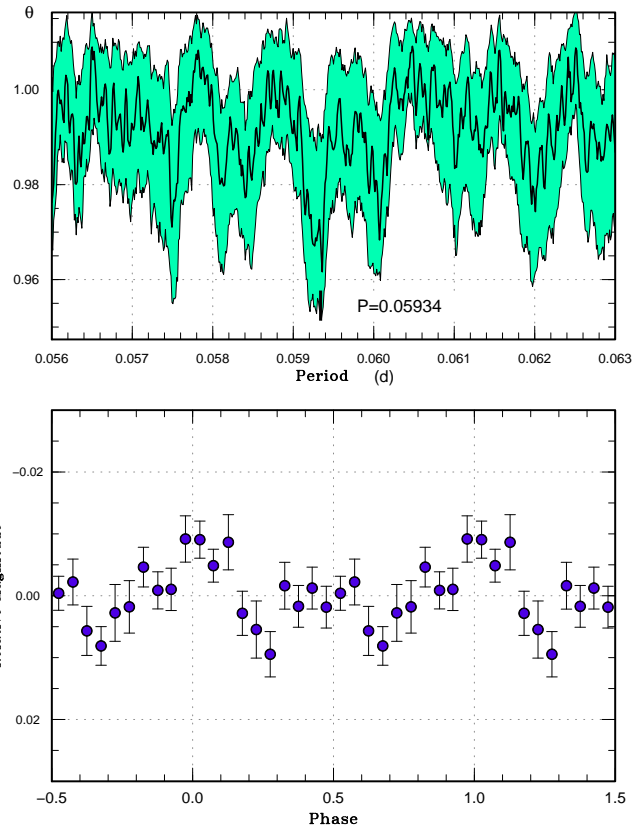


Fig. 135. Possible early superhumps in ASASSN-16bu (2016). The high-quality data before BJD 2457440 were used. (Upper): PDM analysis. (Lower): Phase-averaged profile.

Table 98. Superhump maxima of CRTS J120052 (2016)

E	max*	error	$O - C^\dagger$	N^\ddagger
0	57464.1267	0.0004	-0.0030	153
1	57464.2172	0.0003	-0.0015	190
12	57465.1966	0.0006	-0.0005	84
28	57466.6205	0.0008	0.0002	31
29	57466.7118	0.0006	0.0025	39
40	57467.6882	0.0010	0.0005	40
41	57467.7781	0.0031	0.0014	8
51	57468.6679	0.0027	0.0017	42
52	57468.7623	0.0045	0.0072	19
62	57469.6489	0.0022	0.0043	42
63	57469.7294	0.0056	-0.0042	35
73	57470.6199	0.0032	-0.0031	38
74	57470.7053	0.0047	-0.0068	35
85	57471.6919	0.0025	0.0014	35

*BJD-2400000.

† Against max = 2457464.1298 + 0.088950E.

‡ Number of points used to determine the maximum.

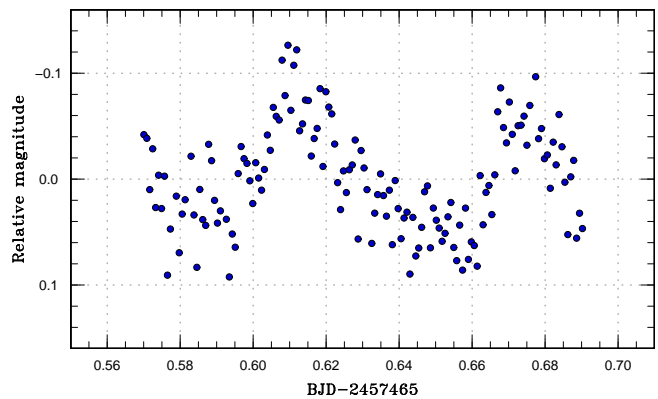


Fig. 136. Superhumps in ASASSN-16de (2016).

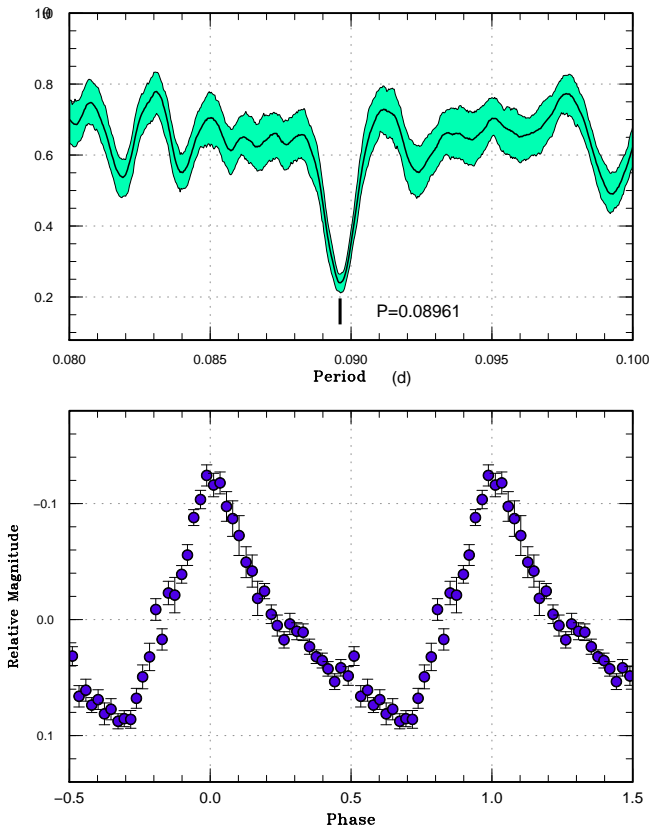


Fig. 137. Superhumps in CRTS J095926 (2015). (Upper): PDM analysis. (Lower): Phase-averaged profile.

Table 99. Superhump maxima of CRTS J163120 (2015)

E	max*	error	$O - C^\dagger$	N^\ddagger
0	57149.6529	0.0023	0.0027	64
1	57149.7092	0.0011	-0.0047	58
2	57149.7790	0.0026	0.0015	63
3	57149.8417	0.0016	0.0006	62

*BJD-2400000.

†Against max = 2457149.6503 + 0.063621E.

‡Number of points used to determine the maximum.

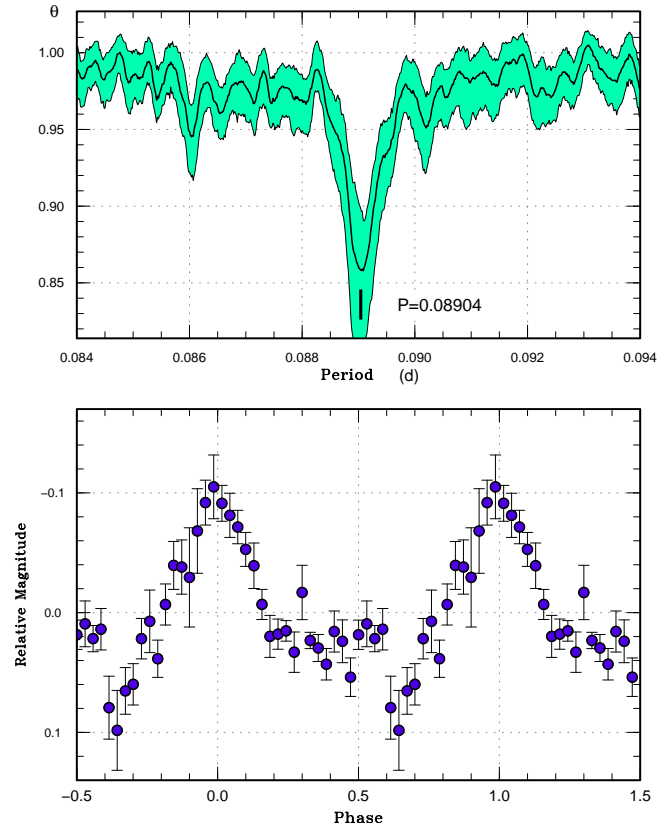


Fig. 138. Superhumps in CRTS J120052 (2016). (Upper): PDM analysis. (Lower): Phase-averaged profile.

Table 100. Superhump maxima of CRTS J200331 (2015)

E	max*	error	$O - C^\dagger$	phase [‡]	N^\S
0	57196.8438	0.0011	-0.0335	0.62	15
1	57196.9019	0.0009	-0.0349	0.62	15
33	57198.8418	0.0008	-0.0028	0.66	19
34	57198.9026	0.0007	-0.0016	0.70	21
49	57199.8111	0.0004	0.0127	0.17	13
50	57199.8717	0.0005	0.0137	0.20	18
66	57200.8240	0.0009	0.0121	0.43	26
67	57200.8846	0.0007	0.0131	0.46	29
82	57201.7783	0.0019	0.0126	0.68	11
83	57201.8396	0.0013	0.0143	0.73	26
84	57201.9067	0.0060	0.0217	0.87	15
250	57211.7723	0.0030	-0.0089	0.92	18
251	57211.8339	0.0020	-0.0068	0.97	28
252	57211.8889	0.0015	-0.0115	0.91	15

*BJD-2400000.

†Against max = 2457196.8773 + 0.059616E.

‡Orbital phase.

§Number of points used to determine the maximum.

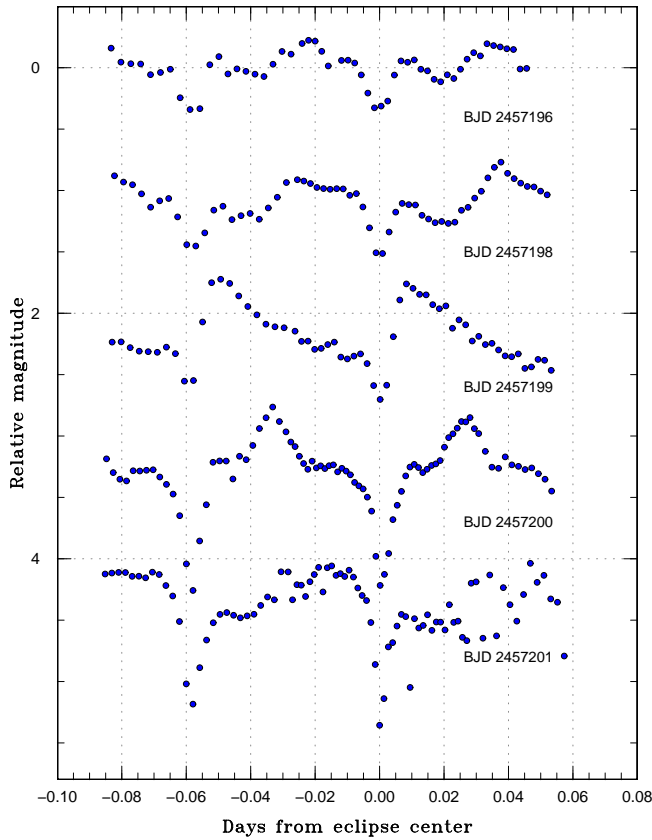


Fig. 139. Light curve of CRTS J200331 on the first five nights. Superposition of growing superhumps and eclipses are well visible.

Table 101. Superhump maxima of CRTS J212521 (2015)

E	max*	error	$O - C^\dagger$	N^\ddagger
0	57259.4157	0.0008	0.0045	43
1	57259.4967	0.0007	0.0058	44
25	57261.3968	0.0025	-0.0038	107
26	57261.4702	0.0009	-0.0100	135
100	57267.3726	0.0016	0.0038	57
101	57267.4480	0.0011	-0.0004	53

*BJD-2400000.

† Against max = 2457259.4113 + 0.079575 E .

‡ Number of points used to determine the maximum.

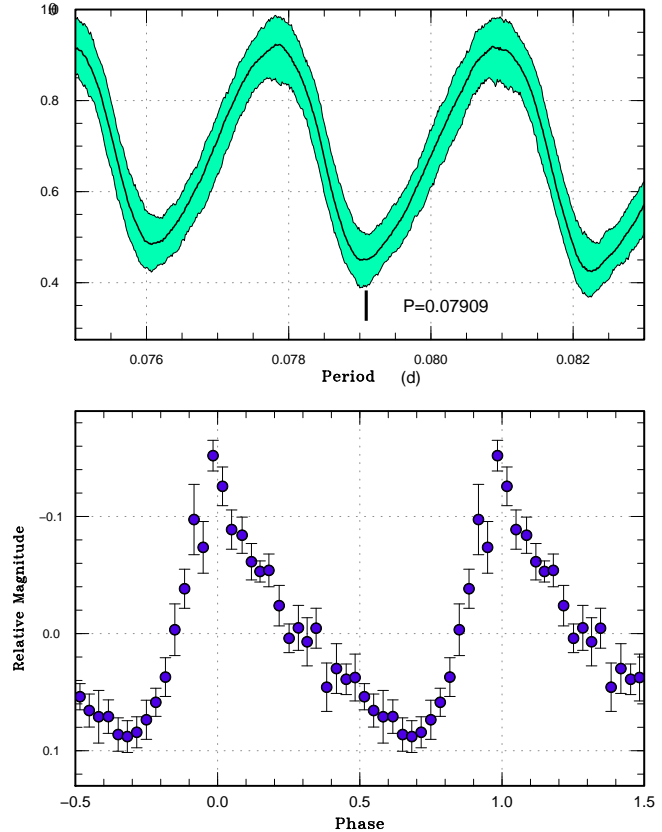


Fig. 140. Superhumps in CRTS J212521 (2015). (Upper): PDM analysis. The data before BJD 2457262 were used. The alias selection was based on $O - C$ analysis. (Lower): Phase-averaged profile.

3.114 CRTS J214738.4+244554

This object (=CSS111004:214738+244554, hereafter CRTS J214738) was discovered by CRTS on 2011 November 4 (Breedt et al. 2014). The 2011 and 2014 superoutbursts were reported in Kato et al. (2013a) and Kato et al. (2015a), respectively.

The 2015 superoutburst was visually detected by C. Chiselbrook on December 15 (cf. vsnet-alert 19351). Only one superhump maximum was recorded: BJD 2457376.8752(4) ($N=84$).

3.115 CSS J221822.9+344511

This object (hereafter CSS J221822) was originally discovered by CRTS (CSS120812:221823+344509) as a suspected dwarf nova on 2012 August 12 at an unfiltered CCD magnitude of 15.85. There is an X-ray counterpart (1RXS J221823.7+344507).

The 2015 outburst was detected by the ASAS-SN team on October 1 at $V=15.42-15.24$ (two measurements). Subsequent observations detected superhumps (vsnet-alert 19109, 19110,

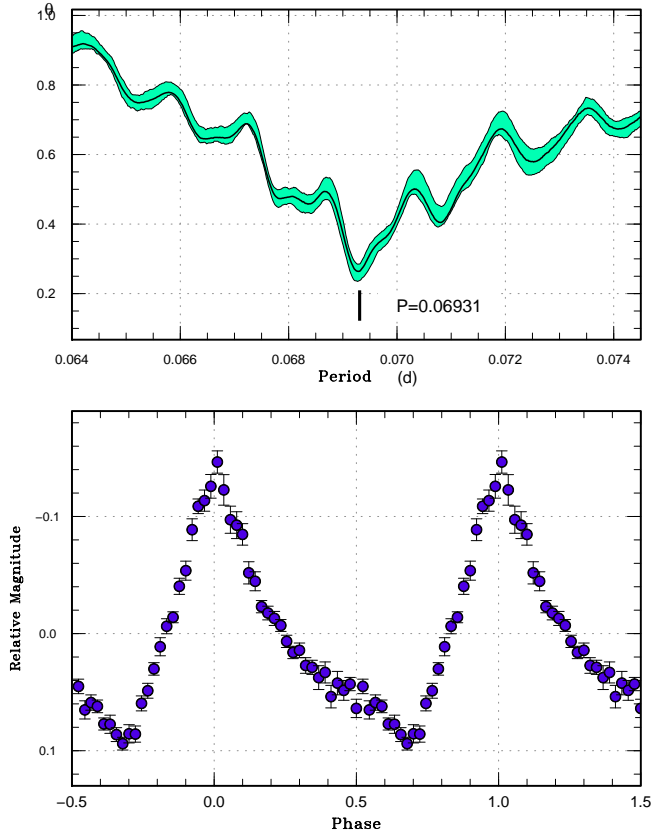


Fig. 141. Superhumps in CSS J221822 (2015). (Upper): PDM analysis. (Lower): Phase-averaged profile.

19118, 19188; figure 141). The times of superhump maxima are listed in table 102.

3.116 DDE 26

DDE 26 is a dwarf nova discovered by (Denisenko 2012). See Kato et al. (2014b) for more information. The 2015 outburst was detected by the ASAS-SN team at $V=15.7$ on December 1 (cf. vsnet-alert 19311, 19320). Subsequent observations detected superhumps (vsnet-alert 19324, 19331). The times of superhump maxima are listed in table 103. A comparison of $O - C$ diagrams (figure 142) indicates that the superhump period was longer in 2012. It may be possible that the 2012 observations recorded stage A superhumps, since some of long- P_{orb} systems are known to show long-lasting stage A (e.g. Kato et al. 2016b; subsection 4.4). This interpretation, however, does not agree with the large amplitudes of superhumps during the 2012 observation. More observations are needed to clarify the superhump variation in this system.

Table 102. Superhump maxima of CSS J221822 (2015)

E	max*	error	$O - C^\dagger$	N^\ddagger
0	57298.0261	0.0030	0.0015	59
1	57298.0923	0.0003	-0.0016	142
2	57298.1628	0.0003	-0.0004	143
3	57298.2300	0.0004	-0.0025	137
4	57298.3020	0.0003	0.0002	63
5	57298.3711	0.0003	0.0000	68
6	57298.4394	0.0003	-0.0009	65
7	57298.5096	0.0004	-0.0001	48
8	57298.5840	0.0011	0.0051	28
19	57299.3403	0.0011	-0.0009	49
47	57301.2789	0.0042	-0.0026	38
48	57301.3491	0.0014	-0.0016	47
50	57301.4931	0.0030	0.0038	45

*BJD-2400000.

† Against max = 2457298.0246 + 0.069294 E .

‡ Number of points used to determine the maximum.

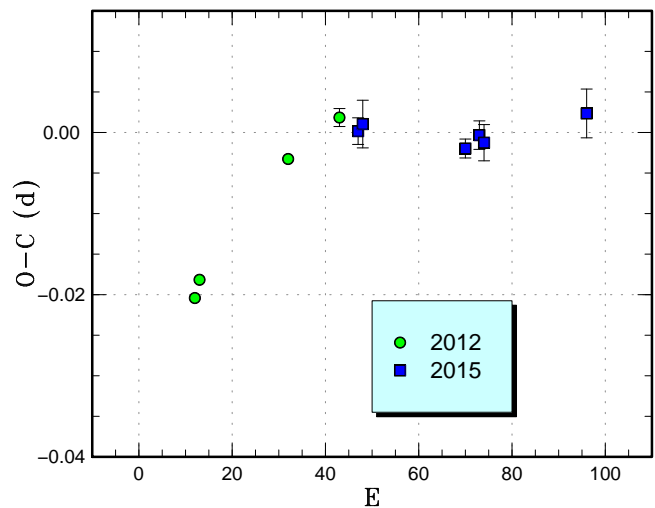


Fig. 142. Comparison of $O - C$ diagrams of DDE 26 between different superoutbursts. A period of 0.08860 d was used to draw this figure. Approximate cycle counts (E) after the outburst detections were used. The actual starts of the outbursts were unknown.

Table 103. Superhump maxima of DDE 26 (2015)

E	max*	error	$O - C^\dagger$	N^\ddagger
0	57361.9325	0.0016	0.0005	108
1	57362.0220	0.0029	0.0014	89
23	57363.9681	0.0012	-0.0020	133
26	57364.2356	0.0018	-0.0004	74
27	57364.3233	0.0022	-0.0014	96
49	57366.2761	0.0030	0.0019	88

*BJD-2400000.

† Against max = 2457361.9320 + 0.088617 E .

‡ Number of points used to determine the maximum.

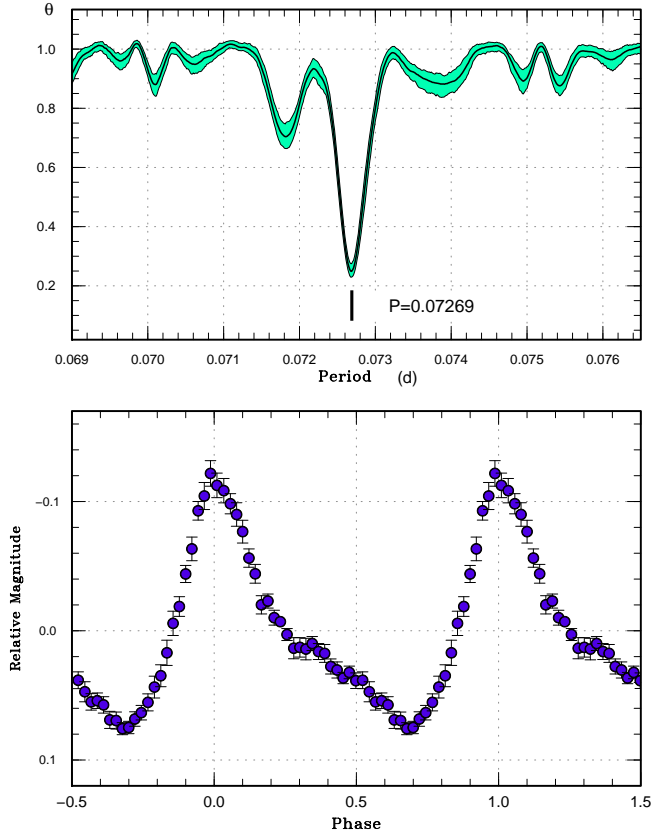


Fig. 143. Superhumps in IPHAS J230538 (2015). (Upper): PDM analysis. The data after BJD 2457182 were used. (Lower): Phase-averaged profile.

3.117 IPHAS J230538.39+652158.7

This object (hereafter IPHAS J230538) was detected as an $H\alpha$ emission line object in INT/WFC Photometric $H\alpha$ Survey (IPHAS: Witham et al. 2008). The first known outburst was detected on 2015 June 4 by the ASAS-SN team (cf. vsnet-alert 18690). The object was still rising (vsnet-alert 18695) and growing superhumps were detected (vsnet-alert 18702, 18709). Further evolution of superhumps were observed (vsnet-alert 18715, 18730, 18789; figure 143). The times of superhump maxima are listed in table 104. Although observations were rather sparse, we could identify stages A–C.

3.118 MASTER OT J003831.10–640313.7

This object (hereafter MASTER J003831) was detected as a transient at an unfiltered CCD magnitude of 12.7 on 2016 January 26 by the MASTER network (Gress et al. 2016a). Although Gress et al. (2016a) suggested either a CV or a BL Lac-type object, the presence of several past outbursts in the ASAS-3 data confirmed the dwarf nova-type classification (vsnet-alert 19443). There is a GALEX counterpart with an NUV magnitude of 18.9(1). Subsequent observations detected

Table 104. Superhump maxima of IPHAS J230538 (2015)

E	max*	error	$O - C^\dagger$	N^\ddagger
0	57181.4144	0.0028	-0.0092	35
1	57181.4980	0.0017	0.0016	65
2	57181.5634	0.0023	-0.0056	24
15	57182.5175	0.0004	0.0031	46
28	57183.4623	0.0003	0.0024	76
29	57183.5358	0.0003	0.0033	77
43	57184.5529	0.0004	0.0022	69
82	57187.3918	0.0004	0.0050	74
83	57187.4664	0.0005	0.0068	74
96	57188.4074	0.0005	0.0024	74
97	57188.4788	0.0004	0.0012	74
110	57189.4218	0.0007	-0.0012	39
111	57189.4945	0.0008	-0.0013	33
123	57190.3708	0.0110	0.0024	9
124	57190.4362	0.0006	-0.0049	51
125	57190.5056	0.0011	-0.0082	49

*BJD-2400000.

† Against max = 2457181.4236 + 0.072722 E .

‡ Number of points used to determine the maximum.

superhumps (vsnet-alert 19449, 19454, 19467; figure 144). The times of superhump maxima are listed in table 105. There are clear stages B and C, with a strongly positive P_{dot} characteristic to this P_{SH} . The object showed a post-superoutburst rebrightening on February 15 (vsnet-alert 19508).

3.119 MASTER OT J073325.52+373744.9

This object (hereafter MASTER J073325) was detected as a transient at an unfiltered CCD magnitude of 15.1 on 2016 February 24 by the MASTER network (Gress et al. 2016b). There was at least one outburst in the CRTS data (15.9 mag on 2008 January 31, vsnet-alert 19528). Subsequent observations immediately detected growing superhumps (vsnet-alert 19532, 19537; figure 145). The times of superhump maxima are listed in table 106. The maxima for $E \leq 19$ were undoubtedly stage A superhumps as judged from the $O - C$ values and growing amplitudes. The likely positive P_{dot} for stage B is typical for this P_{SH} and the early appearance of (ordinary) superhumps indicates that this object is an ordinary SU UMa-type dwarf nova rather than a WZ Sge-type dwarf nova as suspected from the large outburst amplitude (Gress et al. 2016b). The presence of a past outburst is consistent with this identification.

3.120 MASTER OT J120251.56–454116.7

This object (hereafter MASTER J120251) was detected as a transient at an unfiltered CCD magnitude of 16.0 on 2015

Table 105. Superhump maxima of MASTER J003831 (2016)

E	max*	error	$O - C^\dagger$	N^\ddagger
0	57416.5648	0.0004	0.0042	25
1	57416.6248	0.0006	0.0026	25
16	57417.5471	0.0005	0.0013	38
17	57417.6078	0.0004	0.0005	40
32	57418.5269	0.0014	-0.0040	23
33	57418.5910	0.0006	-0.0014	40
49	57419.5725	0.0005	-0.0051	40
50	57419.6339	0.0008	-0.0052	28
65	57420.5594	0.0009	-0.0034	39
66	57420.6209	0.0009	-0.0034	36
81	57421.5486	0.0025	0.0007	39
98	57422.5985	0.0011	0.0039	39
114	57423.5909	0.0008	0.0111	40
130	57424.5676	0.0007	0.0027	40
131	57424.6297	0.0021	0.0032	18
146	57425.5489	0.0008	-0.0012	39
147	57425.6124	0.0009	0.0007	31
179	57427.5747	0.0018	-0.0073	37

*BJD-2400000.

† Against max = 2457416.5606 + 0.061572*E*.

‡ Number of points used to determine the maximum.

Table 106. Superhump maxima of MASTER J073325 (2016)

E	max*	error	$O - C^\dagger$	N^\ddagger
0	57445.4247	0.0009	-0.0114	63
9	57445.9832	0.0026	-0.0042	33
10	57446.0493	0.0018	0.0007	63
11	57446.1046	0.0013	-0.0052	65
14	57446.2989	0.0020	0.0052	17
17	57446.4804	0.0008	0.0030	61
18	57446.5409	0.0011	0.0023	59
19	57446.6046	0.0019	0.0047	28
32	57447.4013	0.0006	0.0051	64
33	57447.4602	0.0005	0.0027	99
34	57447.5226	0.0005	0.0039	80
35	57447.5833	0.0005	0.0034	50
58	57448.9855	0.0008	-0.0032	61
59	57449.0465	0.0006	-0.0035	60
60	57449.1103	0.0017	-0.0009	34
80	57450.3340	0.0008	-0.0023	29
162	57455.3588	0.0012	-0.0002	58

*BJD-2400000.

† Against max = 2457445.4361 + 0.061253*E*.

‡ Number of points used to determine the maximum.

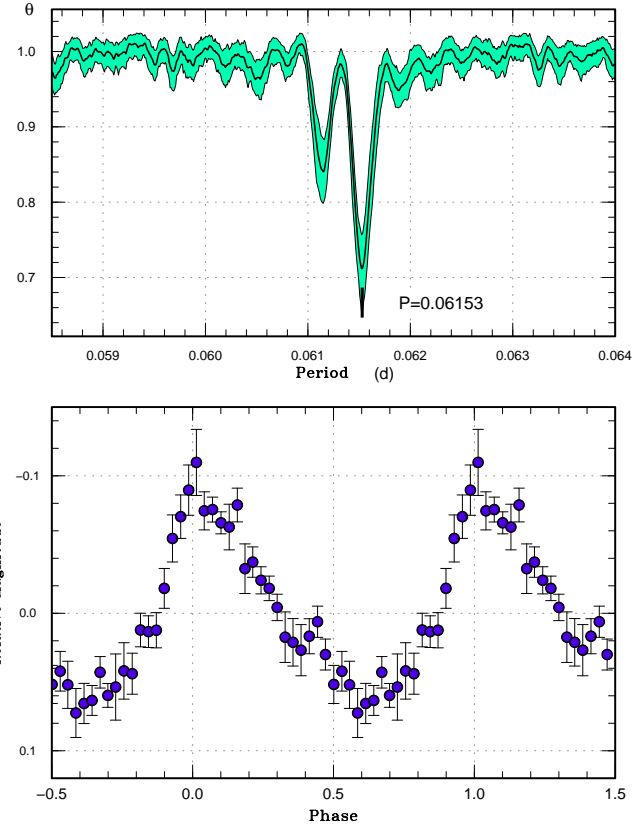


Fig. 144. Superhumps in MASTER J003831 during the plateau phase (2016). (Upper): PDM analysis. (Lower): Phase-averaged profile.

March 15 by the MASTER network (Gress et al. 2015a). This object was also detected at $V=16.7$ on 2015 March 15 by the ASAS-SN team (=ASASSN-15fp, Danilet et al. 2015). The object faded to fainter than $V=17.5$ on March 18 and then brightened to $V=14.4$ on March 20 (Danilet et al. 2015). Superhumps were immediately detected (vsnet-alert 18483, 18486, 18499; figure 146). The times of superhump maxima are listed in table 107. Due to the 4-d gap in the observation, we were not able to identify the stage classification and gave a global value in table 3. The initial part ($E \leq 27$) probably recorded stage B superhumps.

3.121 MASTER OT J131320.24+692649.1

This object (hereafter MASTER J131320) was detected as a transient at an unfiltered CCD magnitude of 14.7 on 2013 May 14 by the MASTER network (Denisenko et al. 2013a). There is a GALEX counterpart with an NUV magnitude of 20.6(2). Two more outbursts were recorded between 2014 and 2015 in the ASAS-SN data. The 2016 outburst was detected on February 15 at $V=15.01$ by the ASAS-SN team (cf. vsnet-alert 19505). Subsequent observations detected superhumps (vsnet-alert 19511; figure 147). The times of superhump maxima are

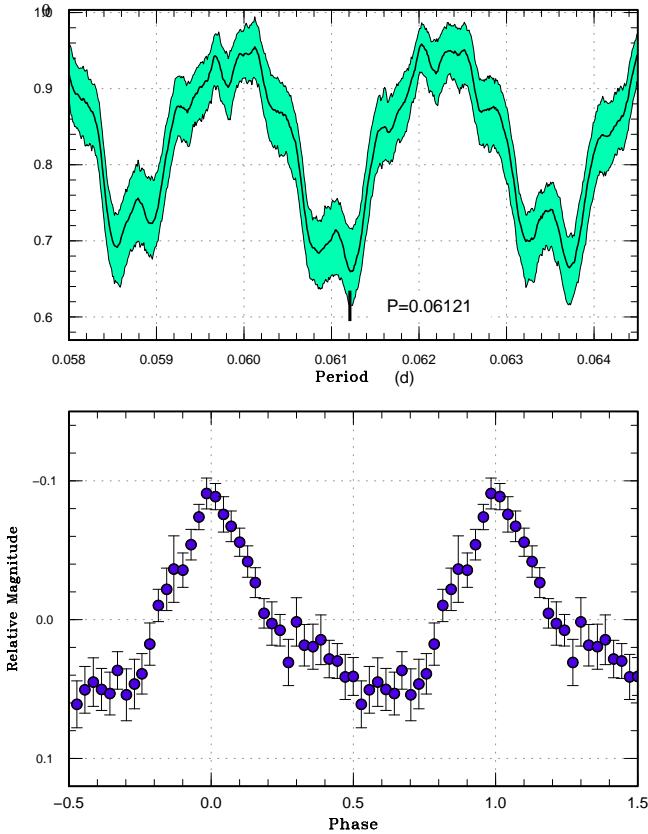


Fig. 145. Superhumps in MASTER J073325 (2016). The data after BJD 2457447 (stage B) were used. (Upper): PDM analysis. The alias selection was based on $O - C$ analysis. (Lower): Phase-averaged profile.

Table 107. Superhump maxima of MASTER J120251 (2015)

E	max*	error	$O - C^\dagger$	N^\ddagger
0	57103.3175	0.0002	-0.0004	146
1	57103.3806	0.0003	-0.0006	146
16	57104.3310	0.0003	-0.0009	145
17	57104.3953	0.0004	0.0001	138
18	57104.4520	0.0023	-0.0066	32
19	57104.5220	0.0003	0.0000	145
20	57104.5925	0.0007	0.0072	47
27	57105.0303	0.0006	0.0014	49
99	57109.5939	0.0026	0.0022	28
111	57110.3510	0.0005	-0.0012	146
112	57110.4143	0.0006	-0.0013	146
113	57110.4828	0.0038	0.0038	18
115	57110.6017	0.0018	-0.0040	34
131	57111.6199	0.0063	0.0003	28

*BJD-2400000.

† Against max = 2457103.3179 + 0.063372E.

‡ Number of points used to determine the maximum.

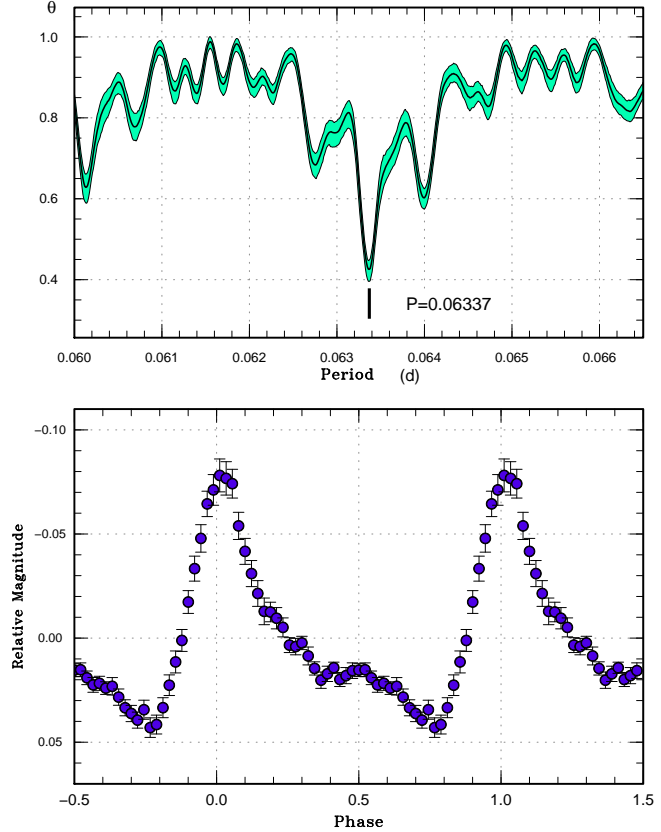


Fig. 146. Superhumps in MASTER J120251 during the plateau phase (2015). (Upper): PDM analysis. (Lower): Phase-averaged profile.

Table 108. Superhump maxima of MASTER J131320 (2016)

E	max*	error	$O - C^\dagger$	N^\ddagger
0	57435.4849	0.0006	-0.0004	65
1	57435.5554	0.0006	0.0004	70
32	57437.7164	0.0009	0.0004	35
33	57437.7836	0.0009	-0.0021	47
34	57437.8569	0.0008	0.0016	46

*BJD-2400000.

† Against max = 2457435.4853 + 0.069709E.

‡ Number of points used to determine the maximum.

listed in table 108. Although we selected the alias period to minimize absolute $O - C$ residuals, the superhump amplitudes were significantly smaller on the first night. It was possible that the stage A superhumps were recorded on the initial night. If there was a strong variation in the period between two nights, our method may have failed to select the correct period. Although there was no indication of such a strong variation in the $O - C$ values, the period should be treated with caution.

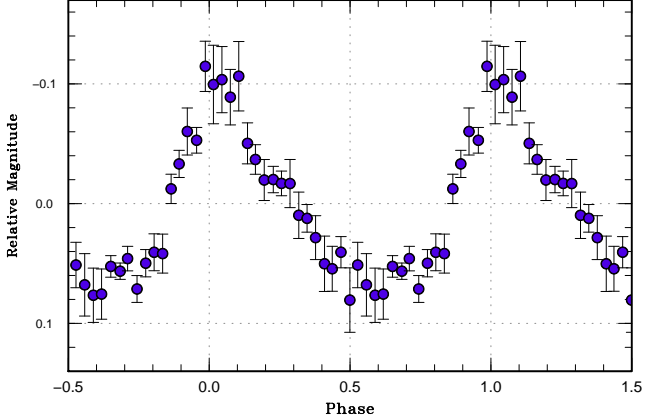
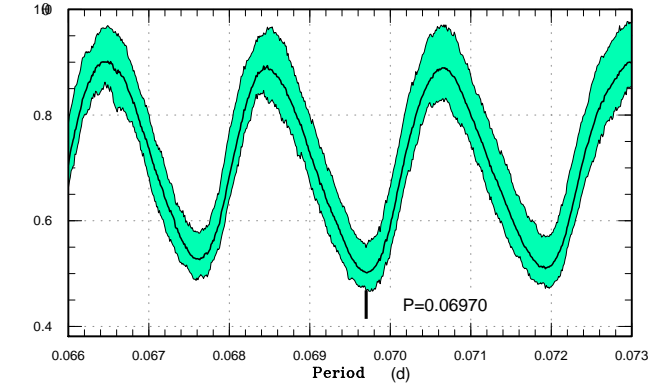


Fig. 147. Superhumps in MASTER J131320 (2016). (Upper): PDM analysis. The alias selection was based on $O - C$ analysis. (Lower): Phase-averaged profile.

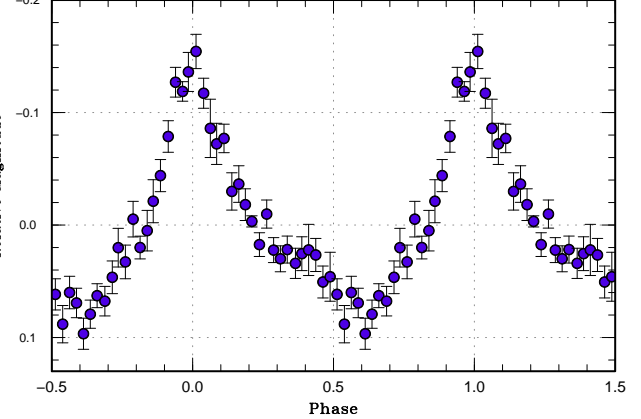
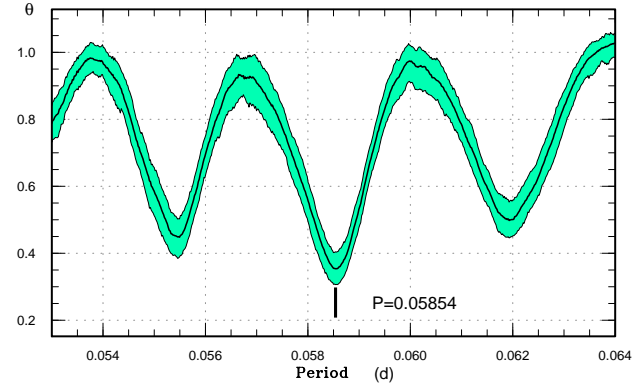


Fig. 148. Superhumps in MASTER J181523 (2015). (Upper): PDM analysis. The alias selection was based on $O - C$ analysis. (Lower): Phase-averaged profile.

Table 109. Superhump maxima of MASTER J181523 (2015)

E	max*	error	$O - C^\dagger$	N^\ddagger
0	57267.4270	0.0005	0.0006	52
1	57267.4830	0.0015	-0.0019	24
2	57267.5448	0.0008	0.0014	38
3	57267.6016	0.0008	-0.0003	51
18	57268.4805	0.0008	0.0009	49
19	57268.5385	0.0006	0.0004	55
20	57268.5954	0.0010	-0.0012	53

*BJD-2400000.

† Against max = 2457267.4264 + 0.058512E.

‡ Number of points used to determine the maximum.

3.122 MASTER OT J181523.78+692037.4

This object (hereafter MASTER J181523) was detected as a transient at an unfiltered CCD magnitude of 15.7 on 2015 August 28 by the MASTER network (Gress et al. 2015b). There is a GALEX counterpart with an NUV magnitude of 22.8(5). Superhumps were soon detected (vsnet-alert 19026, 19041; figure 148). The times of superhump maxima are listed in table 109.

3.123 MASTER OT J212624.16+253827.2

This object (hereafter MASTER J212624) was detected as a transient at an unfiltered CCD magnitude of 14.1 on 2013 June 26 by the MASTER network (Denisenko et al. 2013b). The 2013 superoutburst was well observed and a large positive P_{dot} despite the long P_{SH} was detected (Kato et al. 2014b). For more information, see Kato et al. (2014b).

The 2015 superoutburst was detected by the ASAS-SN team at $V=14.24$ on August 27 (cf. vsnet-alert 19012). Our observation on September 1 recorded superhumps (vsnet-alert 19031). The times of superhump maxima are listed in table 110. Since the observation was 5 d after the outburst detection, our observation did not cover the early part of the superoutburst. Although the 2013 observation started 2 d after the outburst detection, it may have not been detected sufficiently early. Our present observations were insufficient to verify the large positive P_{dot} . Further observations, particularly in the early phase, are still needed.

Table 110. Superhump maxima of MASTER J212624 (2015)

E	max*	error	$O - C^\dagger$	N^\ddagger
0	57267.3587	0.0003	-0.0013	97
1	57267.4486	0.0004	-0.0026	104
2	57267.5407	0.0004	-0.0017	98
3	57267.6397	0.0021	0.0061	41
30	57270.0905	0.0038	-0.0053	57
31	57270.1917	0.0075	0.0047	31

*BJD-2400000.

†Against max = 2457267.3600 + 0.091193*E*.

‡Number of points used to determine the maximum.

3.124 N080829A

This object was originally reported as a transient by H. Mikuz on 2008 August 29 at $R=15.98(4)$ (vsnet-alert 10485). The object was observed at around $R=16.3$ on August 31.

The 2015 outburst was detected by CRTS on October 12 at an unfiltered CCD magnitude of 15.98. Subsequent observations detected superhumps (vsnet-alert 19162, 19164, 19167, 19169; figure 149). The times of superhump maxima are listed in table 111. The strongly positive P_{dot} is typical for stage B superhumps with this superhump period.

3.125 OT J191443.6+605214

This object (hereafter OT J191443) was discovered by K. Itagaki (Yamaoka et al. 2008). The 2008 superoutburst was studied in Boyd et al. (2009) and Kato et al. (2009). See Kato et al. (2014b) for more history.

The 2015 outburst was detected by the ASAS-SN team on July 24. The outburst detection was probably early enough and initial observations detected low-amplitude stage A superhumps (vsnet-alert 18887). The times of superhump maxima are listed in table 112. Although the maxima for $E \leq 1$ were stage A superhumps, we could not determine the period of stage A superhumps (see also figure 150 for the comparison of $O - C$ diagrams).

3.126 SDSS J074859.55+312512.6

This object (hereafter SDSS J074859) is a dwarf nova selected by Wils et al. (2010). The 2015 outburst was detected by CRTS on November 20 at an unfiltered CCD magnitude of 15.86 (cf. vsnet-alert 19292). There were frequent outbursts in the past CRTS data. Observations on Nov. 24 detected eclipses and an analysis of the CRTS data combined with the new data yielded the following ephemeris (vsnet-alert 19297):

$$\text{Min(BJD)} = 2457351.21283(2) + 0.0583110901(7)E. \quad (5)$$

The orbital light curve (figure 151) indicates deep eclipses and

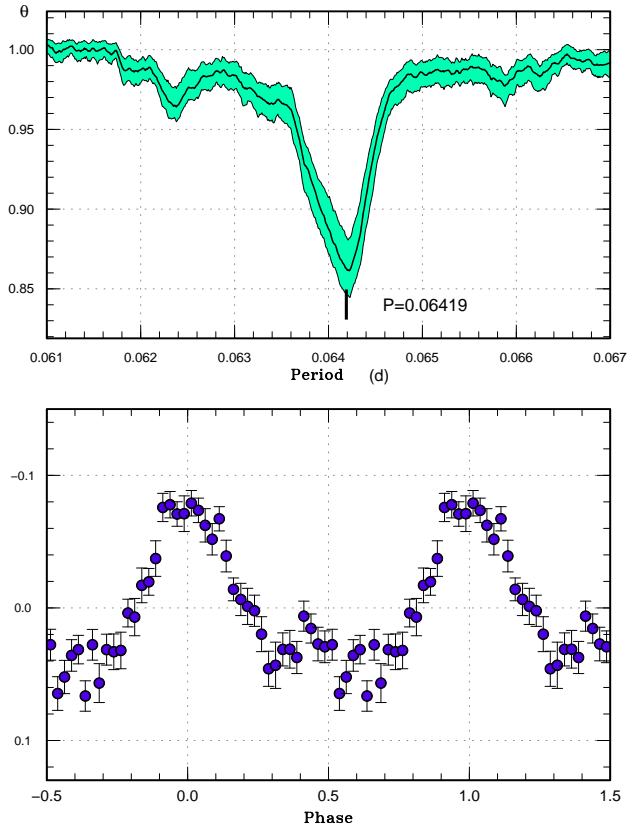


Fig. 149. Superhumps in N080829A (2015). (Upper): PDM analysis. The alias selection was based on $O - C$ analysis. (Lower): Phase-averaged profile.

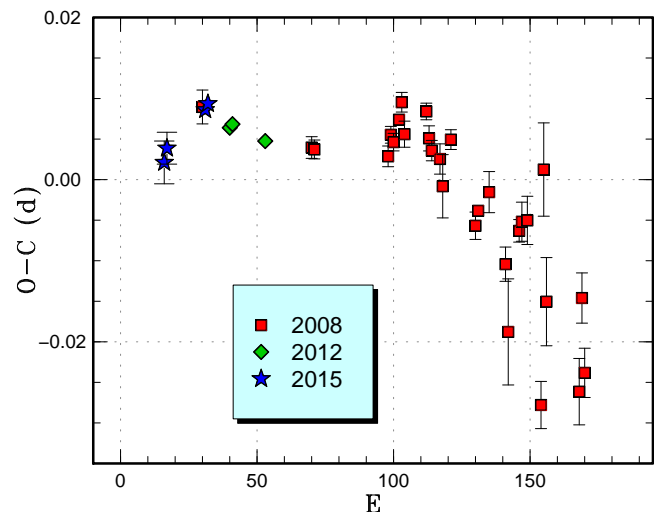


Fig. 150. Comparison of $O - C$ diagrams of OT J191443 between different superoutbursts. A period of 0.07138 d was used to draw this figure. Approximate cycle counts (E) after the start of the superoutburst were used. Since the starts of the 2008 and 2012 superoutbursts were not well constrained, we shifted the $O - C$ diagrams to fit the 2015 one, whose cycle counts are considered to be best determined.

Table 111. Superhump maxima of N080829A (2015)

E	max*	error	$O - C^\dagger$	N^\ddagger
0	57308.9554	0.0012	0.0077	116
2	57309.0800	0.0011	0.0037	160
3	57309.1480	0.0013	0.0075	179
11	57309.6584	0.0004	0.0036	67
12	57309.7199	0.0004	0.0008	66
13	57309.7840	0.0004	0.0006	67
15	57309.9033	0.0087	-0.0086	44
16	57309.9739	0.0015	-0.0023	136
17	57310.0413	0.0011	0.0008	182
18	57310.1046	0.0006	-0.0002	72
19	57310.1658	0.0013	-0.0033	88
32	57311.0006	0.0007	-0.0041	62
33	57311.0686	0.0008	-0.0004	99
34	57311.1323	0.0037	-0.0010	41
47	57311.9633	0.0010	-0.0056	131
48	57312.0358	0.0028	0.0025	138
49	57312.0886	0.0014	-0.0089	74
69	57313.3800	0.0017	-0.0031	67
70	57313.4490	0.0012	0.0016	33
78	57313.9565	0.0035	-0.0052	71
79	57314.0242	0.0034	-0.0017	113
80	57314.0898	0.0043	-0.0004	119
97	57315.1828	0.0116	-0.0002	19
98	57315.2523	0.0042	0.0049	36
99	57315.3162	0.0021	0.0046	33
100	57315.3823	0.0024	0.0065	20

*BJD-2400000.

† Against max = 2457308.9477 + 0.064282*E*.

‡ Number of points used to determine the maximum.

Table 112. Superhump maxima of OT J191443 (2015)

E	max*	error	$O - C^\dagger$	N^\ddagger
0	57229.0977	0.0026	-0.0006	137
1	57229.1709	0.0020	0.0007	146
15	57230.1749	0.0003	-0.0002	68
16	57230.2471	0.0002	0.0001	77

*BJD-2400000.

† Against max = 2457229.0984 + 0.071784*E*.

‡ Number of points used to determine the maximum.

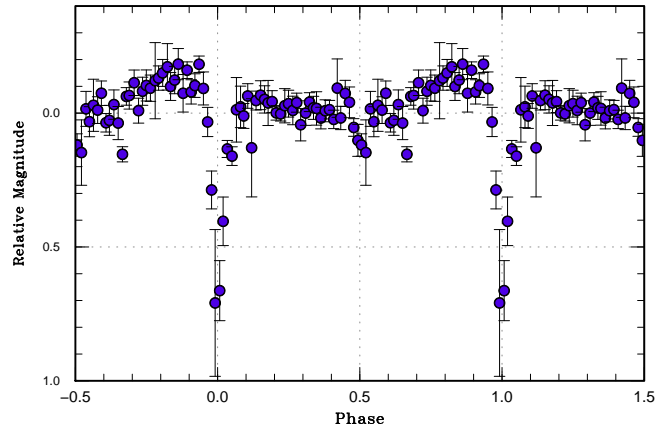


Fig. 151. Mean orbital light curve SDSS J074859. The CRTS data and our observations are used. The ephemeris of equation (5) is used.

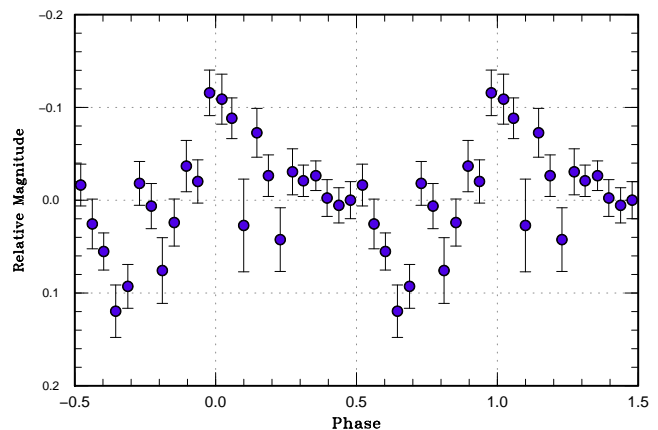
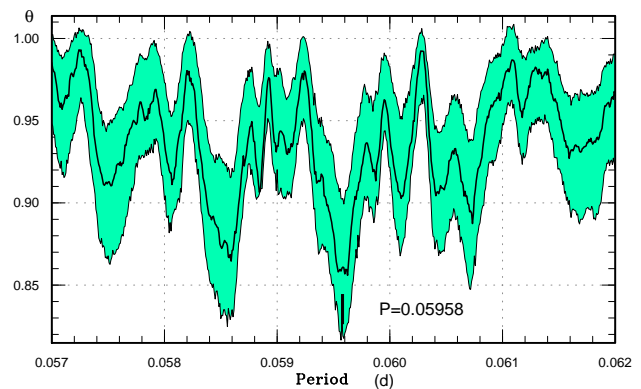


Fig. 152. Superhumps in SDSS J074859 (2015). (Upper): PDM analysis outside the eclipses. (Lower): Phase-averaged profile.

pre-eclipse orbital humps. These features, combined with the short orbital period, suggest that this object is an eclipsing SU UMa-type dwarf nova. Although we could not determine individual superhump maxima, a PDM analysis yielded a superhump period of 0.05958(3) d, 2.1% longer than the orbital period (figure 152). This period is listed in table 3.

Table 113. Superhump maxima of SDSS J145758 (2015)

E	max*	error	$O - C^\dagger$	N^\ddagger
0	57305.2918	0.0006	-0.0075	185
1	57305.3592	0.0032	0.0050	87
6	57305.6266	0.0007	-0.0020	32
7	57305.6832	0.0016	-0.0002	18
91	57310.2907	0.0004	-0.0028	124
92	57310.3503	0.0010	0.0020	61
108	57311.2274	0.0004	0.0010	112
109	57311.2847	0.0009	0.0034	82
110	57311.3373	0.0024	0.0011	40
126	57312.2173	0.0006	0.0030	104
127	57312.2724	0.0005	0.0032	101
128	57312.3273	0.0006	0.0032	82
181	57315.2264	0.0020	-0.0064	59
182	57315.2846	0.0044	-0.0030	57

*BJD-2400000.

 † Against max = 2457305.2993 + 0.054881 E . ‡ Number of points used to determine the maximum.

3.127 SDSS J145758.21+514807.9

This object (hereafter SDSS J145758) is a CV selected by Szkody et al. (2005). The spectrum in Szkody et al. (2005) strongly suggested a dwarf nova with a very low mass-accretion rate. The object was found to contain a pulsating white dwarf as in GW Lib (Uthas et al. 2012). The object has a photometric orbital period of 0.054087(5) d (Uthas 2011). No previous outburst was known.

J. Shears detected the first known outburst on 2015 September 29 at an unfiltered CCD magnitude of 15.3 (vsnet-outburst 18727). The object further rose to 11.9 (visual magnitude) on September 30 (vsnet-alert 19097, 19098). Subsequent observations detected double-wave early superhumps (vsnet-alert 19100, 19103; figure 153). The period of early superhumps was shorter than the orbital period by 0.07(2)%, confirming the relation reported in other WZ Sge-type dwarf novae (Kato 2015).

Due to the short visibility in the evening sky, the development of ordinary superhumps was not well observed. Ordinary superhumps were confidently detected only during the final stage of the plateau phase (vsnet-alert 19187; figure 154). The object started fading rapidly 3 d after these observations of ordinary superhumps. The times of maxima of ordinary superhumps are listed in table 113. The maxima for $E \geq 181$ refer to superhumps during the rapid fading and they were not used in determining the superhump period in table 3. No post-superoutburst observations were available and it was not known whether this fading was a “dip” as in other WZ Sge-type dwarf novae or not.

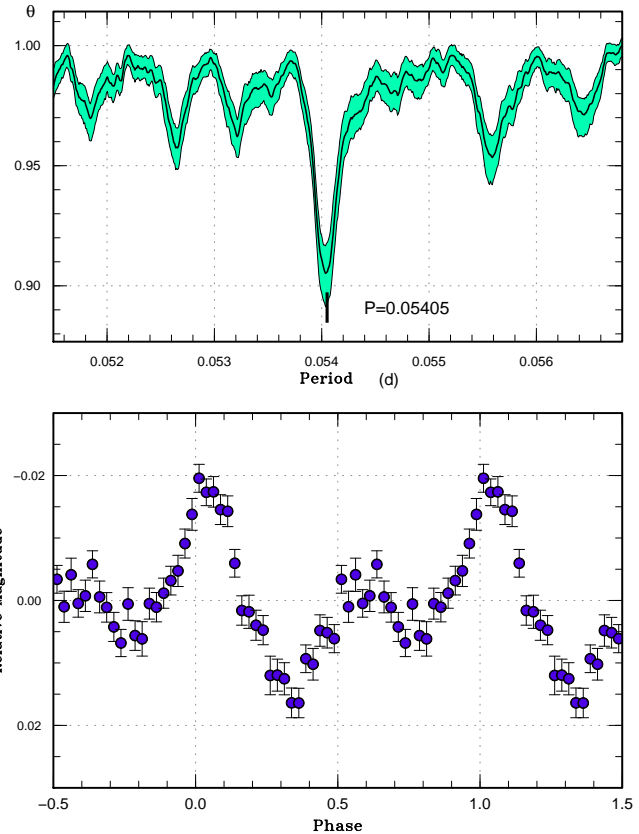


Fig. 153. Early superhumps in SDSS J145758 (2015). (Upper): PDM analysis. The data for BJD 2457296–2457305 were used. (Lower): Phase-averaged profile.

3.128 SDSS J164248.52+134751.4

This object (hereafter SDSS J164248) is a CV selected by Szkody et al. (2009). Szkody et al. (2009) suggested an orbital period of 1.3 hr. Southworth et al. (2008) obtained a spectroscopic orbital period of 0.07889(11) d and also reported Doppler tomography with an unusual brightness distribution in the accretion disk. Despite one well-recorded outburst detection at an unfiltered CCD magnitude of 14.7 in the CRTS data, there had not been outbursts until 2012 September 6, when E. Muylaert recorded an outburst at an unfiltered CCD magnitude of 15.9 (cvnet-outburst 4910). The 2012 outburst quickly faded.

The 2016 outburst was detected at $V=15.46$ by the ASAS-SN team (cf. vsnet-alert 19575). Subsequent observations detected superhumps (vsnet-alert 19582, 19593; figure 155). The times of superhump maxima are listed in table 114. Since the superhump period of 0.07928(2) d is too close to the suggested orbital period, this orbital period does not seem to have been well determined. It is likely that the baseline for the spectroscopic observations was not sufficient to obtain an accurate orbital period. For this reason, we did not include this orbital period in table 3.

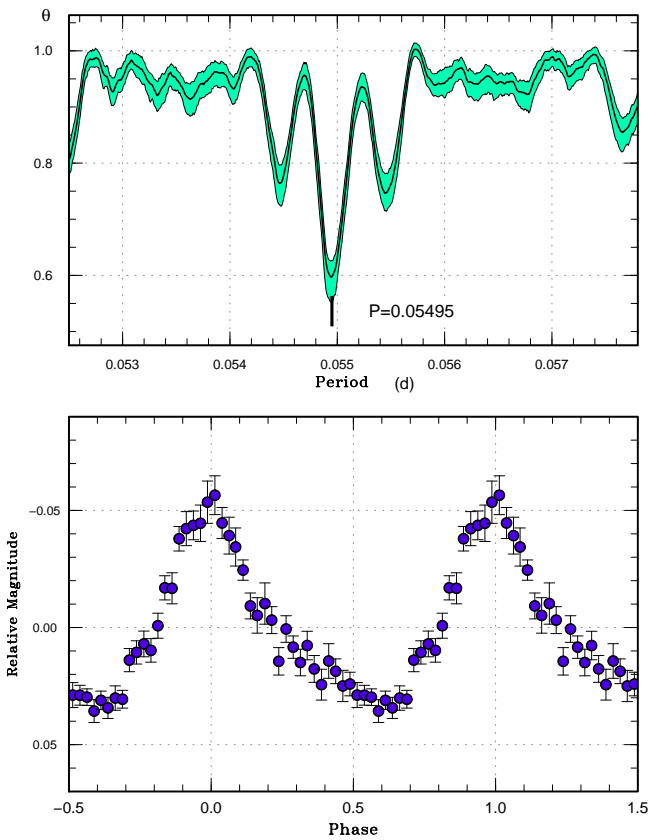


Fig. 154. Ordinary superhumps in SDSS J145758 (2015). (Upper): PDM analysis. The data for BJD 2457305–2457313 were used. (Lower): Phase-averaged profile.

Table 114. Superhump maxima of SDSS J164248 (2016)

E	max*	error	$O - C^\dagger$	N^\ddagger
0	57461.5908	0.0004	-0.0005	81
1	57461.6717	0.0004	0.0011	74
12	57462.5327	0.0038	-0.0105	32
13	57462.6265	0.0005	0.0039	82
14	57462.7048	0.0014	0.0029	20
15	57462.7748	0.0073	-0.0064	13
16	57462.8617	0.0010	0.0012	31
28	57463.8154	0.0013	0.0030	28
29	57463.9027	0.0036	0.0109	13
41	57464.8425	0.0011	-0.0012	25
53	57465.7935	0.0013	-0.0021	18
54	57465.8725	0.0018	-0.0024	25

*BJD-2400000.

† Against max = 2457461.5913 + 0.079327E.

‡ Number of points used to determine the maximum.

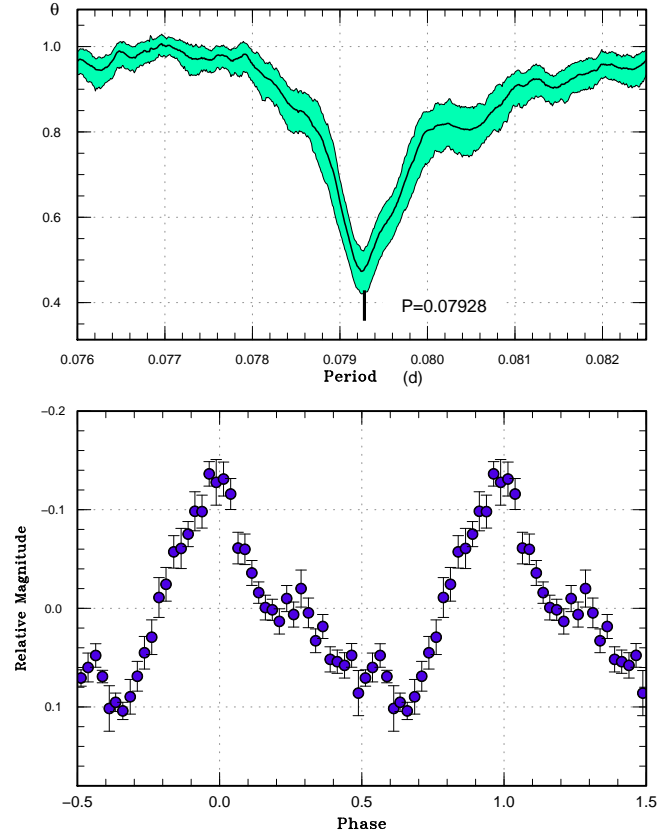


Fig. 155. Ordinary superhumps in SDSS J164248 (2016). (Upper): PDM analysis. (Lower): Phase-averaged profile.

4 Discussion

4.1 Statistics of objects

In Kato et al. (2015a), we introduced the statistics of the sources of the objects studied in our surveys and noticed that the rapid increase of the objects registered as ASAS-SN CVs. Several dwarf novae received new variable star designations in the latest updates of the General Catalog of Variable Stars (Kazarovets et al. 2015a; Kazarovets et al. 2015b) since Kato et al. (2015a), and these newly named objects are included in the GCVS category. The tendency pointed out in Kato et al. (2015a) became more prominent and roughly two thirds of the objects studied in this survey are now ASAS-SN CVs. The present GCVS names appear to be almost complete discoveries up to 2008 in the literature (dwarf novae reported in IAUCs and CBETs appear to be designated more quickly than other literature) and let's hope that the GCVS team could give more final designations to newly discovered dwarf novae.

4.2 Period distribution

In figure 157, we give distributions of superhump and estimated orbital periods (see the caption for details) since Kato

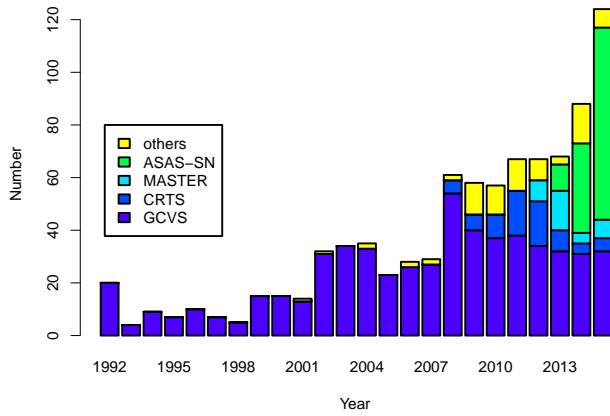


Fig. 156. Object categories in our survey. Superoutbursts with measured superhump periods are included. The year represents the year of outburst. The year 1992 represents outbursts up to 1992 and the year 2015 includes the outbursts in 2016, respectively. The category GCVS includes the objects named in the General Catalog of Variable Stars Kholopov et al. (1985) in the latest version and objects named in New Catalog of Suspected Variable Stars (NSV: Kukarkin et al. 1982). The categories CRTS, MASTER, ASAS-SN represent objects which were discovered in respective surveys. A small fraction of objects discovered by these surveys are already named in GCVS and are included in the category GCVS.

Table 115. Ephemerides of eclipsing systems.

Object	Epoch (BJD)	Period (d)
V2051 Oph	2453189.48679(1)	0.0624278552(2)
ASASSN-15sl	2457341.23671(7)	0.0870484(7)
ASASSN-15ux	2457400.82908(10)	0.056109(2)
CRTS J200331	2457200.79900(6)	0.0587048(3)
SDSS J074859	2457351.21283(2)	0.0583110901(7)

et al. (2009). For readers' convenience, we also listed new ephemerides of eclipsing systems newly determined or updated in this study in table 115. When there are multiple observations of superoutbursts of the same object, we adopted an average of the measurements. Since most of non-magnetic CVs below the period gap are considered to be SU UMa-type dwarf novae, this distribution reflects the distribution of non-magnetic CVs below the period gap. As already pointed out in Kato et al. (2015a), the sharp cut-off at a period of 0.053 d (the objects below this period are either AM CVn-type systems and EI Psc-type objects) and the apparent absence of the strong signature of the lower edge of the period gap are even more apparent. The updated statistics confirms the findings in Kato et al. (2015a). The same statistics using the latest version of RKCAt (Ritter, Kolb 2003; Edition 7.23, 2015 June 30) is shown in figure 158. The result confirms the general trend seen in our sample, although it is not surprising since more than half of dwarf novae in this P_{orb} region in RKCAt are from our surveys. The disrupted magnetic braking may be weaker or more CVs may be formed in the period gap than had been supposed.

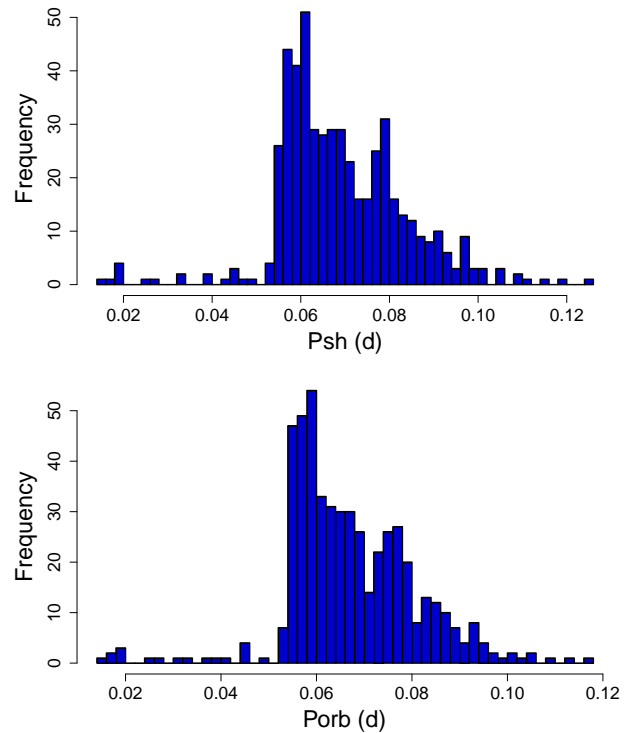


Fig. 157. Distribution of superhump periods in this survey. The data are from Kato et al. (2009), Kato et al. (2010), Kato et al. (2012), Kato et al. (2013a), Kato et al. (2014b), Kato et al. (2014a), Kato et al. (2015a) and this paper. The mean values are used when multiple superoutbursts were observed. The number of objects is 511. (Upper) distribution of superhump periods. (Lower) distribution of orbital periods. For objects with superhump periods shorter than 0.053 d, the orbital periods were assumed to be 1% shorter than superhump periods. For objects with superhump periods longer than 0.053 d, we used the calibration in Kato et al. (2012) to estimate orbital periods.

4.3 Period derivatives during stage B

Figure 159 represents updated relation between P_{dot} for stage B versus P_{orb} . Although this is essentially an updated version of the corresponding figures in the earlier series of papers, we have omitted poor quality observation (quality C) and simplified the symbols. The object listed in this paper with large negative P_{dot} is PM J03338, which had a separate precursor and a long stage A (Kato et al. 2016a). Other objects with large negative P_{dot} in earlier papers are UV Gem (2003), PU UMa (2012) and CY UMa (2014). UV Gem is famous for the large negative P_{dot} and it is possibly interpreted as a stage A-B transition rather than period variation during stage B (cf. Kato et al. 2016b). PU UMa is an eclipsing object and the P_{dot} determination may have suffered from the beat phenomenon. In CY UMa (2014), the stage transition was rather smooth and it was difficult to define the border of stage B. These outliers have their own reasons to be outside the distribution of the majority of objects, and the main trends in this figure seem to apply to most of ordinary superoutbursts.

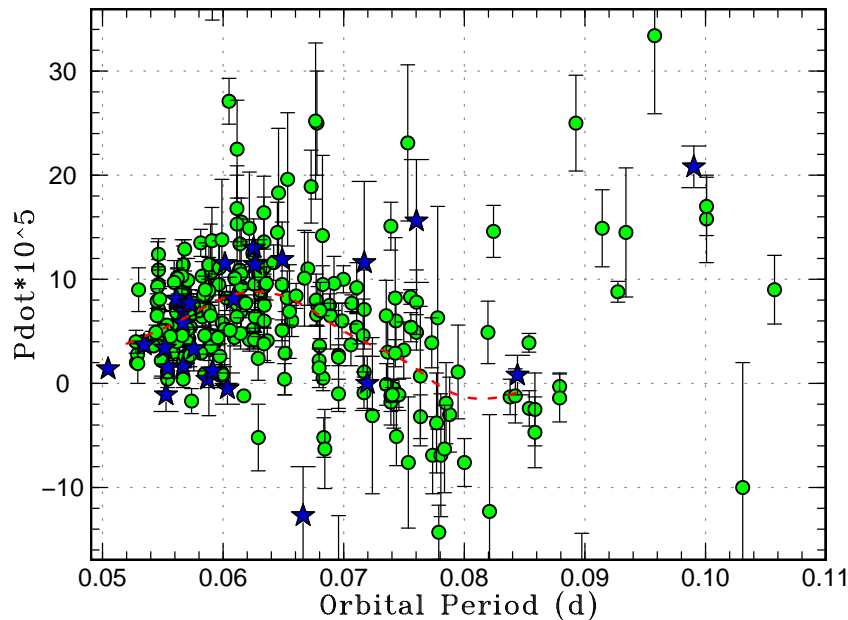


Fig. 159. P_{dot} for stage B versus P_{orb} . Filled circles and filled stars represent samples in Kato et al. (2009)–Kato et al. (2015a) and this paper, respectively. The curve represents the spline-smoothed global trend.

4.4 Long-period objects with long-lasting stage A

It had been known that some long- P_{orb} systems show a strong decrease of the superhump periods [cf. MN Dra and UV Gem, see subsection 4.10 in Kato et al. (2009)]. Although the origin of this strong period variation had remained a mystery, Kato et al. (2014a) proposed a working hypothesis that these strong period variations are a result of the combination of stages A and B. This interpretation requires that stage A in these systems is unusually long. In Kato et al. (2014a), the case of MN Dra was studied, which lacked the spectroscopically determined orbital period. Kato et al. (2016b) presented a more convincing example of V1006 Cyg, whose orbital period had been determined spectroscopically. It appears to have been established that at least some long- P_{orb} systems show long-lasting stage A, which implies that the 3:1 resonance grows slowly in these systems. Kato et al. (2014a) and Kato et al. (2016b) suggested that the mass ratios close to the borderline of the 3:1 resonance is responsible for this phenomenon.

An updated list of long- P_{orb} SU UMa-type objects with long phase of stage A superhumps is given in table 116. For V452 Cas, we used the best observed superoutburst (2007) in Shears et al. (2009) and modified the superhump stages listed in Kato et al. (2009) according to the modern interpretation (see also subsection 3.5 and figure 6). The duration of stage A in KK Tel is from the combined $O - C$ diagram (see also subsection 3.27 and figure 28). ASASSN-15rs (subsection 3.87) and DDE 26 (subsection 3.116) may belong to this category.

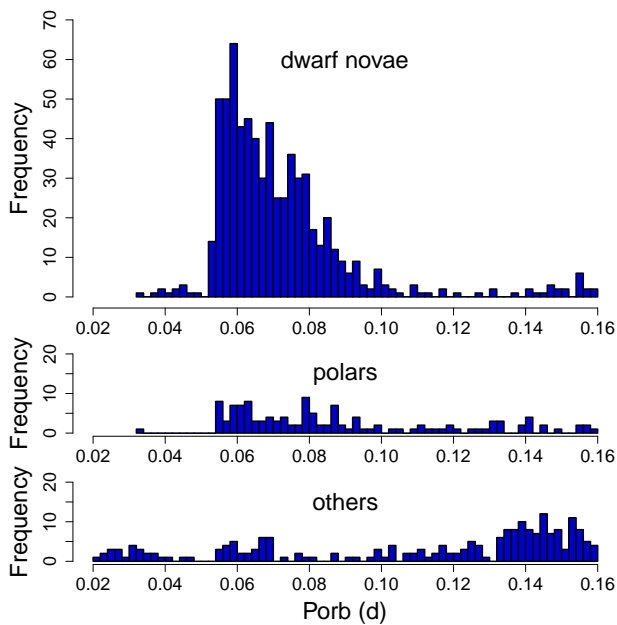


Fig. 158. Distribution of orbital periods in the latest version of RKCAt (Ritter, Kolb 2003; Edition 7.23, 2015 June 30). The three histograms represent distributions of dwarf novae (DN in RKCAt), polars (AM in RKCAt) and others. The number of dwarf novae in the region of 0.02–0.12 d (corresponding to figure 157) is 676.

Table 116. Comparison of SU UMa-type objects with long phase of stage A superhumps

Object	P_{orb}^*	P_A^\dagger	P_B^\ddagger	P_C^\S	dur	$q^\#$	References
V1006 Cyg (2015)	0.09903(9)	0.1093(3)	0.10541(4)	0.10444(5)	≥ 32	0.34(2)	Kato et al. (2016b)
MN Dra (2012)	0.0998(2)	0.10993(9)	0.10530(6)	–	≥ 39	0.327(5)	Kato et al. (2014a)
MN Dra (2013)	0.0998(2)	0.1082(1)	0.10504(7)	–	≥ 18	0.258(5)	Kato et al. (2014a)
CRTS J214738.4+244554 (2011)	0.09273(3)	0.0992(3)	0.09715(2)	–	≥ 21	0.204(11)	Kato et al. (2015a)
OT J064833.4+065624 (2014)	–	0.1052(4)	0.10033(3)	–	≥ 38	–	Kato et al. (2015a)
V452 Cas (2007)	–	0.08943(7)	0.08869(2)	–	20–35	–	this work
KK Tel (2015)	–	0.09005(12)	0.08761(2)	–	≥ 25	–	this work
ASASSN-15cl (2016)	–	0.0961(3)	0.09463(10)	0.09391(7)	≥ 22	–	this work

*Orbital period (d).

†Period of stage A superhumps (d).

‡Period of stage B superhumps (d).

§Period of stage C superhumps (d).

||Duration of stage A (cycles).

#Determined from stage A superhumps.

4.5 Mass ratios from stage A superhumps

Since the new interpretation of stage A as representing the dynamical precession rate at the 3:1 resonance in Kato, Osaki (2013b), the application of this method produced a steady stream of q measurements. We list new estimates for q from stage A superhumps in table 117. This table also includes new objects that were studied in detail in other papers. The appropriate references are listed in table 3.

In table 118, we list all stage A superhumps recorded in the present study.

A updated distribution of mass ratios is shown in figure 160 [for the list of objects, see Kato, Osaki (2013b) and Kato et al. (2015a)]. We have newly added PHL 1445 with $P_{\text{orb}}=0.052985$ d and $q=0.087(6)$ (McAllister et al. 2015, eclipse observation). It would be worth mentioning that Harrison (2016) derived $q \leq 0.071$ for WZ Sge ($P_{\text{orb}}=0.056688$ d) by infrared spectroscopy of the secondary (not plotted in this figure). The present study has strengthened the concentration of WZ Sge-type dwarf novae around $q = 0.07$ just above the period minimum, as reported in Kato et al. (2015a).

4.6 WZ Sge-type objects

In table 119, we list the parameters of WZ Sge-type dwarf novae (including likely ones).

It has been known that P_{dot} and P_{orb} are correlated with the rebrightening type [starting with figure 36 in Kato et al. 2009 and refined in Kato et al. (2009)–Kato et al. (2015a) and Kato (2015)]. The five types of outbursts based on rebrightenings are: type-A outbursts (long-duration rebrightening), type-B outbursts (multiple rebrightenings), type-C outbursts (single

Table 117. New estimates for the binary mass ratio from stage A superhumps

Object	ϵ^* (stage A)	q from stage A
V1006 Cyg	0.094(3)	0.34(2)
V493 Ser	0.0449(13)	0.129(5)
ASASSN-15gq	0.038(2)	0.107(8)
ASASSN-15hd	0.028(4)	0.076(12)
ASASSN-15na	0.030(2)	0.081(5)
ASASSN-15ni	0.0027(2)	0.074(2)
ASASSN-15po	0.0251(5)	0.067(2)
ASASSN-15pu	0.028(5)	0.074(16)
ASASSN-15uj	0.0243(13)	0.064(4)
ASASSN-16bh	0.0283(3)	0.076(1)
ASASSN-16bu	0.037(4)	0.10(1)
CRTS J200331	0.0310(2)	0.084(1)
PM J03338	0.0604(13)	0.172(4)

rebrightening), type-D outbursts (no rebrightening) and type-E outbursts (double superoutburst, with ordinary superhumps only during the second one). In figure 161, we show the updated result up to this paper. In this figure, we also added objects without known rebrightening types. These objects have been confirmed to follow the same trend, which we consider the evolutionary track.

ASASSN-16bh, the very noteworthy and well-observed WZ Sge-type dwarf nova in this study is located at the minimum period [$P_{\text{orb}}=0.05346$ d, $P_{\text{dot}}=+3.7(3)$]. This object showed a typical type-A rebrightening, in agreement with the trend in other WZ Sge-type dwarf novae.

ASASSN-15po is an outlier ($P_{\text{orb}}=0.05092$ d) in the figure below the period minimum of most of the objects. This ob-

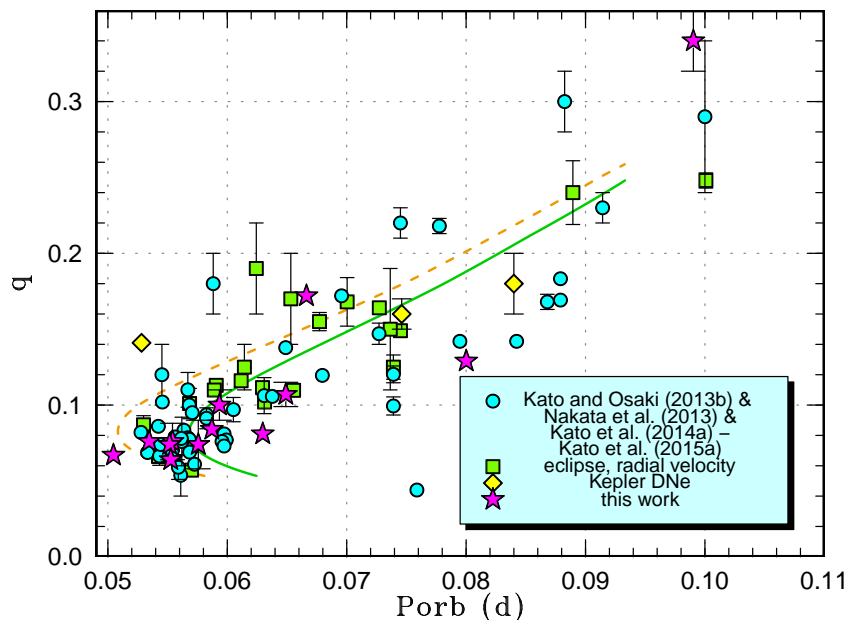


Fig. 160. Mass ratio versus orbital period. The dashed and solid curves represent the standard and optimal evolutionary tracks in Knigge et al. (2011), respectively. The filled circles, filled squares, filled stars, filled diamonds represent q values from a combination of the estimates from stage A superhumps published in four preceding sources (Kato, Osaki 2013b; Nakata et al. 2013; Kato et al. 2014a; Kato et al. 2014a; Kato et al. 2015a), known q values from quiescent eclipses or radial-velocity study (see Kato, Osaki 2013b for the data source), q estimated in this work and dwarf novae in the Kepler data (see text for the complete reference), respectively. The objects in “this work” includes objects studied in other papers but listed in table 1

ject may be similar to OV Boo = SDSS J150722.33+523039.8, which has an orbital period of 0.046258 d (Littlefair et al. 2007; Patterson et al. 2008; Uthas et al. 2011). Although the spectroscopic features strongly suggest the dwarf nova-type (probably WZ Sge-type) nature, OV Boo has not been yet recorded in major outburst. ASASSN-15po is the first object below the period minimum which has undergone a typical WZ Sge-type superoutburst. The details of the outburst are discussed in K. Namekata et al. in preparation.

4.7 Lessons from recent observations

Thanks to the increase of discoveries of new dwarf novae and detections of outbursts by modern surveys (such as ASAS-SN), the number of studied objects has dramatically increased in recent years. This increase has indeed improved our knowledge in the distribution of CVs below the period gap (e.g. subsection 4.1). The fraction of well-observed superoutbursts, however, largely decreased. For example, the number of “A”-class (well-observed) observations decreased from 58 (out of 363 outbursts) in Kato et al. (2009), 6 (out of 65 outbursts) in Kato et al. (2010) to 5 (out of 107 outbursts). Although such qualification of observations are subjective and the criteria may have not necessarily been the same, the increase of “underobserved” outbursts is apparent despite the increase of observations (figure 162).

The same trend is even more apparent in WZ Sge-type outbursts. In Kato et al. (2009)–Kato et al. (2013a), 55 WZ Sge-

type outbursts (out of 66) had observations to classify the rebrightening pattern. In the present study, only 5 WZ Sge-type outbursts (out of 18) have rebrightening classifications. Such a trend is fatal since rebrightenings are one of key elements in the study of WZ Sge-type dwarf novae (cf. Kato 2015).

These trends in observations probably reflect the increase of freshly discovered objects or outbursts, which would easily divert observers’ attention. In order that the observations will be more astrophysically beneficial and rewarding to observers, we propose the following lessons from recent observations. Although some of the lessons may be evident, we list them since they will be useful for those who wish to start contributing to this field, and they are not usually written in practical textbooks (such as Hellier 2001).

- Single-night observations have very limited value (except classification of the object and the initial detection of superhumps). If there are more than observations on two nights (hopefully consecutive nights), we can determine the superhump period better than to 0.2% (1σ error), necessary to make comparison with the orbital one. Periods from single-night observations have large errors typically 1–3%, which is entirely insufficient to make comparison with the orbital one.
- Once the object is observed, do not lightly change the target. In general, fresh outbursts tend to be “overobserved” (observations are sometimes redundant) while they become underobserved as the progress of the outbursts. There may not be many observations in the later phase and observations such

Table 119. Parameters of WZ Sge-type superoutbursts.

Object	Year	P_{SH}	P_{orb}	P_{dot}^*	err*	ϵ	Type [†]	N_{reb}^{\ddagger}	delay [§]	Max	Min
RZ Leo	2016	0.078675	0.076030	15.6	5.9	0.035	C	1	–	13.0	18.5
V2051 Oph	2015	0.064708	0.062428	–	–	0.037	–	–	–	–	–
ASASSN-15dp	2015	0.060005	–	0.4	1.1	–	–	–	–	14.1	19.4:
ASASSN-15ee	2015	0.057136	–	8.1	1.2	–	–	–	6	12.6	19.9:
ASASSN-15gq	2015	0.066726	0.06490	11.9	0.8	0.028	–	–	≥ 5	15.4	[21.6
ASASSN-15hd	2015	0.056105	0.05541	1.5	0.3	0.013	C?	≥ 1	11	14.0	21.7
ASASSN-15hn	2015	0.061831	–	–0.5	1.5	–	–	–	13–14	12.9	21.9:
ASASSN-15kh	2015	0.060480	–	1.2	1.6	–	–	–	13	13.2	[21.0
ASASSN-15na	2015	0.063720	0.06297	3.1	2.6	0.012	–	–	≥ 9	14.8	21.5:
ASASSN-15ni	2015	0.055854	0.05517	3.4	0.6	0.012	–	–	10	12.9	21.0:
ASASSN-15po	2015	0.050916	0.050457	1.1	0.1	0.009	A/B	≥ 5	11	13.7	21.6
ASASSN-15pu	2015	0.058254	0.05757	3.3	2.1	0.012	–	–	10	13.7	22.1:
ASASSN-15se	2015	0.063312	–	–	–	–	A/B or B	≥ 2	≥ 5	13.0	20.6
ASASSN-15sl	2015	0.091065	0.087048	9.1	2.6	0.046	–	–	–	–	–
ASASSN-15uj	2015	0.055805	0.055266	–1.1	1.6	0.010	–	–	10	14.3	21.0:
ASASSN-15ux	2015	0.056857	0.056109	–	–	0.013	–	–	14	14.4	[21.0
ASASSN-16bh	2016	0.054027	0.05346	3.7	0.3	0.011	A	1	7	12.7	20.3:
ASASSN-16bi	2016	–	0.05814	–	–	–	–	–	12:	14.3	[20.6
ASASSN-16bu	2016	0.060513	0.05934	–	–	0.020	–	–	9	14.5	22.1
CRTS J200331	2015	0.059720	0.058705	–	–	0.017	–	–	–	–	–
SDSS J074859	2015	0.05958	0.058311	–	–	0.022	–	–	–	–	–
SDSS J145758	2015	0.054912	0.054087	2.2	2.9	0.015	–	–	–	11.9	29.5

*Unit 10^{-5} .

†A: long-lasting rebrightening; B: multiple rebrightenings; C: single rebrightening; D: no rebrightening.

‡Number of rebrightenings.

§Days before ordinary superhumps appeared.

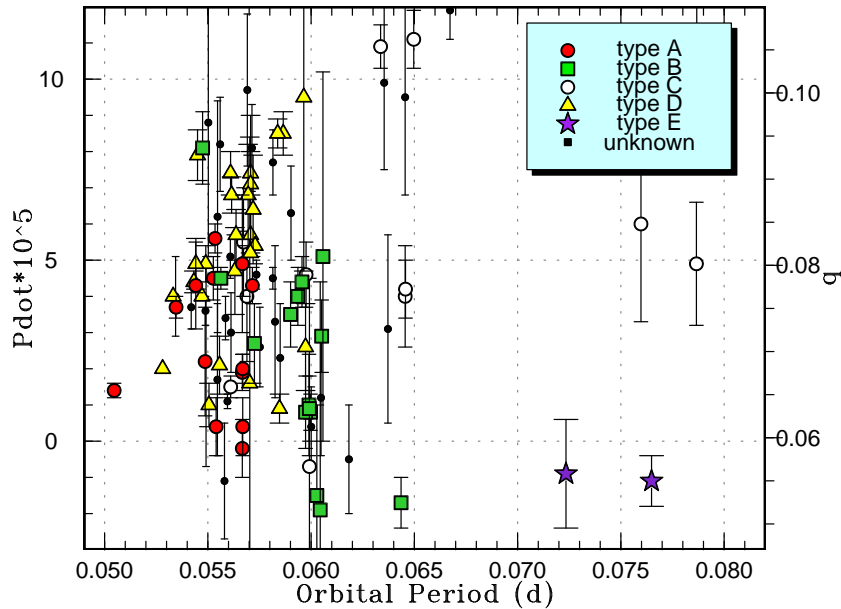
**Fig. 161.** P_{dot} versus P_{orb} for WZ Sge-type dwarf novae. Symbols represent the type of outburst: type-A (filled circles), type-B (filled squares), type-C (filled triangles), type-D (open circles) and type-E (filled stars) (see text for details). On the right side, we show mass ratios estimated using equation (6) in Kato (2015). We can regard this figure as to represent an evolutionary diagram.

Table 118. Superhump Periods during Stage A

Object	Year	period (d)	err
EG Aqr	2015	0.08109	0.00022
V1006 Cyg	2015	0.10930	0.00030
V844 Her	2015	0.05703	0.00019
V493 Ser	2015	0.08377	0.00011
KK Tel	2015	0.09005	0.00012
ASASSN-15cl	2016	0.09613	0.00027
ASASSN-15dp	2015	0.06145	0.00013
ASASSN-15ee	2015	0.05794	0.00009
ASASSN-15gn	2015	0.06453	0.00003
ASASSN-15gq	2015	0.06748	0.00018
ASASSN-15hd	2015	0.05703	0.00024
ASASSN-15hm	2015	0.05662	0.00010
ASASSN-15hn	2015	0.06322	0.00016
ASASSN-15kh	2015	0.06155	0.00003
ASASSN-15lt	2015	0.06213	0.00024
ASASSN-15na	2015	0.06491	0.00012
ASASSN-15ni	2015	0.05673	0.00017
ASASSN-15po	2015	0.05178	0.00001
ASASSN-15pu	2015	0.05920	0.00030
ASASSN-15sc	2015	0.05867	0.00009
ASASSN-15uj	2015	0.05664	0.00008
ASASSN-15ux	2015	0.05743	0.00031
ASASSN-16bh	2016	0.05502	0.00010
ASASSN-16bu	2016	0.06159	0.00023
CRTS J095926	2015	0.09079	0.00090
CRTS J200331	2015	0.06058	0.00002
MASTER J073325	2016	0.06209	0.00017
PM J03338	2015	0.07067	0.00005

a phase can be relatively more important. We should note, however, that objects may become too faint or the amplitudes of superhumps became too small to make useful observations. In such cases, we recommend nightly snapshots.

- Even after the superoutburst ends, regularly visit the target and obtain snapshot observations. This is particularly true for WZ Sge-type dwarf novae. If there is a major rebrightening, restart time-resolved photometry.
- For detecting stage A superhumps, which is very important to estimate mass ratios, early observations are very important. Even a 1-d gap in the observation could be fatal. In WZ Sge-type dwarf novae, there is usually a long waiting time (~ 10 d) before stage A superhumps appear. Although observations in this phase may not appear so appealing since early superhumps may become less apparent and amplitudes of variations became smaller, this phase is astrophysically more important (compared to the phase after full growth of superhumps) and it is a waste to miss this phase.

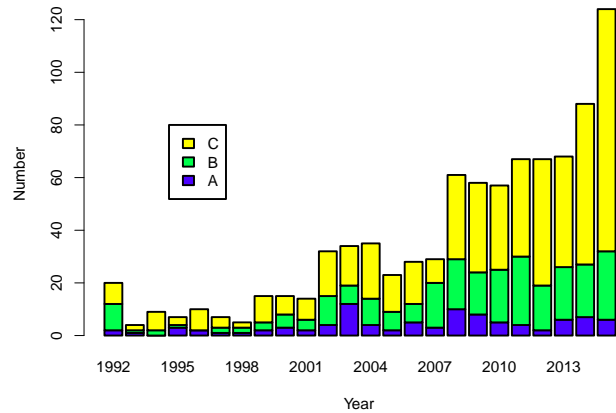


Fig. 162. Quality of observations (A: excellent, B: partial coverage or slightly low quality, C: insufficient coverage or observations with large scatter). The year represents the year of outburst. The year 1992 represents outbursts up to 1992 and the year 2015 includes the outbursts in 2016, respectively.

5 Summary

In addition to the updated statistics of the period distribution, $P_{\text{orb}}-P_{\text{dot}}$ relation, the updated evolutionary track using stage A superhumps and refined relationship between $P_{\text{orb}}-P_{\text{dot}}$ versus the rebrightening type in WZ Sge-type dwarf novae, the objects of special interest in this paper can be summarized as follows.

- V452 Cas ($P_{\text{SH}} \sim 0.0888$ d), KK Tel ($P_{\text{SH}} \sim 0.0876$ d) and ASASSN-15cl ($P_{\text{SH}} \sim 0.0946$ d) appear to have a long-lasting stage A. They would be members of growing group of long- P_{orb} objects with slowly growing superhumps. A slow growth of the 3:1 resonance near the stability border has been proposed (Kato et al. 2016b; also Kato et al. 2014a). If the mass ratios for these objects are determined by measuring P_{orb} , they would provide an excellent test for this interpretation.
- The WZ Sge-type object RZ Leo underwent a well-observed superoutburst in 2016. No clear evidence of early superhumps was detected. This object showed a strong beat phenomenon between the superhump and orbital periods.
- ASASSN-15cy is an object below the period minimum ($P_{\text{SH}} \sim 0.0500$ d). This object showed a superoutburst resembling the EI Psc-type object CSS J174033.5+414756.
- ASASSN-15hd is a WZ Sge-type dwarf nova showing large-amplitude early superhumps with a “saw-tooth”-like profile.
- ASASSN-15gn ($P_{\text{SH}} \sim 0.0636$ d), ASASSN-15hn ($P_{\text{SH}} \sim 0.0618$ d), ASASSN-15kh ($P_{\text{SH}} \sim 0.0605$ d) and ASASSN-16bu ($P_{\text{SH}} \sim 0.0609$ d) are possibly period bouncers as judged from the slow growth of ordinary superhumps and small amplitudes of superhumps.
- ASASSN-15na is a WZ Sge-type dwarf with a relatively long orbital period (0.06297 d). The object, however, appears to have a larger q than expected for a period bouncer.
- ASASSN-15ni is a WZ Sge-type dwarf nova showing a su-

peroutburst typical for this class.

- ASASSN-15sl and SDSS J074859 are eclipsing systems and we have also determined the orbital periods using eclipse observations.
- ASASSN-15uj is a WZ Sge-type dwarf nova with a low $q=0.064(4)$, indicating the relatively evolved state.
- ASASSN-15ux is a rare eclipsing WZ Sge-type dwarf nova.
- ASASSN-16bh is a WZ Sge-type dwarf nova showing a relatively rare plateau-type, long rebrightening (without small rebrightenings in it). This object also showed early superhumps with three maxima in one cycle.
- CRTS J200331 is an eclipsing SU UMa-type or WZ Sge-type dwarf nova probably near the border of SU UMa-type and WZ Sge-type objects.

Acknowledgements

This work was supported by the Grant-in-Aid “Initiative for High-Dimensional Data-Driven Science through Deepening of Sparse Modeling” (25120007) from the Ministry of Education, Culture, Sports, Science and Technology (MEXT) of Japan. The authors are grateful to observers of VSNET Collaboration and VSOLJ observers who supplied vital data. We acknowledge with thanks the variable star observations from the AAVSO International Database contributed by observers worldwide and used in this research. We are also grateful to the VSOLJ database. This work is deeply indebted to outburst detections and announcement by a number of variable star observers worldwide, including participants of CVNET and BAA VSS alert. The CCD operation of the Bronberg Observatory is partly sponsored by the Center for Backyard Astrophysics. We are grateful to the Catalina Real-time Transient Survey team for making their real-time detection of transient objects available to the public. This research has made use of the SIMBAD database, operated at CDS, Strasbourg, France. This research has made use of the International Variable Star Index (VSX) database, operated at AAVSO, Cambridge, Massachusetts, USA.

References

- Abazajian, K. N., et al. 2009, *ApJS*, 182, 543
- Ahn, C. P., et al. 2012, *ApJS*, 203, 21
- Ahnert-Rohlf, E. 1952, *Mitteil. Veränderl. Sterne*, 158
- Andrade, E. L., & Baptista, R. 2014, *Rev. Mexicana Astron. Astrof. (Serie de Conferencias)*, 44, 145
- Angel, R., Liebert, J., & Stockman, H. 1977, *IAU Circ.*, 3065, 3
- Antipin, S. V. 1996a, *IBVS*, 4343
- Antipin, S. V. 1996b, *IBVS*, 4360
- Antipin, S. V. 1999, *IBVS*, 4673, 1
- Baba, H., Kato, T., Nogami, D., Hirata, R., Matsumoto, K., & Sadakane, K. 2000, *PASJ*, 52, 429
- Bakowska, K., Olech, A., Zloczewski, K., & Wisniewski, M. 2010, *Acta Astron.*, 60, 137
- Balayan, S. K. 1997, *Astrophysics*, 40, 211
- Baptista, R. 2012, *Mem. Soc. Astron. Ital.*, 83, 530
- Baptista, R., Borges, B. W., Bond, H. E., Jablonski, F., Steiner, J. E., & Grauer, A. D. 2003, *MNRAS*, 345, 889
- Baptista, R., & Bortoletto, A. 2004, *AJ*, 128, 411
- Baptista, R., Catalán, M. S., Horne, K., & Zilli, D. 1998, *MNRAS*, 300, 233
- Baptista, R., Santos, R. F., Faúndez-Abans, M., & Bortoletto, A. 2007, *AJ*, 134, 867
- Barentsen, G., et al. 2014, *MNRAS*, 444, 3230
- Bateson, F., McIntosh, R., & Stubbings, R. 2000, *Publ. Variable Stars Sect. R. Astron. Soc. New Zealand*, 24, 48
- Bateson, F. M. 1982, *Publ. Variable Stars Sect. R. Astron. Soc. New Zealand*, 9, 1
- Berardi, P. 2015, *Astron. Telegram*, 7854
- Bertaud, C. 1951, *Annales d’Astrophysique*, 14, 199
- Bond, H. E. 1978, *PASP*, 90, 526
- Bond, H. E. 2004, in *IAU Colloq. 53: White Dwarfs and Variable Degenerate Stars*, ed. H. M. van Horn, & V. Weidemann (University of Rochester), p. 495
- Bond, H. E., Wagner, R. L., & Tapia, S. 1977, *IAU Circ.*, 3049
- Boyd, D., Graham, K., Kato, T., Koff, R., Miller, I., Oksanen, A., Pickard, R., & Poyner, G. 2009, *J. Br. Astron. Assoc.*, 119, 251
- Boyle, B. J., Shanks, T., Croom, S. M., Smith, R. J., Miller, L., Loaring, N., & Heymans, C. 2000, *MNRAS*, 317, 1014
- Breedt, E., et al. 2014, *MNRAS*, 443, 3174
- Bruch, A. 2000, *A&A*, 359, 998
- Bruch, A., Fischer, F.-J., & Wilmsen, U. 1987, *A&AS*, 70, 481
- Bruch, A., & Schimpke, T. 1992, *A&AS*, 93, 419
- Brun, A., & Petit, M. 1957, *Perem. Zvezdy*, 12, 18
- Busch, H., Häussler, K., & Splittergerber, E. 1979, *Veröff. Sternw. Sonneberg*, 9, 125
- Cannizzo, J. K., Still, M. D., Howell, S. B., Wood, M. A., & Smale, A. P. 2010, *ApJ*, 725, 1393
- Cao, Y., & Kulkarni, S. R. 2014, *Astron. Telegram*, 6221
- Cleveland, W. S. 1979, *J. Amer. Statist. Assoc.*, 74, 829
- Cook, M. C., & Brunt, C. C. 1983, *MNRAS*, 205, 465
- Cristiani, H., Duerbeck, H. W., & Seitter, W. C. 1985, *IAU Circ.*, 4027
- Cutri, R. M., et al. 2003, *2MASS All Sky Catalog of point sources (NASA/IPAC Infrared Science Archive)*
- Dai, Z., Szkody, P., Garnavich, P. M., & Kennedy, M. 2016, *AJ*, in press (arXiv/1603.03859)
- Danilet, A. B., et al. 2015, *Astron. Telegram*, 7260
- Davis, A. B., Shappee, B. J., Archer Shappee, B., & ASAS-SN 2015, *American Astron. Soc. Meeting Abstracts*, 225, #344.02
- Davis, A. B., et al. 2014, *Astron. Telegram*, 6211
- Denisenko, D., et al. 2013a, *Astron. Telegram*, 5065
- Denisenko, D., et al. 2013b, *Astron. Telegram*, 5111
- Denisenko, D. V. 2012, *Astron. Lett.*, 38, 249
- Dong, S., et al. 2015, *Astron. Telegram*, 7850
- Downes, R., Webbink, R. F., & Shara, M. M. 1997, *PASP*, 109, 345
- Downes, R. A. 1990, *AJ*, 99, 339
- Drake, A. J., et al. 2009, *ApJ*, 696, 870
- Drake, A. J., et al. 2014, *MNRAS*, 441, 1186
- Drew, J. E., et al. 2005, *MNRAS*, 362, 753
- Echevarria, J., & Alvarez, M. 1993, *A&A*, 275, 187
- Fernie, J. D. 1989, *PASP*, 101, 225

- Goranskij, V. P. 1972, *Astron. Tsirk.*, 696
- Gorbovskoy, E. S., et al. 2013, *Astron. Rep.*, 57, 233
- Green, R. F., Ferguson, D. H., Liebert, J., & Schmidt, M. 1982, *PASP*, 94, 560
- Greiss, S., et al. 2012, *AJ*, 144, 24
- Gress, O., et al. 2015a, *Astron. Telegram*, 7237
- Gress, O., et al. 2016a, *Astron. Telegram*, 8596
- Gress, O., et al. 2015b, *Astron. Telegram*, 7972
- Gress, O., et al. 2016b, *Astron. Telegram*, 8730
- Hamilton, R. T., Harrison, T. E., Tappert, C., & Howell, S. B. 2011, *ApJ*, 728, 16
- Haro, G., & Chavira, E. 1960, *Boletín de los Observatorios de Tonantzintla y Tacubaya*, 2, 11
- Harrison, T. E. 2016, *ApJ*, 816, 4
- Hellier, C. 2001, *Cataclysmic Variable Stars: How and why they vary* (Berlin: Springer)
- Herbig, G. H. 1958, *PASP*, 70, 605
- Hirose, M., & Osaki, Y. 1990, *PASJ*, 42, 135
- Hirose, M., & Osaki, Y. 1993, *PASJ*, 45, 595
- Hoffleit, D. 1935, *Harvard Coll. Obs. Bull.*, 901, 20
- Hoffmeister, C. 1949, *Erg. Astron. Nachr.*, 12, 1
- Hoffmeister, C. 1957, *Mitteil. Veränderl. Sterne*, 245
- Hoffmeister, C. 1963a, *IBVS*, 24
- Hoffmeister, C. 1963b, *Veröff. Sternw. Sonneberg*, 6, 1
- Hoffmeister, C. 1966, *Astron. Nachr.*, 289, 139
- Hoffmeister, C. 1967, *Astron. Nachr.*, 290, 43
- Hoppe, J. 1935, *Astron. Nachr.*, 254, 369
- Howell, S., & Szkody, P. 1988, *PASP*, 100, 224
- Howell, S. B., De Young, J., Mattei, J. A., Foster, G., Szkody, P., Cannizzo, J. K., Walker, G., & Fierce, E. 1996, *AJ*, 111, 2367
- Howell, S. B., Dobrzycka, D., Szkody, P., & Kreidl, T. J. 1991, *PASP*, 103, 300
- Howell, S. B., Harrison, T. E., Szkody, P., & Silvestri, N. M. 2010, *AJ*, 139, 1771
- Hurst, G. M., Lubbock, S., & McNaught, R. H. 1987, *IAU Circ.*, 4504
- Imada, A., Kato, T., Monard, L. A. G., Retter, A., Liu, A., & Nogami, D. 2006, *PASJ*, 58, 383
- Imada, A., et al. 2008, *PASJ*, 60, 1151
- Ishioaka, R., et al. 2001, *PASJ*, 53, 905
- Ishioaka, R., Uemura, M., Kato, T., Iwamatsu, H., Matsumoto, K., Billings, G., Masi, G., & Kiyota, S. 2000, *IAU Circ.*, 7552
- Ishioaka, R., et al. 2002, *A&A*, 381, L41
- Kato, T. 1991, *IBVS*, 3671
- Kato, T. 1995, *IBVS*, 4239
- Kato, T. 2001a, *IBVS*, 5107
- Kato, T. 2001b, *IBVS*, 5110
- Kato, T. 2002, *PASJ*, 54, L11
- Kato, T. 2015, *PASJ*, 67, 108
- Kato, T., et al. 2016a, *PASJ*, in press (arXiv/1604.01103)
- Kato, T., et al. 2014a, *PASJ*, 66, 90
- Kato, T., et al. 2015a, *PASJ*, 67, 105
- Kato, T., Fujino, S., & Iida, M. 1989, *VSOLJ Variable Star Bull.*, 9, 33
- Kato, T., et al. 2013a, *PASJ*, 65, 23
- Kato, T., et al. 2014b, *PASJ*, 66, 30
- Kato, T., Hamsch, F.-J., & Monard, B. 2015b, *PASJ*, 67, L2
- Kato, T., et al. 2009, *PASJ*, 61, S395
- Kato, T., Kunjaya, C., Okyudo, M., & Takahashi, A. 1994, *PASJ*, 46, L199
- Kato, T., et al. 2012, *PASJ*, 64, 21
- Kato, T., et al. 2010, *PASJ*, 62, 1525
- Kato, T., & Matsumoto, K. 1999a, *IBVS*, 4765
- Kato, T., & Matsumoto, K. 1999b, *IBVS*, 4767
- Kato, T., Monard, B., Hamsch, F.-J., Kiyota, S., & Maehara, H. 2013b, *PASJ*, 65, L11
- Kato, T., & Nogami, D. 1995, *IBVS*, 4260
- Kato, T., Nogami, D., Baba, H., Matsumoto, K., Arimoto, J., Tanabe, K., & Ishikawa, K. 1996a, *PASJ*, 48, L21
- Kato, T., Nogami, D., Masuda, S., & Hirata, R. 1996b, *PASJ*, 48, 45
- Kato, T., Nogami, D., Moilanen, M., & Yamaoka, H. 2003a, *PASJ*, 55, 989
- Kato, T., et al. 2014c, *PASJ*, 66, L7
- Kato, T., & Osaki, Y. 2013a, *PASJ*, 65, 97
- Kato, T., & Osaki, Y. 2013b, *PASJ*, 65, 115
- Kato, T., et al. 2016b, *PASJ*, 68, L4
- Kato, T., et al. 2003b, *MNRAS*, 339, 861
- Kato, T., Stubbings, R., Monard, B., Butterworth, N. D., Bolt, G., & Richards, T. 2004a, *PASJ*, 56, S89
- Kato, T., Stubbings, R., Nelson, P., Pearce, A., Garradd, G., & Kiyota, S. 2001, *IBVS*, 5159
- Kato, T., & Uemura, M. 2000, *IBVS*, 4902
- Kato, T., Uemura, M., Ishioaka, R., Nogami, D., Kunjaya, C., Baba, H., & Yamaoka, H. 2004b, *PASJ*, 56, S1
- Kazarovets, E. V., Kireeva, N. N., Samus, N. N., & Durlevich, O. V. 2003, *IBVS*, 5422
- Kazarovets, E. V., Samus, N. N., Durlevich, O. V., Kireeva, N. N., & Pastukhova, E. N. 2011, *IBVS*, 5969
- Kazarovets, E. V., Samus, N. N., Durlevich, O. V., Kireeva, N. N., & Pastukhova, E. N. 2015a, *IBVS*, 6151
- Kazarovets, E. V., Samus, N. N., Durlevich, O. V., Kireeva, N. N., & Pastukhova, E. N. 2015b, *IBVS*, 6155
- Kepler Mission Team 2009, *VizieR Online Data Catalog*, 5133
- Khatsov, A. Sh. 1971, *Abastumanskaya Astrofiz. Obs. Byull.*, 40, 13
- Kholopov, P. N., et al. 1985, *General Catalogue of Variable Stars*, fourth edition (Moscow: Nauka Publishing House)
- Khruslov, A. V. 2005, *Perem. Zvezdy, Prilozh.*, 5, 4
- Kimura, M., et al. 2016a, *PASJ*, 68, L2
- Kimura, M., et al. 2016b, *PASJ*, in press (arXiv/1604.06344)
- Kiyota, S., & Kato, T. 1998, *IBVS*, 4644
- Knigge, C., Baraffe, I., & Patterson, J. 2011, *ApJS*, 194, 28
- Koch, D. G., et al. 2010, *ApJ*, 713, L79
- Kryachko, T. V. 2001, *IBVS*, 5058
- Kukarkin, B. V., et al. 1982, *New Catalogue of Suspected Variable Stars* (Moscow: Nauka Publishing House)
- Kurochkin, N. E. 1977, *Astron. Tsirk.*, 974, 4
- Lasker, B., Lattanzi, M. G., McLean, B. J., & et al. 2007, *VizieR Online Data Catalog*, 1305
- Levitan, D., Groot, P. J., Prince, T. A., Kulkarni, S. R., Laher, R., Ofek, E. O., Sesar, B., & Surace, J. 2015, *MNRAS*, 446, 391
- Littlefair, S. P., Dhillion, V. S., Marsh, T. R., Gänsicke, B. T., Baraffe, I., & Watson, C. A. 2007, *MNRAS*, 381, 827
- Liu, Wu., Hu, J. Y., Zhu, X. H., & Li, Z. Y. 1999, *ApJS*, 122, 243
- Longa-Peña, P., Steeghs, D., & Marsh, T. 2015, *MNRAS*, 447, 149
- Lubow, S. H. 1991, *ApJ*, 381, 259
- Lubow, S. H. 1992, *ApJ*, 401, 317
- Luyten, W. J., & Haro, G. 1959, *PASP*, 71, 469
- McNaught, R. H. 1985, *IAU Circ.*, 4036

- Mattei, J., Ducoty, R., Stanton, R., & Scovill, C. 1985, *IAU Circ.*, 4026
- Mattei, J., Isles, J., & Lubbock, S. 1987, *IAU Circ.*, 4506
- Mattei, J. A., Stubbings, R., & Dubovsky, P. 2000, *IAU Circ.*, 7547
- Mayall, M. W. 1968, *JRASC*, 62, 141
- Mayall, M. W. 1970, *JRASC*, 64, 205
- McAllister, M. J., et al. 2015, *MNRAS*, 451, 4633
- Mennicken, R., & Vogt, N. 1993, *Rev. Mexicana Astron. Astrof.*, 26, 111
- Mennickent, R. E., & Diaz, M. P. 2002, *MNRAS*, 336, 767
- Mennickent, R. E., Sterken, C., Gieren, W., & Unda, E. 1999, *A&A*, 352, 239
- Mennickent, R. E., & Tappert, C. 2001, *A&A*, 372, 563
- Meyer, F., & Meyer-Hofmeister, E. 2015, *PASJ*, 67, 52
- Monet, D. B. A., et al. 1998, *VizieR Online Data Catalog*, I/252
- Montgomery, M. M. 2001, *MNRAS*, 325, 761
- Morgenroth, O. 1934, *Astron. Nachr.*, 253, 441
- Motch, C., et al. 1998, *A&AS*, 132, 341
- Munari, U., & Zwitter, T. 1998, *A&AS*, 128, 277
- Murray, J. R. 1998, *MNRAS*, 297, 323
- Nakata, C., et al. 2014, *PASJ*, 66, 116
- Nakata, C., et al. 2013, *PASJ*, 65, 117
- Narumi, H., Korth, S., Dyck, G., Iida, M., & Hurst, G. 1989, *IAU Circ.*, 4757
- Nesci, R., Caravano, A., Falasca, V., & Villani, L. 2013, *IBVS*, 6059
- Nogami, D., & Kato, T. 1997, *PASJ*, 49, 109
- Nogami, D., Kato, T., Baba, H., Matsumoto, K., Arimoto, J., Tanabe, K., & Ishikawa, K. 1997, *ApJ*, 490, 840
- Nogami, D., Monard, B., Retter, A., Liu, A., Uemura, M., Ishioka, R., Imada, A., & Kato, T. 2004, *PASJ*, 56, L39
- Nogami, D., Uemura, M., Ishioka, R., Kato, T., & Pietz, J. 2004, *PASJ*, 56, S155
- Nogami, D., et al. 2003, *A&A*, 404, 1067
- Novák, R. 1997, *IBVS*, 4489
- O'Donoghue, D., Chen, A., Marang, F., Mittaz, J. P. D., Winkler, H., & Warner, B. 1991, *MNRAS*, 250, 363
- Ohshima, T., et al. 2014, *PASJ*, 66, 67
- Oizumi, S., et al. 2007, *PASJ*, 59, 643
- Olech, A., Schwarzenberg-Czerny, A., Kędzierski, P., Złoczewski, K., Mularczyk, K., & Wiśniewski, M. 2003, *Acta Astron.*, 53, 175
- Osaki, Y. 1989, *PASJ*, 41, 1005
- Osaki, Y. 1996, *PASP*, 108, 39
- Osaki, Y., & Kato, T. 2013a, *PASJ*, 65, 50
- Osaki, Y., & Kato, T. 2013b, *PASJ*, 65, 95
- Osaki, Y., & Kato, T. 2014, *PASJ*, 66, 15
- Osaki, Y., & Meyer, F. 2002, *A&A*, 383, 574
- Osaki, Y., & Meyer, F. 2003, *A&A*, 401, 325
- Papadaki, C., Boffin, H. M. J., Steeghs, D., & Schmidtbreich, L. 2008, *A&A*, 487, 611
- Parsamyan, E. S., Oganyan, G. B., Kazaryan, E. S., & Yankovich, I. I. 1983, *Astron. Tsirk.*, 1269, 7
- Patterson, J. 1980, *J. American Assoc. Variable Star Obs.*, 9, 49
- Patterson, J. 1998, *PASP*, 110, 1132
- Patterson, J., Augustejin, T., Harvey, D. A., Skillman, D. R., Abbott, T. M. C., & Thorstensen, J. 1996, *PASP*, 108, 748
- Patterson, J., et al. 2003, *PASP*, 115, 1308
- Patterson, J., Thorstensen, J. R., & Knigge, C. 2008, *PASP*, 120, 510
- Pavlenko, E. P., et al. 2014, *PASJ*, 66, 111
- Pearson, K. J. 2006, *MNRAS*, 371, 235
- Petit, M. 1960, *Journal des Observateurs*, 43, 17
- Pinto, G., & Romano, G. 1972, *Mem. Soc. Astron. Ital.*, 43, 135
- Pinto, G., & Romano, G. 1976, *Mem. Soc. Astron. Ital.*, 47, 229
- Pojmański, G. 2002, *Acta Astron.*, 52, 397
- Prieto, J. L., et al. 2013, *Astron. Telegram*, 4999
- Prieto, J. L., et al. 2014, *Astron. Telegram*, 6249
- Richter, G. A. 1969, *Mitteil. Veränderl. Sterne*, 5, 69
- Richter, G. A. 1985, *IBVS*, 2714
- Ritter, H., & Kolb, U. 2003, *A&A*, 404, 301
- Romano, G., & Minello, S. 1976, *IBVS*, 1140
- Rosino, L., & Candeo, G. 1989, *IAU Circ.*, 4900
- Rutkowski, A., Olech, A., Mularczyk, K., Boyd, D., Koff, R., & Wisniewski, M. 2007, *Acta Astron.*, 57, 267
- Rutkowski, A., Pietrukowicz, P., Olech, A., Ak, T., Złoczewski, K., Poleski, R., Tappert, C., & Eker, Z. 2011, *Acta Astron.*, 61, 345
- Saito, R. K., & Baptista, R. 2006, *AJ*, 131, 2185
- Sanduleak, N. 1972, *IBVS*, 663
- Shappee, B. J., et al. 2014, *ApJ*, 788, 48
- Shappee, B. J., et al. 2013, *Astron. Telegram*, 5052
- Shears, J., Lloyd, C., Boyd, D., Brady, S., Miller, I., & Pickard, R. 2009, *J. Br. Astron. Assoc.*, 119, 31
- Shears, J., Wils, P., Bolt, G., Hamsch, F.-J., Krajci, T., Miller, I., Sabo, R., & Staels, B. 2011, *J. Br. Astron. Assoc.*, 121, 155
- Sheets, H. A., Thorstensen, J. R., Peters, C. J., Kapusta, A. B., & Taylor, C. J. 2007, *PASP*, 119, 494
- Shurpakov, S., et al. 2013, *Astron. Telegram*, 5083
- Simonian, G., et al. 2015, *Astron. Telegram*, 7809
- Simonian, G., et al. 2016, *Astron. Telegram*, 8648
- Skiff, B. A. 1999, *IBVS*, 4675
- Skinner, J. N., Thorstensen, J. R., & Lépine, S. 2014, *AJ*, 148, 115
- Smak, J. I. 1991, *Acta Astron.*, 41, 269
- Smart, R. L. 2013, *VizieR Online Data Catalog*, 1324
- Southworth, J., et al. 2008, *MNRAS*, 391, 591
- Stanek, K. Z., et al. 2015, *Astron. Telegram*, 8068
- Stanek, K. Z., et al. 2013, *Astron. Telegram*, 5082
- Steeghs, D., O'Brien, K., Horne, K., Gomer, R., & Oke, J. B. 2001, *MNRAS*, 323, 484
- Stellingwerf, R. F. 1978, *ApJ*, 224, 953
- Szkody, P. 1987, *ApJS*, 63, 685
- Szkody, P., et al. 2002, *AJ*, 123, 430
- Szkody, P., et al. 2009, *AJ*, 137, 4011
- Szkody, P., et al. 2005, *AJ*, 129, 2386
- Szkody, P., & Howell, S. B. 1992, *ApJS*, 78, 537
- Tappert, C., Mennickent, R. E., Arenas, J., Matsumoto, K., & Hanuschik, R. W. 2003, *A&A*, 408, 651
- Tchäpe, R. 1963, *Mitteil. Veränderl. Sterne*, 2, 3
- Thorstensen, J. R., & Fenton, W. H. 2003, *PASP*, 115, 37
- Thorstensen, J. R., Patterson, J. O., Kemp, J., & Vennes, S. 2002, *PASP*, 114, 1108
- Thorstensen, J. R., Patterson, J. O., Shambrook, A., & Thomas, G. 1996, *PASP*, 108, 73
- Uemura, M., et al. 2008, *IBVS*, 5815, 1
- Uthas, H. 2011, Ph. D. thesis, (arXiv/1105.1164)
- Uthas, H., Knigge, C., Long, K. S., Patterson, J., & Thorstensen, J. 2011, *MNRAS*, 414, L85
- Uthas, H., et al. 2012, *MNRAS*, 420, 379
- Voges, W., et al. 1999, *A&A*, 349, 389
- Vogt, N. 1983, *A&A*, 118, 95
- Vogt, N., & Bateson, F. M. 1982, *A&AS*, 48, 383

- Vrielmann, S., & Offutt, W. 2000, *New Astron. Rev.*, 44, 39P
- Vrielmann, S., & Offutt, W. 2003, *MNRAS*, 338, 165
- Vrielmann, S., Stiening, R. F., & Offutt, W. 2002, *MNRAS*, 334, 608
- Warner, B. 1995a, *Cataclysmic Variable Stars* (Cambridge: Cambridge University Press)
- Warner, B. 1995b, *Ap&SS*, 226, 187
- Warner, B., & Cropper, M. 1983, *MNRAS*, 203, 909
- Warner, B., & O'Donoghue, D. 1987, *MNRAS*, 224, 733
- Watts, D. J., Bailey, J., Hill, P. W., Greenhill, J. G., McCowage, C., & Carty, T. 1986, *A&A*, 154, 197
- Webbink, R. F., Hazen, M. L., & Hoffleit, D. 2002, *IBVS*, 5298
- Wenzel, W. 1984, *IBVS*, 2481
- Whitehurst, R. 1988, *MNRAS*, 232, 35
- Wils, P., Gänsicke, B. T., Drake, A. J., & Southworth, J. 2010, *MNRAS*, 402, 436
- Witham, A. R., Knigge, C., Drew, J. E., Greimel, R., Steeghs, D., Gänsicke, B. T., Groot, P. J., & Mampaso, A. 2008, *MNRAS*, 384, 1277
- Wojcikiewicz, E., & Baptista, R. 2014, *Rev. Mexicana Astron. Astrof. (Serie de Conferencias)*, 44, 170
- Wolf, M. 1919, *Astron. Nachr.*, 209, 85
- Wood, M. A., Still, M. D., Howell, S. B., Cannizzo, J. K., & Smale, A. P. 2011, *ApJ*, 741, 105
- Woudt, P. A., & Warner, B. 2010, *MNRAS*, 403, 398
- Yamaoka, H., Itagaki, K., Maehara, H., & Nakano, S. 2008, *Cent. Bur. Electron. Telegrams*, 1535
- Zacharias, N., et al. 2015, *AJ*, 150, 101